The Electricity and Transportation Infrastructure Convergence Using Electrical Vehicles

Final Project Report

Power Systems Engineering Research Center

Empowering Minds to Engineer
the Future Electric Energy System

The Electricity and Transportation Infrastructure Convergence Using Electrical Vehicles

Final Project Report

Project Team

Faculty:
Mladen Kezunovic, Project Leader
Texas A&M University

Sakis Meliopoulos
Georgia Institute of Technology

Ross Baldick
University of Texas at Austin

Students:
Qin Yan, Bei Zhang
Texas A&M University
Thamer Alquthami
Georgia Institute of Technology

PSERC Publication 14-8

September 2014

For information about this project, contact

Mladen Kezunovic, Ph.D., P.E.
Eugene E. Webb Professor
Texas A&M University
Department of Electrical Engineering
College Station, TX 77843-3128
Phone: 979-845-7509
Fax: 979-845-9887
Email: kezunov@ece.tamu.edu

Power Systems Engineering Research Center

The Power Systems Engineering Research Center (PSERC) is a multi-university Center conducting research on challenges facing the electric power industry and educating the next generation of power engineers. More information about PSERC can be found at the Center's website: http://www.pserc.org.

For additional information, contact:

Power Systems Engineering Research Center
Arizona State University
527 Engineering Research Center
Tempe, Arizona 85287-5706
Phone: 480-965-1643
Fax: 480-965-0745

Notice Concerning Copyright Material

Acknowledgements

This is the final report for the project entitled "The Electricity and Transportation Infrastructure Convergence Using Electrical Vehicles" (PSERC project T-50G).

We express our appreciation for the support provided by the Electric Vehicle Transportation and Electricity Convergence (EV-TEC) members, Power Systems Engineering Research Center (PSERC) members, and by the National Science Foundation for the grant received under the Industry / University Cooperative Research Center Collaborative Opportunities for Research between I/UCRCs (CORBI) program.

We wish to thank the following project advisors:

Jay Giri, ALSTOM Grid
Art Mander, TriState G&T
Kip Morison, BC Hydro
Mark Westendorf, Midcontinent ISO.

Executive Summary

Electric vehicles (EVs) introduce environmental advantages when compared to conventional gasoline-powered vehicles. They reduce air pollutants and greenhouse gas emissions while contributing to energy security through reduction in oil imports. They can be also utilized to dynamically control the apparent load or contribute to ancillary services. Market penetration of EVs is foreseen to grow significantly in the future. Therefore, the investigation on how EVs, both Plug-in Hybrid Electric Vehicles (PHEVs) and Battery Electric Vehicles (BEVs), can be utilized in an optimal way in both electricity and transportation networks is necessary.

Specifically, this project mainly: a) provides State of Charge (SoC) model that integrates electricity and transportation impact of EVs, b) uses the model to study optimal use of EVs in individual and aggregated mode, and c) shows some practical examples using testbeds for monitoring impact on transformers, participation in ancillary services, and integration of communication and information management for charging stations from multiple vendors.

First, the impact of vehicle movement on SoC is investigated. The relationship between the vehicle's movement and SoC is simulated and analyzed. An algorithm is proposed to calculate and analyze the optimal velocity during a driving cycle with respect to battery energy consumption. Such algorithm can be inserted in the vehicle imbedded systems and provides the drivers suggestions about the optimal driving speed according to the real-time driving condition and the preset driving cycle.

Second, the design of the proposed communication center between charging infrastructures and its functionality are introduced. The survey results on different charging station vendors are summarized. In addition, database design and data acquisition methods are described, according to the information that each vendor would provide to the customers.

Third, physically based models of various components that are considered to be part of the overall model of the system are presented. These include energy resources such as roof top solar PV, energy storage system in the form of battery systems, etc. and house appliances such as smart dishwasher, refrigerator, and air conditioner. Averaged models of power electronics converters are used to connect various parts of the system together. A demonstration case study of most of these new models is also provided to display the various characteristics of the model. The overall model is managed by a house management system that provides appropriate control for the entire system connected to a distribution transformer. The coordinated control of EVs and PHEVs with other residential resources and the power grid is achieved by real time control utilizing a real time model of the system via state estimation.

Last, a systematic method for an Energy Services Company, particularly one that serves EV load, to participate in a multi-settlement market structure is provided. The challenges in scenario generation in case of EV load are discussed and a data driven approach for generating scenarios is proposed.

Project Publications:

Mahdi Kefayati and Ross Baldick, "Scheduling Flexible Loads in Multi-settlement Electricity Markets," *INFORMS Annual Meeting*, Minneapolis, MN, 5-10 October 2013.

B. Zhang, M. Kezunovic, "Impact of Available Electric Vehicle Battery Power Capacity on Power System Reliability," *Power and Energy Society Meeting*, 2013 IEEE

T. Alquthami, A.P. Meliopoulos, "Hierarchical optimization and control of a distribution system" *Proceedings of the IEEE North American Power Symposium (NAPS)*, 2013.

T. Alquthami, R. Huang, E. Polymeneas, A.P. Meliopoulos, "Hierarchical optimization and control of a power system", *Proceedings of the 2014 IEEE Innovative Smart Grid Technologies (ISGT-US)*, 2014.

T. Alquthami, A.P. Meliopoulos, "Distribution Transformer Load Management System", Accepted: *IEEE PES General Meeting*, July 2014.

Q. Yan, B. Zhang, M. Kezunovic, "Optimization of Electric Vehicle Movement for Efficient Energy Consumption," The 46th North American Power Symposium (NAPS), Pullman, WA, USA, September 2014

Table of Contents

List of Figures

List of Tables

1. Introduction

1.1 Problem Definition

In recent years, the market share of Electric Vehicles (EVs) including Plug-in Hybrid Electric Vehicles (PHEV) and Battery Electric Vehicles (BEV) has been dramatically increased. Due to the environmental and sustainable energy advantages of EVs compared with conventional fuel transportation, the related topics have been discussed and studied, such as the impact of EV penetration on the power grid or how to develop the technologies to improve its performance. It can be foreseen that, in the near future, the penetration of EVs will continue to grow significantly in the worldwide market [1]. In some open literatures, it is easily found that the attitude towards the market penetration estimation is quite optimistic [2]. Clement et al. (07-08) stated that the amount of PHEVs would reach 28% of the total vehicle fleet in Belgian in 2030. It was estimated in Hadley and Tscetkova (2008) [3] that, PHEVs would reach a market share of 25% by the year 2020 and achieve the vehicle amount of 50 million by 2030 in US. Although current penetration situation of EVs does not seem to support such inferences, these estimations have been confirmed by other studies [2].

In a previous PSERC project (T-34) [4, 5], by Sakis Meliopoulos (lead), Jerome Meisel and Tom Overbye, the impact of PHEVs on the power grid was studied in different aspects, and it drew a conclusion that, the impact is beneficial in terms of environment, economy and reliability, in general. The impact can be more beneficial to assist the regulation of the power grid when needed by implementing certain controls. Negative effect has been revealed as well, on the service lifetime of distribution components such as distribution transformers and local circuits. However, the unfavorable effect is manageable by certain optimization strategies. As a result, the benefits of EVs to the power grid can be maximized by extra control algorithms and appropriate devices or circuits. In addition to maximize the performance of EVs on electricity networks, certain optimization algorithms can profit transportation networks as well by regarding electricity as another source of "fuel" for vehicles. In another PSERC project (T-40) by Mladen Kezunovic (lead), Ross Baldick, and Ivan Damnjanovic [6, 7], the impacts of PHEVs on both the electricity and transportation networks have been discussed. Besides the mentioned project, two EV TEC projects – "Information Exchange Between ISOs, Aggregators, and PEVs to Procure Ancillary Services" led by Ross Baldick and "Impact of EVs charging on Distribution Systems" led by Mladen Kezunovic – have investigated how the utilization of renewable energy sources will be influenced by the charging of electricity-required EVs and analyzed the deterioration of the battery's state of charge (SOC).

As identified in the above-mentioned projects, the benefits of EVs penetrations into electricity and transportation fields need to be investigated on how to achieve it simultaneously. The investigations may include the combination of the benefits that are concluded in the previous studies and the extension of the previous results by making further improvement. In addition to the benefits, measurements should also be proposed to alleviate the negative impacts on distribution system and local components, such as local circuits and distribution transformers.

When discussing about the growing market of electric vehicles, charging stations and charging standards are required to be investigated and established. Development has been made in terms of unification. There are some standards being established, with the SAE J1772 connector becoming the one used in most of the world [8]. The chargers that safely allows electricity to flow into the vehicle batteries and the protocols proposed to create the chargers are called electric vehicle supply equipment (EVSE). The EVSE supports two-way communication between EV charging stations and EVs and hence improves the safety. The term EVSE has been used for a long time and it was defined in the 1996 NEC and California Article 625 as:

> "The conductors, including the ungrounded, grounded, and equipment grounding conductors, the electric vehicle connectors, attachment plugs, and all other fittings, devices, power outlets or apparatuses installed specifically for the purpose of delivering energy from the premises wiring to the electric vehicle."[9]

The two-way communication between the charger and vehicle guaranteed the charging current passed to the vehicle to be both under the maximum current the charger can provide and under the maximum current the vehicle can receive. In addition to the current limit, there are other safety designs, such as lockout, detecting hardware faults, electrical shortage, and fire, disconnecting the power flow, and preventing battery damage. For instance, lockout feature prevents current from flowing from wall charger to the car when the plug is not physically connected to the car. Although the EVSE builds the two-way communication between charger and vehicle pairs, there is no communication and information exchange between charging stations since different standards may exist. In fact, many different vendors of EVSE are providing products that are compatible only with their own infrastructure. Thus, to better coordinate the use of electric vehicles and better schedule the charging to realize certain applications, the communication between charging stations need to be investigated and established.

1.2 Project Scope

To better understand how the problems defined in the previous section may be solved, a complementary set of activities will be pursued through this joint CORBI project in the following three areas:

1. Modeling the impact of EVs on distribution systems by incorporating results from a power transformer testbed and measuring impacts of long and short terms stresses due to EV charging on asset management. An example of the previous work is shown on Fig. 1 and Fig 2. A recommendation that was developed in previous work is the development of a low cost monitor of the electro-thermal model of distribution transformers that will allow tracking of the loss of life and will provide information for managing the fleet of distribution transformers by moving transformers to other locations serving customers with less load and upgrading the size of transformers that are losing life at very high rates;

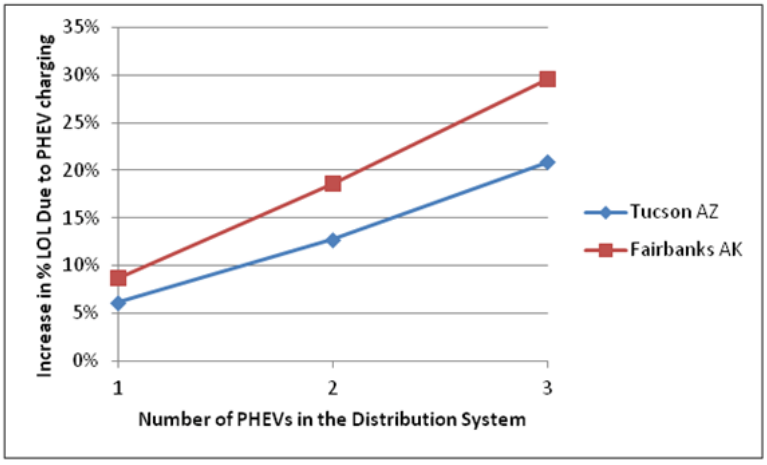

Figure 1.2.1 Increased Transformer LOL as PHEV are Added to the System

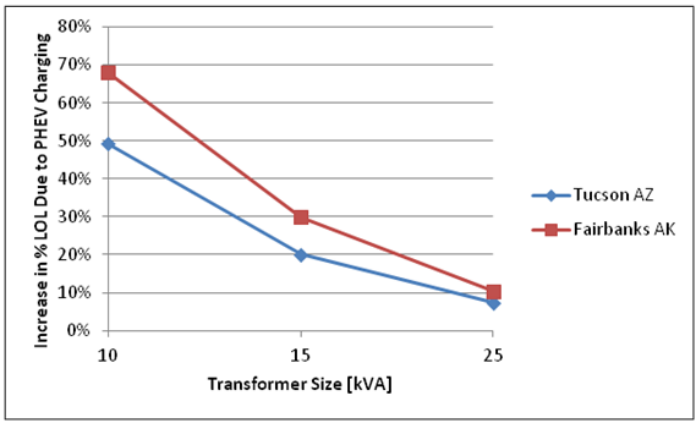

Figure 1.2.2 Effect of Transformer Size of Loss of Life

2. Modeling the impact of large number of EVs charged in a parking garage. An example of a testbed study from the previous PSERC work is shown in Fig 3 and Fig. 4. In this example a model of an actual distribution system in downtown Houston is modeled to show how outage management affect various customers (loads) with and without the energy supply available in a parking garage where a number of EVs are parked. The demand study of the garage can offer solutions for short outages in the distribution systems where the garage becomes an energy supply using energy stored in the EV batteries;

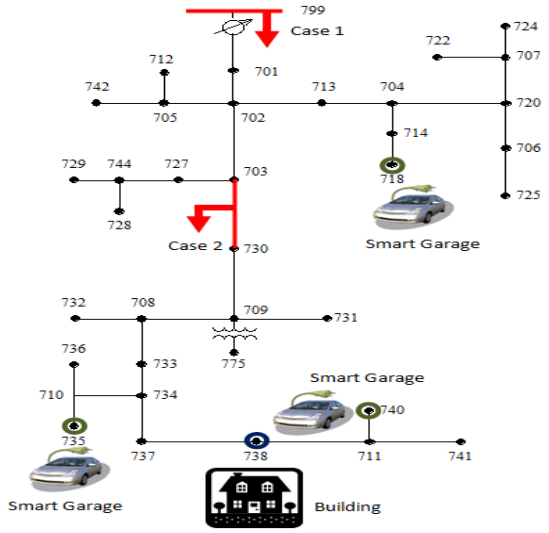

Figure 1.2.3 Position of Garages vs. Critical Feeders

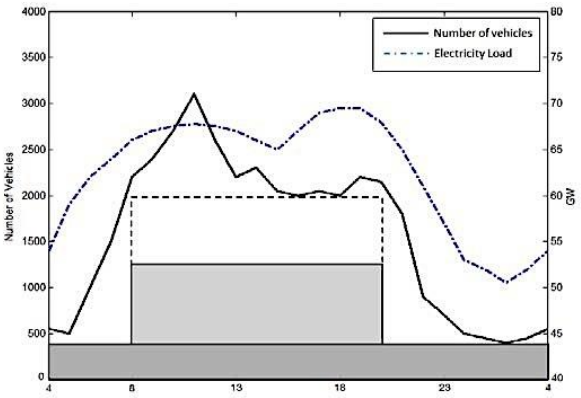

Figure 1.2.4 Demand for Charging in a Garage

3. Modeling the use of EVs in outage management by studying the impact of both electricity and transportation on EVs focusing on testbed simulation scenarios with real state of charge (SOC) data as shown in Fig. 5 and Fig. 6. This scenario allows study of the behavior of state of charge for various EVs taking into account their properties and properties of the driving cycle. Such examples are created using a testbed using data from College Station where specific driving cycles are modeled in detail and SOC tracked accordingly [10];

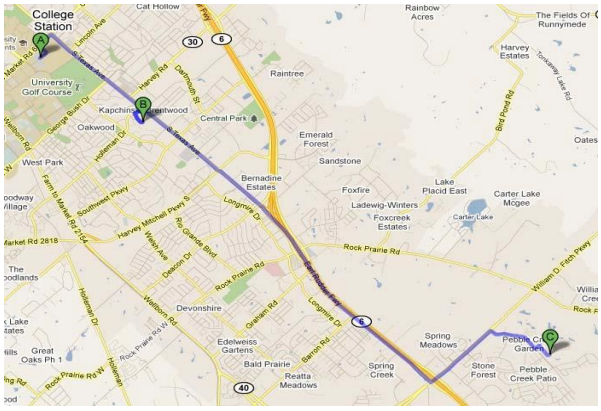

Figure 1.2.5 Typical Traffic Route of an EV

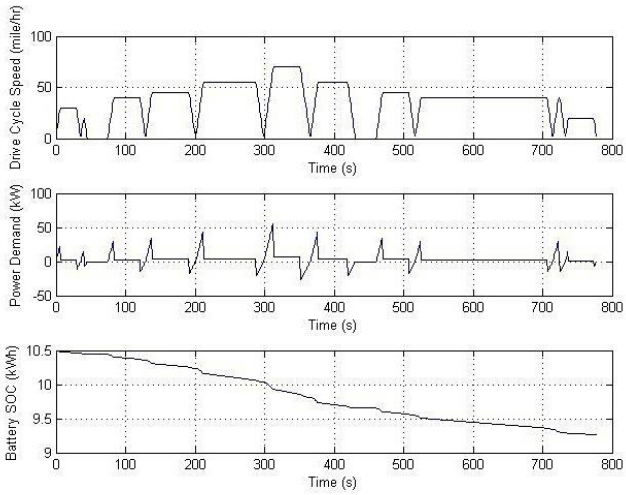

Figure 1.2.6 SOC Pattern for EV Battery

4. Modeling the use of controlled charging as a demand-side resource both in the context of participating in the energy market and in the Ancillary Services market through an appropriate model of interaction between an aggregator and EVs. Figure 7 illustrates that the aggregator intermediates between the market, as represented by the grid operator or ISO, and a potentially large number of EVs. Key issues include communication and control performance between aggregator and cars over a heterogeneous collection of possibly imperfectly reliable communication paths, together with ISO communication and control performance requirements that are modeled on generator performance standards. If the communication and control can be provided cost-effectively, then the inherent charging flexibility of EVs can be harnessed to provide services to the grid that will offset the cost of energy purchased for charging. For example, figure 8 shows historical responsive reserves and regulation prices in ERCOT. Bearing in mind that the EV can be providing for ancillary service (AS) while being charged, the market value of the AS provided will allow for a discount between the wholesale energy price and the price for combined charging and provision of AS. The

practicalities of large-scale aggregation will be investigated using a testbed of EVSEs being installed at the ERCOT Taylor facilities.

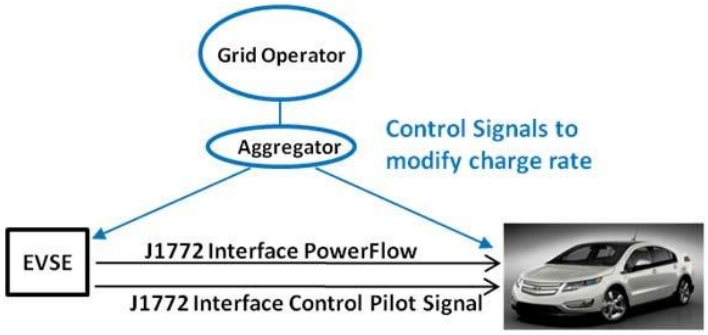

Figure 1.2.7 Communication and Control Structure

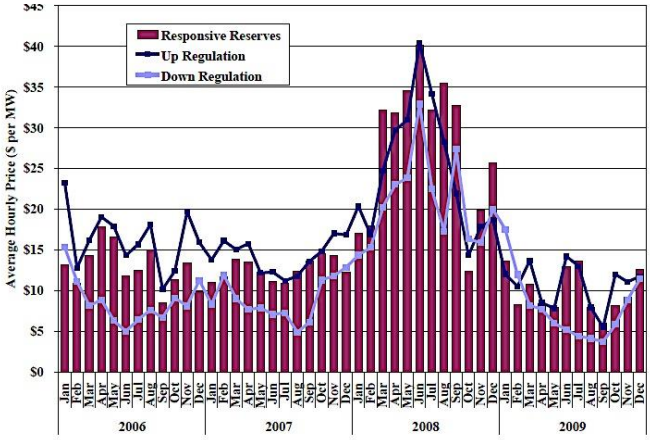

Figure 1.2.8 Typical Prices in ERCOT

As part of the joint CORBI project, our scope of the project is to analyze how the SOC of the vehicle batteries gets affected by vehicle movement and EV charging and study the impacts of EVs on both electricity and transportation infrastructure. In addition, the establishment of the testbed for communication and information management system for fleet owners to monitor the usage of charging infrastructure is realized in our project by establishing a communication channel for charging stations from different vendors.

As an extension of the project "TEC-1: The Role of PHEV/BEV in Outage/Asset and Demand Side Management", this project investigated how Electrical vehicles, can be utilized in an optimal way in both electricity and transportation networks. Specifically, the study: a) provided State of Charge (SoC) model that integrates electricity and transportation impact of EVs, b) used the model to study optimal use of EVs in individual and aggregated mode, and c) showed some practical examples using testbeds for monitoring impact on transformers, participation in ancillary services, and integration of communication and information management for charging stations from multiple vendors.

1.3 Goals and Objectives

This project aims to achieve the following outcomes:

1. Report identifying the benefits of simultaneous impacts of EVs on electricity and transportation infrastructures;
2. Low cost monitoring device of the electro-thermal model of distribution transformers and loss of life monitor for accurate management of the distribution transformer fleet;
3. Modeling and simulation software for analysis of the impacts of transportation needs of EVs on their State of Charge (SoC) Capabilities;
4. Demonstration example of the studies that may be performed using the SoC information;
5. Demonstration of practical information management approach when using EVs in various aggregator programs;
6. Demonstration of communication networks for integration of the EV charging stations from diverse vendors.

This project aims to achieve the following outcomes and benefits:

1. Methodology of mitigating the negative impacts of EVs on the electricity system by the development of a low cost monitoring device;
2. Recommendations on how to specify power transformers to sustain additional load from EVs;
3. Identification of market benefits of EV aggregation with respect to ancillary services and integration of renewables;
4. Development of common modeling and simulation framework to investigate interaction between electricity and transportation infrastructures during asset, outage and demand side management;
5. Demonstration of simultaneous environmental, economic and reliability impacts EVs may have on electricity and transportation networks;
6. Demonstration of feasibility of aggregation of large numbers of EVs and impact on demand response, provision of ancillary services, outage management and asset management.

1.4 Organization of Report

This project report will be organized as follows. Chapter 2 presents some background information including introduction of vehicle battery state of charge (SOC), EV roles in transportation and power systems, charging station development. In Chapter 3, impacts of vehicle movement on SOC are introduced in terms of the relationship and optimization analysis. Chapter 4 investigates some specifications and features of EV charging infrastructures. Chapter 5 to 6 illustrate in detail the survey result on different vendors, the

communication center proposed and the communication between charging infrastructures and communication center. A conclusion is given in Chapter 7. References, project publications and the appendix will be presented at the end of this report.

2. Background

2.1 Introduction

This part briefly introduces the state of charge of the vehicle batteries and the roles of EVs in both transportation and power systems current technology development and the current research status of electric vehicles. Related works that have been studied in terms of battery SOC and charging stations are also described here.

2.2 Vehicle Battery State of Charge

Analyzing state-of-charge (SOC) in a battery has been a significant topic for the industries for decades. In terms of material field, SOC is a static thermo-dynamic concept of battery chemistry and should be determined at each equilibrium point [11]. However, making driving cycle analysis with trip data collected from either plug-in hybrid electric vehicles (PHEVs) or battery electric vehicles (BEVs) operation in real-world situations is arduous and challenging. Similarly, investigating the performance of a battery including the variance of SOC in real life faces the same challenge [12]. It varies dramatically with respect to the driving speed, distance travelled, drivers' personal driving habit, the road condition, the battery aging condition, the regenerative braking, and etc. For the battery, the values of voltage and resistant depend on the SOC, the temperature, the current and the aging state of the battery [13].

In addition, the operation of PHEVs and BEVs are designed differently. Since PHEVs are operating using two dynamic resources, there are two operating mode, namely charge-depleting mode and charge-sustaining mode. Thus, a fully charged PHEV will be operating in charge-depleting mode until at one point, that the battery is consumed to a targeted SOC, then the operation switches to use the internal combustion engine, namely charge-sustaining mode, to maintain the targeted SOC [14]. Figure 2.1 [15] shows the typical SOC variation of a battery in the above-described PHEVs in terms of different operating modes.

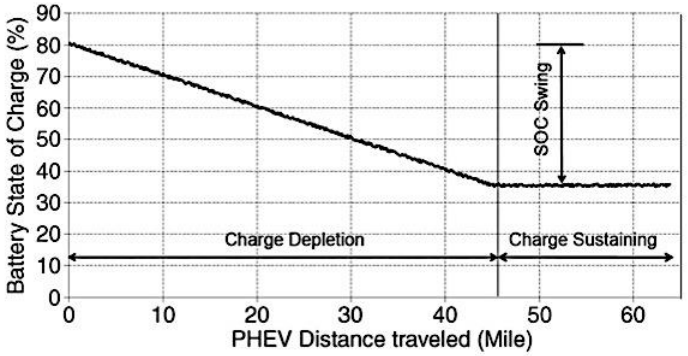

Figure 2.2.1 Typical SOC Variation of a PHEV Battery

There are plenty of papers that have discussed different method to simulate or estimate the battery SOC [16-21]. To name a few, paper [16] presented a method to simulate artificial

driving cycles based on mean velocity and mean positive acceleration which are two easily accessible parameters; paper [17] provided a description of an advanced vehicle simulator developed by the National Renewable Energy Laboratory; paper [18] stated how to estimate the SOC of the EV batteries using Elman neural network method; paper [19] introduced an observer-based SOC estimator for batteries where the estimation strategy is based on the battery's state space model. Detailed analysis of the impacts of vehicle movement on SOC will be discussed in Chapter 3.

2.3 Electric Vehicle Roles in Transportation and Power Systems

PHEVs/BEVs can create multiple benefits in electricity networks while playing a major role in transportation networks at the same time. The adoption of PHEVs/BEVs ties these two systems together. With the use of electric energy as a propulsion fuel in transportation networks rapidly growing, EVs are becoming a reality to face the fact that volatility increase of the crude oil market, unexpected price increase of oil, and the threat of global climate change. Thus, it is stated that it is significant to understand the consumers' choices in consideration of the travel patterns, as well as the future government regulations, retailers' incentives, aggregation opportunities, etc. as they transcend the traditional boundaries. The price of charging and discharging of the vehicles can cause a fundamental shift in the behavior of PHEV/BEV drivers. If the pricing schemes are developed with both the electricity and transportation systems in mind, PHEVs/BEVs could help mitigate problems plaguing the traffic network, particularly congestion issues. Another crucial reason of changing PHEV/BEV driver behavior and affecting driver's route planning includes the charging infrastructures, their location and the charging duration.

In addition, PHEVs/ BEVs can also contribute to the utilization rate of the road network. Vehicle miles traveled (VMT) has risen consistently since the emergence of the automobile, while with dips when gasoline prices rise quickly. The willingness of vehicle use is expected to increase into the foreseeable future if the transportation-needed energy is shifted to an alternative fuel source with more stable price schemes, such as electricity, and especially if the source of the fuel is renewable.

Besides the effect that PHEVs/BEVs have on the transportation system, the penetration also brings about great opportunities, as well as significant challenges, to the existing power grid. Charging of PHEVs/BEVs will increase the demand of electricity, but if not properly controlled, will increase the peak-valley difference and regional imbalance which may result in overvoltage and overcurrent of the existing lines, transformers and other equipment, and thus will reduce equipment utilization rate. Moreover, non-linearity and asymmetric of charging equipment will increase the harmonic currents in the distribution network, resulting in three phase imbalance and increase of the neutral current. All of these issues may reduce the reliability of power supply and power quality [22].

Despite the challenges that PHEVs/BEVs may bring to the power grid, it can benefit power grid based on the controllable nature of charging. The energy stored in PHEV/BEVs' batteries can be used as emergency backup power for the commercial facilities/buildings, and thus the reliability of the power supply for that load will be increased. Furthermore, they can discharge the batteries as distributed resources and sent back the power to the grid

to smooth the load curve, increase backup capacity and improve the reliability and security of the power system. PHEVs/BEVs can also provide ancillary service (including spinning reserves and regulation). In the future, PHEVs/BEVs can be integrated to support renewable energy in emerging power markets [23].

2.4 Charging Station Development

An electric vehicle charging station, also called EV charging station, electric recharging point, charging point and EVSE, is an element in an infrastructure that supplies electric energy for the recharging of plug-in electric vehicles, including BEVs, PHEVs, and neighborhood electric vehicles [24].

In order for the use of PHEVs and BEVs to be widely accepted and outspreaded, the infrastructure of charging stations need to be developed for the individual consumers and fleet owners first. To be more general, it is obvious that the installation of charging station should be ahead of the selling of electricity-needed vehicles. In this regard, consumers may take the convenience and amount of the existing charging stations as the priority consideration when considering purchasing an EV. The need for EV charging stations in residential, industrial and commercial facilities is increasing and will continue to rise as the amount of EVs grows [25]. Drivers need affordable, convenient and compatible choices for charging at residential place or fleet facilities for fleet drivers. Charging stations at their workplace buildings and public locations will also encourage the market growth of EVs. Thus, the development of charging station is of the same significance as the development of electric-consuming vehicles.

Some of the chargers are installed at residential places using the domestic supplies; some of the charging stations support faster charging at higher voltages and currents than are available from the domestic supplies; some charging stations are on-street facilities provided by electric utility companies. With the development of charging strategies, some new forms of charging stations have been introduced and implemented. The solar panel has been used in some charging stations to utilize photovoltaic energy for the chemical energy of the batteries (see Figure 2.4.1). Mobile charging stations have been introduced [24]. Some of the special charging stations provide one or a range of heavy duty or special connectors and/or charging without a physical connection using parking places equipped with inductive charging mats. The wireless charging methods are being investigated. A special form of a charging station is a battery swapping station. In those stations, the batteries are switched instead of charged which is a convenient and time-saving choice for the customers. This type of stations has already been applied in some cities around the world.

Figure 2.4.1 Charging Stations Supplied by Solar Panel

Safety is the primary reason that charging equipment and safety standards have progressed. There are numerous safety codes and standards related to charging stations. The rest of this part will introduce the background and history of the charging equipment and code development.

In 1991, the issues of EV charging began to be faced by people including equipment manufacturers, a national consortium of automakers, utilities, building officials and government officials. Applying a systems approach, the national consortium formed the National Electric Vehicle Infrastructure Working Council (IWC) and began parallel efforts for vehicle and charging equipment development. As a result of their efforts, the equipment and safety standards have been created, that bring on equipment which uses technology to deal with shock hazards and battery hydrogen off-gassing. These standards were recommended by IWC to other associations including the Institute of Electrical and Electronic Engineers (IEEE), the American National Standards Institute, Underwriters Laboratories (UL), the Society of Automotive Engineers (SAE), and the National Fire Protection Association (NFPA) [26].

To be more specifically,

- The SAE developed equipment standards that detail operational and architectural specifications for charger and vehicle components;
- The UL developed safety standards for listing of charging equipment;
- The NFPA adopted safety standards in the form of the 1996 NEC.

In 1994, the California Energy Commission started to work with IWC, California Building Officials and the State Fire Marshal to modify the 1996 NEC Article 625. It aimed to accommodate California specific issues and adopt it prior to California's normal triennial adoption schedule. As a result, a modified version of the 1996 NEC Article 625 became effective as the California Electrical Code's new Article 625 in June 1996 [26].

2.5 Distribution Transformer Impact of Distribution Resources Including EVs/PHEVs

In a previous PSERC project (T-34) [4, 5], the impact of EVs/PHEVs on the power grid was studied from different aspects. The conclusions were: a) the impact is beneficial in terms of environment, economy and reliability, in general, b) the impact can be more beneficial by implementing certain controls to assist the regulation of the power grid when needed, and c) a negative effect was identified regarding the service lifetime of distribution transformers. The unfavorable effect is manageable by properly designed control strategies. As a result, the benefits of EVs/PHEVs to the power grid can be maximized by properly designed control algorithms and possibly using additional devices such as smart appliances, intelligent control of charging cycles of EVs and PHEVs, intelligent control of air conditioning and heating loads. The implementation and management of these controls requires an infrastructure that continuously monitors the system operation from the transmission to the residential and commercial level which enables real time coordinated control of the various resources and the utilization of EVs and PHEVs s the loads in such a way that the power components are not overloaded, thus avoiding loss of life and at the same time provides load managements services to the utility. A brief description regarding the current energy management is provided next.

2.6 Energy Management System

In the heart of the power system, the control center, lays one of the most important and critical components, the energy management system. It is a combination of software and hardware, used by the system operators to monitor, control, and optimize the operation of the system. The functions of the energy management system are designed to increase the reliability of the power system. A historical prospective on the development of EMS is given in [22]. A traditional energy management system is illustrated in Figure 2.6.1. Data coming from the field though the SCADA system are used to perform state estimation. Results of the estimation are used to visualize, monitor, control, and optimize the operation of the power system. New operating points (commands) are sent back to the field through the SCADA system.

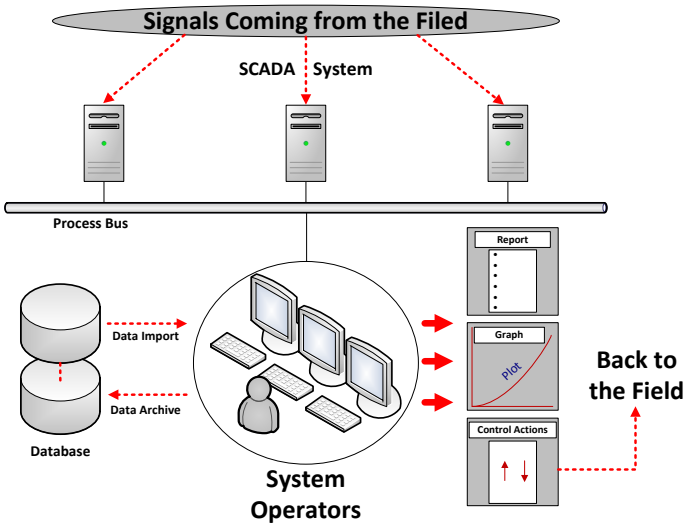

Figure 2.6.1 Traditional Energy Management System (EMS)

The increasing integration of renewable generation resources, energy storage systems such as batteries, and large deployment of EVs/PHEVs and residential/commercial smart appliances in the distribution system have increased the importance of optimization and coordinated control methodologies to take advantage of the new possibilities. As the number of controls increases, the legacy centralized approach may not be workable anymore. New decentralized approaches to the energy management system are necessary. The decentralized approach can be deployed to distribution systems and customer owned resources using a combination of data provided by advanced metering infrastructure (AMI), phasor measurement units (PMUs), digital relays, and traditional SCADA to extract in real time operating model of the system, optimize and control the system to achieve stated objectives. This process is extended to residential and commercial systems. For example, a house level energy management system or a commercial building energy management system is assumed to be part of the overall approach. We have focused on the house energy management system for which an overview is provided next.

2.6.1 House Energy Management System

The house energy management system is devoted to monitor, operate, optimize, and control the flow and use of energy though a single or a group of houses in an automated way and coordinate this operation with the electric power grid. The system, continuously, monitors the operation of various resources including EVs/PHEVs and domestic appliances and controls various loads in such a way to achieve specific objectives, such as peak load levelization, system loss minimization, provide VAR support and other objectives that may be depended on the operating conditions of the power grid at the time. One requirement that is placed on the design of this system is that it will not inconvenience customers. This translates to not overriding customer selected settings and controls of their electrical system, such as air-conditioning controls, required charge of EVs, etc. The system should be able to perform specific applications, such demand response (DR), load peak shaving, load shifting, and cost minimization, when requested. It should also co-optimize the operation

of the overall system when the power grid does not experience any unusual operating conditions that will require changes in the operating objectives.

EVs and PHEVs are the most important components of the electrical system of the house and enablers of the increased controllability of the house system. The home energy management system provides the means to maximize the benefits from EVs and PHEVs. It is described in Section 7.

3. Impacts of Vehicle Movement on State of Charge

3.1 Introduction

Since the energy shortage and environmental destruction have gradually attracted people's attention, Electric Vehicles (EVs) have been proposed and designed aiming at alleviating the mentioned problems. Compared with the traditional vehicles, EVs don't pollute the environment while running. Moreover, since they charge through the power grid, the widespread of EVs will help to centralize the pollution spots to the generation system, which is easier to control than the mobile pollutant as the case of traditional vehicles.

One of the important indices of EVs is their State of Charge (SOC) which is defined as "the percentage of the remained charge inside the battery to the full charge" [27]. Due to the limitation on the battery technique nowadays, the range of EVs are still quite limited. Other than the purpose to save energy, this makes another necessity for us to manage and estimate the SOC of EVs according to their movements.

There are basically two kinds of estimation of SOC according to EVs' movement, one is the estimation based on the parameters of battery measured in real time, and the other is based on the trip information and drivers' behavior.

However, standing from the aggregators' view or power grid's view, the real-time estimation on SOC may not be that helpful, and on the contrary, the statistical estimation and evaluation may be more helpful. That is because EVs will be able to have influence on the power grid only after they are aggregated into a large number considering the huge capacity difference between the power grid and a single EV. Moreover, load prediction will be needed during the operation and planning in the power system. And EVs will be able to participate into the electricity market with the introduction of aggregators. Therefore, the statistical estimation data of SOC will be more helpful in this purpose.

3.2 Current Research

This section investigates various feasible scenarios depending on various adoption rates of EVs, different charging methods, time-of-charge and driver's charging inclination. The driving cycles used in this section are based on Pang's previous research results. Do I need to also consider EV with fast charging, which will obviously lead to enormous impact? None of the papers have considered this. Since the energy shortage and the limitation on the battery capacity, there have been a lot of papers working on power management of EVs so as to increase the efficiency. For example, In [28], intelligent transportation system (ITS) is used to minimize the fuel use; in [29], dynamic programming is used to do the power management of EVs; in [30], deep charge-discharge cycle and battery size are reduced by power management, etc.

In order to apply the power management technique, the estimation of SOC in EVs is of vital importance. As to the first way of estimation on SOC, as mentioned in the introduction part, which is based on the real-time battery parameters, there have been several methods such as impedance spectroscopy method, open-circuit voltage method, Coulomb counting

method, electro-chemical modeling method, current integral method, etc., as mentioned in [27, 31-35]. [36] takes into account drivers' behavior while estimating the power consumption of EVs. [37, 38] simulate the SOC result based on the modeling of the battery and auxiliary unit considering the regenerative braking. Learning mechanism and fuzzy logic are utilized in [39, 40] to estimate the SOC in EVs. As to the other method which is mainly based on the trip information, [41, 42] describe the way to simulate SOC based on the driving cycle which provides the trip information in which Newton's second law is utilized.

As described in the introduction part, the statistical estimation on SOC should be of more help than the real time estimation. Therefore, the choice of driving cycle which provide the detail information of the trips becomes crucial. There have been some standard driving cycles which are mainly used for measuring the energy consumption or the emission of the vehicles [43], and ARTEMIS European driving cycles are designed in [44] for measuring pollutant emissions. Besides, there have been some particular driving cycles designed for different purposes: in [45], the a driving cycle is designed to test the battery of EV; a driving cycle for hybrid city bus is proposed in [46]; in [47], a particular driving cycle is developed for EV test in Hong Kong; a driving cycle for mail delivery use is described in [41]. However, most of those driving cycles are designed to be used as the baseline for some particular purpose and may not be able to reflect the real world needs from EV drivers. Hence, probability way is applied in [48] to evaluate the energy consumption of EVs. Stochastic Markov model adopted in [49] to simulate the SOC in real life in order to propose a vehicle mission model. Besides, statistical ways are also developed in [50, 51] based on the real vehicle data.

3.3 Model on Energy Consumption of Electric Vehicle

The second method which is based on the trip information as described in the introduction is adopted in this report in order to simulate the relationship between vehicle movement and energy consumption. The questions lie in 1) how to analyze the energy consumption based on the trip information, and 2) how to generate driving cycles for test.

Newton's second law will be applied, and therefore, a model should be established to conduct the force analysis on the vehicle during its trip. As shown in Figure 3.3.1, the inclination of the ground is also considered during the analysis. The acceleration of the vehicle is decided by the forced applied on it. There are mainly four kinds of forces as donated in Figure 3.3.1, i.e. friction, gravity, propulsion and supporting force from the ground. The friction *f* which prevents the vehicle from going ahead can be caused by the friction between tires of the vehicle and the ground, the wind blow against the vehicle, etc. The F in the figure is the propulsion force of that car which can be provided by electricity in the battery for an EV.

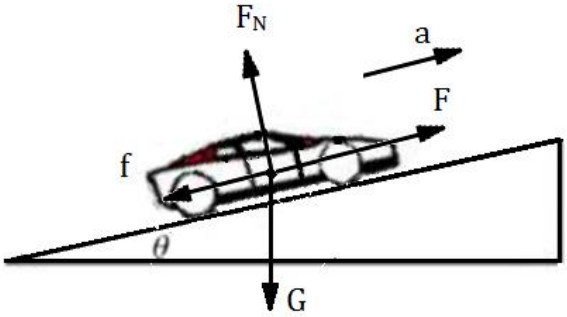

Figure 3.3.1 The Force Analysis of Vehicle on the Slope

From Newton's law, we can model the system in the following equations:

$$f = F_D + F_F + F_G \tag{3.1}$$

$$F_D = \frac{1}{2}\rho A_f C_D \left(v + v_w\right)^2 \tag{3.2}$$

$$F_F = \left(C_r + C_v v\right) mg\cos\theta \tag{3.3}$$

$$F_G = mg\sin\theta \tag{3.4}$$

Where ρ is the air density, A_f is the vehicle frontal area, C_D is the aerodynamic drag coefficient, C_r is the constant rolling friction coefficient, C_v is the viscous rolling friction coefficient, v_w is the head-wind speed, m is the mass of the vehicle, g is the gravitational constant, and θ is the grade angle of the road. Then the propulsion force F can be expressed as follows according to the Newton's second law:

$$F = m\frac{dv}{dt} + F_D + F_F + F_G \tag{3.5}$$

The power of the propulsion force is:

$$p = Fv = (m\frac{dv}{dt} + F_D + F_F + F_G) \tag{3.6}$$

The power of the propulsion force comes from battery of the electric vehicle, and due to the loss such as mechanical friction inside the vehicle, the energy of the electricity cannot entirely transform into the energy to make the vehicle move. And we suppose that the efficiency of this transformation is η, then the energy consumption of a vehicle can be expressed as:

$$E = \frac{1}{\eta}\int_0^t \left(m\frac{dv}{dt} + F_D + F_F + F_G \right) v dt \tag{3.7}$$

From the equation (3.7), we can be able to analyze the energy consumption based on the trip information.

One of the advantages of EV is that if designed properly, the kinetic energy of the vehicle can be stored back to the battery when braking so as to save energy. Regenerative braking is a process in which the kinetic energy of the vehicle can be partially recuperated. During this period, the battery can be discharged and thus is a way to save energy. Likewise, the kinetic energy can neither be totally discharged into the battery, and we suppose the efficiency here to be ξ. Then the energy regained during regenerative braking can be expressed as:

$$E_R = \xi \left(E_{b1} - E_{b2} \right) \tag{3.8}$$

E_R - the energy to be regained; E_{b1} - the kinetic energy of the vehicle at the beginning of the regenerative braking; E_{b2} - the kinetic energy of the vehicle at the end of the regenerative braking.

3.4 Driving Cycle Establishment

As described in the introduction, new driving cycles should be generated which can represent the movement of vehicles in the daily life for the purpose of finding the relationship between the movement of electric vehicles in daily life and their SOC condition. Usually, a lot of stochastic factors will be included into daily driving, for example, drivers' behavior, the traffic condition, the weather condition, etc. which should be taken into account during the establishment of driving cycle. In this report, the probability way will be adopted in order to deal with the stochastic factors.

The driving cycle generator developed here is based on normal distributions. The driving cycle is generated by a succession of driving phases. Each driving phase is defined by its duration in seconds and its final velocity, while the initial velocity is defined by the former step. In order to facilitate the creation of the driving cycle some assumptions have been made. The main assumptions are: a) acceleration and deceleration values are constant; and b) the vehicle is not doing any backtracking.

The working principle of the driving cycle generator is shown in Figure 3.4.1. During the process of generating the driving cycle, stochastic factors which are caused by drivers' behavior, the condition of the traffic and so on are taken into account. As a result, the speed of vehicles running on the road cannot be constant, and the variance of speed always exists due to the some stochastic factors.

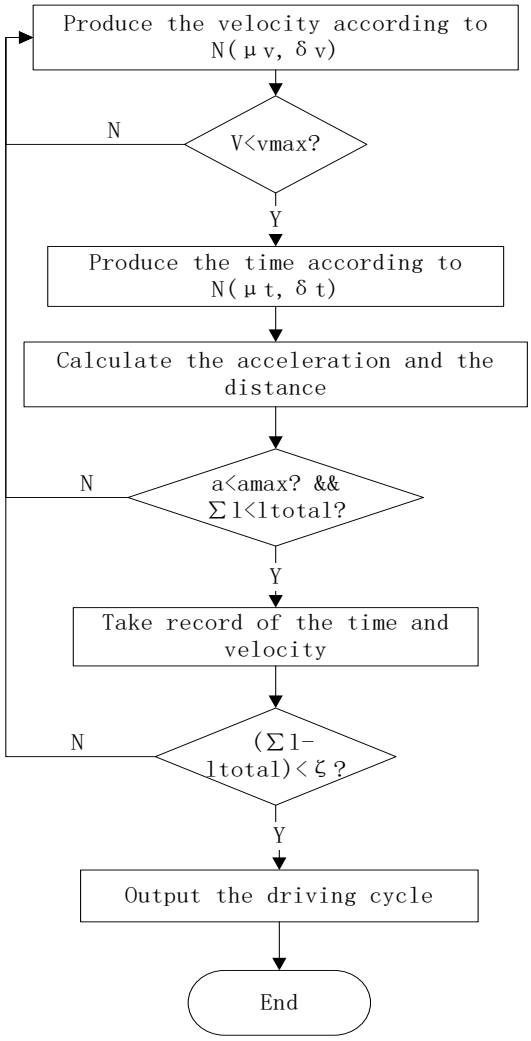

Figure 3.4.1 Working Principle of Driving Cycle Generator

3.5 The Relationship between the Vehicle's Movement and SOC

There are a lot of factors that can affect the energy consumption of electric vehicles such as velocity, the stop times, wind speed, whether or not have regenerative brake, etc. and their effect on SOC will be studied below.

3.5.1 Mean Velocity

In order to study how the mean velocity of the vehicle affects the SOC, other factors are set to be the same. Three mean velocities are selected for test, 9.7m/s, 16m/s and 20m/s while the variance of the velocity is 8.3. Meanwhile, the maximum acceleration is 2.8m/s^2. And the scheduled distance is 10000m with no stop and we suppose that the vehicle is fully charged at the beginning of the travel. Other parameters are shown in Table 3.1.

Table 3.1 The Parameters of Vehicle Model-1

ρ	A_f	C_D	C_r	C_v	v_w	m	g	θ	η
1.28kg/m^3	3m^2	0.31	10^{-2}N	10^{-4}Ns/m	0m/s	1800kg	9.81m/s^2	0	0.8

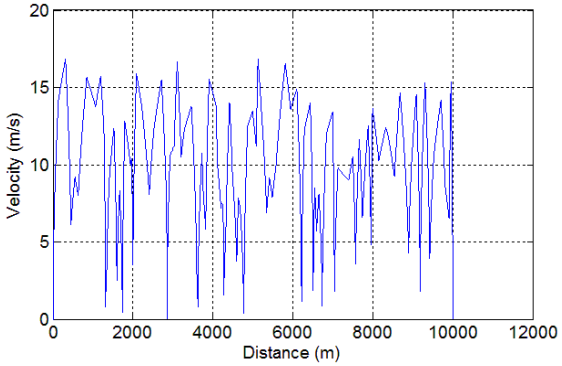

Figure 3.5.1 Velocity – Distance Diagram (Mean Velocity = 9.7m/s)

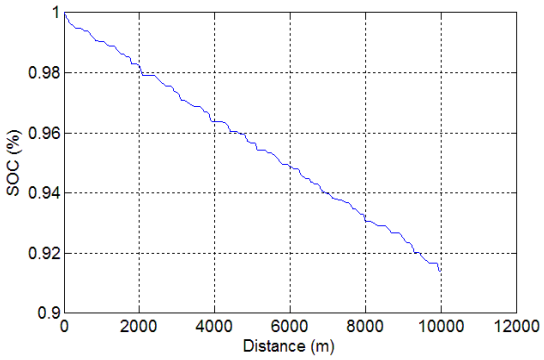

Figure 3.5.2 SOC – Distance Diagram (Mean Velocity = 9.7m/s)

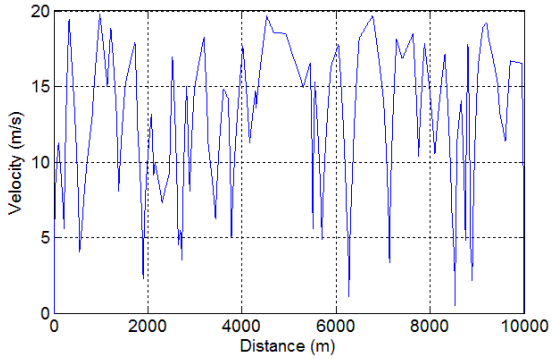

Figure 3.5.3 Velocity – Distance Diagram (Mean Velocity = 16m/s)

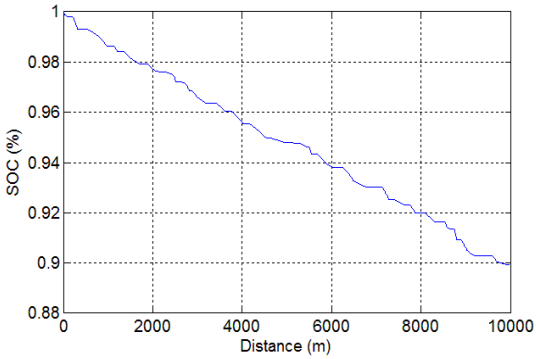

Figure 3.5.4 SOC – Distance Diagram (Mean Velocity = 16m/s)

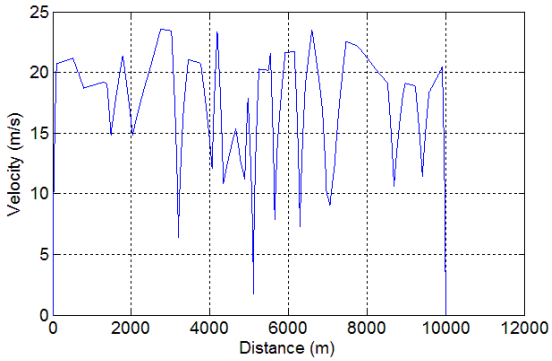

Figure 3.5.5 Velocity – Distance Diagram (Mean Velocity = 20m/s)

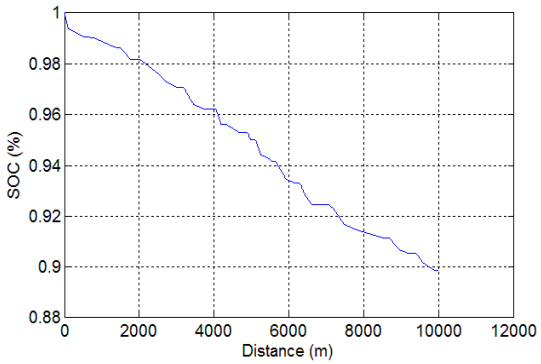

Figure 3.5.6 SOC – Distance Diagram (Mean Velocity = 20m/s)

The final SOC in the above three conditions are listed in Table 3.2.

Table 3.2 The Final SOC in Three Conditions

Mean velocity	**9.7m/s**	**16m/s**	**20m/s**
Final SOC	0.9139	0.8993	0.8986

From the figures and the data listed in Table 3.2, we find that more electricity energy will be consumed if the mean velocity of the vehicle is increased. However, we find that the difference between the final SOC in 16m/s case and that in 20m/s case is very small, this is because that the velocity in 16m/s case changes more frequently than that in 20m/s case which cause energy consumption.

3.5.2 Standard Deviation of the Speed

The impact of standard deviation on the energy consumption is studied in this section in which 16m/s is selected to be the mean velocity and three different standard deviation of velocity are applied: 8.3, 10 and 12. Meanwhile, the maximum acceleration is 2.8m/s^2. And the scheduled distance is 10000m with no stop and we suppose that the vehicle is fully charged at the beginning of the travel. Other parameters are shown in Table 3.1.

Figure 3.5.3 and 3.5.4 are the ones that describe the velocity and SOC condition in the case when the mean velocity is selected to be 16m/s and standard deviation is selected to be 8.3.

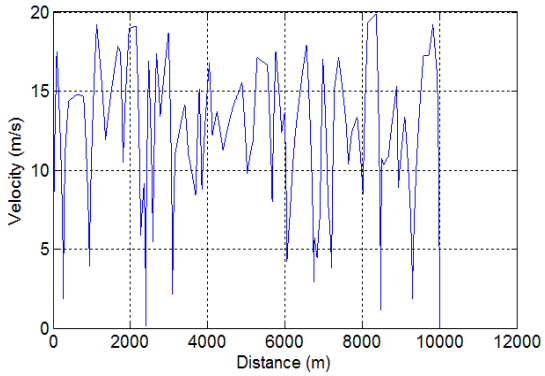

Figure 3.5.7 Velocity – Distance Diagram (Mean Velocity = 16m/s, Standard Deviation = 10)

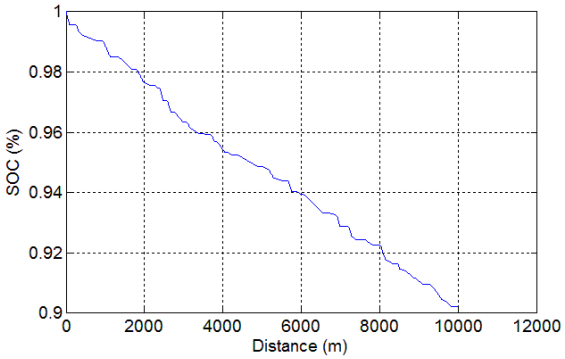

Figure 3.5.8 SOC – Distance Diagram (Mean Velocity = 16m/s, Standard Deviation = 10)

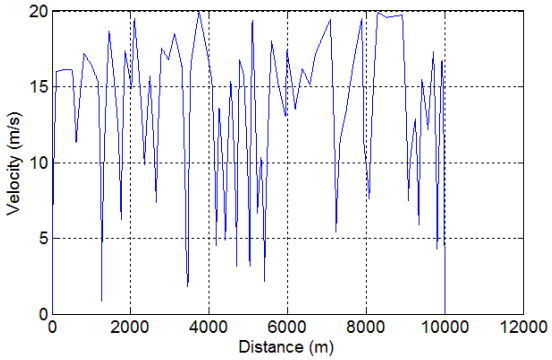

Figure 3.5.9 Velocity – Distance Diagram (Mean Velocity = 16m/s, Standard Deviation = 12)

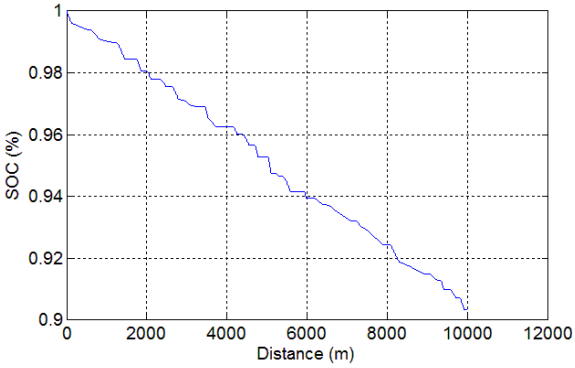

Figure 3.5.10 SOC – Distance Diagram (Mean Velocity = 16m/s, Standard Deviation = 12)

The final SOC in the above three conditions are listed in Table 3.3.

Table 3.3 The Final SOC in Three Conditions

Standard Deviation	8.3	10	12
Final SOC	0.8993	0.9023	0.9034

From the result, the final SOC in the above three conditions are quite close to each other. We can see that the standard deviation does not affect the energy consumption of electric vehicles a lot. The reason why larger standard deviation causes less energy consumption is that speed of vehicle changes less frequently in that case due to the stochastic factor. Next, we will study the impact of change of speed on the SOC.

3.5.3 Speed Variation Frequency

The traffic condition influences speed of vehicles a lot, for example, the speed of vehicles running on the high way is much more stable than those running on the roads in cities where the traffic tends to be busy and there are traffic lights everywhere. In order to study the effect of speed-changing frequency on the energy consumption of vehicles, average time period between the changes of speed is selected to be 10s, 15s, 20s, 30s and 40s. Meanwhile, the mean velocity is set to be 16m/s, while the standard deviation is 10. The maximum acceleration is 2.8m/s^2. And the scheduled distance is 10000m with no stop and we suppose that the vehicle is fully charged at the beginning of the travel. Other parameters are shown in Table 3.1.

The case with average time period of 10s is shown in Figure 3.5.7 and 3.5.8.

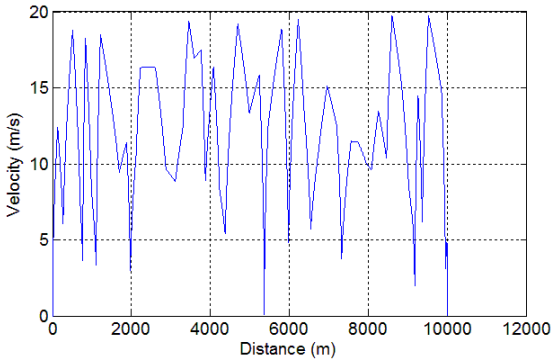

Figure 3.5.11 Velocity – Distance Diagram (Mean Velocity = 16m/s, Time Period = 15)

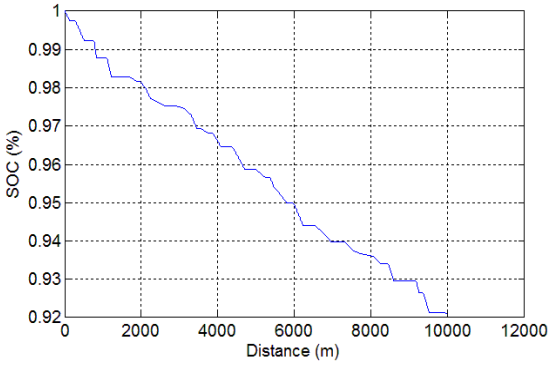

Figure 3.5.12 SOC – Distance Diagram (Mean Velocity = 16m/s, Time Period = 15)

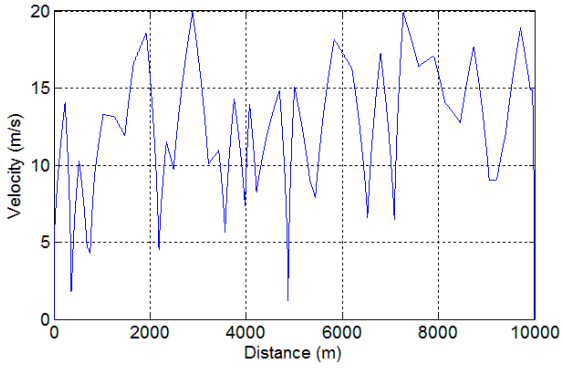

Figure 3.5.13 Velocity – Distance Diagram (Mean Velocity = 16m/s, Time Period = 20)

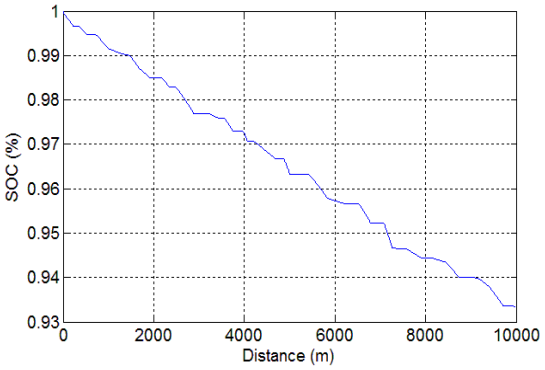

Figure 3.5.14 SOC – Distance Diagram (Mean Velocity = 16m/s, Time Period = 20)

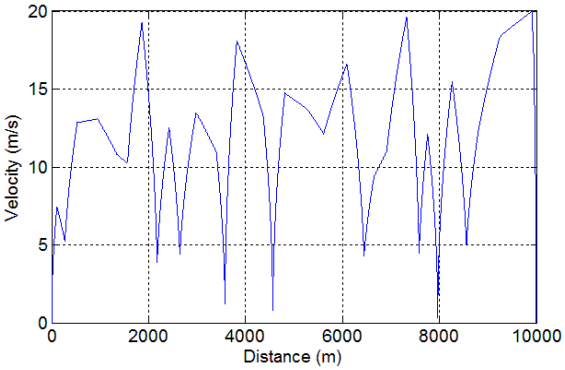

Figure 3.5.15 Velocity – Distance Diagram (Mean Velocity = 16m/s, Time Period = 30)

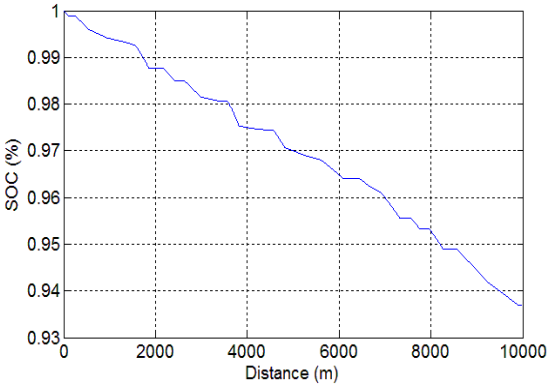

Figure 3.5.16 SOC – Distance Diagram (Mean Velocity = 16m/s, Time Period = 30)

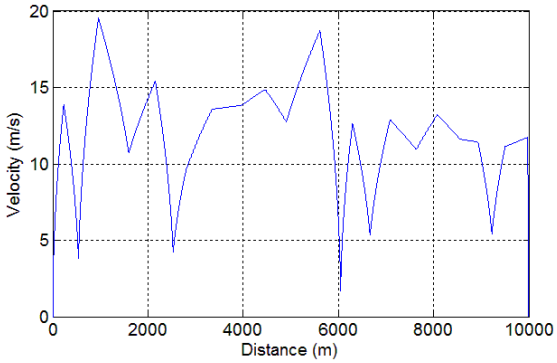

Figure 3.5.17 Velocity – Distance Diagram (Mean Velocity = 16m/s, Time Period = 40)

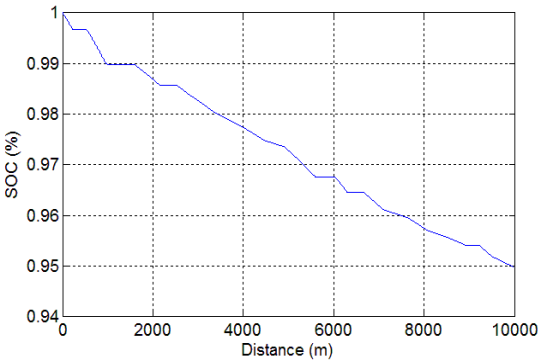

Figure 3.5.18 SOC – Distance Diagram (Mean Velocity = 16m/s, Time Period = 40)

The final SOC in the above five scenarios are listed in Table 3.4.

Table 3.4 The Final SOC in Five Scenarios

Time period	10s	15s	20s	30s	40s
Final SOC	0.9023	0.921	0.9335	0.9368	0.9499

From the figures, we can observe that the frequency of the speed change decreases with the increase of the time period between the changes of the speed. And the result in Table 3.4 shows that the frequency of the speed change has greater impact on the energy consumption of electric vehicles compared with the factors discussed above. And the smoother the vehicles run, the less energy they will consume.

3.5.4 Regenerative Brake

During the period of regenerative brake, the kinetic energy of vehicles can partially be converted into electricity energy and stored back into the battery, which can help save energy. During the analysis of the effect of regenerative brake on the energy consumption, the five scenarios in the former section are studied again to calculate the SOC with regenerative brake. The efficiency ξ of the conversion from kinetic energy to electricity energy is chosen to be 0.06.

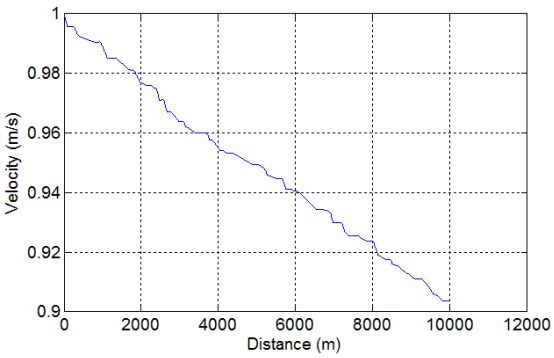

Figure 3.5.19 SOC – Distance Diagram (With Regenerative Brake, Time Period = 10s)

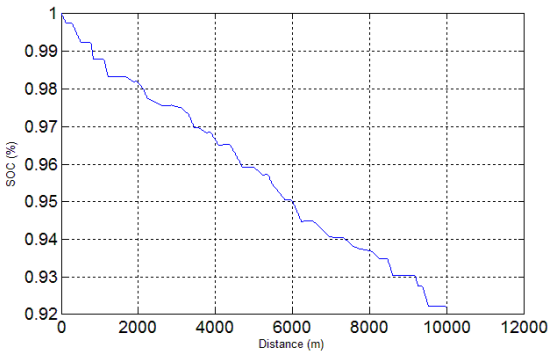

Figure 3.5.20 SOC – Distance Diagram (With Regenerative Brake, Time Period = 15s)

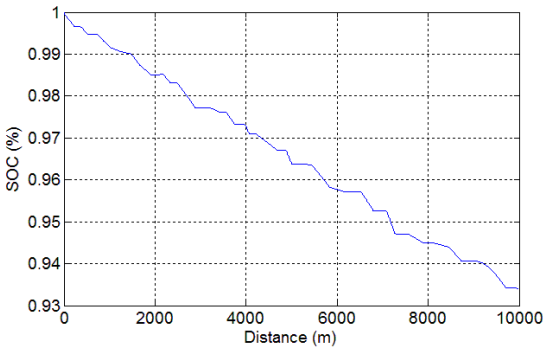

Figure 3.5.21 SOC – Distance Diagram (With Regenerative Brake, Time Period = 20s)

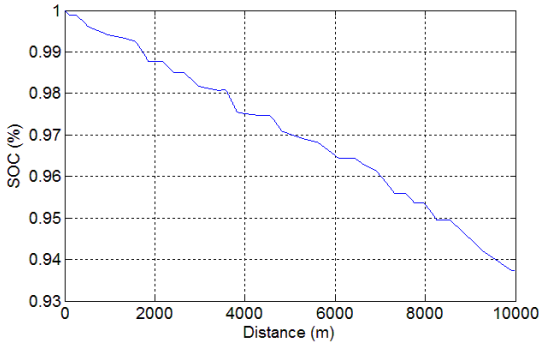

Figure 3.5.22 SOC – Distance Diagram (With Regenerative Brake, Time Period = 30s)

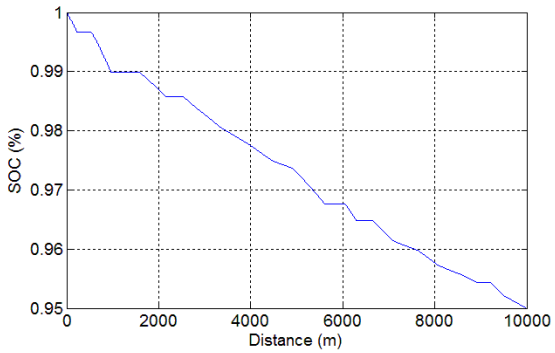

Figure 3.5.23 SOC – Distance Diagram (With Regenerative Brake, Time Period = 40s)

The final SOC in the above five scenarios with and without regenerative brake are listed in Table 3.5.

Table 3.5 The Final SOC in Five Scenarios with Regenerative Brake

Time period	10s	15s	20s	30s	40s
Final SOC without regenerative brake	0.9023	0.921	0.9335	0.9368	0.9499
Final SOC with regenerative brake	0.9038	0.922	0.9341	0.9374	0.9502
The difference	0.0015	0.001	0.0006	0.0006	0.0003

From the result we can see that the regenerative brake can to some extend help save energy, which cannot be achieved by the conventional vehicles. The amount of energy saved through regenerative brake is small because the efficiency here is just 0.06. However, with the development of the technology, we can believe that the energy to be saved through regenerative brake will become considerable.

Another thing that we can observe from the result is that, the more frequently the vehicle changes its speed, the more energy will be able to be saved through regenerative brake. This result implies that for those vehicles which frequently change their speed, for example, those running in the city, it is more necessary to install the regenerative brake.

3.5.5 Stop Times

The stop frequency will also affect the energy consumption of electric vehicles. In this section, mean velocity of the vehicle is chosen to be 9.7m/s, 16m/s and 20m/s respectively, and the standard deviation of velocity is selected to be 8.3. And the scheduled distance is 10000m with no stop, 5 stops, 10 stops, 15 stops, 20 stops and 25 stops. We suppose that the vehicle is fully charged at the beginning of the travel. Other parameters are shown in Table 3.1.

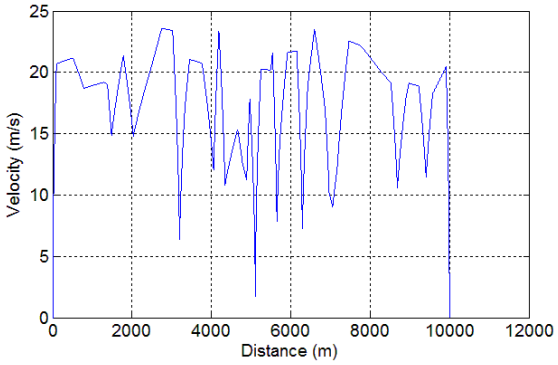

Figure 3.5.24 Velocity – Distance Diagram (No Stop, Mean Velocity=20m/s)

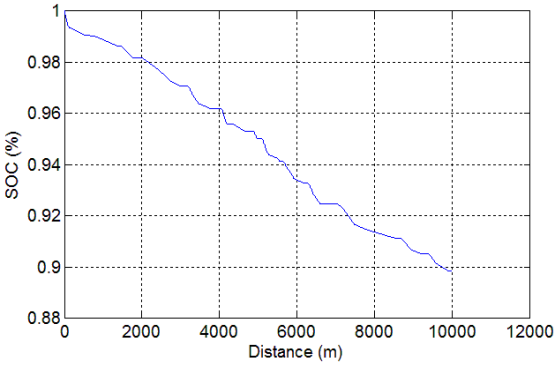

Figure 3.5.25 SOC – Distance Diagram (No Stop, Mean Velocity=20m/s)

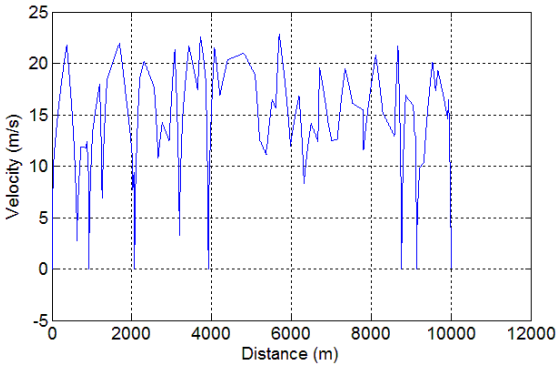

Figure 3.5.26 Velocity – Distance Diagram (5 Stops, Mean Velocity=20m/s)

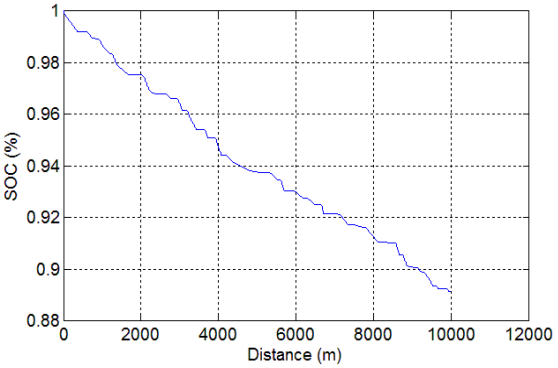

Figure 3.5.27 SOC – Distance Diagram (5 Stops, Mean Velocity=20m/s)

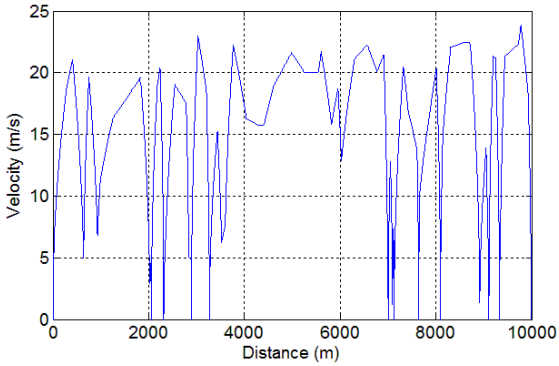

Figure 3.5.28 Velocity – Distance Diagram (10 Stops, Mean Velocity=20m/s)

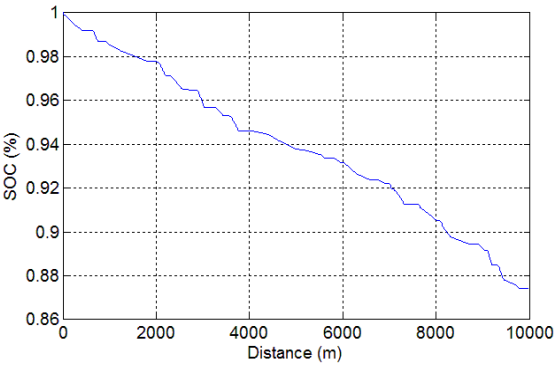

Figure 3.5.29 SOC – Distance Diagram (10 Stops, Mean Velocity=20m/s)

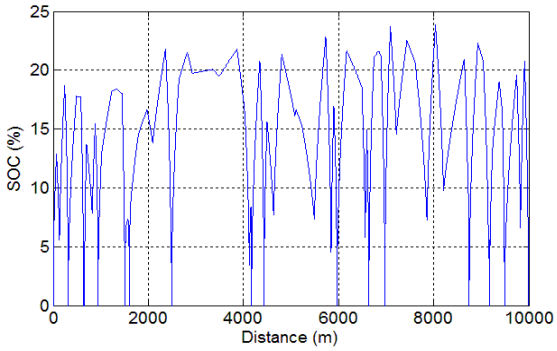

Figure 3.5.30 Velocity – Distance Diagram (15 Stops, Mean Velocity=20m/s)

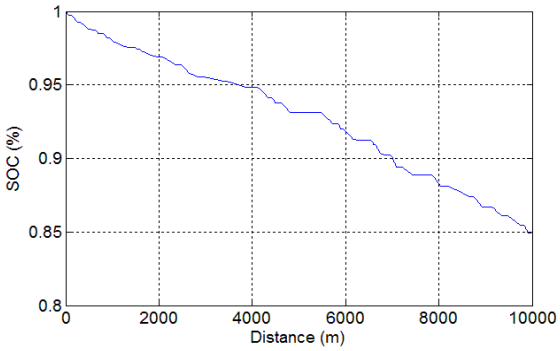

Figure 3.5.31 SOC – Distance Diagram (15 Stops, Mean Velocity=20m/s)

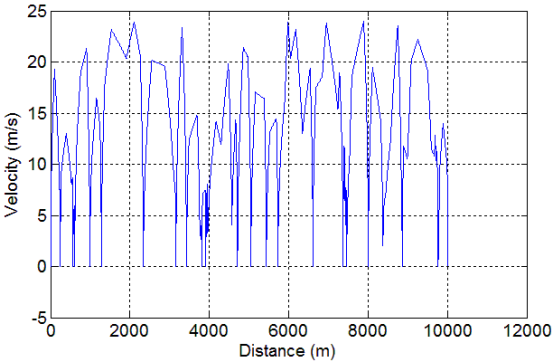

Figure 3.5.32 Velocity – Distance Diagram (20 Stops, Mean Velocity=20m/s)

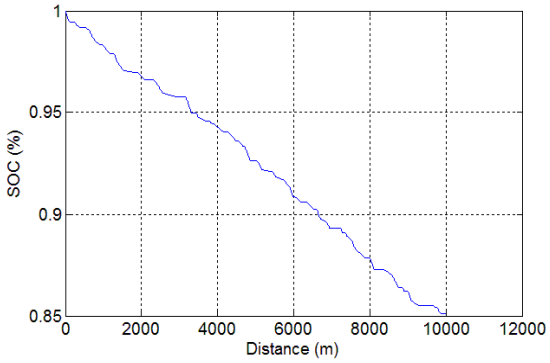

Figure 3.5.33 SOC – Distance Diagram (20 Stops, Mean Velocity=20m/s)

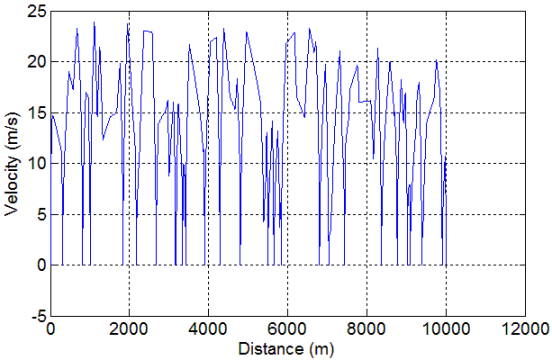

Figure 3.5.34 Velocity – Distance Diagram (25 Stops, Mean Velocity=20m/s)

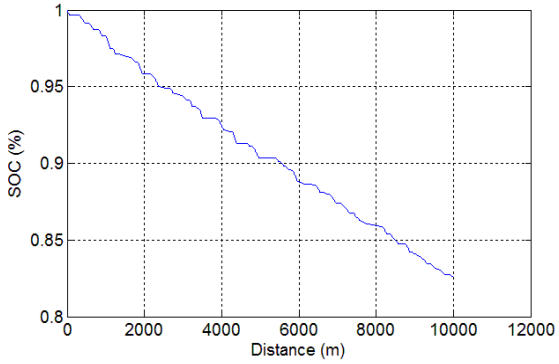

Figure 3.5.35 SOC – Distance Diagram (25 Stops, Mean Velocity=20m/s)

The final SOC in the above six scenarios with different mean velocities are listed in Table 3.6.

Table 3.6 The Final SOC in Six Scenarios with Different Velocities

Stop times	0	5	10	15	20	25
9.7m/s	0.9139	0.9099	0.9041	0.8976	0.9075	0.9001
16m/s	0.8993	0.9055	0.8935	0.881	0.882	0.876
20m/s	0.8986	0.8916	0.8744	0.8491	0.851	0.826

Two main observations can be obtained from the results listed in Table 3.6: 1) higher speed will result in greater energy consumption and at the same time, and the stop frequency will have greater impact on energy consumption during higher speed; 2) the energy consumption augments with the incensement of the stop times, however when the stop frequency increase to 20 times, the energy consumption does not increase as it does in the smaller stop frequency which is caused by the limit on the maximum acceleration and velocity of the vehicle.

3.5.6 Inclination of Ground

From Figure 3.1, we can tell that the inclination of the ground will have impact on vehicle's energy consumption; this is because the bigger θ is, the bigger F will be to achieve the same acceleration. Here the velocity is set to be 9.7m/s, and standard deviation to be 8.3. θ is selected to be 0, 10 and 20 degrees. The scheduled distance is 10000m with no stop and we suppose that the vehicle is fully charged at the beginning of the travel. Other parameters are shown in Table 3.7.

Table 3.7 The Parameters of Vehicle Model-2

ρ	A_f	C_D	C_r	C_v	v_w	m	g	η
1.28kg/m^3	3m^2	0.31	10^{-2}N	10^{-4}Ns/m	0m/s	1800kg	9.81m/s^2	0.8

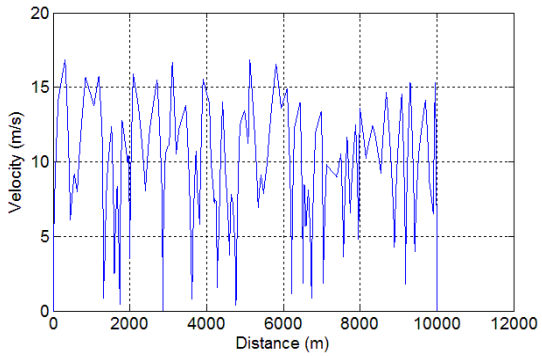

Figure 3.5.36 Velocity – Distance Diagram (No Stop, Mean Velocity=9.7m/s)

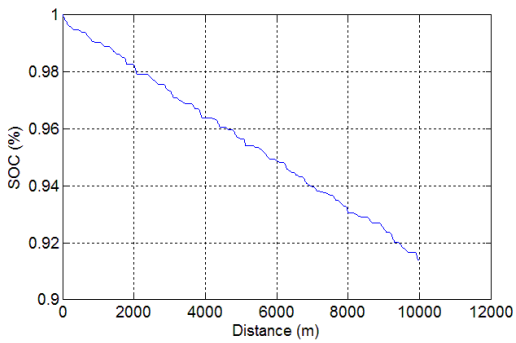

Figure 3.5.37 SOC – Distance Diagram (No Stop, Mean Velocity=9.7m/s, θ=0)

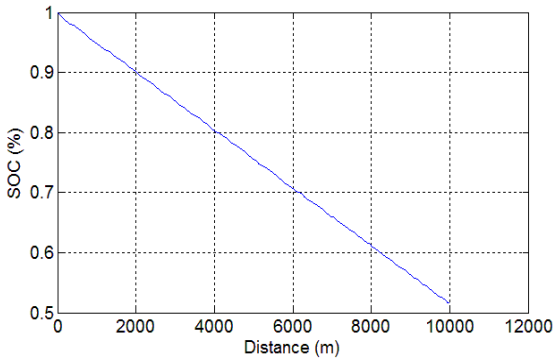

Figure 3.5.38 SOC – Distance Diagram (No Stop, Mean Velocity=9.7m/s, θ=10)

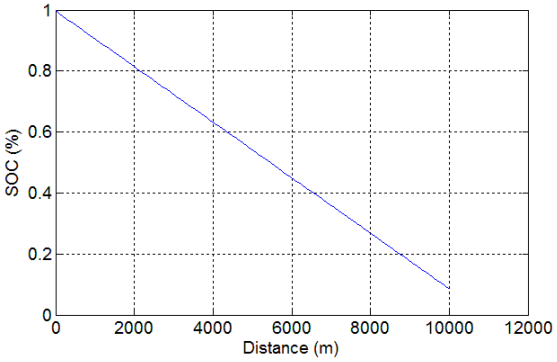

Figure 3.5.39 SOC – Distance Diagram (No Stop, Mean Velocity=9.7m/s, θ=20)

The final SOC in the above three scenarios are listed in Table 3.8.

Table 3.8 The Final SOC with Different Inclination

$\boldsymbol{\theta}$	0	10	20
SOC	0.9139	0.516	0.0881

From the result, we can observe that the inclination of the ground will have huge impact on the energy consumption of the vehicles. When the θ increase to 20 degrees, the vehicle has to consume almost all energy it has to finish the travel of 10000m.

3.5.7 Wind Speed

The wind can either be a propulsion force when the direction of the wind is the same as that of the vehicle, and be a resistance force to the vehicle vice versa. Here the velocity is set to be 9.7m/s, and standard deviation to be 8.3. v_w is selected to be 0, 2m/s, 5m/s, 10m/s, -2m/s, -5m/s and -10m/s respectively. The scheduled distance is 10000m with no stop and

we suppose that the vehicle is fully charged at the beginning of the travel. Other parameters are shown in Table 3.9.

Table 3.9 The Parameters of Vehicle Model-3

ρ	A_f	C_D	C_r	C_v	θ	m	g	η
1.28kg/m^3	3m^2	0.31	10^{-2}N	10^{-4}Ns/m	0m/s	1800kg	9.81m/s^2	0.8

The driving cycle of the vehicle is shown in Figure 3.5.36, and the results of SOC in different wind speed are illustrated in the following figures.

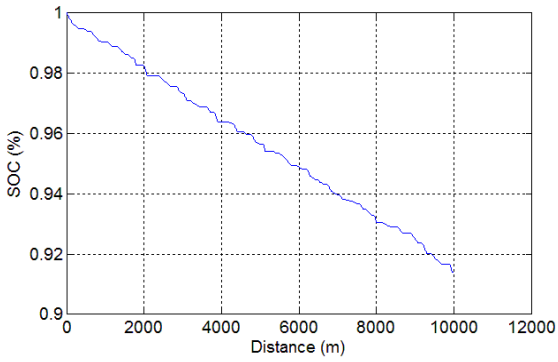

Figure 3.5.40 SOC – Distance Diagram (No Stop, Mean Velocity=9.7m/s, v_w =0)

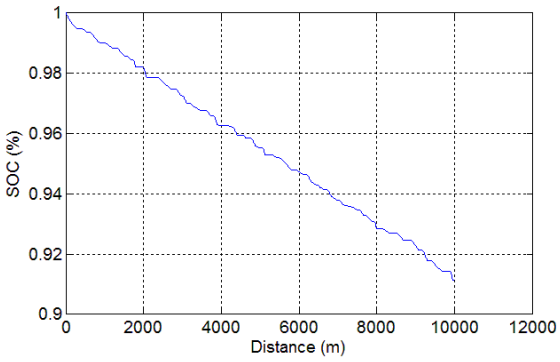

Figure 3.5.41 SOC – Distance Diagram (No Stop, Mean Velocity=9.7m/s, v_w =2m/s)

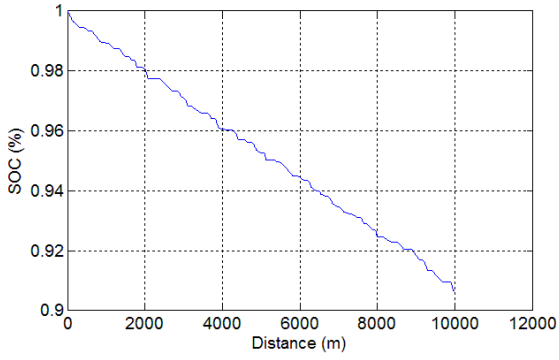

Figure 3.5.42 SOC – Distance Diagram (No Stop, Mean Velocity=9.7m/s, v_w =5m/s)

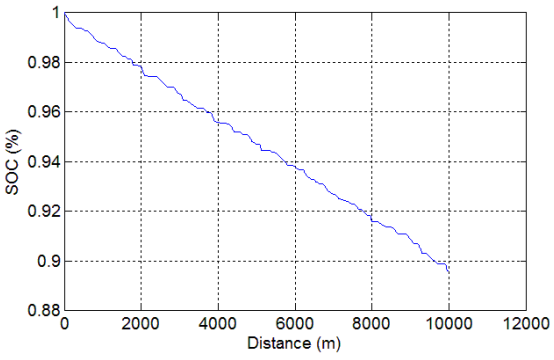

Figure 3.5.43 SOC – Distance Diagram (No Stop, Mean Velocity=9.7m/s, v_w =10m/s)

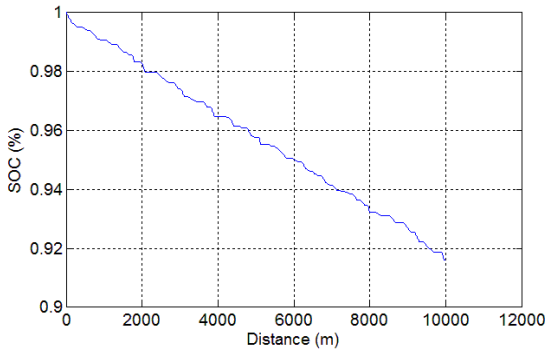

Figure 3.5.44 SOC – Distance Diagram (No Stop, Mean Velocity=9.7m/s, v_w =-2m/s)

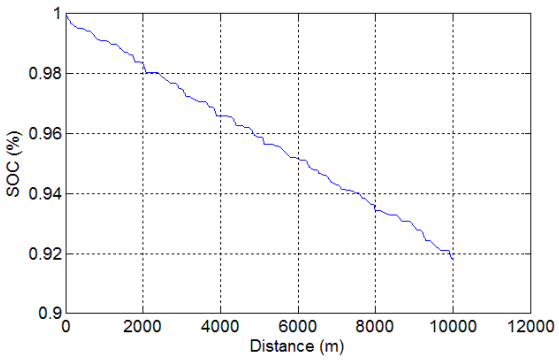

Figure 3.5.45 SOC – Distance Diagram (No Stop, Mean Velocity=9.7m/s, v_w =-5m/s)

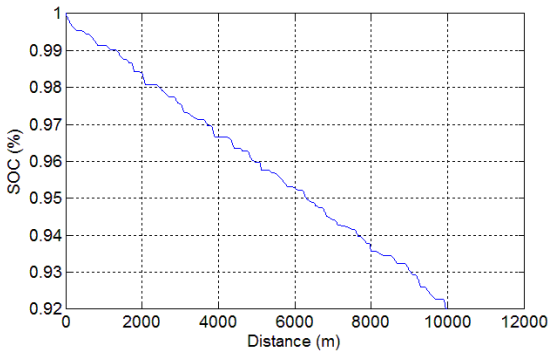

Figure 3.5.46 SOC – Distance Diagram (No Stop, Mean Velocity=9.7m/s, v_w =-10m/s)

The final SOC in the above seven scenarios are listed in Table 3.10.

Table 3.10 The Final SOC with Different Wind Speed

v_w	0	2m/s	5m/s	10m/s	-2m/s	-5m/s	-10m/s
SOC	0.9139	0.9114	0.9068	0.8961	0.916	0.9184	0.9201

Form the results shown above we can observe that the wind speed impacts the energy consumption of electric vehicle like other factors.

3.5.8 Conclusion

From the analysis above, we know that there are many factors that will affect the energy consumption of EVs.

1. The velocity of EVs including the mean velocity and the standard deviation of it

can influence the energy consumption, and the higher velocity or standard deviation, the more energy EVs will consume during the travel. But compared with other factors, the influence of velocity is the least one.

2. The wind speed is the second least factor that influences the SOC status. This implies that bad weather condition can lead to more energy consumption.
3. The frequency of changing speed and the stop times of EVs during travel are the two factors that influence the SOC status more than the factors listed in 1 and 2, but less than other factors mentioned above. From above, we can tell that the more frequently EVs change their speed or the more they stop during travel, the more energy they tend to consume. But be aware that, because of the limit of the acceleration of EVs, the energy consumption will not always increase when the stop times reach some point. This conclusion implies that the traffic condition will have effect on EVs' energy consumption. For example, when an EV is running on a busy downtown road, it may probably has to change its speed more frequently or stop more often because of the traffic lights, then it may result in a larger energy consumption than an EV running on a highway with light traffic and few traffic light although higher mean velocity.
4. The inclination of the ground is the very factor that has the greatest effect on energy consumption. This is because the vehicle has to overcome its own weight which is generally huge in order to get to a place with higher altitude, and thus leading to high energy consumption.

One of the differences between EVs and conventional vehicles is that EVs can have regenerative braking which can help save energy to some extent. The amount of energy saving is not quite impressive in the above analysis because the efficiency ξ of the conversion from kinetic energy to electricity energy is just 0.06. But with the development of technology and the increase of the efficiency, the regenerative braking can help saving considerable energy in the future especially for those EVs running on the downtown area with frequent speed change.

3.6 Optimization Analysis of Vehicle Movement in regard to SOC

Here comes a question that what is the most cost-effective way to go from one place to the destination. Because of the limit of the battery of EVs, people may want to save energy before they can get to the charging station and obtain energy for their EVs.

In order to analyze this problem, equation (3.7) will be used here. We can see that η is just a constant and does not matter in the following analysis, so we neglect this parameter here and then the equation becomes:

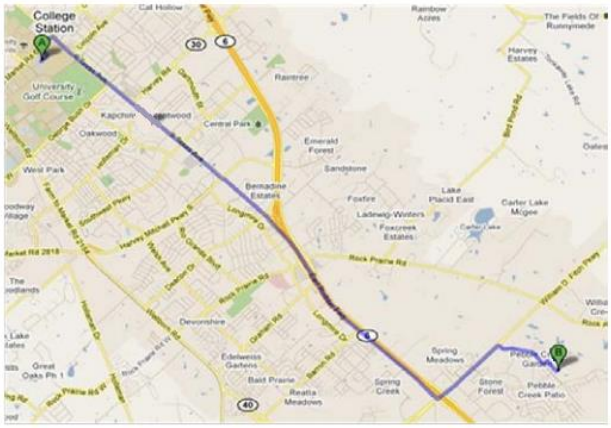

Figure 3.6.1 Problem Illustration

$$E = \int_0^t \left(m\left(\frac{dv}{dt}\right) + F_D + F_F + F_G \right) * v * dt \tag{3.9}$$

To simplify the equations, we assume

$$A = \frac{1}{2} * \rho * A_f * C_D \tag{3.10}$$

$$B = C_r * \ m * g \tag{3.11}$$

$$C = C_v * m * g \tag{3.12}$$

Thus, Equation (3.9) can be simplified as

$$E = \int_0^t \left(m\left(\frac{dv}{dt}\right) + A * (v + v_m)^2 + (B + C * v) * \cos\theta + m * g * \sin\theta \right) * v * dt \tag{3.13}$$

We choose the parameters shown in Table 3.11:

Table 3.11 Illustration of Choice of Parameters

$\boldsymbol{\rho}$	$\boldsymbol{A_f}$	$\boldsymbol{C_D}$	$\boldsymbol{C_r}$	$\boldsymbol{C_v}$	$\boldsymbol{v_w}$	**m**	**g**	$\boldsymbol{\theta}$
1.28 kg/m^3	2.74 m^2	0.29	0.012 N	10^{-4} N ·s/m	0 m/s	1520+70 (driver)kg	9.8 m/s^2	0

Then A in (equation 3.10) is calculated as 0.5085, B in equation (3.11) as 186.984, and C in equation (3.12) as 1.5582.

3.6.1 Energy Consumption Analysis

3.6.1.1 Driving at Constant Velocity

When the electric vehicle is moving a distance of s including acceleration, constant velocity v, and deceleration periods, the energy consumption during constant velocity period can be calculated as:

$$E_2 = \int_0^t \left(A * v^2 + (B + C * v)\right) * v * dt = \int_0^{(s-\frac{v^2}{a})/v} (A * v^3 + B * v + C * v^2) * dt$$

$$= (A * v^2 + B + C * v) * \left(s - \frac{v^2}{a}\right) \quad (3.14)$$

3.6.1.2 During Acceleration Period

Assume that the acceleration rate is constant as a and the objective speed is v, then the energy consumption during the acceleration period is:

$$E_1 = \int_0^{v/a} \left(m * a + A * (a * t)^2 + \left(B + C * (a * t)\right)\right) * (a * t) * dt$$

$$= \frac{1}{2}mv^2 + \frac{Av^4}{4a} + \frac{Bv^2}{2a} + \frac{Cv^3}{3a} \quad (3.15)$$

3.6.1.3 During Deceleration/ Break Period

Assume that the deceleration rate is constant as$-a$ and the starting speed is v, then the energy consumption during the deceleration period is:

$$E_3 = 0 \quad (3.16)$$

If the regenerative energy is taken into consideration, it is assumed that some of the energy supplied by the battery to speed up is recovered by charging the battery when braking. Let ξ be the fraction of the kinetic energy that is stored in the battery when decelerating the electric vehicle. Then the energy consumption during the deceleration period is:

$$\mathrm{E}_3' = \frac{1}{2}\mathrm{mv}^2 * (-\xi) \quad (3.16)'$$

While v=20 m/s, the ratio of the energy loss because of aerodynamic drag, rolling friction, road grade force, etc. and the stored kinetic energy is:

$$\frac{\frac{\mathrm{Av}^4}{4\mathrm{a}} + \frac{\mathrm{Bv}^2}{2\mathrm{a}} + \frac{\mathrm{Cv}^3}{3\mathrm{a}}}{\frac{1}{2}\mathrm{mv}^2} \approx 0.0584$$

Thus, if electric vehicle technology permits, the highest efficiency of regenerative energy ξ can be as high as 94.16%.

3.6.2 Case 1: Driving in a Distance without Stop

The total energy consumption estimation E should be the addition of three periods (Equation (3.14)-(3.16)).

$$E = E_1 + E_2 + E_3 \tag{3.17}$$

$$E' = E_1 + E_2 + E_3' \tag{3.17}'$$

$$E_1 + E_3 = \frac{1}{2}mv^2 + \frac{Av^4}{4a} + \frac{Bv^2}{2a} + \frac{Cv^3}{3a} \tag{3.18}$$

$$E_1 + E_3' = \frac{1}{2}mv^2 * (1 - \xi) + \frac{Av^4}{4a} + \frac{Bv^2}{2a} + \frac{Cv^3}{3a} \tag{3.18}'$$

$$E_2 = (A * v^2 + B + C * v) * \left(s - \frac{v^2}{a}\right) \tag{3.19}$$

According to Nissan Leaf customer reviews, Nissan Leaf can drive at speed of up to 90 mph and deliver a 0-60 mph time of around 8 seconds. Thus, in this study, the average acceleration rate is assumed to be $a = \frac{20}{6}\ m/s^2$. While the constant velocity is assumed to be 20 m/s and the distance to be 5000 m, the estimated $E_2/(E_1 + E_3')\ \approx 6.48$

Therefore, for the given acceleration rate, objective speed and total distance, even when the driving cycle is without any stop, the accelerating /decelerating periods cannot be neglected and will be taken into consideration. In addition, the constraint condition for the constant speed depending on the stop times is as follows:

$$v \leq \sqrt{\frac{s * a}{(n+1)}} \tag{3.20}$$

Thus, theoretically, for the objective speed$v = 20\ m/s$, the maximum stop times is 40. The optimization analysis of driving cycles without stop will be formulated and discussed in the case 2.

3.6.3 Case 2: Driving in a Distance with Multiple Stops

Generally, for driving cycles with multiple stops, the accelerating and decelerating periods are taken into consideration. According to Equation (3.17), the energy consumption including$E_1,\ E_2, E_3$, for n stops, is function of the velocity as:

$$E(n) = (n+1) * (E_1 + E_3) + E_2(n)$$
$$= (n+1) * \left(\frac{1}{2}mv^2 + \frac{Av^4}{4a} + \frac{Bv^2}{2a} + \frac{Cv^3}{3a}\right) + (A * v^2 + B + C * v)$$
$$* \left(s - (n+1) * \frac{v^2}{a}\right) \quad (3.21)$$

When the regenerative energy is considered, Equation (3.21)' is used to calculate the total energy consumption:

$$E(v,n,\xi)' = (n+1) * (E_1 + E_3') + E_2(v,n)$$
$$= (n+1) * \left(\frac{1}{2}mv^2 * (1-\xi) + \frac{Av^4}{4a} + \frac{Bv^2}{2a} + \frac{Cv^3}{3a}\right)$$
$$+ (A * v^2 + B + C * v) * \left(s - (n+1) * \frac{v^2}{a}\right) \quad (3.21)'$$

In order to calculate the optimal velocity with the minimum energy consumption, the derivative of the formula is analyzed. The derivative of the energy consumption with respect to the velocity is:

$$\frac{dE(v,n)}{dv} = (n+1) * \left(mv + \frac{Av^3}{a} + \frac{Bv}{a} + \frac{Cv^2}{a}\right) - \frac{4Av^3(n+1)}{a} - \frac{3Cv^2(n+1)}{a}$$
$$+ \left(2As - \frac{2B(n+1)}{a}\right)v + Cs = 0 \quad (3.22)$$

$$\frac{dE(v,n,\xi)'}{dv} = (n+1) * \left(mv * (1-\xi) + \frac{Av^3}{a} + \frac{Bv}{a} + \frac{Cv^2}{a}\right) - \frac{4Av^3(n+1)}{a}$$
$$- \frac{3Cv^2(n+1)}{a} + \left(2As - \frac{2B(n+1)}{a}\right)v + Cs = 0 \quad (3.22)'$$

Flowchart of the algorithm to calculate the optimal velocity with respect to battery energy saving:

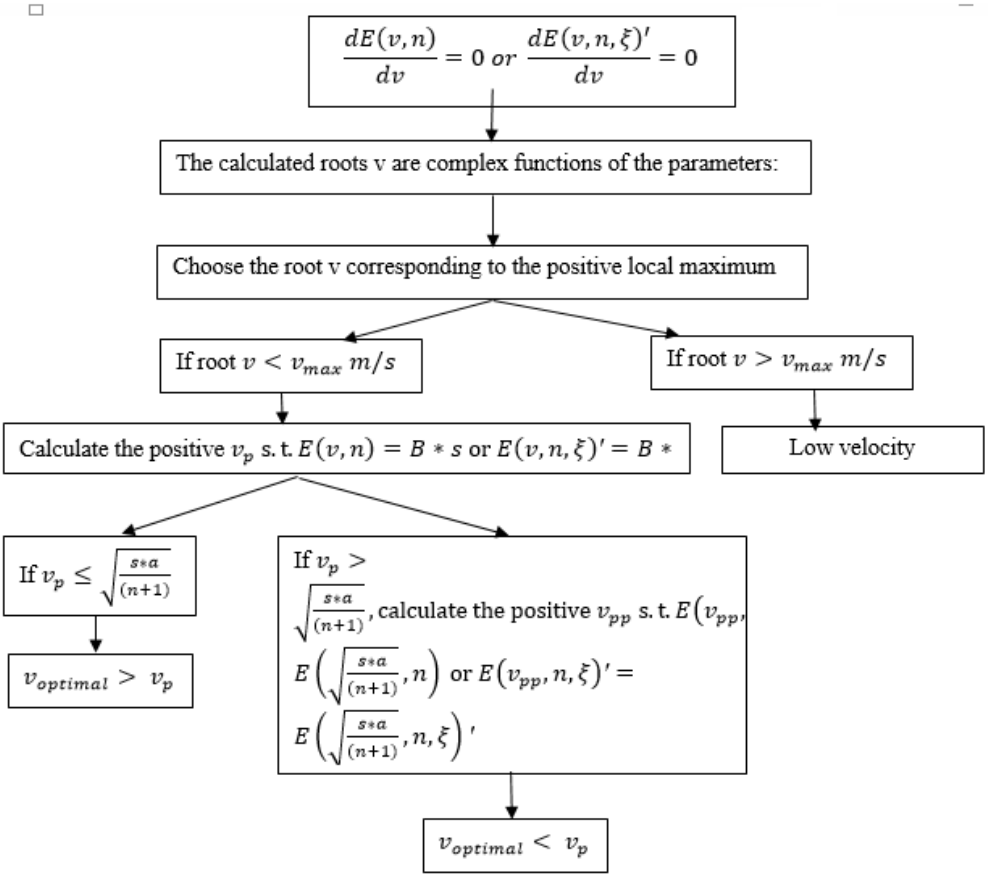

Figure 3.6.2 Flowchart of Calculating the Optimal Velocity

3.6.3.1 Calculation Results of the Derivative for n=0:

The case studies below are based on the assumption that a = $15/6\ \mathrm{m/s^2}$. Calculation Results of the derivative for n=0 without regenerative energy:

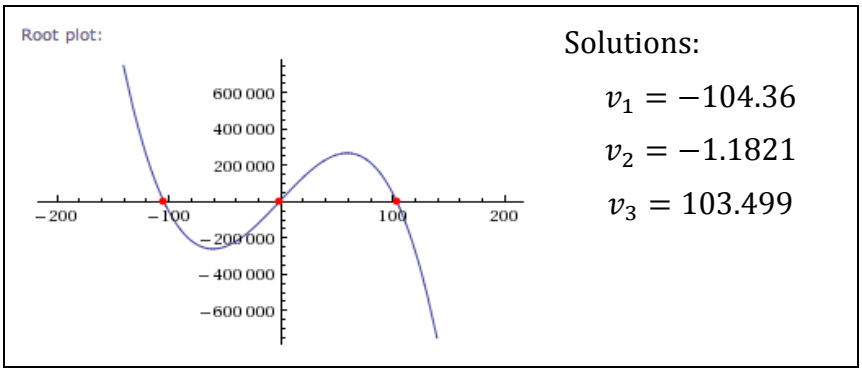

Figure 3.6.3 Illustration of Calculation Results (1)

From the root plot, based on mathematic theories, energy consumption at v = −1.1821 m/s should be a local minimum value, while the energy consumptions at v = −104.36 m/s

(ignore) and v = 103.499 m/s should be local maximum values. Since the speed ranges from 0 up to 90 mph, the value at v = −1.1821 m/s is a global minimum and will be increasing with the increase of speed through 90 mph (40 m/s). This is also indicated in the results below.

Calculation results of the energy consumption for n=0 without regenerative energy:

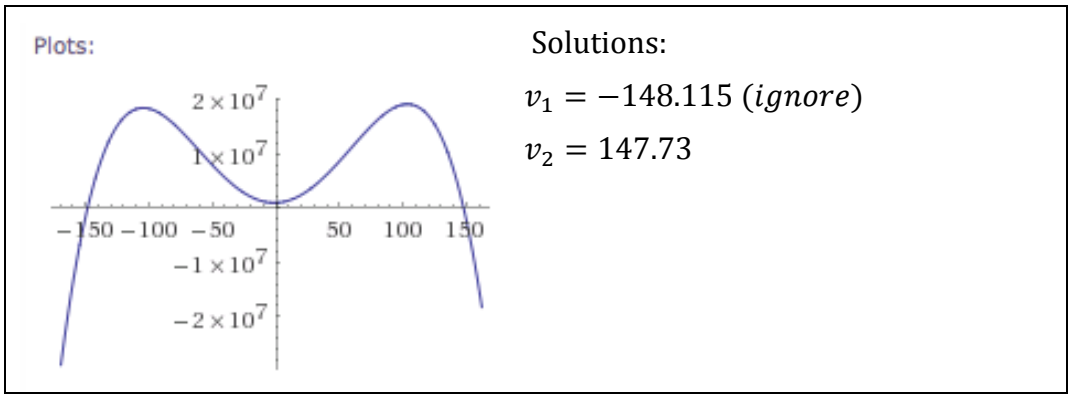

Figure 3.6.4 Illustration of Calculation Results (2)

Calculation results of the derivative for n=0 with regenerative energy, assuming that ξ = 20%:

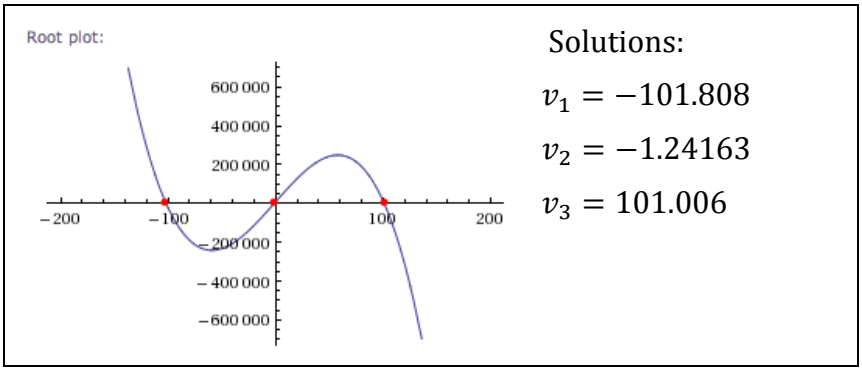

Figure 3.6.5 Illustration of Calculation Results (3)

From the root plot, based on mathematic theories, energy consumption at v = −1.24163 m/s should be a local minimum value, while the energy consumptions at v = −101.808 m/s (ignore) and v = 101.006 m/s should be local maximum values. Since the speed ranges from 0 up to 90 mph, the value at v = −1.24163 m/s is a global minimum and will be increasing with the increase of speed through 90 mph (40 m/s). This is also indicated in the results below.

Calculation results of the energy consumption for n=0 with regenerative energy:

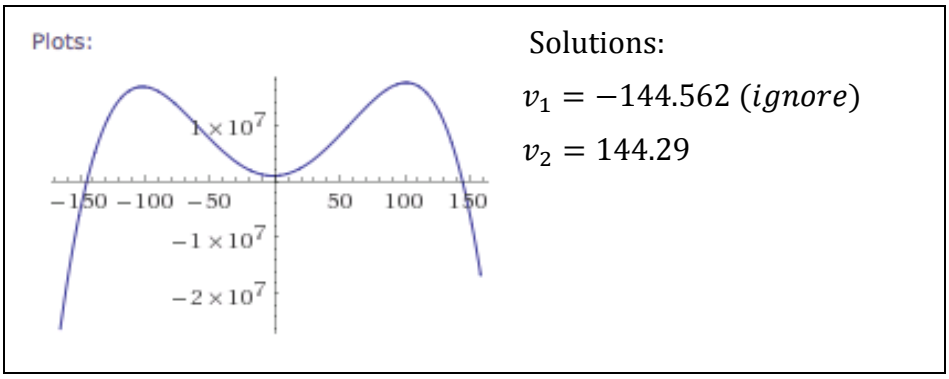

Figure 3.6.6 Illustration of Calculation Results (4)

Calculation results of the derivative for n=20 without regenerative energy:

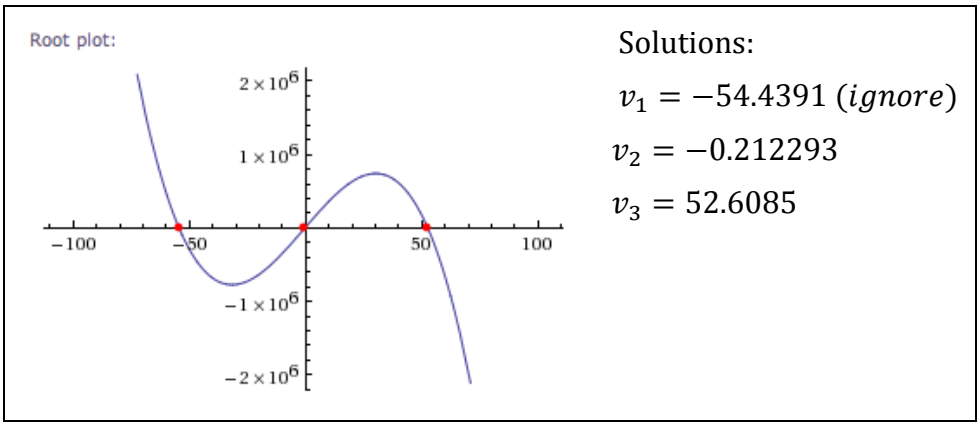

Figure 3.6.7 Illustration of Calculation Results (5)

From the root plot, based on mathematic theories, energy consumption at $v = -0.212293$ m/s should be a local minimum value, while the energy consumptions at $v = -54.4391$ m/s (ignore) and $v = 52.6085$ m/s should be local maximum values. Since the speed ranges from 0 up to 90 mph, the value at $v = -0.212293$ m/s is a global minimum and will be increasing with the increase of speed through 90 mph (40 m/s). This is also indicated in the results below.

3.6.3.2 Calculation Results of the Derivative for n=20:

Calculation results of the energy consumption for n=20 without regenerative energy:

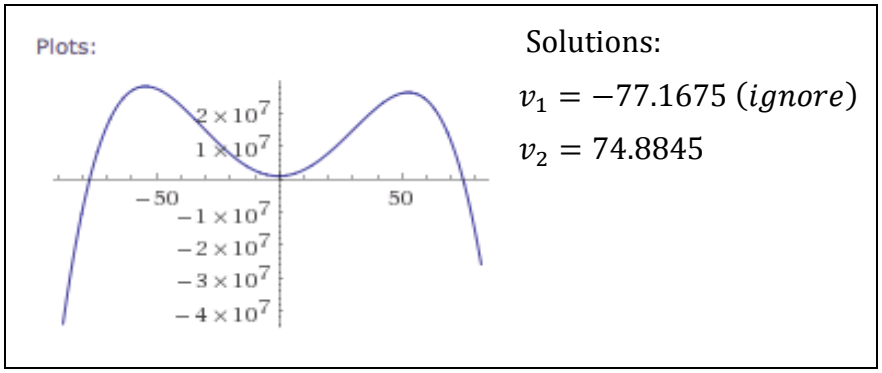

Figure 3.6.8 Illustration of Calculation Results (6)

Calculation Results of the derivative for n=20 with regenerative energy, assuming that $\xi = 90\%$:

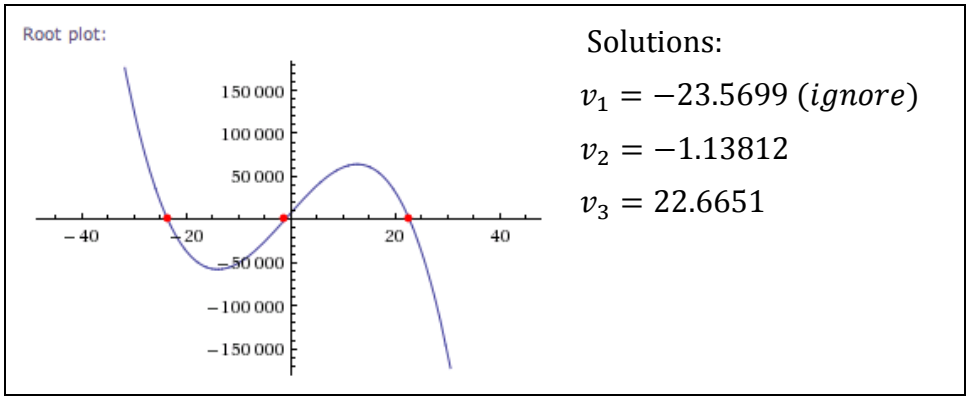

Figure 3.6.9 Illustration of Calculation Results (7)

From the root plot, based on mathematic theories, energy consumption at $v = -1.13812$m/s should be a local minimum value, while the energy consumptions at $v = -23.5699$ m/s (ignore) and $v = 22.6651$ m/s should be local maximum values. Since the speed ranges from 0 up to 90 mph, the value at $v = -1.13812$ m/s may not be a global minimum. The energy consumption will be increasing from $v = 0$ through 22.6651 m/s (60 mph). In order to check whether the value at $v = 0$ is the global minimum within the speed range of 0-90 mph, the curve of the original equation need to be displayed.

Calculation results of the energy consumption for n=20 with regenerative energy, assuming that $\xi = 90\%$:

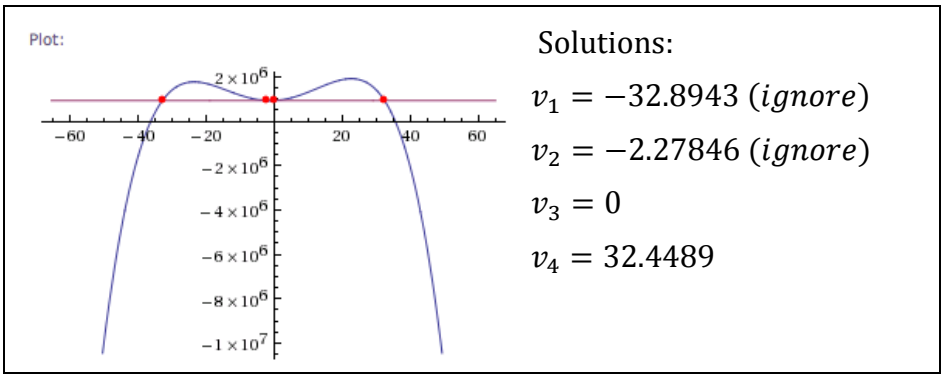

Figure 3.6.10 Illustration of Calculation Results (8)

The horizon line in the plot crosses the point at $v = 0$. The other point of intersections in the right half-plane is at $v = 32.4489$ m/s. Thus, when the speed is over 32.4489 m/s, the higher the speed is, the lower the energy consumption will be. However, according to Equation (19), the constraint for the speed is that it cannot exceed $v = 24.4$ m/s when the stop times is n=20. Thus, In this case, the less speed you are driving at, the lower energy the vehicle will consume. When the speed reaches 22.6651 m/s, the energy consumption during the driving cycle will be the maximum value. By calculating the v_{pp} s.t. $E(v_{pp}, 20, 0.9) = E(24.4, 20, 0.9)$, we obtain $v_{pp} = 20.792$. Thus, $v_{optimal} < 20.792$ will be suggested.

3.6.4 Conclusion

An algorithm is proposed to calculate and analyze the optimal velocity during a driving cycle with respect to battery energy consumption. The energy consumption is a complex function of vehicle specifications, driving situation and road conditions, such as velocity, total mass, acceleration rate, driving distance, stop times, regenerative efficiency, etc. Once the vehicle specifications are fixed and the road conditions are predicted according to the driving cycles preset by the vehicle owners and the GPS data, the energy consumption is a nonlinear function with regard to velocity, stop times and regenerative efficiency. The relation between the average constant velocity and the total energy consumption can be described as a mound-shaped curve. Thus, the optimal velocity is determined by the constraint conditions of maximum velocity bound and velocity-stop times relationship. Such algorithm can be inserted in the vehicle imbedded systems and provides the drivers suggestions about the optimal driving speed according to the real-time driving condition and the preset driving cycle.

4. Charging Infrastructures

4.1 Introduction

As discussed before, charging infrastructure (see Figure 4.1.1) is a crucial part to support the market share growing of electric vehicles. Important choices have to be made regarding the required number of chargers, location (residential or public places), and type of charging infrastructure (slow or fast, conductive or inductive or swapping). The decision should also be based on the city, regional, or country level. Many aspects need to be taken into consideration to make these decisions, such as user acceptance, user comfort, safety, standardization, and costs.

Making such decisions requires the involvement of all stakeholders: federal, regional and local governments, industry from different sectors (automotive, energy, mobility), academia, and regulators—and of course the users of the electric vehicles. The suppliers of charging infrastructure also play an important role in the new innovation platform, for example, Smart Grids Flanders, which brings together various stakeholders to develop the future electricity grid in Flanders. [52]

Nowadays, a lot of the EV buyers would charge their vehicles at home. One reason is the charging infrastructures are still not quite convenient in some cities; one of the reasons is to take advantage of charging overnight considering the long duration of vehicle charging; while another important reason is that, a lot of EV selling companies provide almost free-charge installation of the home chargers from the companies that they are cooperating with. In addition, most of the driving is local over short distances, which decreases the need for charging in the middle of the trip. In US, for example, 78% of commutes are less than 40 miles round-trip [53]. Nevertheless, longer drives between cities and towns require a network of public charging stations or another method to extend the range of electric vehicles beyond the normal daily commute. One challenge in such infrastructure is the level of demand: an isolated station along a busy highway may see hundreds of customers per hour if every passing electric vehicle has to stop there to complete the trip. In the first half of the 20th century, internal combustion vehicles faced a similar infrastructure problem [54].

Figure 4.1.1 Charging Infrastructures [52]

4.2 Electric Vehicle Supply Equipment (EVSE) and Their Functionality

Figure 4.2.1 shows how the EVSE is interfaced with vehicles and utilities. Promotion of public charging stations is encouraged as the EVSEs can convey the following benefits to the grid and customers [55, 56]:

- Help to divert the charging peak from network demand peak, while home based EV charging will probably fall on the network demand peak;
- Reduce network upgrade requirements to accommodate EV charging at the end distribution feeder level;
- Alleviate the overloading impact on distribution lines/cables and transformers. Furthermore, this does not disturb normal cooling cycles of distribution transformers as home based EV charging does. Thus, less impact will be induced on the distribution transformer service life;
- The uncertain mobile EV load can be transformed into a more predictable load;
- It is easier to constitute regulations on chargers to a bulk charging than to distributed charging. It is more convenient to implement smart charging concepts;
- Provide an incentive to customers who drive PEVs by providing EVSEs in the parking area;
- Benefit employees who drive PEVs by providing the ability for them to recharge their vehicles while they work;
- Demonstrate support for sustainable development; furthermore, leadership in energy and environmental design credits can be obtained when 3% of the total facility parking area provides alternative-fuel fueling stations, and parking spaces with EVSEs would satisfy the requirement.

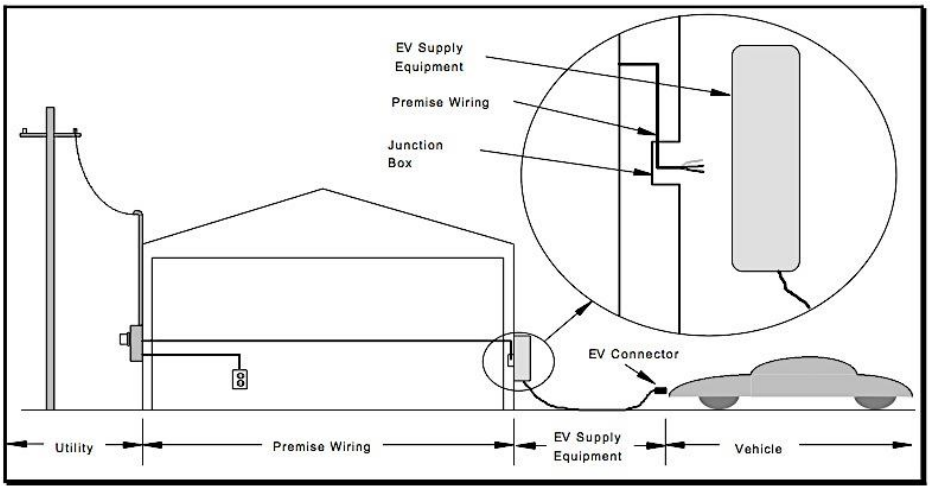

Figure 4.2.1 EV Charging System Configuration [57]

An EVSE will typically comprises of the following components [56]:

- An overcurrent device: for protection against overloads and short circuits;
- A contactor: to switch power to the connector and keep the connector's terminals deenergized when not plugged in;
- A controller: to interface with the vehicle's onboard charging system and provides ground fault protection; it may also have some power metering capabilities;
- Displays and indicators on the exterior: to provide status and alarm information and guide the user through the operational sequence;
- A cable: to connect the EVSE to the charging receptacle on the vehicle;
- A conductive connector that plugs into the vehicle.

There are four main safety devices incorporated into "Smart" EVSE that make for safe operation. [57]

- Connection Interlock: The device that creates a dead interface between the charging device, EVSE and the EVs. The Connection Interlock will prevent the power from flowing through the EV Connector or the cable, if the connector is not connected to the vehicle, while a signal will be passed from EVSE to check whether the vehicle is connected to the EV Connector and the EVSE will act a system check, if the vehicle is connected. The EVSE will allow the power to flow through the EV Connector or the cable after confirming system integrity. This device is required by Section 625-18 of the 1996 and 1999 NEC®, and California Electrical Codes.
- Charge Circuit Interrupt Device: In Section 625-22 of both the 1996 NEC® and the California Electrical Code, ground-fault protection is required for all charging levels, which is "when a current to ground exceeds some predetermined value that is less than the current required to operate the overcurrent protective device of the supply circuit, the system shall de-energize the electric vehicle supply equipment within an established period of time." Although traditional Ground-Fault Circuit Interrupters (GFCIs) for 60 Hertz systems trip at 5 milliamperes (mA) when they detect a possible ground-fault current, the GFCIs cannot differentiate possible hazardous ground currents with the harmless transient currents on the utility distribution system. Thus, the personnel protection systems for EVSE utilize ground or isolation monitoring, a circuit interrupting device, and basic, double, or reinforced insulation.
- Automatic De-energization Device: The device is a mechanism that will de-energize the EVSE if a strain occurs to the cable or EV connector that could make the live parts to be exposed. This device is required in Section 625-19 of the 1996 and 1999 NEC®, and the California Electrical Code.
- Ventilation Interlock: The ventilation interlock is required in Section 625- 29 of the 1996 and 1999 NEC and section 625-29 (c) and 1206 of the California Electrical and Building Codes. It provides three functions: querying the vehicle to determine

if the vehicle requires ventilation during charging, checking whether the EVSE can provide ventilation, and ensuring the ventilation function during the entire charging process if ventilation is available.

The control pilot circuit [58, 59] is the primary control aims to ensure proper operation when connecting an EV to the EVSE. According to SAE J1772 standard, the control pilot provides the following functions: a) verification of vehicle connection, b) indication of EVSE standby state, c) indication of EVSE state- ready to supply energy, d) indication of EV/PEV state- ready to accept energy, e) determination of indoor ventilation, and f) checking of the EVSE current capacity.

In addition to control pilot circuit, it also includes other functions, such as proximity detection, digital data transfer and the communication between plug-in vehicles and the utility grid [58].

4.3 Charging Level

Charging equipment for PHEVs and BEVs is classified by the rate at which the batteries are charged. Charging times vary based on how depleted the battery is, how much energy it holds, the type of battery, and the type of EVSE. The charging time can range from 15 minutes to 20 hours or more, depending on these factors. The levels and the corresponding characteristics are as follows (Table 4.1) [57,56,60-63]:

Table 4.1 Charging Levels

Charging Levels	**Voltage**	**Maximum Current**
AC Level 1	120 Vac, single phase	16 A
AC Level 2	208-240 Vac, single phase	80 A
DC Level 1	200-450 V DC	80 A
DC Level 2	200-450 V DC	200 A

- AC Level 1: Level 1 charging is the slowest method. This charging level is designed to allow a vehicle to plug into the common 120-Vac receptacle and requires electrical installation according to the National Electrical Code. Recharging a battery at this level can take a significant amount of time, from 12–18 hours, based on the capacity of the vehicle battery and its discharge level. EV charging employs cord & plug connected portable EV supply equipment (EVSE) that can be transported with an EV. Most PEVs will come with an AC Level 1 EVSE cordset so that no additional charging equipment is required. On one end of the cord is a standard, three-prong household plug, as NEMA 5-15 connector. On the other end is a J1772 standard connector, which plugs into the vehicle. Based on the battery type and vehicle, AC Level 1 charging adds about 2 to 5 miles of range to a PEV per hour of charging time.
- AC Level 2: level 2 chargers are required by national electric code (NEC) Article 625 to be hardwired into the facility's wiring system. This level provides a faster rate of charge than ac level 1. The 30-A rated EVSEs will reduce the charging time

down to 4-8 h. AC Level 2 EVSE requires installation of home charging or public charging equipment and a dedicated circuit of 20 to 100 amps, depending on the EVSE requirements. This charging option can operate at up to 80 amperes and 19.2 kW. However, most residential AC Level 2 EVSE will operate at lower power. Many such units operate at up to 30 amperes, delivering 7.2 kW of power. These units require a dedicated 40 amp circuit. Most homes have 240 V service available, and because AC Level 2 EVSE can charge a typical EV battery overnight, this will be a common installation for homes. AC Level 2 equipment uses the same connector on the vehicle that Level 1 equipment uses. Based on the vehicle and circuit capacity, AC Level 2 adds about 10 to 20 miles of range per hour of charging time.

- DC charging: DC fast charging, also called level 3 commercial fast charging, can be installed in highway rest areas and city refueling points, analogous to gas stations. It typically operates with a 480 V or higher three-phase circuit and requires an off-board charger to provide regulated ac-dc conversion. EV charging employs permanently wired EVSE that is operated at a fixed location. This equipment is used specifically for EV charging and is rated at greater than 14.4 kW. A DC fast charge can add 60 to 80 miles of range to a light-duty PHEV or EV in 20 minutes.

At one time, there was also an AC level 3 method defined by SAE J1772, but it was never implemented. Information concerning AC level 3 is provided in the appendix of SAE J1772-2010 for reference purposes only [56].

Nowadays, inductive charging has also been introduced. Inductive charging equipment, which uses an electromagnetic field to transfer electricity to a PEV without a cord, has been recently introduced commercially for installation as an aftermarket add-on. Currently available wireless charging stations operate at power levels comparable to AC Level 2[60].

4.4 OEM and Service Providers

OEM (original equipment manufacturer) refers to the company that originally manufactured the product. A brief summary of the OEM and service providers are listed in the table 4.2 below:

Table 4.2 OEM and Service Providers

Vendor	Category	Specifications
LEVITON	OEM	Level 2; Input Amperage: 16A ; Input Voltage: 240VAC ; Output Power: 3.8kW (16A @240VAC)
Siemens	OEM	Level 1 Level 2
Coulomb Technologies	Service Provider	Residential Level 2 Commercial Level 1 and Level 2 Commercial Dual Level 2

Table 4.2 OEM and Service Providers (continued)

Vendor	Category	Specifications
Delta-Q	OEM	DC Output Voltage (nominal): 24V; 36V; 48V; 72V Output Current-max: 25A; 21A; 18A; 12A AC Input Voltage – range: 85 - 265 VAC AC Input Voltage – nominal: 120 VAC / 230 VAC rms
EVI	OEM	Level 2; Continuous Vehicle Current: 16A; 24A; 32A; Level 2; Current: 24A (30A Breaker) Level 2; Current: 60A Circuit Breaker.
Blink	OEM	Level 2; Input Current: maximum 30A; 12A, 16A and 24A;
ECOtality	Service Provider	Same with EVI DS-50 Same with EVI MCS-100 Same with EVI ICS-200
GE	OEM	Level 2; AC Charging Power Output: 7.2kW; Voltage and Current Rating: 208-240VAC @ 30A;
GoSmart Technologies	OEM	Level 2; Voltage: 208-240 VAC; Current: 15-30A; Power: 3.12-7.2 kW;
EV-Charge America	OEM	Level 1; Voltage:110- 120 VAC; Current: 20 A (max); Level 2; Voltage: 208VAC/240 VAC; Current: 40 A (max);
Tesla	OEM	Maximum Current: 15A Voltage: 120V Maximum Power: 1.8 kW Maximum Current: 40A Voltage: 120-240V Maximum Power: 9.6 kW Maximum Current: 70A Voltage: 208-240V, Single phase Maximum Power: 16.8 kW
Eaton	OEM	Level 2; Incoming voltage and connections: 208–240 Vac, Line 1, Line 2, Neutral and Earth ground;
OpConnect	OEM	Level 1 (NMEA 5-20); Level 2 (SAE J1772).

Table 4.2 OEM and Service Providers (continued)

Vendor	Category	Specifications
Shorepower Technologies	OEM	Level 1; Input Power: 240 Volt or 208 Volt, 100 amp (min. 50 amp) 4 Wire Circuit; Output Power: 4 Level 1 GFCI 120 Volt 20 Amp Outlets (NEMA 5-20R) One Station Serves up to 4 Vehicles;
Voltec	OEM	Level 2; Input Voltage: 208 / 240V – 15A (20A circuit), single phase, 2 wire, with ground; Output Voltage: 208 / 240V – 15A, single phase;
SPX	OEM	Level 2; Amperage: 32Amax (Field Adjustable) Voltage: 95 VAC – 264 VAC;
ClipperCreek	OEM	Level 1; Level 2; Input Voltage & Wiring: 240V AC single-phase - L1, L2, and Safety Ground; 208V AC 3-phase wye-connected - Any 2 phases and Safety Ground;240V AC 3-phase, delta-connected. Voltage Range: 185V AC to 264V AC; Input Current: 20amps, max; Output Power: At 240V AC, approximately 5KW Level 2; Service Entrance: 208V to 240V - 30 to 100 Amps, single phase, 2 wire w/ground; Continuous Current: 80A; 72A; 64A; 56A; 48A; 40A; 32A; 24A.

4.5 Communication Protocol

The formats of exchanging messages are well defined for the communication systems to use. Since each message has an exact meaning aiming to evoke a particular response of the receiver, a protocol must define the syntax, semantics, and synchronization of communication. Typically, the specified behavior is not based on how it is implemented, thus the protocol can be implemented as hardware, software, or both. Communication protocols may be designed as a technical standard and need to be agreed upon by all the involved parties. The relationship between protocols and communications can be an analogy as programming languages and computations [64].

Communication systems operate in parallel using concurrent programming which is a collection of the programming tools and techniques for parallel processes. Concurrent programming only deals with the synchronization of communication. The syntax and semantics of the communication for a low-level protocol usually have modest complexity, while high-level protocols with relatively large complexity could implement language

interpreters, i.e., the HTML language. Systems use a set of cooperating protocols, sometimes called a protocol family or protocol suite, to handle a transmission. The current communications protocols on the Internet are designed with very complex and diverse settings. The layering scheme is called the TCP/IP model, as shown in Figure 4.5.1.

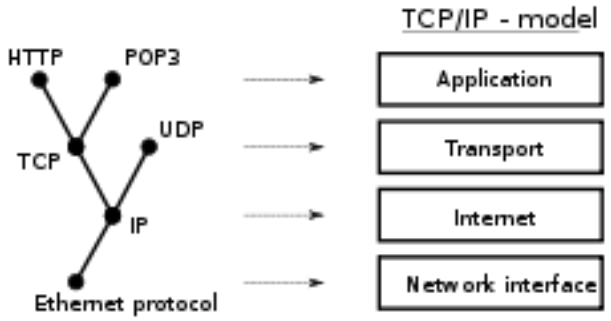

Figure 4.5.1 The TCP/IP Model or Internet Layering Scheme and Its Relation to Some Common Protocols. [64]

Some of the standards organizations for communications protocols are listed below:

- International Organization for Standardization (ISO);
- International Telecommunications Union (ITU): it is an umbrella organization of telecommunications engineers designing the public switched telephone network (PSTN), and also many radio communication systems. The NMEA standards are used for marine electronics. For Web technologies, the World Wide Web Consortium (W3C) provides protocols and standards;
- Institute of Electrical and Electronics Engineers (IEEE): it controls many software and hardware protocols in the electrical industry for commercial and consumer devices;
- Internet Engineering Task Force (IETF): it maintains the current protocols on the Internet.

International standards organizations are supposed to be more unbiased than local organizations with a national or commercial self-interest to consider. Standards organizations also research and develop standards for the future. In fact, the standards organizations cooperate closely with each other [64, 65].

5. Communication Center

5.1 Introduction

Many different vendors of Electrical Vehicle Supply Equipment (EVSE) are offering products that are compatible only with their communication infrastructure, which means that it is hard for EVSEs from different vendors to communicate with each other.

However, this will greatly harm the further widespread of EVs. First of all, this situation will definitely bring inconvenience and difficulty for EV drivers and fleet owners, since they will have to manage separately the data and account if they charge their vehicles through facilities from different vendors. And it is so hard for the facilities from one vendor to be available everywhere so that vehicle owners can stick to just one vendor. Besides, the lack of communication among facilities from various vendors may bring difficulty for fleet owners to optimize their charging schedule or travel route.

Moreover, EVs might be able to participate into the electricity market after being widely adopted since they have batteries inside and hence can be viewed as storage to some extent. In order for EVs to better bid into electricity market, aggregators, who perform as "a commercial middleman between a system operator and plug-in electrical vehicles (EV)"[66], will be introduced. Consequently, the communication among infrastructures from various vendors, with which necessary data can be gathered by aggregators, will be in great need so as to ensure the proper and efficient work of aggregators.

Besides, as one of the consequence of widespread of EVs to replace the conventional vehicles, the charging need and their potential to store electricity therefore cannot be ignored by the grid anymore. The utility will have to forecast the electricity need from EVs and cooperate well with EVs so as to better perform their job. In this sense, the communication among infrastructures from different vendors may help EVs better integrated into the power grid.

To sum up, the communication among infrastructures from various vendors needs to be established so as to lay down the groundwork for the future popularization of EVs. The data from infrastructures manufactured by different vendors need to be collected and stored properly. This will bring convenience to vehicle owners and help them better optimize and manage their charging behavior. And this can also help with aggregators' performance and EVs future integration into the power grid.

5.2 Survey on Different Vendors

In order to set up the communication among infrastructures from various vendors, a survey is first conducted among different vendors on their network and communication protocol, service to drivers and charging station owners, method of payment, etc.

5.2.1 Vendors and Websites

The following vendors are covered in the survey and the information on each vendor mainly comes from their website which is also shown below in Table 5.1:

Table 5.1 List of Vendors and Their Websites

Vendor	Website
Ecotality	http://www.ecotality.com/
Blink network	http://www.blinknetwork.com/index.html
PEP stations	http://www.pepstations.com/
LilyPadEV	http://www.lilypadev.com/?gclid=CP-Tg4uL47ICFUWnPAodiGkALg
DBT	http://www.dbtus.com/charging-solutions/fleet-chargers/
(Coulomb Technologies) ChargePoint Networked Charging Stations	http://chargepoint.com/
Clipper Creek	http://www.clippercreek.com/products.html
Aerovironment	http://evsolutions.avinc.com/
Better Place	http://www.betterplace.com/
Levition	http://www.leviton.com/
EV-go	http://www.evgonetwork.com/
Legrand	http://www.legrand.us/
EV charge America	http://www.ev-chargeamerica.com/
SemaConnect	http://www.semaconnect.com/
Shorepower	http://shorepower.com/komfortkits.html
Aker Wade	http://www.akerwade.com/
Andromeda power	http://andromedapower.com/Orca_Mobile.php
Control Module Industries	http://www.controlmod.com/
Delta	http://www.delta.com.tw/product/rd/evcs/evcs_main.asp
EATON	http://www.eaton.com/
EFACE	http://www.efacec.pt/
ABB	http://www.abb.com/
EVTEC	http://www.evtec.ch/
Fuji Electric	http://www.americas.fujielectric.com/
GE	http://www.geindustrial.com/
Evcollective	http://www.evcollective.com/
Parkpod	http://us.parkpod.com/home/
Schneider	http://products.schneider-electric.us/

5.2.2 Payment and Authorization

The results of the survey on the method of payment and authorization from different vendors are shown in the following Table 5.2.

Table 5.2 Results on Method of Payment and Authorization

Vendor	Payment and Authorization
Blink Network	Mobile-phone based payment options, and credit card payments
PEP Station	Credit card Internet Payment Gateway services ensure transactions are processed safely and securely using the latest standards of encryption and transmission
LilyPadEV	Contactless Credit Card Reader and Provisioning
(Coulomb Technologies) ChargePoint Networked Charging Stations	ChargePoint cards, contactless credit cards and MIFARE-based transportation cards
Levition	Major credit cards and ChargePass Card
EV Charge America	A small RFID (Radio Frequency Identification) tag: Each user on the network is provided with a small RFID (Radio Frequency Identification) tag that they carry on their key ring that only works in the proximity of a charging station. When they arrive at a charging station, the RFID tag authenticates them as a subscriber to the service and the station is activated, electricity is turned on, and the charging unit further secures their plug-in cord so that it cannot be removed by anyone else.
SemaConnect	Smart Card Authentication: for open or closed access. SemaCharge Passes available for EV drivers
Shorepower	Industrial outdoor card reader accepting all major credit/debit cards and/or proprietary cards (e.g. fleet, student or employee card)
Delta	RFID card reader, ISO 14443 complaint
ABB	RFID
Schneider	Authentication for commercial units using a Radio Frequency Identification (FID) card scan ensures that only approved users can access the charging station
EATON	Eaton can interface with third- party authentication systems including but not limited to: Outdoor-rated credit card swipe; RFID and HID card readers; Key fob readers; Synchronous-code keypads

5.2.3 Network and Communication Protocol

The results of the survey on the network and communication protocol or interface from different vendors are shown in the following Table 5.3.

Table 5.3 Network and Communication Protocol of Different Vendors

Vendors	Network and Communication Protocol
Blink Network	• The residential and commercial chargers are linked to the Blink Network via the Internet; • Certified energy and demand metering, SAE J1772 connector, supports electric utility EV building when certified to ANSI 12.20 and IEC standards; • Multiple modes of communications are supported, including Wireless IEEE 802.11g, cellular, LAN/Ethernet, and LAN capable Web-based bi-directional delivery and data flow; • Access to the Blink Network and Blink Membership portal.
PEP Station	• Required to be connected to the Internet via an Ethernet cable; • TCP/IP, IPv4/IPv6, DHCP Addressing, HTTPS/SSL.
LilyPadEV	• Local Area Network 2.4 GHz 802.15.4 dynamic network; • Wide Area Network Commercial GPRS or CDMA cellular data network.
(Coulomb Technologies) ChargePoint Networked Charging Stations	• Wireless and cellular network interfaces; • Local Area Network: 2.4 GHz 802.15.4 dynamic network; • Wide Area Network: Commercial GPRS or CDMA cellular data network.
Aerovironment	• Communication: Wireless IEEE 802.11g, 3G/4G cellular, and Ethernet; • An optional module for Ethernet, WiFi, Zigbee, or cellular communication is available.
EV Charge America	• Wireless, and Ethernetconnectivity
SemaConnect	• CDMA & Wireless Networking, Wireless Technology: allows the station to communicate with the software and produce real-time data; • Networking: 802.15.4 (Zigbee) Dynamic Mesh Network (LAN), CDMA or GPRS (WAN) ; • Network: SemaCharge.
Shorepower	• Wireless, cellular and Ethernet communication.
Andromeda Power	• Communication: Wireless IEEE 802.11g, 3G/4G cellular, and Ethernet.
Control Module Industries	• Communication: Zigbee (HAN compliant), WiFi, Cellular & Bluetooth; • Networks: Web-Based, LAN, WAN, Cellular.

Table 5.3 Network and Communication Protocol of Different Vendors (continued)

Vendors	Network and Communication Protocol
Delta	• Communication: Charger to back office: Ethernet RJ-45, Charger to EV: CAN; Network interface: Ethernet, wireless (option).
EATON	• Standard Ethernet, Serial (RS-232), ModBus (RS485/4-wire), Wi-Fi, Cellular (optional); • Eaton offers direct building management integration via the open zzModbus standard. Two types of physical layers can be used for this protocol: RS-485 (Modbus RTU) or Ethernet (Modbus TCP).
EFACE	• Communication protocol(others under request): Web services over IP
ABB	• Network connection: GSM / UMTS modem10/100 Base-T Ethernet; • Web connected; • Data transportation and security: your charger data, settings and software updates are transported via TLS and X509 certificates, a security standard widely used to protect classified industrial and governmental information.
EVTEC	Connectivity: Ethernet, Powerline, GSM/GPRS/UMTS
EV Collective	• Network Communication: Kanematsu Platform; • EVSEs have to be network-integrated especially if they are installed on the street. EV Collective Platform evolves such EVSEs into cash cows with billing capability and online presence.
Parkpod	• All ParkPods of a local group are communicating in a local wireless network; • An additional communications gateway connects this local group to the Internet or a local server. This modular design accommodates any existing or future network configuration easily.
Schneider	• GPRS communication

5.2.4 Services for Drivers or Charging Station Owners

1. Ecotality

Ecotality enables members to charge when rates are lowest, receive updates on their EV's charging status, and easily locate available chargers within the network's growing number of partner locations such as Ikea, Best Buy, Cracker Barrel, BP, and many more.

2. Blink network

For drivers:

- Deploy state-of-the-art GPS and location-based tools for their mobile device and Smartphone and accessible via the Blink Network web portal;
- Remotely scheduling and starting their charge via the web or on their Smartphone or mobile device;
- The Blink Portal customizes their experience by bringing all the information they need to one place. With a customizable dashboard they can quickly view and interact with the Blink Network. Access dynamic information any time, any place, on their Smartphone or mobile device, via the Web, or by connecting through Wireless IEEE 802.11g, cellular, LAN/Ethernet, or LAN capable devices. Personalize their experience by customizing the dashboard, choose their view point and favorites to easily plan your trips, reserve a charger, and see real-time the availability of Blink charging stations and the location of any EV charging station nationwide.

For charging station owners:

- They use sophisticated software to communicate with power companies, meter power, operate efficiently, and save charging station owner money on each charge;
- The charger can also determine the lowest times and rates available for charging;
- A wealth of information can be accessed via customizable gauges and dashboard that provide them with real time information about their anything related to your EV and Blink charging stations.

3. PEP Station

PEP*Advantage*™ for the PS2000 provides an open station management system for electric car drivers and PEP Station owners. Unlike other networked charging stations, there are no membership requirements for electric car drivers and no revenue sharing for PS2000 owners. The PEP*Advantage*™ network is designed to be flexible, user-friendly and is offered at a fraction of the cost of other station management networks.

For charging station owners:

- Access management: PEP Stations can be configured for access cards, credit cards or free charging and can be configured for time of day operation. (Figure 5.2.1 shows an sample usage report produced by the software used for help owners manage their charging stations);
- Rate management: Station owners may set the hourly fee for credit card billing;
- Usage reporting: PEP maintains usage statistics on a per-station and aggregate

basis. This information will be distributed to registered users monthly;

- Software updates;
- Monitoring, diagnostics and service by Diebold, Inc.

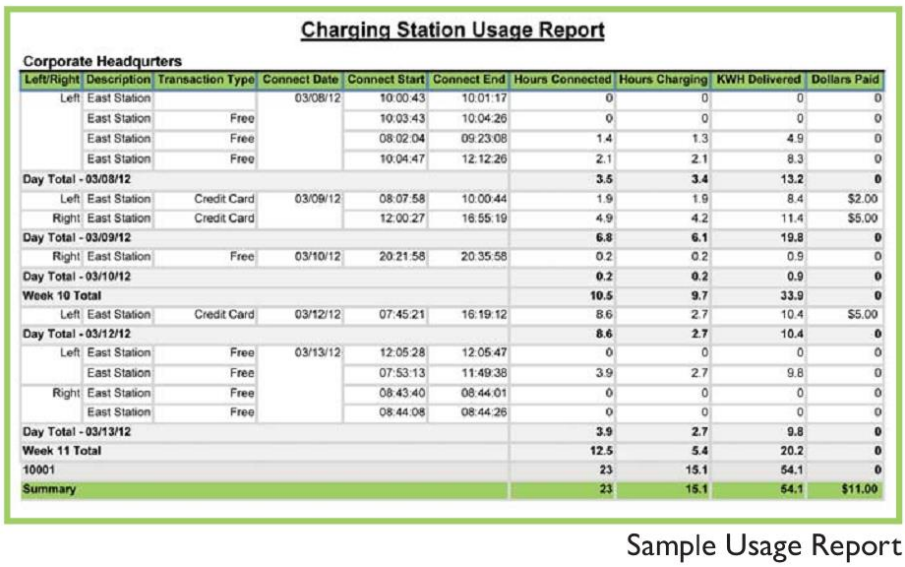

Charging Station Usage Report

Corporate Headquarters

Left/Right	Description	Transaction Type	Connect Date	Connect Start	Connect End	Hours Connected	Hours Charging	KWH Delivered	Dollars Paid
Left	East Station		03/08/12	10:00:43	10:01:17	0	0	0	0
	East Station	Free		10:03:43	10:04:26	0	0	0	0
	East Station	Free		08:02:04	09:23:08	1.4	1.3	4.9	0
	East Station	Free		10:04:47	12:12:26	2.1	2.1	8.3	0
Day Total - 03/08/12						**3.5**	**3.4**	**13.2**	**0**
Left	East Station	Credit Card	03/09/12	08:07:58	10:00:44	1.9	1.9	8.4	$2.00
Right	East Station	Credit Card		12:00:27	16:55:19	4.9	4.2	11.4	$5.00
Day Total - 03/09/12						**6.8**	**6.1**	**19.8**	**0**
Right	East Station	Free	03/10/12	20:21:58	20:35:58	0.2	0.2	0.9	0
Day Total - 03/10/12						**0.2**	**0.2**	**0.9**	**0**
Week 10 Total						**10.5**	**9.7**	**33.9**	**0**
Left	East Station	Credit Card	03/12/12	07:45:21	16:19:12	8.6	2.7	10.4	$5.00
Day Total - 03/12/12						**8.6**	**2.7**	**10.4**	**0**
Left	East Station	Free	03/13/12	12:05:28	12:05:47	0	0	0	0
	East Station	Free		07:53:13	11:49:38	3.9	2.7	9.8	0
Right	East Station	Free		08:43:40	08:44:01	0	0	0	0
	East Station	Free		08:44:08	08:44:26	0	0	0	0
Day Total - 03/13/12						**3.9**	**2.7**	**9.8**	**0**
Week 11 Total						**12.5**	**5.4**	**20.2**	**0**
10001						**23**	**15.1**	**54.1**	**0**
Summary						**23**	**15.1**	**54.1**	**$11.00**

Sample Usage Report

Figure 5.2.1 Illustration of Sample Usage Report

4. (Coulomb Technologies) ChargePoint Networked Charging Stations

Every station is network-enabled and embedded with an on-board computer, a fluorescent display, a standards-based RFID reader and a utility-grade meter that provides precise, bi-directional energy measurement.

For Charging Station Owners:

- They can set pricing and collect fees, provide 24x7 driver assistance, control access, enable reservations, display advertisements, track usage and monitor the station remotely using the growing suite of ChargePoint cloud-based service plans;
- Integrated Fault Detection;
- Enable Time-Of-Use (TOU) pricing and demand response by integrating with Advanced Metering Infrastructures (AMIs);
- They can also view all usage history for your public charging including: Start and End Times, Energy (kWh) Used, Greenhouse Gases Saved, Occupied Time, Location.

5. Aerovironment

The Smart Charging Station is designed to communicate with a wide area network grid and turn consumers' homes into grid-connected smart charging hubs – charging when energy consumption is low, and delaying the charge when energy demand is high.

- Smartphone application to control/monitor the charging;
- Embedded ORCA-EDM (Energy Demand Management);
- Remotely controlled via third-party software control system.

6. Levition

For charging station owners:

Charging stations connected to the ChargePoint Network provide more value for charging station owners than non-networked stations. The ChargePoint Network Standard Service combines software applications and network services so that station owners can monitor their stations, view usage reports, and collect station fees from anywhere with an internet connection. The software can (5.2.2 illustrates the ChargePoint Network):

- Provide driver assistance;
- Generate revenue;
- Provide high reliability;
- Advertise ;
- Eliminate energy theft and enhance safety;
- Optimize return on investment and measure green initiative success.

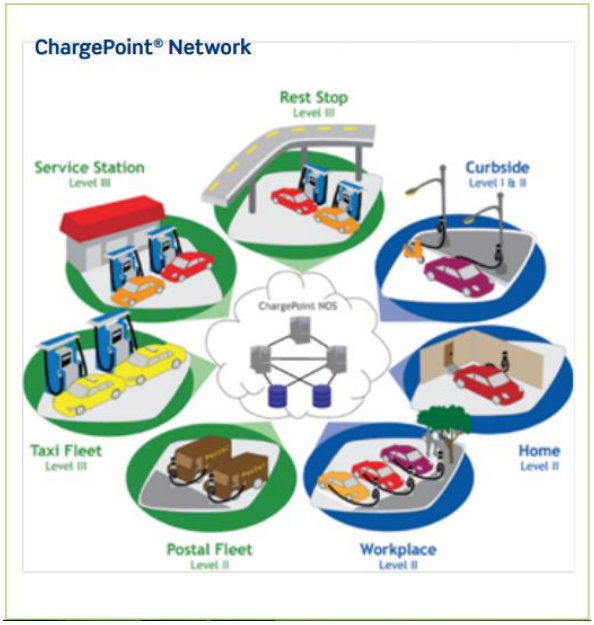

Figure 5.2.2 Illustration of ChargePoint Network

For Fleet Managers:

The ChargePoint Network Fleet Manager provides fleet management staff a centralized point of management and control for charging their Electric Vehicle fleet on ChargePoint Network Stations.

- Determine real-time fleet-wide charging status: View the status and location of every EV in their fleet currently charging within the ChargePoint Network;
- Ensure daily EV availability;
- Organize the EV fleet: Organize vehicles by fleet, department and driver;
- Track greenhouse gas and fuel efficiency savings;
- Real time EV charging location and status;
- Fleet summary alert;
- Vehicle charged alert;
- Vehicle charging fault alert;
- Usage reports.

7. EV Charge America

For drivers:

This environmentally responsible and economically sustainable approach to EV Charging Stations includes distributing and deploying a wireless, networked, meshed-LAN array of subscription-based EV Charging Stations that can be located anywhere on earth via Google Maps, OnStar™, Hand-held devices such as BlackBerrys and iPhones, or any other standard GPS enabled cell phone using the Charge Point Network.

8. SemaConnect

For drivers: the ChargePro Driver Manager software is for electric vehicle drivers. Easily register, manage, monitor and update their charging account through the ChargePro Driver Manager. The web-based management system makes it simple, convenient and effortless to use. The Driver Manager software also has mapping tools for identifying station locations, availability and pricing. Text-based messaging makes it easy to immediately communicate important information such as charging-fault detection, current state-of-charge and charging-complete. The system also allows the driver to specify means of payment, schedule charging times, and monitor charging costs and energy usage. The system also includes mapping and messaging features.

For charging stations owners: the ChargePro Station Manager software is for station owners and operators. Easily manage, monitor and update their charging stations through the ChargePro portal by logging in with their secure username and password. The web-based management system makes it simple, convenient and effortless to use from any internet connected-computer within their enterprise. Through the Station Manager application, station owners have the ability to register users, monitor costs, set pricing, track system usage and even print out environmental reports.

The ChargePro Charging Station has many features well suited to fleet applications such as monitoring, messaging and management tools. Monitoring tools include: Vehicle plug-in, plug-out times, state-of-charge information and electricity usage reports. Messaging tools include: Late plug-in, plug-out, charging fault event and incomplete charge at plug-out. Management tools include: Charging scheduler, configurable alarm triggers and user access control.

9. Shorepower

For station owners:

- Web-based monitoring/reporting system - detailed information about usage, access times, energy consumed and billing;
- Optional Features: Energy and time use monitor, Remote on and off control, Payment & control system, Automatic evening globe illumination.

10. Andromeda Power

- Smartphone application to control/monitor the charging;
- Embedded ORCA-EDM (Energy Demand Management);
- Remotely controlled via third-party software control system.

11. Delta

Delta Electric Vehicle Supply Equipment (EVSE): Delta provides efficient, reliable, and user friendly AC chargers and DC Quick Chargers for various charging demand and installations.

Delta Site Management System (SMS): The Delta SMS is designed for perfect integration with Delta EVSE. It features a web-based graphical user interface (GUI) that makes remote setup, management, and maintenance easy for single and multiple site management.

Delta Charging Network Management System (CNMS): Delta's CNMS gives smart and centralized management of EV charging network for multiple system integration capabilities and scalability.

12. EATON

Remote management and control:

- Eaton's optional Pow-R-Station Network Manager Software provides remote-management and control services for the charging station.
- Eaton's Pow-R-Station Network Manager Software allows a user or a fleet manager to check the status of the station, including if it is idle or in use, the amount of power flowing to the vehicle, and any required preventative maintenance.
- Further, the user is able to gather usage data and reports, manage and control how fast charging takes place, and access maps of where each station is located, all from Internet portal dashboards.

13. ABB

ABB complements its fast charging solutions with web-based control, management and maintenance systems. All Terra chargers are connected to the Power Routing network. ABB provides a suite of APIs, which enables the Terra chargers to interface to 3rd party billing servers, fleet management systems, smart grids or demand-response applications, via the Power Routing network.

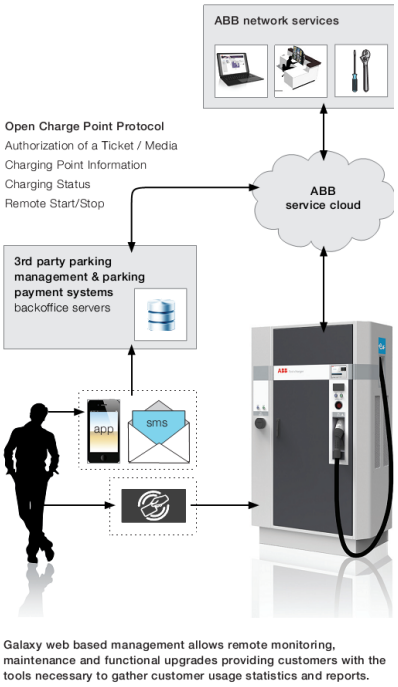

Figure 5.2.3 Illustration of ABB Galaxy Web Based Management Tool

ABB also offers the Galaxy online management tool (illustrated in Figure 5.2.3). This user-friendly web application allows a charging infrastructure operator to access status information and statistics from the Terra chargers at their sites, including kWh consumption and session statistics on a daily, weekly, or monthly basis. Additionally, an operator can use the Galaxy tool to configure chargers and sites according to their preferences.

ABB's Power Routing network is a robust IT backbone operated by ABB's service center to provide support, software updates and upgrades, remote maintenance, servicing and monitoring of Terra chargers. The Power Routing network ensures the best possible uptime and performance for your charging infrastructure.

14. Fuji

According to TonyWilliams at MyNissanLEAF, the charger can communicate with other units so that the overall load is kept below a user configured threshold. The charger can be configured with two nozzles, so that a second car can be queued up and start charging when the first car is done.

15. EV Collective

EVSEs have to be network-integrated especially if they are installed on the street.EV Collective Platform evolves such EVSEs into cash cows with billing capability and online presence.

For EV Drivers:

- Station Status;
- Their account/Billing;
- Reservation.

For Station Managers:

- Troubleshooting;
- Charger/Member Management;
- Statistics.

16. Parkpod

ParkPod Software is a comprehensive suite, covering end user operation functions, operator administration (local and central), communications and data transfer (internal, external) as well as interfacing/integration with critical functions of third parties (e.g. auto OEMs, energy utilities). Key Software Features include:

- Database enabled client/server solution;
- OS MS Windows 7 / MS Windows XP Professional;
- Ergonomic user menus with expanded tree hierarchy;
- User guidance;
- Complex rights management, all rights can be granted user specific, several user classes enabled;
- Integrated reporting tools for complex protocol definitions, unlimited number of protocols or export formats can be defined, including different languages;
- Support- and remote maintenance software, realized though Internet connectivity;
- Input masks with expanded plausibility checks;
- Integrated data base access;
- Expandability through modular system design;
- Foreign language support (online language switching, Standard: German and English, user installed extensions possible);
- Statistical data analysis, by ParkPod unit or customer.

17. Schneider

Remote monitoring and control allows users to not only monitor energy use, the charging station, and usage data, but also control remote access.

5.3 Introduction of Communication Center

As mentioned in the introduction, many EVSEs from different vendors may have problem communicating with each other, since they may adopt different communication protocols. Figure 5.3.1 illustrates this limitation.

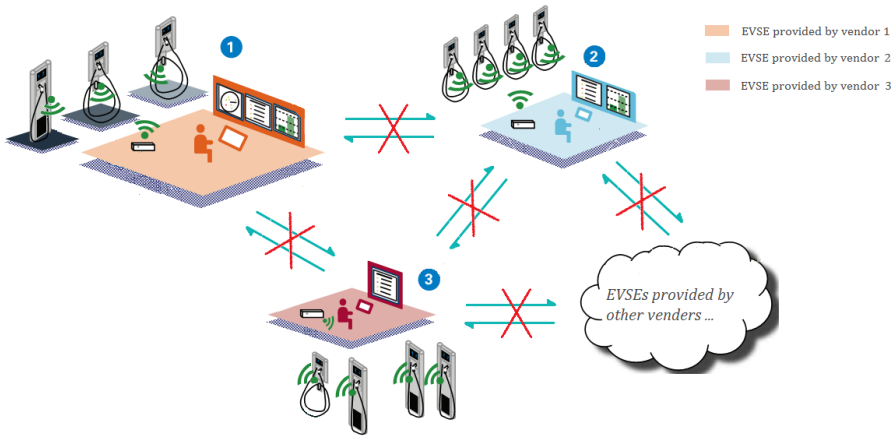

Figure 5.3.1 Limitation of Communication among EVSEs from Different Vendors

As a consequence, it is also hard for aggregators or utilities to access or control those EVSE at a time, thus leading to the difficulty for the future widespread of EVs. Therefore, Communication Center will be introduced here to help alleviate this issue.

5.3.1 The Functionality of Communication Center

In order to help alleviate the negative impact EVs may exert to the power grid and at the same time enable EVs to participate into electricity market, communication among EVSEs from different vendors needs to be established. Therefore, in this project, the concept of Communication Center is introduced to ease the communication as well as to promote the future widespread of EVs. Figure 5.3.2 illustrates the concept of Communication Center.

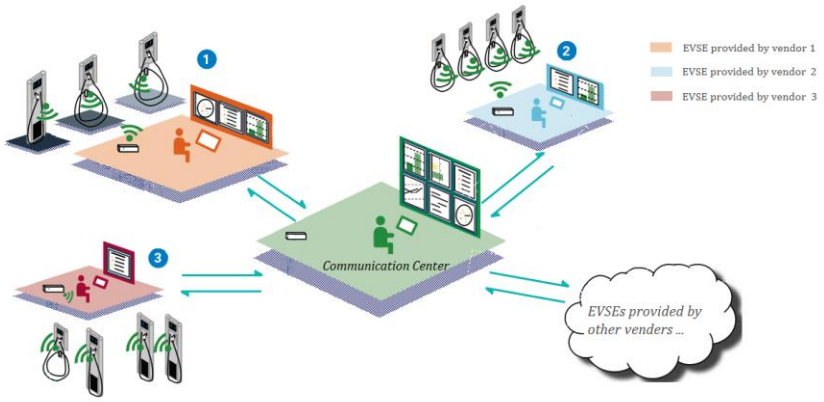

Figure 5.3.2 Illustration of Communication Center

The functionality of the introduced Communication Center includes:

- Communication realization and management: as is shown in Figure 5.5, the communication center is designed to be able to communicate bi-directionally with EVSEs provided by various vendors, and therefore, a uniform protocol compatible with all EVSEs might be required. Through this bidirectional communication between Communication Center and EVSEs, the Communication Center can not only gather data and information from EVSEs but also control those EVSEs according to different purposes. Besides, the communication among EVSEs from different vendors can also be realized indirectly through Communication Center. However, through Communication Center, the indirect communication among EVSEs can be better managed, for example, the information to be communicated will be first sent to and examined by Communication Center so as to verify the validness of the information before it is sent to the destination EVSE. The effectiveness of the communication as well as the controllability on EVSEs can therefore be greatly guaranteed.
- Data acquisition and management: through the bidirectional communication, the Communication Center is able to gather all the data from EVSEs provided by various vendors by whom different communication protocol might be adopted. Through the proper management on those data, it will provide significantly meaningful and useful information to drivers, charging station owners, utilities, aggregators, etc. For example, the data can help aggregators to better make their decision on how to bid into market so as to make profit for EV drivers as well as to help alleviate the negative impact EVs may exert on the power grid; the data can also help drivers better optimize their charging schedule to some extent; also, the data can help utilities better forecast the electricity need from EVs so as to upgrade the facility if needed and make wiser decision on how to purchase the electricity in the wholesale market, etc. In all, the collection and management of the data is of great importance in helping building safer and stronger power grid and at the same time in expediting the acceptance and future popularization of EVs.

- Information provision to drivers: another important functionality of Communication Center is to provide information to EV drivers. Since EV drivers are the direct target customers of EVs, their need and convenience should be taken into serious consideration. If without the Communication Center, EV drivers might have to visit different interface in order to check their charging information since it is hard for them to always charge through the EVSEs from the same vendor if they need to go to different places regularly. This will bring EV drivers great inconvenience and lead to harder optimization of their charging activity. Hence, the proposed Communication Center should be able to provide the information needed for those EV drivers and provide them with statistic report and tools to help them optimize their charging activity since it will take quite a long time for an EV to get fully charged unlike the conventional vehicle, under which circumstance, the schedule of charging activity in advance appears particularly important and necessary. In a word, the introduction of Communication Center can bring great convenience for EV drivers.
- Control and optimization: with the bidirectional communication between Communication Center and various EVSEs, Communication Center can control EVSEs according to different purposes. For example, when the load of the power grid is at its peak time, Communication Center may be able to limit the charging from EVs by control the state of EVSEs. By proper strategy, Communication Center may be able to realize some optimization function such as optimize the charging according to the price of the electricity market by sending the control signal to EVSEs as well as the incentives to EV drivers. The control and optimization functionality can thus help EVs alleviate their negative impact on the grid and better participate into the electricity market.

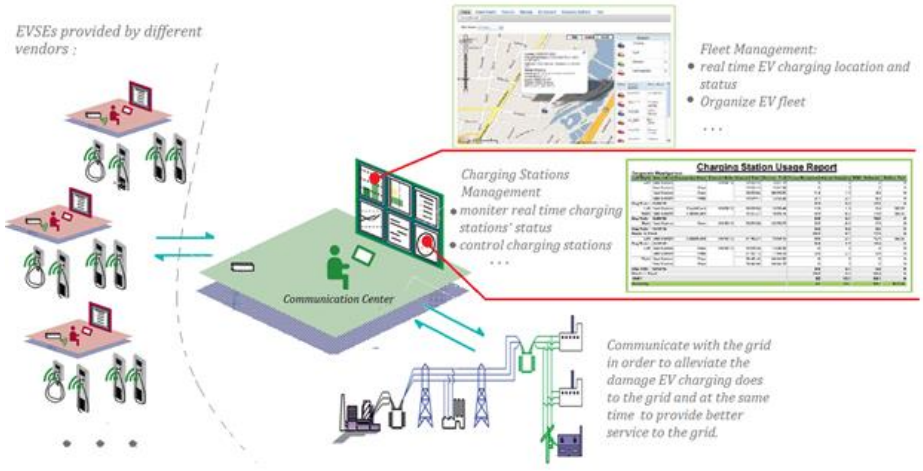

Figure 5.3.3 Illustration of Communication Center as Interface with Other Entities

- Interaction with other entities: in order to enable EVs to bid into electricity market, aggregators will be needed to assist with that. Hence the Communication Center should be able to communicate with aggregators and provide them with the information needed so as to help them make better decision. Moreover,

Communication Center can become one of the ways to help aggregators implement their bidding by sending control signal to EVSEs and incentives to EV drivers. Other than aggregators, Communication Center should also be able to interact with other entities such as utilizes, etc. It should be able to provide utilities with necessary data and assist them when needed. Communication Center can be therefore viewed as the interface between EVs and other entities. Figure 5.3.3 illustrates this concept.

5.3.2 The Advantage of Adopting Communication Center

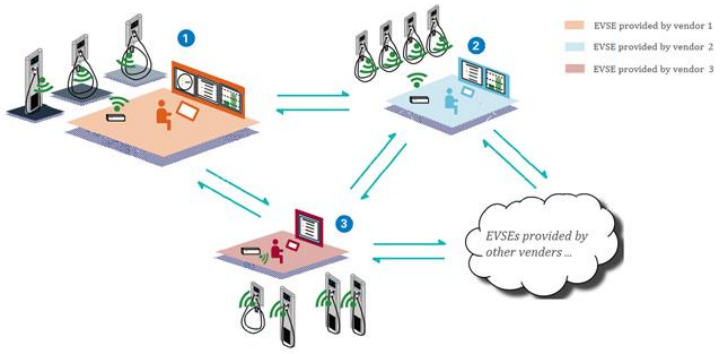

Figure 5.3.4 Illustration of Direct Communication among EVSEs from Different Vendors

As described in the introduction part, the communication among EVSEs will be needed in order for the future development of EVs. Compared with the direct communication structure which is illustrated in Figure 5.3.4, the multilayered structured in which the Communication Center is introduced as a new layer illustrated in Figure 5.3.2 has some advantages.

- Efficiency in utilizing charging resources: as stated in [67], " Network structure is critical to improve charging station utilization efficiency and to charge as much as possible EV with limited resource." Usually, EVSEs distribute into different regions, even the EVSEs from the same vendor, and may belong to different power grade according to different types of charging facilities. Therefore, the layered network structure based on the region or power grade might be appropriate and help improving the efficiency in making full use of the charging resources. Since it will be more convenient and realistic to optimize the charging or resource utilization in one region or under one power grade because of the similar characteristic under the same region or power grade.
- Easier to implement: EVSEs provided by various vendors have their own ways of communication, a new protocol will have to be studied and invented in order to enable those EVSEs from different vendors to directly communicate with each other if the direct communication structure is going to be adopted. If the layered structured is adopted, those EVSEs can first communicate with the monitor in the charging station and then different charging station can communicate with

Communication Center located in that area by using TCP/IP protocol which is already a quite mature protocol. Besides, in the direct communication structure, every EVSE or charging station monitor has to deal with the problem of simultaneous communication, for example, when A requests to communicate with B, C also requests to communicate with B. However, if Communication Center is introduced, only the Communication Center will have to deal with this issue which greatly ease the implementation.

- Compatible with future aggregative architecture: in order for EVs to participate into the electricity market, aggregators will be needed in order to help and coordinate EVs to better bid into market. As described in [68], there are two architectures for EVs to provide ancillary services: deterministic architecture (as shown in Figure 5.3.5) and aggregative architecture (as illustrated in Figure 5.3.6). It is also concluded that compared with the deterministic architecture, the aggregative architecture is more reliable and provide more convenience for EVs and aggregators to better bid into electricity market under a large scale of adoption of EVs in the future. Compare the aggregative architecture with our proposed multilayered structure where Communication Center is introduced, we can observe that our proposed Communication Center structure is quite compatible with the aggregative architecture. Since the Communication Center in every region or power grade can act as the aggregator or at least provide information or control functionality to some extent for aggregator who is responsible for that area to perform his task. The Communication Center can therefore assist the work of aggregators because of the similarity in the communication structures.
- Data and communication management: with the introduction of Communication Center, data from EVSEs and communication among them can be better managed. Unlike the direct communication structure, the Communication Center can collect data from EVSEs and store them properly. With the collected data, more analysis can be done than the limited data within one charging station or EVSEs from one vendor. Moreover, with those data, it will be easier to optimize the charging and for aggregators to bid into the market. Besides, the communication among different EVSEs can be better managed by the proposed Communication Center who acts as an intermediary among them. Since the information to be communicated among EVSEs will have to be first sent to and assessed by the Communication Center. Those EVSEs owners or charging station owners care most their own interest instead of the condition or the interest for others. Under some circumstances, the decision they make may harm the grid or other people's interest, therefore, the Communication Center will be needed to manage the communication with the consideration of optimizing the interest in that region.

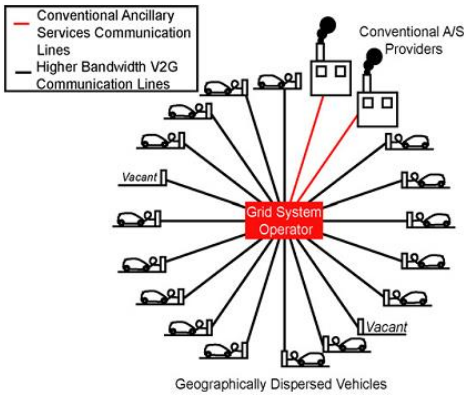

Figure 5.3.5 Illustration of Deterministic Architecture

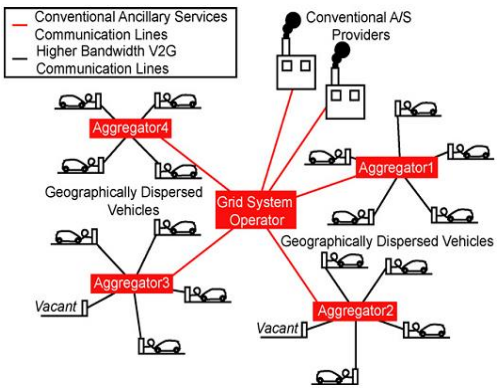

Figure 5.3.6 Illustration of Aggregative Architecture

- Intercommunication with other entity: the proposed concept of Communication Center, as an intermediary among EVSEs or charging stations, can act as the interface for EVs to interact with other entities, such as aggregators, utilities, system operators, etc. Through the Communication Center, EVs can better cooperate with other entities in order to alleviate their negative impact and provide ancillary service if needed. Moreover, EVs can also get information from other entities, such as the price of the electricity and so on, so that they can better operate in the real-time and make more interest based on the information. The multilayered structure may ease this functionality compared with the direct communication structure.

5.3.3 Communication Center Design

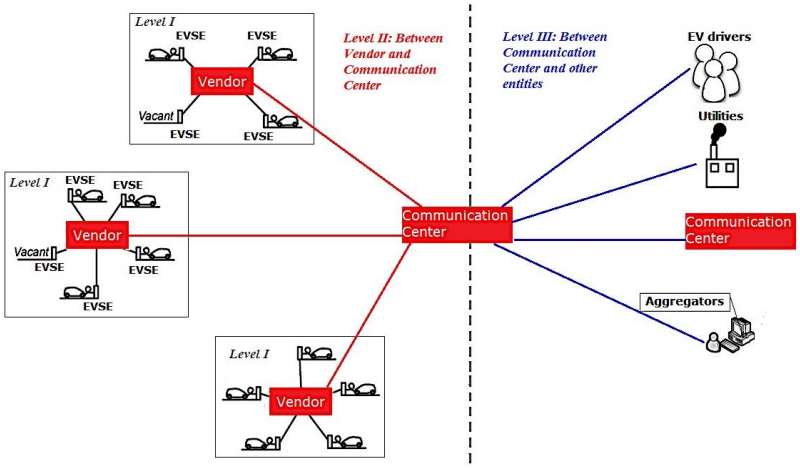

Figure 5.3.7 Illustration of Multi-layered Communication Structure

1. Communication structure

As mentioned above, multi-layered structure of communication will be selected to realize the communication among EVSEs from different vendors which is illustrated in Figure 5.3.7. Three layers are shown in the Figure 5.3.7:

- First layer is shown on the left of the dashed grey line which is between EVSEs and charging stations or EVSEs and their belonging vendors. For different vendors or charging stations, different communication protocol might be adopted and the data from those EVSEs will be first collected and stored into the database of their belonging charging stations or vendors.
- Second layer lies between different vendors or charging stations and our proposed Communication Center. During this layer, the data from EVSEs will be collected from different vendors or charging stations if needed. The bidirectional communication may allow the Communication Center to realize some control functionality and help realize the indirect communication among EVSEs provided by different vendors.
- The third layer is the communication between Communication Center and other entities, which could be aggregators, utilities, EV drivers or even another Communication Center in other region. With this third layer, the proposed Communication Center can cooperate with each other or aggregators and provide information to other entities which is of vital importance to the future widespread of EVs.

2. Communication protocol

With this multi-layered communication structure, vendors or charging stations just have to deal with the communication with their own product or facilities, and there is no direct communication among EVSEs from different vendors. Moreover, since every vendor server or charging station can have the access to the internet, TCP/IP protocol, which is a quite mature protocol, will be enough to realize the communication. Hence, TCP/IP protocol will be adopted here for the Communication Center to communicate with charging station or vendors.

3. Database

One of the functionality of the proposed Communication Center is to collect and store data from EVSEs provided by different vendors, and therefore database will be needed by the Communication Center where those necessary data can be stored appropriately. The database will be updated in real-time and be backup in time so that the data needed will be available for calculation and operation.

4. Interface with other entities

As another functionality of the Communication Center, it should be able to provide EV drivers with their charging information. This requires that the Communication Center should have the interface to communicate with those EV drivers. Besides, since the Communication Center will have to communicate bi-directionally with charging stations or vendors, interface to deal with the communication with charging stations or vendors will also be needed. Moreover, since the Communication Center is supposed to communicate with other entities like aggregators or utilizes, the interface to deal with that communication should also be developed and integrated into the Communication Center. One of the common and easiest way to realize those interface might be to develop particular webpages for those target customer to login and communicate with the Communication Center. Therefore, no more particular software will be needed to develop or installed in the customer side. However, this method may also has its own limitation when realizing some control schemes.

6. Communication between Charging Infrastructures and Communication Center

6.1 Data Requirement Analysis and Data Acquisition

The proposed Communication Center is designed to have multi-functionalities as described in the Section 5.3.1. In order to realize those functionalities, different data should be available from charging stations or vendors at specified time interval. However, the fact is that the data needed from Communication Center might not be accessible due to various reasons, for example, the data needed are not collected by vendors or charging stations; the data are available but cannot be transmitted to the Communication Center at the required time interval, etc. As a result, the functionality of the Communication Center should be therefore adjusted according to the practical condition.

This section will first analyze the data need according to the ideal functionality design of Communication Center. Then a survey on the practical available data from different vendors will be conducted.

6.1.1 Data Requirement Analysis

According to the direction of the data transmission, the data can be classified into two main categories, one is transmitted from charging stations to the Communication Center, and the other is transmitted in the opposite direction. In each category, the data can be further grouped according to how often they will be requested.

1. Data direction: From charging stations/vendors to the Communication Center

In order for the Communication Center to better perform its duty, it should store some basic information of the charging centers in the region such as the address, number of chargers of the charging station, etc. Such basic information cannot be easily changed as compared with those real-time data, and therefore can be transmitted just once especially when the charging station is first put into operation. Table 6.1 lists the possible required one-time data needed from charging stations.

Table 6.1 List of One-time Data Needed from Charging Stations

As <actor>	I want to <do something>	So that <goal>
Charging station	Send location to communication center	The center can know some basic information of the new charging station
Charging station	Send the number of chargers in the station to communication center	The center can know some basic information of the new charging station
Charging station	Send the power supply capability of the station to communication center	The center can know some basic information of the new charging station

Table 6.1 List of One-time Data Needed from Charging Stations (continued)

As <actor>	I want to <do something>	So that <goal>
Charging station	Send the type of chargers in the station to communication center	The center can know some basic information on chargers in the new charging station
Charging station	Send the ranges of rated voltage of chargers in the station to communication center	The center can know some basic information on chargers in the new charging station
Charging station	Send the ranges of rated current of chargers in the station to communication center	The center can know some basic information on chargers in the new charging station

For the purpose of enabling Communication Center to better monitor the state of the charging stations, real-time data will be requested from the Communication Center. Some data will be triggered by the event, for example, when there is a vehicle starting charging, there will be a charger whose state will change from idle to busy. And other real-time can be sent during interval, for example, the charging voltage and current should be sent based on small intervals so as to be better monitored. Table 6.2 and Table 6.3 list the event-triggered data and interval based data needed by the Communication Center respectively.

Table 6.2 List of Event-triggered Data Needed from Charging Stations

As <actor>	I want to <do something>	So that <goal>
Charging station	Send the real-time price to communication center	The center can know the prices of all charging stations
Charging station	Send the status of EVSE units (ready, busy or fault) to the communication center	The center can know the availability of EVSE units
Charging station	Send the customer ID to the communication center when the status of chargers is changed to busy	The center can know the charging information of EVSE units
Charging station	Send the charging type to the communication center when the status of chargers is changed to busy	The center can know the charging information of EVSE units
Charging station	Send the total energy consumption to the communication center when the status of chargers is changed to ready or fault from busy	The center can know the charging information of EVSE units
Charging station	Send the charging duration to the communication center when the status of chargers is changed to ready or fault from busy to busy	The center can know the charging information of EVSE units

Table 6.3 List of Interval-based Data Needed from Charging Stations

As <actor>	I want to <do something>	So that <goal>
Charging station	Send the exact charging voltage to the communication center when the status of a charger is busy	The center can know the power of the charger at that time
Charging station	Send the exact charging current to the communication center when the status of a charger is busy	The center can know the power of the charger at that time
Charging station	Send the exact SOC of the vehicle which is connected to that charger to the communication center when the status of a charger is busy	The center can know the SOC of the vehicle

2. Data direction: from communication center to charging stations

The data sent from the Communication Center to charging stations will help realize the control functionality and provide necessary information for charging stations. Like the real-time data needed from charging stations, the data needed from the Communication Center can also be divided into two groups, one is triggered by the event and the other is based on the time interval. Table 6.4 and Table 6.5 list the interval-based data and event-triggered data needed from the Communication Center respectively.

Table 6.4 List of Interval-based Data needed from the Communication Center

As <actor>	I want to <do something>	So that <goal>
Communication center	Send the prices of all other charging stations to that charging station	The charging station can know about prices of all other charging stations

Table 6.5 List of Event-triggered Data needed from the Communication Center

As <actor>	I want to <do something>	So that <goal>
Communication center	Send limitation of power to that charging station especially during the peak time	The communication center can adjust the power consumption from vehicle charging so as to alleviate the burden of peak power consumption

6.1.2 Practical data from vendors

In this project, we did a survey to the vendors on whether they pull data from their chargers, how they manage the obtained data, whether they provide the data to their customers and how the customers can manage the data. The table below summarized partial results of the survey based on their current availabilities.

Table 6.6 Results of the Survey

Vendors	Collect Data	Where to store	Provide data to users	Communication Details
ECOtality	Yes	Network	Yes, only to users	API: HTTPS POST
ChargePoint	Yes	Network	Yes, only to users	APT: HTTPS POST
Aerovironment	Yes	Network, intranet	Yes, only to users	API access, users have no access
eVgo	Yes	Network	No, only provide services	
PEP Station	Yes	Software	Yes, only to users	Send usage reports through emails
SemaConnect	Yes	Network	Yes, only to users	API access
GE	Yes	Network	Yes, only to users	API access, users have access
ABB	Yes	Network	Yes, only to users	Online Management Tool

6.2 Database Design for Communication Center

This part will summarize the development and current research status of outage management based on related papers. The possible impact of PHEVs/BEVs on utility distribution system in the area of outage management will be stated.

As described from the previous Section 6.1.2, not all data needed from our proposed Communication Center can be obtained due to various reasons such as the data are not collected; the data cannot be revealed to the third party because of the policy, etc. However, the hope can be held that those data will be accessible with the further development and popularization of EVs in the future.

As a consequence, the designed functionality of the Communication Center should therefore be modified according to the data available. From the survey in the above section, we can see that in most cases, vendors will be responsible for collecting the data from the EVSEs they provided and then send the data to charging stations through some software or communication methods if requested by the charging stations. Moreover, the data provided by different vendors may differ a little bit, and the common available data are as follows:

- Basic information of the charging station: location name, address (including street address, city, state and postal code), serial number;
- Charging event: connection time, disconnection time, cumulative energy, charger status;
- About customer: customer ID, fee, fee reason.

Therefore, some designed functionality cannot be realized because of the lack of data, for example, real time monitoring the charging voltage, current as well as the SOC of the vehicle, etc.

As stated in the Chapter 5, one of the most important functionality of the proposed Communication Center is to collect and manage data from EVSEs. Therefore, the database will be needed as a part of the Communication Center and it should be well designed to classify and store those data before we start collecting data from EVSEs.

First of all, we will have to know which data will be stored and managed in our database to be designed. Other than the common available data from vendors concluded above, as the Communication Center, it will also have to include the data on EV drivers, since it will have to provide the information for them and help them schedule their charging scheme as mentioned in the Chapter 5. Those data may include the Customer ID, their car brand, their battery capabilities, etc.

Besides, since the Communication Center will also have to perform as an interface with other entities, it may also have to store some data obtained from entities such as aggregators, utilities, etc. However, those data from other entities are not considered here in our design since they are not quite the focus of this project, but the database will be easily expanded in the future to include those data.

After the analysis on what data will be stored and managed in the database to be designed, we will have to properly design the database. As a good database, the redundancy and the "bad dependency" of the data should be avoided. Since the redundancy of the data will significantly increase the need of storage when there are a lot of data needed to be stored. Moreover, the "bad dependency" of the data will cause the misoperation of the database such as the accidental delete of information. Therefore, the database to be designed needs to be normalized according to some forms shown as follows:

- First Normal Form (1NF): "A relation is in first normal form if the domain of each attribute contains only atomic values, and the value of each attribute contains only a single value from that domain."[69]
- Second Normal Form (2NF): "No non-prime attribute in the table is functionally dependent on a proper subset of any candidate key."[69]
- Third Normal Form (3NF): "Every non-prime attribute is non-transitively dependent on every candidate key in the table. The attributes that do not contribute to the description of the primary key are removed from the table. In other words, no transitive dependency is allowed."[69]

There are more forms like Elementary Key Normal Form (EKNF), Boyce-Codd Normal Form (BCNF), Fourth Normal Form (4NF), Fifth Normal Form (5NF), etc. However, here in our design in this project, we just refer to the 1NF, 2NF and 3NF.

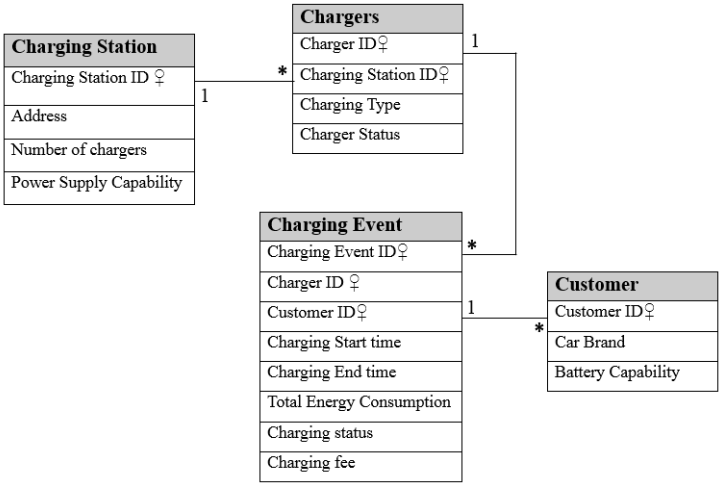

Figure 6.2.1 Illustration of the Relationship among Four Tables

Based on the three normal forms, the data we are going to store in our database can be divided into four tables:

- Charging Station: this table contains mainly the basic information of a charging station which includes the charging station ID, which is the key information used to differentiate different charging stations, address, number of chargers it owns, and its power supply capability;
- Chargers: this table is used to describe the basic information and relationship between chargers and their belonging charging stations, which includes the information like: Charger ID, its belonging charging station ID, its current status, and the charging Type of this charger (whether it is a slower charger, fast charger, etc.);
- Charging Event: this table mainly characterizes the charging event and it established the relationship between chargers and customers. It includes the information like: charging event ID, charger ID, customer ID, charging start time, charging end time, total energy consumption of this charging event, charging status and charging fee.
- Customer: as stated before, the Communication Center also has to have EV drivers' information, and this table has the items as follows: customer ID, the car brand of the EV, and its battery capability.

And the relationship among each table can be shown as Figure 6.2.1.

6.3 Data Acquisition Methods

After the proper design of the database for the Communication Center described in the previous section, next step is obtain those data and store them into the database automatically. From the survey on the available data from other vendors, we can also know the fact that usually the vendor will be responsible for collecting the data from the EVSEs provided by themselves to the charging station owners or operators if requested.

There are different ways of transmitting data back to the charging station side. One of the common ways among different vendors is to establish website for charging station owners to register and log in to obtain their data. Also, the Application Programming Interface (API) can be found in some of the websites provided by vendors such as Blink. As described in [70], "An application programming interface (API) specifies how some software components should interact with each other. In addition to accessing databases or computer hardware, such as hard disk drives or video cards, an API can be used to ease the work of programming graphical user interface components." Therefore, with the help of API, it will be much easier for charging station to develop their own software to obtain the data from vendor side automatically. For those vendors who do not provide API, it will be harder for charging station owners to get access to the data automatically, hence new methods need to be explored. In this section we will talk about how to acquire data from vendors automatically, and two scenarios will be mainly discussed, one is the one with API provided and the other is the one without API.

Before we go on to talk about the acquisition of the data, there is one more thing that needs to be clarified which is how often the Communication Center can get access to those data. As mentioned in Section 6.1.1, the Communication Center needs two kinds of data based on the frequency of the data being transmitted: one is the interval-based data, and the other is the event-triggered data. However, it is hard for vendors to send those data when triggered by the event, since their original software may need to be modified in order to realize that function. The way we are going to handle with that is to treat those supposed event-triggered data the same way as interval-based data, i.e. to acquire them in intervals. Although this might cause a little error on time, the error can be controlled within certain limit when the time interval is chosen to be small. The reason for that is: 1) the Communication Center is a new concept and it is not easy at this stage to convince vendors to modify their software; 2) it will be easier for the concept of Communication Center to be accepted by vendors since they won't have to do a lot if they choose to erect the communication with the Communication Center.

6.3.1 Data Acquisition from Vendors through API

The purpose here for the Communication Center is to obtain data automatically from the charging stations and store them into its own database. Since vendors will be responsible for collecting and transmitting the data, instead of collecting data from charging stations, the Communication Center can obtain data directly from the vendors.

As mentioned above, it will be easier to develop the software with the help of the API provided by the vendors. With the API, the Communication Center can directly go to websites provided by vendors and use the API tool to access the data automatically through the software properly developed.

The target of the software: automatically get access to the data of charging stations from belonging websites provided by vendors and then store them properly into the database in the Communication Center with the help of API.

The choice of tool: here in this project, we choose JAVA as the programming tool to develop the targeted software, since 1) it can work well with API; 2) it has well developed interfaces with different database software, such as Oracle, Access, etc. 3) it is mature regarding to communication functions and can be easily connected to other software; 4) the function of the Communication Center can be easily expanded in the future by using JAVA.

Decomposition of the task: the whole task of the software can be decomposed into the following parts:

- Connect to the website by using API: by importing the proper classes or libraries in JAVA, the program will be able to connect to the website provided by vendors without manually opening the internet explorer, clicking on different items, etc. with certain information given by vendors such as a token. The following classes will be needed for realizing this function:
    - org. apache. Commons. httpclient. HttpClient
    - org. apache. Commons. httpclient. HttpMethod
    - org. apache. Commons. httpclient. NameValuePair
    - org. apache. Commons. httpclient. method. PostMethod
    - By applying the PostMethod, all the data information can be returned as a long string which can be input for the next parts;
- Connect and write data into the database: in this project, as a testbed, we choose Access to build up the database of the Communication Center. The program here acts like the interface between the website and the database realized through Access. The good thing is that JAVA also supports the connection with several database software including Access, and it support the Structured Query Language (SQL) which "is a special-purpose programming language designed for managing data held in a relational database management system (RDBMS)."[71] And the classes enable the use of SQL to operate the database in JAVA program is under the package of java. sql.
- String operation: after obtaining the data from the website, since they are in string format, necessary operation will be needed to filter the string to get the data interested. But before doing that, the format of the string value should be studied so as to find the way to further filter that string. The rough flowchart of string operation can be illustrated in Figure 6.3.1.

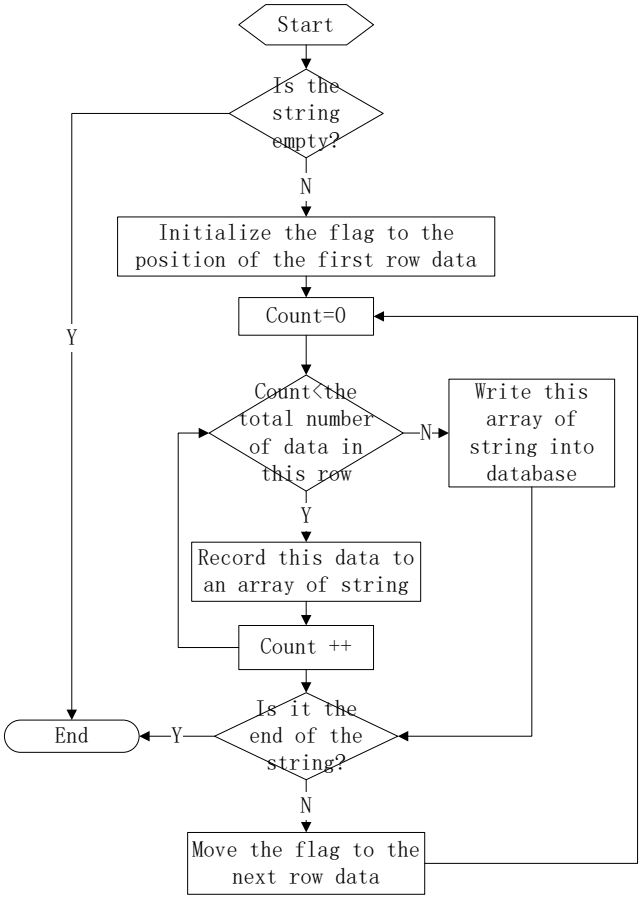

Figure 6.3.1 Illustration of Flowchart of String Operation

And the flow of the acquiring data from vendors with API provided can be shown in Figure 6.3.2.

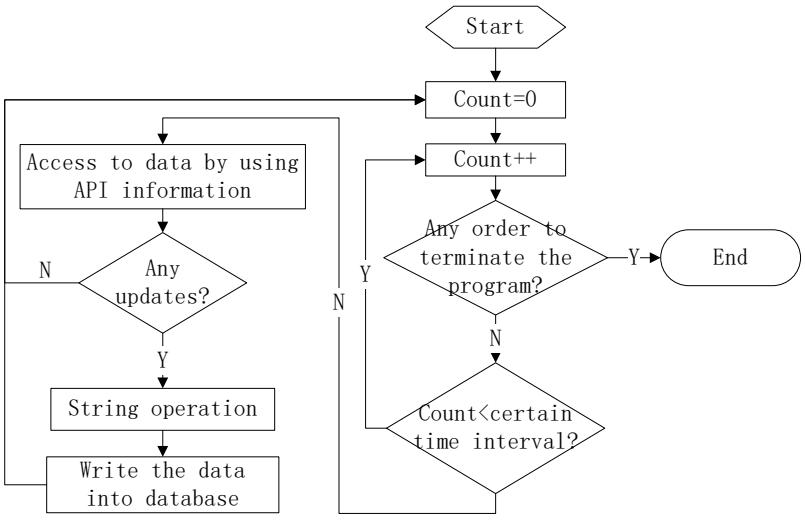

Figure 6.3.2 Flowchart of Acquisition of Data through API

6.3.2 Data Acquisition from Vendors through other Method

As is mentioned in the survey on the available data from vendors, not all the vendors provide API in their website, and thus leading to the difficulty for automatically collecting data from vendors. However, we notice that although API may not be available, some vendors can still send those data through emails to their customers in a required format and at the required frequency. This provides another possibility to acquire data from vendors automatically.

The target of the software: automatically get access to the data of charging stations from belonging vendors through emails and then store them properly into the database in the Communication Center. This means the software to be developed will have to check the email box at a fixed frequency and extract the data from the.

The choice of tool: here, again, JAVA will be chosen as the programming tool to realize this function, since it has interface to interact with the email system when certain classes or libraries are included in the program. Besides, the software to be developed to interact with the email system can be easily integrated with the one connecting with the website by API, as developed in the previous section, since they are both developed in JAVA language.

Decomposition of the task: the whole task of the software can be decomposed into the following parts:

- Connect to the email system: the software will have to connect to the designated email box automatically. By including certain classes or libraries under the package of javax.mail, JAVA program can connect to the email system. The flowchart to check emails is shown in Figure 6.3.3.
- Read file and string operation: after downloading the files from those unread emails sent from vendors, the next step is to read files, extract the data from files and convert them into string. File operation can be realized by including some classes under package java.io. After that, the string operation will be needed and the procedures are quite similar to the one shown in Figure 6.3.1.
- Connect and write data into the database: this part is also pretty similar to the same part described in the Section 6.3.1.

Therefore, the whole program to realize the function of connecting to the email system can be illustrated in the Figure 6.3.4.

As mentioned above, these two programs can be easily merged into one program, since they are both programed in JAVA. The flow chart of the merged program can be shown in Figure 6.3.5, and the detail on how to connect to the data through email or API and how to store the data into database can be referred to the content discussed above.

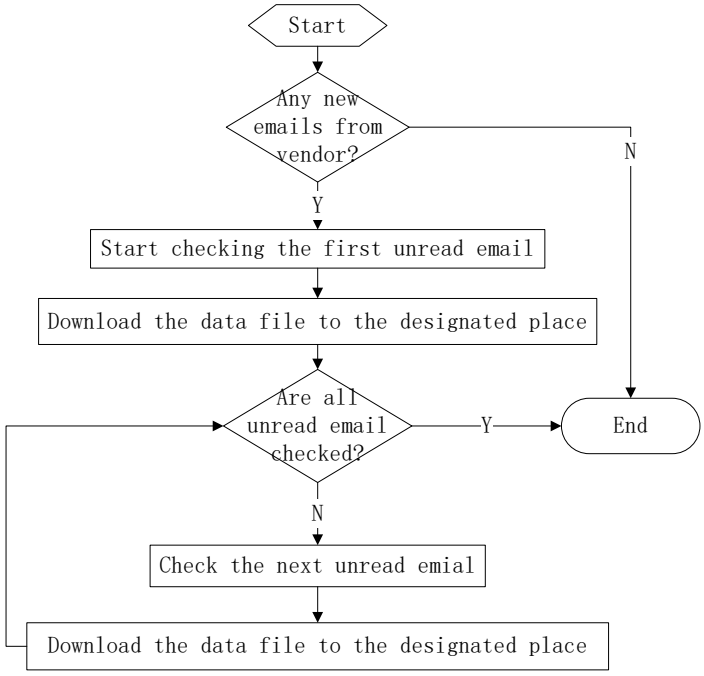

Figure 6.3.3 Flowchart of Checking Emails

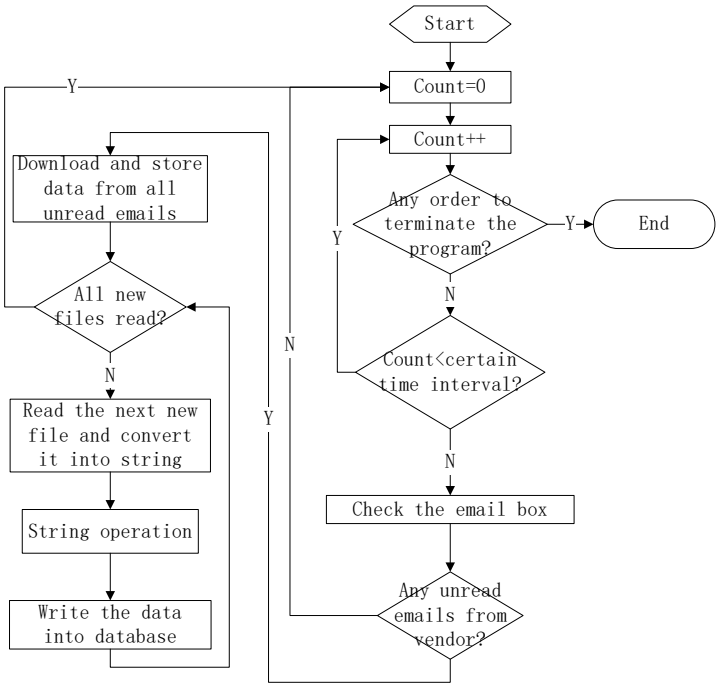

Figure 6.3.4 Flowchart of Acquisition of Data through Email

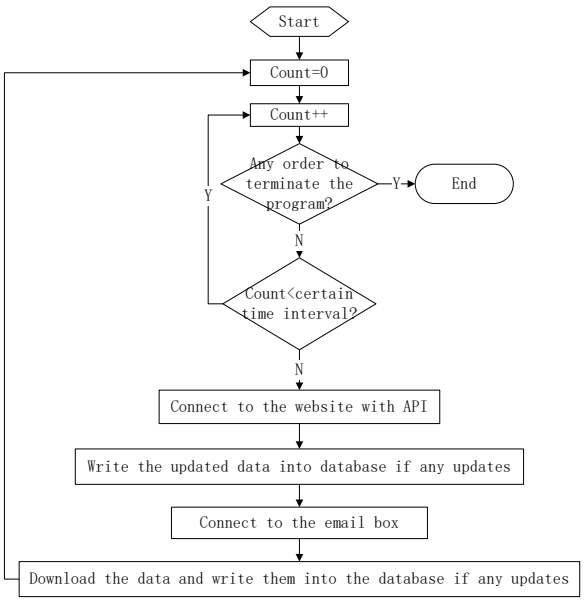

Figure 6.3.5 Flowchart of the Merged Program

7. Advanced Infrastructures for Optimal Utilization of EVs and PHEVs

7.1 Introduction

This section introduces a new infrastructure that takes advantage of state of art technologies. The infrastructure is used as the basic framework for a house energy management system. This new infrastructure has the potential to optimize the operation of the overall distribution feeder of an electric power grid, assist the grid operations via ancillary services and mitigate the negative impacts on distribution transformers. The key elements of the approach are (a) coordinated integration of EVs/PHEVs in the electric distribution system and (b) no inconvenience to the customers, i.e. no changes in the life style of the residential/commercial customer. A description of the proposed infrastructure is given next.

7.2 Description of House Energy Management System Infrastructure

The new approach assumes that the system that it monitors is highly penetrated with distributed energy resources (DER) such as roof-top solar photovoltaic (PV), energy storage system such as battery, intelligent electronic devices (IED), EVs/PHEVs, and smart and controllable/non-controllable appliances. This assumption provides an important base for the data necessary to perform real time system monitoring and control of the system various components. The advantages of implementing this new approach are many. The major one is that it will enable for real time management and control of all the different components that are connected to the residential/commercial building that the customer owned. Therefore, the burden of integrating new loads such as EVs/PHEVs is lessened. Furthermore, it will enable the implementation of different desired optimization functions for the operation of the distribution power grid to extract the maximum benefits to both the utility and the customer, without incurring any inconvenient to the end-user (customer). The overall approach of the newly designed scheme is illustrated in
Figure . The infrastructure consists of the following three modules:

- Physically based model of every component in the system,
- Distributed State Estimation (DSE),
- Asset scheduling optimization.

The advanced infrastructure scheme works as the following: measurements, whether synchronized or non-synchronized from various power distribution components and residential/commercial buildings devices … etc. are collected. Residential/commercial building resources and appliances measurements can be collected by what is known as Home Area Network (HAN); while other filed measurements can be collected by instrumentation meters such as Universal GPS Synchronized Meter (UGPSSM) [72]. All of these measurements are sent to a local hardware (computer) where the distribution state estimation algorithm is. The estimation process is performed on the collected measurements and the outcome is a well reliable and validated real time model of the entire system. Real time model of the system is then used by the house/commercial management system to perform various functions.

An important function is the optimization. Results of the optimization are the in the form of scheduling control signals of the building smart appliances and energy resources such as electric vehicles charging/discharging, open/close smart switches, smart dishwasher operation, and energy storage battery system charging/discharging… etc. To perform an optimization over a finite horizon of time, the developed system needs information regarding the environmental future forecast for solar irradiance, outside temperature, relative humidity, and building loads … etc. Therefore, a forecasted module is integrated into the system to perform parameters forecasting and stream the resulted data to the optimization. It provides, in particular, forecasted data to the system for the short term horizon, maximum a day. Also, it updates the forecasted data as the time progresses and real data are coming in. All these modules and algorithms (energy resource and appliances models, state estimation algorithm, and optimization) can be integrated in a hardware that is located at house/commercial building, which can provide the customer with the latest and most updated energy usage and saving. More details regarding every module is provided in the following sections. The physical based modeling approach adopted in this work is explained next.

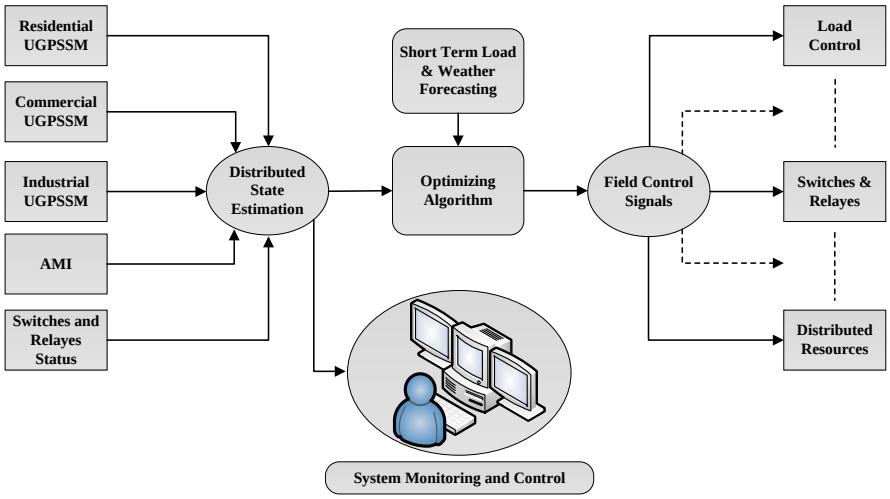

Figure 7.2.1 Illustration of the New House Energy Management System Infrastructure

8. System Component Modeling

8.1 Introduction

There are several different approaches that one can use to designing systems and models. However, the physically-based modeling approach is the most desired one, because it is based on how the system lays out in the physical world. Basically, the physical system is represented by a detailed, yet well understood, abstract mathematical model. This mathematical model is then used to simulate the physical system and further develop various applications. In this section, the general modeling approach used to model various system components; and the integration method used to solve the differential equations, if exists in the model, are discussed. In addition, new electro-thermal models for important components in the residential/commercial building are physically modeled.

8.2 Object Orientation Modeling Approach

Several methods are available in the literature to model a system or a device. Yet, one powerful approach is the object orientation modeling approach. It is a popular technical approach to analyzing, designing an application, a device, or a system by applying the object oriented paradigm and visual modeling throughout the development life cycles. The advantages of this approach are many; however salient benefits are listed below:

- Provides a unified syntax to all various power system components, associates controls, and also advanced applications such as state estimation, optimization, and protection.
- Simplifies communication between various parts of the developed application in an efficient and reliable manner and without losing information.
- Improves the stability and thus the quality of the application.
- Facilitates and simplifies the integration of new device, system, or application with other existed components (Plug and Play concept). Therefore, no need for alternation of existing applications.
- This generalization enables standardization for utilizing and exchanging the model of a device for other advanced smart grid applications.

In the next section, the procedure used from abstracting the mathematical model to integrate various devices in one system is discussed.

8.3 Description of Device or System Modeling Procedure

Every device, system, or application goes through a number of steps to become in one unified standard form. The modeling procedure followed is illustrated in Figure 8.3.1 and explained as the following:

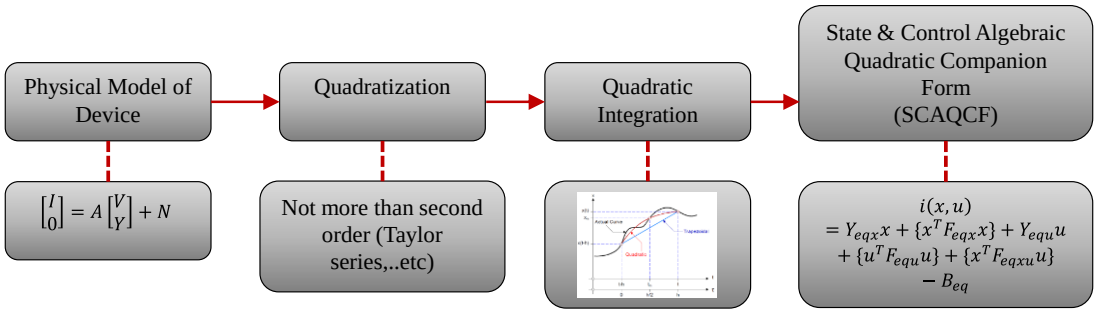

Figure 8.3.1 Device, System, or Application Modeling Procedure

1. Mathematical Model Extraction

The abstract mathematical model of a device is derived based on the physical system as it is the physical world. This model is, simply, formulated as a set of linear and nonlinear differential algebraic equations (DAEs) and algebraic equations in terms of the device various state and control variables. The derived mathematical model is then cast in a simple compact form as given in (8.1).

$$\begin{bmatrix} \mathrm{i(t)} \\ 0 \end{bmatrix} = \mathrm{A} \begin{bmatrix} \mathrm{v(t)} \\ \mathrm{Y(t)} \end{bmatrix} + \mathrm{B} \tag{8.1}$$

Where
i(t): Vector defining the through variable of the model.
v(t): Vector defining the across (external) state variables of the model.
Y(t): Vector defining the internal state variables of the model.
A: Matrix defining the linear and nonlinear part of the model with appropriate dimension.
B: Vector defining the constant part of the model with appropriate dimension.

2. Model Quadratization

The extracted mathematical model is then quadratized. Simply, any nonlinear equation that is above degree two is reduced to degree not higher than two. The reduction procedure is performed by introducing slack variables. Nonlinear functions such as exponential function or logarithm function is also quadratized by using Maclaurin series expansion around zero. Slack variables are used as necessary to reduce the order of the model to a degree that is not higher than the second order. Several examples of function or system quadratization can be found in [73-75].

3. Model Quadratic Integration

The resulting differential and algebraic system of equations are integrated using the quadratic integration method based on [76]. For a system of equations, whether linear or nonlinear, especially for stiff systems when power electronics with IGBTs switches or induction machines are part of the model, the quadratic integration method has exhibited superiority over other integration methods such as Trapezoidal method. Below is a list of advantages of using it in the power system:

- Numerical oscillation free method and therefore a stable integration.
- The method is of the order of four. Solution is achieved with high numerical accuracy and precision.
- Fast convergence with low number of iteration.

Based on three point collocation method, the quadratic method is formulated; and used to convert the system of equations into a set of algebraic linear or quadratic equations. The concept of the quadratic integration method adopted in this work is illustrated in Figure 8.3.2. It is unlike the Trapezoidal integration method, where the system model states are assumed to vary linearly throughout the time step, the quadratic integration method is assumed that within every integration time step, the system states variables vary quadratically. In principle, within every integration time step of length h, which is defined by an interval [τ − h,τ], the two end points x[τ – h] and x[τ], and the midpoint xm , defined by (xm = x[τ – (h / 2)]), can define a quadratic function in the interval [t − h,t]. This function is then integrated in the time interval [τ − h,τ] resulting in a set of algebraic equations for this integration step. The solution of the equations is obtained via Newton's method. Note that the resulting algebraic equations are either linear or quadratic [76].

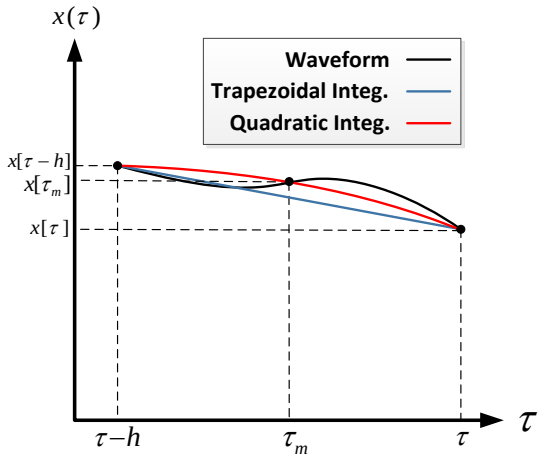

Figure 8.3.2 Illustration of Quadratic Integration Method

To show the difference between the quadratic integration and the trapezoidal integration, a case study of a series RLC circuit is modeled. Results of this case including the difference between the two integration methods are reported in Appendix A.

4. State and Control Algebraic Quadratic Companion Form (SCAQCF)

Then, the state and control variables are separated and then formed according to the State and Control Algebraic Quadratic Companion Form (SCAQCF) given by (8.2) in a detailed notation and (8.3) in a matrix notation. The main advantage of the SCAQCF model is that this formulation gives the generalized and abstract model for any component of the power

system, which is independent of the type of the device and is suitable for implementation of object-oriented algorithms for any application.

SCAQCF in detailed format:

$$\begin{bmatrix} \tilde{I}(t) \\ 0 \\ \tilde{I}(t_m) \\ 0 \end{bmatrix} = Y_{eq\_x} \begin{bmatrix} \tilde{V}(t) \\ Y(t) \\ \tilde{V}(t_m) \\ Y(t_m) \end{bmatrix}$$

$$+ \begin{bmatrix} [\tilde{V}^T(t) \quad Y^T(t) \quad \tilde{V}^T(t_m) \quad Y^T(t_m)] \quad F_{eq\_x\_1} \quad \begin{bmatrix} \tilde{V}(t) \\ Y(t) \\ \tilde{V}(t_m) \\ Y(t_m) \end{bmatrix} \\ \vdots \\ [\tilde{V}^T(t) \quad Y^T(t) \quad \tilde{V}^T(t_m) \quad Y^T(t_m)] \quad F_{eq\_x\_n} \quad \begin{bmatrix} \tilde{V}(t) \\ Y(t) \\ \tilde{V}(t_m) \\ Y(t_m) \end{bmatrix} \end{bmatrix} \tag{8.2}$$

$$+ Y_{eq\_u} \begin{bmatrix} \tilde{U}(t) \\ \tilde{U}(t_m) \end{bmatrix} + \begin{bmatrix} [\tilde{U}^T(t) \quad \tilde{U}^T(t_m)] \quad F_{eq\_u\_1} \quad \begin{bmatrix} \tilde{U}(t) \\ \tilde{U}(t_m) \end{bmatrix} \\ \vdots \\ [\tilde{U}^T(t) \quad \tilde{U}^T(t_m)] \quad F_{eq\_u\_n} \quad \begin{bmatrix} \tilde{U}(t) \\ \tilde{U}(t_m) \end{bmatrix} \end{bmatrix}$$

$$+ \begin{bmatrix} [\tilde{V}^T(t) \quad Y^T(t) \quad \tilde{V}^T(t_m) \quad Y^T(t_m)] \quad F_{eq\_xu\_1} \quad \begin{bmatrix} \tilde{U}(t) \\ \tilde{U}(t_m) \end{bmatrix} \\ \vdots \\ [\tilde{V}^T(t) \quad Y^T(t) \quad \tilde{V}^T(t_m) \quad Y^T(t_m)] \quad F_{eq\_xu\_n} \quad \begin{bmatrix} \tilde{U}(t) \\ \tilde{U}(t_m) \end{bmatrix} \end{bmatrix}$$

$$- B_{eq}$$

SCAQCF in a matrix format:

$$i(x, u) = Y_{eqx}x + [x^T F_{eqx} x] + Y_{equ}u + [u^T F_{equ} u] + [x^T F_{eqxu} u] - B_{eq} \tag{8.3}$$

where
x: the external and internal states at time t and time tm.
u: the control variables at time t and time tm.
Y_{eqx}: matrix defining the linear part of device state variables.
F_{eqx}: matrix defining the nonlinear part of device state variables.
Y_{equ}: matrix defining the linear part of device control variables.
F_{equ}: matrix defining the nonlinear part of device control variables.

F_{eqxu}: matrix defining the nonlinear part of device state control variables.
B_{eq}: vector defining the constant part of device model.
t_m: a middle point in the integration time step h.

More details concerning the extraction of the final model in SCAQCF format is provided in Appendix A.

To better manage the undesirable impact of increasing number of EVs/PHEVs, the house management system model has to be able to monitor and control, in continuous fashion, the house appliances and resources. These domestic appliances and resources should be physically modeled. The model should take into account the thermodynamics behavior of the system since it is in a large part would determine, mostly, the energy consumption. In this project, the electromagnetic transient phenomenons are not of interest because of their small time scale feature and thus not considered in the model of the resources and appliances. In other word, the modeling domain that is considered is the quasi-dynamic time domain, which ignores the fast moving behavior such as power electronics switching; but it considers the slow moving behavior such as house temperature, EV's battery charge … etc.

Therefore, the following devices are considered to be part of the house management system: electro-thermal center tap transformer, electro-thermal model of a house, smart appliances including, smart dishwasher, electro-thermal refrigerator, electro-thermal air conditioner. Other house loads such as lighting, cloth washer and dryer …, are modeled as a time variable load. Distributed energy resources (DER) such as roof top solar photovoltaic (PV), energy storage battery system (BESS), and EV/PHEV, modeled as lithium ion battery, are also modeled. Averaged models of battery system charger in the form of a DC-DC buck-boost converter, DC-DC boost converter, DC/AC inverter, and all devices associated control circuits are additionally considered. It should be noted that these modeled devices can be connected together in different configurations as they exist in the physical house and how they are connected to the distribution transformer. This feature facilitates modeling different houses with different arrangements as they are different in reality. Starting with electro-thermal model of the center-tap transformer, detailed description of each model component of the system is provided next.

8.4 "Center Tap" Single Phase Distribution Transformer Electro-Thermal Model

8.4.1 Introduction

Typical residential/commercial distribution transformer is connected a one or several house(s) through a service drop. The service drop is an overhead wires connected from the power provider pole, where the transformer usually is, to the premise such as a residential house(s) or a commercial building(s). Voltage ratings are different depending on the customer. Residential transformer is, usually, rated 7.2/(0.240/0.12) kV with power ratings up to 50 kVA; in contrast commercial transformer is, usually, rated 13.8/(0.48/0.24) kV with power ratings up to 500 kVA. Depending on the type of application, special configuration of distribution transformer is also existed. In Figure 8.4.1, two examples of single phase distribution transformer are presented. It is a usual practice to use a pole

mounted transformer in case if the power is provided to a residential customer and a pad mounted transformer in the case of a commercial one. The electro-thermal model used in the house management system is described next.

Figure 8.4.1 Example of Center-Tap Transformer, a) Right: Pole-Mounted Center-Tap Transformer, b) Left, Pad Mounted Center-Tap Transformer

8.4.2 Electrical Model of a Single Phase Center Tap Transformer

The electrical model used to compute the transformer electrical currents for a specific electric load demand is the standard electrical model. In this project, a single phase transformer is only used and is designed to adapt various voltage and power ratings to be able to accommodate different types of customers (residential /commercial). The electrical model circuit of that model is illustrated in Figure 8.4.2. It is assumed that this center tap transformer is used to provide a low voltage level to a residential house through a service drop. Normal voltage rating of these types of transformers is 110-140 V phase to ground and 210-240 V two phases. Also, normal rated size is ranged between 10-50 kVA. The electrical model equations are provided in Appendix B.

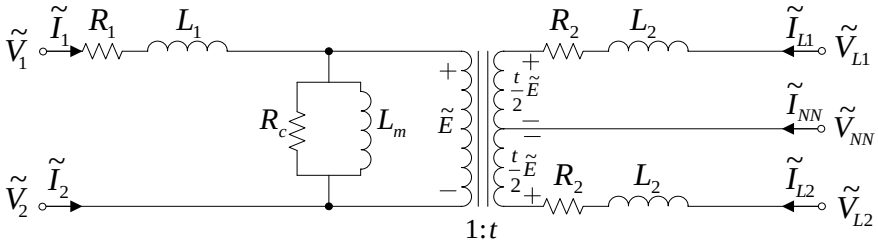

Figure 8.4.2 Electrical Circuit of the Center-Tap Transformer

8.4.3 Thermal Model of a Single Phase Center Tap Transformer

Transformer's overall insulation life expectancy and overloading capabilities depend on several factors. However, it is determined primarily by the hot spot temperature in the transformer. It is, therefore, essential to predict thermal behaviors of a transformer during normal loadings and, in particular, during transformer abnormal (overloading) conditions. Furthermore, the improved knowledge of transformer thermal characteristics can predict the expected life of the distribution transformer insulation. This can indicate whether the transformer is properly sized for particular application or not. Therefore, this improved

realization can, a) allow the enhancement of the operation of the transformer, and b) provide better load management optimization decisions. In this section, the development of a novel, thorough, and detailed thermal model is accordingly discussed.

8.4.4 Modified Thermal Model

Although there are exists thermal models of the transformer in the literature, a new model is needed. Most of these already existed models are lacking accuracy and are modeled mainly for power transformers. Therefore, a new detailed thermal model of a single phase center-tap transformer is developed. The high level of details, in fact, enables better monitoring of the gradient temperatures inside the transformer and thus accurately assesses the hot spot temperature and the loss of insulation life. The parameters of this model indicate that the thermal time constants are in the order of 10 to 20 minutes. This means that there is plenty of time for the house management system to reschedule the use of electricity and avoid overheating the transformer in case of an overloading condition. The process of developing the thermal model is explained next.

8.4.4.1 Temperature Spot Definition

To monitor the rapid temperature change and to locate the hot spot temperature inside the center tap transformer with high accuracy, several temperature spots are selected. It is determined to select 21 temperature spots in total. Location of each one of these temperature spots is illustrated in Figure 8.4.3. Specifically, three temperature spots are selected for the transformer primary winding, six temperature spots for the transformer secondary winding, four temperature spots for the transformer core, four temperature spots for the oil tank, and lastly another four temperature spots for the transformer case. The reference temperature used in the model is the ambient temperature, which is designed and built separately than the transformer model.

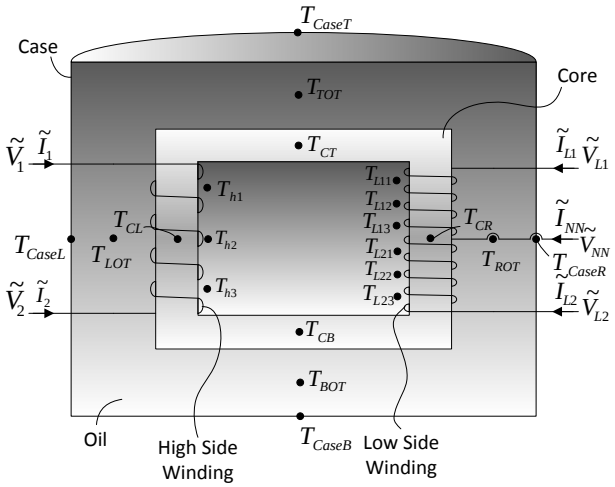

Figure 8.4.3 Single Phase Center-Tap Transformer Temperature Spots Locations

Next, each temperature spot is explained briefly:

Primary Temperature Spots: The transformer primary winding is divided into three segments as illustrated in Figure 8.4.4. Each one of these segments has a temperature spot located in the middle of the segment. In total, there are three temperature spots: T_{h1}: High-side temperature spot for segment one in [^{o}C]; T_{h2}: High-side temperature spot for segment two in [^{o}C]; and T_{h3}: High-side temperature spot for segment three in [^{o}C].

Secondary Temperature Spots: The transformer secondary winding is segmented into two main parts: Secondary winding part between phase L1 and NN; and Secondary winding part between phase L2 and NN. Each one of these parts is divided into three segments as illustrated in Figure 8.4.4, where each segment has a temperature spot located in the middle of the segment. In total, there are six temperature spots as the following: T_{L11}: Low-side temperature spot for part one segment one in [^{o}C]; T_{L12}: Low-side temperature spot for part one segment two in [^{o}C]; T_{L13}: Low-side temperature spot for part one segment three in [^{o}C]; T_{L21}: Low-side temperature spot for part two segment one in [^{o}C]; T_{L22}: Low-side temperature spot for part two segment two in [^{o}C]; T_{L23}: Low-side temperature spot for part two segment three in [^{o}C].

Transformer Core Temperature Spots: The core of the transformer is divided into four regions as illustrated in Figure 8.4.4, where each one has a temperature spot located in the middle of the region. In total, there are four temperature spots as: T_{CT}: Core-Top temperature spot for region one in [^{o}C]; T_{CB}: Core-Bottom temperature spot for region two in [^{o}C]; T_{CR}: Core-Right temperature spot for region three in [^{o}C]; T_{CL}: Core-Left temperature spot for region four in [^{o}C].

Transformer Oil Region Temperature Spots: The transformer oil tank is divided into four sub-spaces, where each one has a temperature spot. In total, there are four temperature spots as the following: T_{TOT}: Top of the Oil temperature spot for region one in [^{o}C]; T_{BOT}: Bottom of the Oil temperature spot for region two in [^{o}C]; T_{ROT}: Right of the Oil temperature spot for region three in [^{o}C]; T_{LOT}: Left of the Oil temperature spot for region four in [^{o}C].

Transformer Case Temperature Spots: The transformer case is divided into four segments, where each one has a temperature spot. In total, there are four temperature spots as: T_{CaseT}: Case-Top temperature spot for region one in [^{o}C]; T_{CaseB}: Case-Bottom temperature spot for region two in [^{o}C]; T_{CaseR}: Case-Right temperature spot for region three in [^{o}C]; T_{CaseL}: Case-Left temperature spot for region four in [^{o}C].

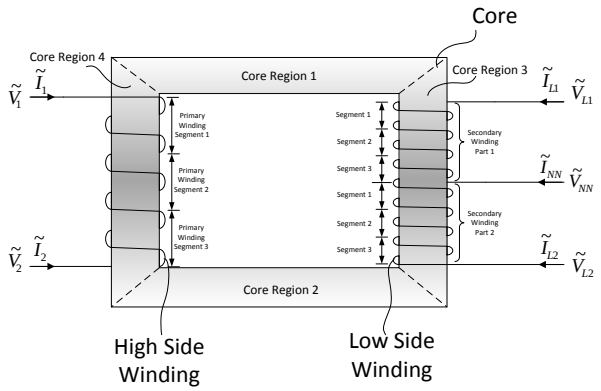

Figure 8.4.4 Single Phase Center-Tap Transformer Primary and Secondary Windings and Core divided Segments

8.4.4.2 Thermal Conductance (Gth), Thermal Capacitance (Cth), and Heat Source (Q̇) Definition

The first thermal element is the thermal conductance. In principle, the heat at each spot is experienced a thermal resistance as it propagates to other spots. The reciprocal of that thermal resistance is the thermal conductance. It is defined as the quantity of heat transmitted between every temperature spot and another. So, for every selected temperature spot in the physical model, there are 21 thermal conductances connected to it. On the other hand, the thermal capacitance is defined as the amount of the heat energy required to raise the temperature specific amount. For every selected temperature spot in the model, it is assumed that there is a thermal capacitance associates with it. The thermal capacitance is connected between the corresponding spot and a specific reference near to the corresponding spot. The connections of these thermal capacitances are provided in Table 8.1. The third thermal element is the heat source, which is in the form of ohmic losses in the specific area. Therefore, there are 13 heat sources in total. The location of these heat sources are provided in Table 8.2.

Table 8.1 Transformer Thermal Model Heat Capacity

Thermal Capacitance (C_{th})	Spot 1	Spot 2
C_{h1}	T_{h1}	T_{CT}
C_{h2}	T_{h2}	T_{CL}
C_{h3}	T_{h3}	T_{CB}
C_{L11}	T_{L11}	T_{CT}
C_{L12}	T_{L12}	T_{CR}
C_{L13}	T_{L13}	T_{CR}
C_{L21}	T_{L21}	T_{CR}
C_{L22}	T_{L22}	T_{CR}
C_{L23}	T_{L23}	T_{CB}
C_{CT}	T_{CT}	T_{TOT}
C_{CB}	T_{CB}	T_{BOT}
C_{CR}	T_{CR}	T_{ROT}
C_{CL}	T_{CL}	T_{LOT}
C_{TOT}	T_{TOT}	T_{Case_T}
C_{BOT}	T_{BOT}	T_{Case_B}
C_{ROT}	T_{ROT}	T_{Case_R}
C_{LOT}	T_{LOT}	T_{Case_L}
C_{CaseT}	T_{CaseT}	T_{amb}
C_{CaseB}	T_{CaseB}	T_{amb}
C_{CaseR}	T_{CaseR}	T_{amb}
C_{CaseL}	T_{CaseL}	T_{amb}

Table 8.2 Transformer Heat Source

Heat Source ($\dot{Q}$)	Spot
$\dot{Q}_{h1}$	T_{h1}
$\dot{Q}_{h2}$	T_{h2}
$\dot{Q}_{h3}$	T_{h3}
$\dot{Q}_{L11}$	T_{L11}
$\dot{Q}_{L12}$	T_{L12}
$\dot{Q}_{L13}$	T_{L13}
$\dot{Q}_{L21}$	T_{L21}
$\dot{Q}_{L22}$	T_{L22}
$\dot{Q}_{L23}$	T_{L23}
$\dot{Q}_{CT}$	T_{CT}
$\dot{Q}_{CB}$	T_{CB}
$\dot{Q}_{CR}$	T_{CR}
$\dot{Q}_{CL}$	T_{CL}

8.4.4.3 Thermal Model

The thermal model is developed by using the analogy of thermal – electrical physical laws. The electrical laws govern the capacitance and resistance are as the following:

$$v(t) = i(t)R \tag{8.4}$$

$$i(t) = C\frac{dv(t)}{dt} \tag{8.5}$$

Similarly the thermal laws are:

$$T(t) = Q(t)R_{th} \tag{8.6}$$

$$Q(t) = C_{th}\frac{dT(t)}{dt} \tag{8.7}$$

So, the temperature dynamic is given by the following general differential equation:

$$Q(t) = C_{th}\frac{dT(t)}{dt} + G_{th}\Delta T(t) \tag{8.8}$$

where
T(t): the spot temperature at time t in [k^{o}C]
Q(t): Heat flow rate at time t in [MBtu/h]
R_{th}: Thermal resistance in [k^{o}C.h/MBtu]
G_{th}: Thermal conductance in [MBtu/k ^{o}C.h]
C_{th}: Heat capacity in [MBtu/k ^{o}C]

The model equations of the thermal model are provided in Appendix B.

8.4.5 Computation of Thermal Quantities

The methods used to compute the thermal capacitance and conductance are presented in this section.

8.4.5.1 Computation of Thermal Capacitance (C_{th})

The heat capacity is a function of the volume, mass density, and specific heat of the matter as given by

$$C_{th} = Vol\ \rho\ C_p \tag{8.9}$$

$$Vol = \pi r^2 h \tag{8.10}$$

where
Vol: the volume in [m^3]
ρ: the mass density [kg/m^3]
Cp: Specific heat [Btu/kg.^oC]
r: radius of the tank [in]
h: the height of the tank [in]

In the electro-thermal model of the transformer, the volume of each part is computed considering the following assumptions:

- Inner radius is 96% of the outer radius;
- A number of inches are subtracted of the transformer height due to bushing as necessary. Some manufacture provides exact height without bushing;
- Each winding side volume is assumed to be 2% of the resulted transformer volume (Core and Windings Volume).

8.4.5.2 Computation of Thermal Conductance (G_{th})

Thermal conductance circuit parameters are computed considering the transformer nameplate full rated load. Rated temperature for every temperature spot is considered as provided in Table 8.3. The steady state equations of the single phase center-tap transformer set equations (provided in Appendix B) are used to compute the circuit conductance. This procedure is designed to be performed automatically.

Table 8.3 Center-Tap Distribution Transformer Rated Temperature at each Temperature Spot (^oC)

Temperature Spot	Rated Temp [^oC]
T_{h1}	103
T_{h2}	95
T_{h3}	91
T_{L11}	105
T_{L12}	100
T_{L13}	95
T_{L21}	94
T_{L22}	93
T_{L23}	92
T_{CT}	94
T_{CB}	88
T_{CR}	92
T_{CL}	90
T_{TOT}	80
T_{BOT}	70
T_{ROT}	77

Table 8.3 Center-Tap Distribution Transformer Rated Temperature at each Temperature Spot (^oC) (continued)

Temperature Spot	Rated Temp [^oC]
T_{LOT}	73
T_{caseT}	65
T_{caseB}	55
T_{caseR}	62
T_{caseL}	59
T_{amb}	40

Due to the large number of conductances, which is larger than the number of equations, each conductance is represented by a percent of a collective main conductance. The total number of main conductances is 21, which equals to the number of equations. Thus, all thermal circuit thermal conductances can be calculated using the assumed percentage provided in Table B-1 – Table B-21 in Appendix B.

8.4.6 Transformer Loss of Insulation Life (LOIL)

The degradation of the transformer insulation life attributes to three different factors, namely moisture, oxygen, and temperature [77, 78]. Each one of these contributes separately to the degree of the transformer insulation degradation; therefore, they must be controlled independently. The contamination of the transformer oil resulted from either moisture or oxygen can be controlled by the transformer Oil-Preservation System [OPS]. Thus, they, moisture and oxygen, are excluded from the analysis provided in this thesis. Therefore, the transformer considered here is assumed to be well dried and oxygen free. It is only assumed that the temperature factor is the only factor considered in the LOIL computation procedure, which is explained next.

The Loss of Insulation Life during time interval t can be explained by the equivalent total hours life consumed divided by the predefined normal insulation life, which is usually given in hours. Thus, LOIL mathematically can be computed using the following equation [78, 79],

$$\mathrm{LOIL} = \exp\left(-\left(\mathrm{A} + \frac{\mathrm{B}}{\mathrm{T_{HotSpot}}}\right)\right)\mathrm{h} \tag{8.11}$$

where
$T_{HotSpot}$: Hot spot temperature at time t in [^oK].
t: time period in [h].
A & B: Empirical constants depending on the design of the transformer. Numerical values of A & B are summarized in Table 8.4.

Table 8.4 Transformer Empirical A & B Numeric [80]

Constant	65 °C Insulation System	55 °C Insulation System
A	-11.269	6328.8
B	-11.968	6328.8

8.4.7 Model Simulation

A 13.8 kV system is used to test the electro-thermal transformer model. The test system consists of mainly slack generator, step up and down transformers, transmission line, distribution substation (13.8 kV), overhead distribution line, electro-thermal distribution transformer. Two cases are simulated to test the electro-thermal transformer model. The electrical circuit parameters for the center tap electro-thermal transformer are provided in Table 8.5.

Table 8.5 Case Study Transformer Electrical Impedance Parameters

Z1 [pu]	0.00428+j0.03422
ZL1, ZL2 [pu]	0.00699+j 0.01399
Ym [pu]	0.0068+j 0.09

To estimate the volume of typical transformer parts, a number of transformers physical dimensions and volumetric quantity of oil data are needed. Such data can be found in the transformer manufacture data sheet. As an example, a 10 kVA ABB transformer data is provided in Table 8.6.

Table 8.6 Transformer Dimension and Oil Volume for ABB 10 kVA [81]

Height h [in]	Radius r [in]	Oil Volume [Gallon]
22.0	8.27	5.8

Given the height and radius data, the transformer including the transformer case volume is computed. The case volume is computed using the transformer inner and outer radius. This case volume is subtracted from the transformer volume. Next, the oil volume was subtracted from the transformer volume resulting in an approximation of the transformer less oil volume, representing the total volume for transformer core and windings. Finally, each one of the transformer windings volume is assumed to be 2% of the total core and winding volume. Table 8.7 summarizes the volume, mass density, and specific heat, and the resulting heat capacity of each transformer part. Finally, the thermal capacity is divided by the total number of temperature spots assigned to each part of the transformer. Table 8.8 provides the final computed heat capacity for every spot in the transformer.

Table 8.7 Volume, Mass Density, Specific Heat, and Heat Capacity of Various Parts of ABB 10 kVA Transformer

	Volume [m^3]	**Mass density (ρ)[kg/m^3]**	**Specific heat, C_p [J/kg.°C]**	**Thermal Capacity, C_{th} [Btu/ °C]**
Primary Winding	0.0009886	(Copper) 8930	385	C_h = 3399.01
Secondary Winding	0.0009886	(Copper) 8930	385	C_L = 3399.01
Transformer Core	0.0474556	(Iron) 7874	450	C_{core} = 168150
Transformer Oil	0.0219553	(Mineral Oil) 800	1860	C_{oil} = 32669.6
Transformer Case	0.0060729	(Steel) 7874	450	C_{case} = 21518.3

Table 8.8 Thermal Capacities for ABB 10 kVA Transformer

Thermal Cap., C_{th} [Btu/ °C]	**Value**	**Thermal Cap., C_{th} [Btu/ °C]**	**Value**
C_{h1}	1133.019609	C_{CR}	42037.382166
C_{h2}	1133.019609	C_{CL}	42037.382166
C_{h3}	1133.019609	C_{TOT}	8167.400615
C_{L11}	566.5098	C_{BOT}	8167.400615
C_{L12}	566.5098	C_{ROT}	8167.400615
C_{L13}	566.5098	C_{LOT}	8167.400615
C_{L21}	566.5098	C_{CaseT}	5379.584307
C_{L22}	566.5098	C_{CaseB}	5379.584307
C_{L23}	566.5098	C_{CaseR}	5379.584307
C_{CT}	42037.382166	C_{CaseL}	5379.584307
C_{CB}	42037.382166		

8.4.7.1 Extreme Case

The objective of this case is to show the rise time of the electro-thermal model. In this case, the outside temperature is assumed to be 40 °C over the simulation period, two hours. No load is considered in the beginning of the simulation; by the end of the half hour, full load equals 100% of the transformer rating is connected to the transformer low side and the response is measured. This case is simulated with 1 second time step. Results are reported for two different ratings 10 and 25 kVA. Table 8.9 summarizes the transformer dimension and oil volume data taken from the manufacture data sheet and used in this case [81]. Before the simulation starts, the computation of the transformer thermal circuit values is performed. Results for each rating are tabulated in Table 8.10. Note that every thermal connected to every temperature spot can be computed as provided in the previous section.

Table 8.9 ABB Transformer Physical Parameters (Dimension and Oil Volume) [81]

	10 kVA	***25 kVA***
Height *h* [in]	22.0	24.2
Radius *r* [in]	8.27	9.0
Oil Volume [US Gal]	5.8	7.92

Table 8.10 Derived Thermal Circuit Parameters Results for ABB Transformers

	10 kVA	***25 kVA***
C_{h1}, C_{h2}, C_{h3},	1133.019609	1453.1590
C_{L11}, C_{L12}, C_{L13}, C_{L21}, C_{L22}, C_{L23}	566.5098	726.57953
C_{CT}, C_{CB}, C_{CR}, C_{CL}	42037.382166	53915.221
C_{TOT}, C_{BOT}, C_{ROT}, C_{LOT}	8167.400615	11011.90910
C_{CaseT}, C_{CaseB}, C_{CaseR}, C_{CaseL}	5379.584307	7008.34387
G_{h1}	0.9392	2.34804
G_{h2}	4.9646	12.41160
G_{h3}	9.2251	23.06277
G_{L11}	1.3173	3.29348
G_{L12}	5.1539	12.88472
G_{L13}	15.9001	39.75033
G_{L21}	6.6761	16.69016
G_{L22}	12.7690	31.92241
G_{L23}	13.8044	34.51093
G_{CT}	114.4823	286.20563
G_{CB}	342.9088	857.27202
G_{CR}	411.6648	1029.16195
G_{CL}	638.6320	1596.57994
G_{TOT}	93.6341	234.08525
G_{BOT}	557.5581	1393.89515
G_{ROT}	235.7097	589.27419
G_{LOT}	608.0865	1520.21629
G_{CaseT}	179.2948	448.2369
G_{CaseB}	1091.0020	2727.505025
G_{CaseR}	264.8116	662.0288
G_{CaseL}	487.5559	1218.8897

Temperature rise time for various temperature signals considering two transformer ratings and for ABB are shown in Figure 8.4.5 and Figure 8.4.6. Approximate rise times are

reported in Table 8.11 for three different manufactures ABB, Power Partners, and Cooper Power Systems with two ratings 10 and 25 kVA. Physical data used to approximate the rise time are taken from the manufacture data sheet [81-83].

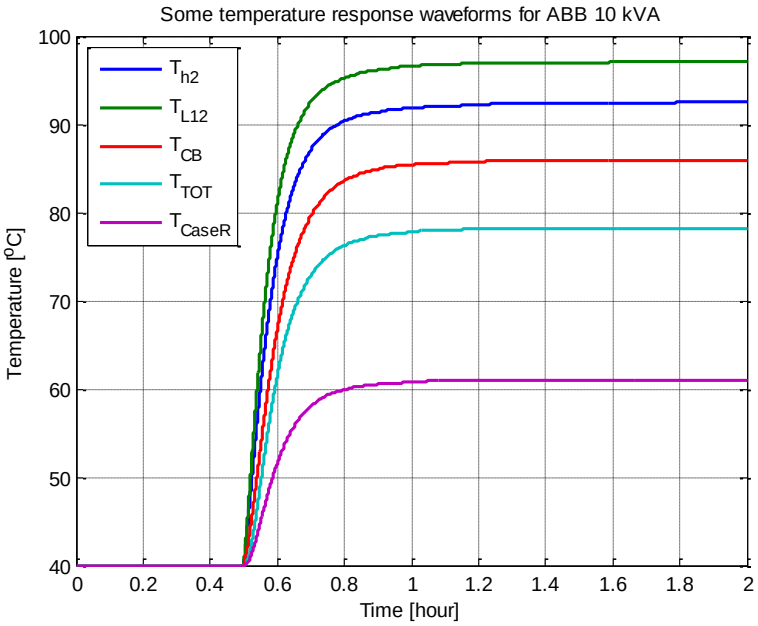

Figure 8.4.5 ABB 10 kVA Transformer Temperature Rise Time

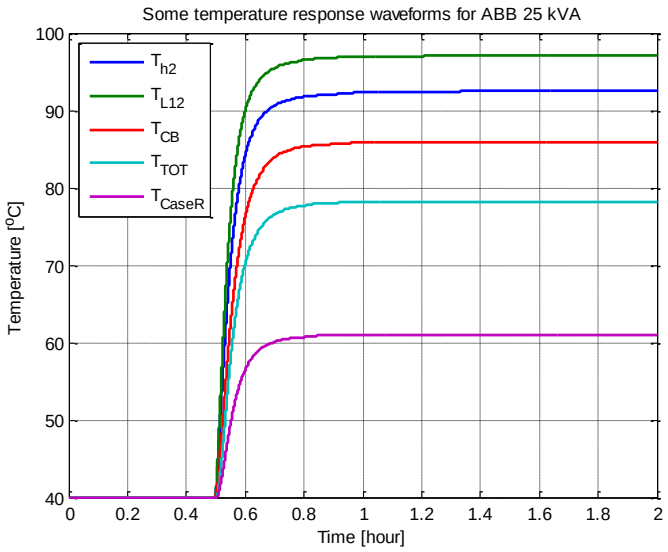

Figure 8.4.6 ABB 25 kVA Transformer Temperature Rise Time

According the data provided in Table 8.11, the rise time depends on the manufacture specification and transformer rating. However, the results of this case indicate that there is an adequate amount of time for the house management system to reschedule the operation of various components and thus averting transformer overheating.

Table 8.11 Approximate Rise Time in [min]

Manufacture	*10 kVA*	*25 kVA*
ABB	20.45	19.3
Cooper Power Systems	21.55	20.4
Power Partners Inc.	22.15	17.72

8.4.7.2 Simulation of Different Loading Conditions with 10 kVA ABB Electro-Thermal Transformer

A 10 kVA center tap distribution transformer loss of insulation life is computed. Figure 8.4.7 shows the single line diagram of the test case. The test system consists of infinite bus, transmission system, distribution lines, center-tap transformer, service drop, and finally variable load. Various temperature spots are monitored and reported.

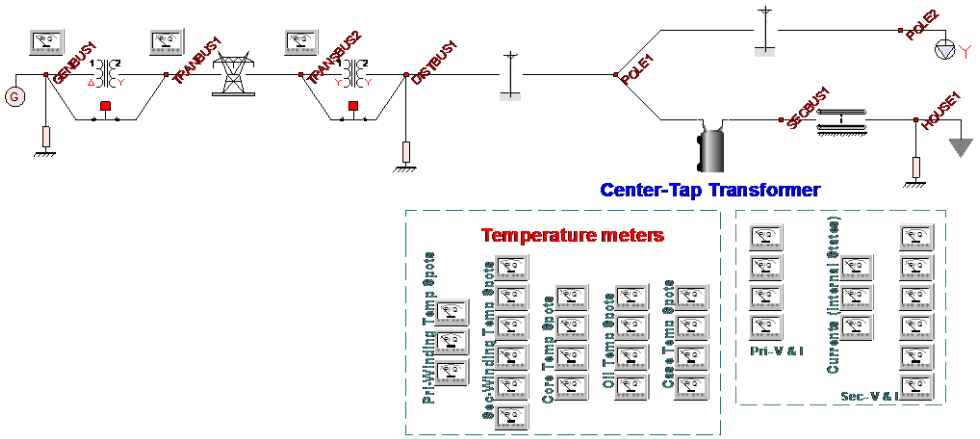

Figure 8.4.7 Test System Single Line Diagram

One important environmental condition is the ambient temperature. It is assumed fixed for both below cases.

Figure shows the ambient temperature on hourly basis considered in this analysis.

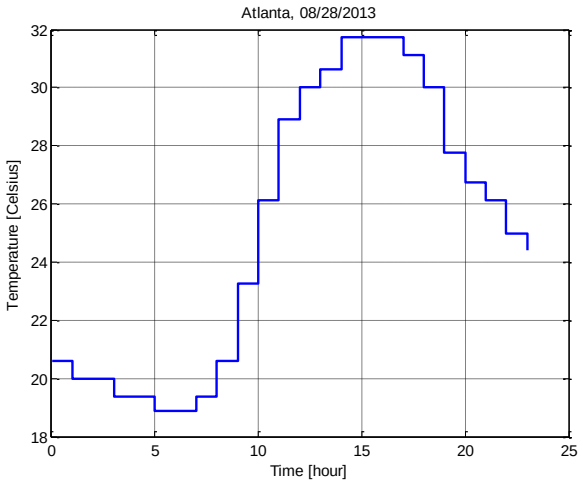

Figure 8.4.8 Ambient Temperature Condition

8.4.7.2.1 Mild Overloading

The Center-Tap transformer is assumed to be mildly overloaded between 15:00 pm and 17:00 pm with a rated 1.2 pu load during the sixteenth hour. Figure 8.4.9 depicts the load connected to the transformer.

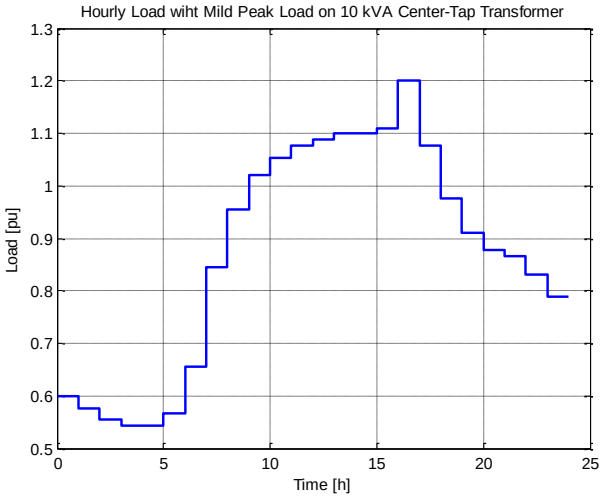

Figure 8.4.9 Hourly Load with 1.2 pu Peak Load Applied to 10 kVA Center-Tap Transformer

The aging acceleration factor along with the aging cumulative hours calculations are reported in Table 8.12. The hottest spot and the spot name are provided, too. The computations are based on aging rate constant equals to 14580 and normal insulation life equals to 150000.

Table 8.12 Aging Calculation for 10 kVA Transformer and for 24 Hours Period

Time	Load (pu)	Amb. Temp. (ºC)	Hottest Spot Temp (ºC)	Spot Name	LOIL (%)	Cumulative LOIL (%)
0:00:00	0.599	20.611	42.785	L11	0.00000017	0.00000017
1:00:00	0.577	20.000	40.576	L11	0.00000012	0.00000029
2:00:00	0.555	20.000	39.038	L11	0.00000010	0.00000039
3:00:00	0.544	19.389	37.680	L11	0.00000008	0.00000047
4:00:00	0.544	19.389	37.678	L11	0.00000008	0.00000055
5:00:00	0.566	18.889	38.684	L11	0.00000009	0.00000064
6:00:00	0.655	18.889	45.397	L11	0.00000025	0.00000088
7:00:00	0.844	19.389	63.448	L11	0.00000287	0.00000376
8:00:00	0.955	20.611	77.083	L11	0.00001552	0.00001928
9:00:00	1.021	23.278	87.868	L11	0.00005386	0.00007314
10:00:00	1.054	26.111	94.967	L11	0.00011739	0.00019053
11:00:00	1.077	28.889	100.798	L11	0.00021773	0.00040827
12:00:00	1.088	30.000	103.394	L11	0.00028490	0.00069317
13:00:00	1.099	30.611	105.504	L11	0.00035352	0.00104669
14:00:00	1.099	31.722	106.616	L11	0.00039574	0.00144244
15:00:00	1.11	31.722	108.128	L11	0.00046083	0.00190327
16:00:00	1.2	31.722	121.067	L11	0.00161726	0.00352052
17:00:00	1.077	31.111	103.043	L11	0.00027480	0.00379532
18:00:00	0.977	30.000	89.145	L11	0.00006211	0.00385743
19:00:00	0.91	27.778	79.057	L11	0.00001960	0.00387704
20:00:00	0.877	26.722	74.332	L11	0.00001116	0.00388820
21:00:00	0.866	26.111	72.527	L11	0.00000897	0.00389717
22:00:00	0.832	25.000	67.834	L11	0.00000502	0.00390218
23:00:00	0.788	24.389	62.801	L11	0.00000264	0.00390483

The expected transformer loss of insulation life during that day is 0.004 %.

8.4.7.2.2 Extreme Overloading

The Center-Tap transformer is assumed to be extremely stressed with a high load between 15:00 pm and 17:00 pm with a rated 1.4 p.u. load during the sixteenth hour. Figure 8.4.10 depicts the load connected to the transformer.

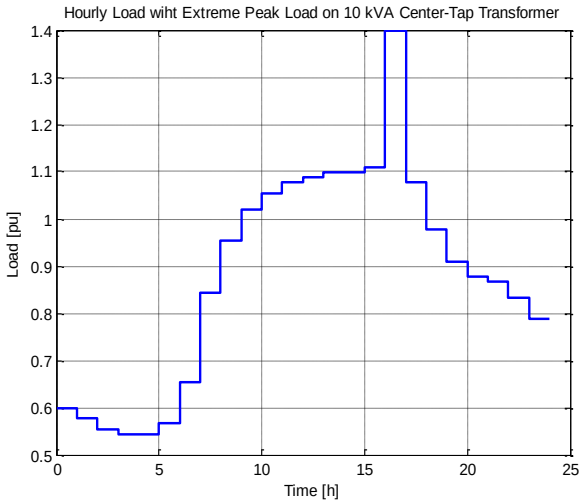

Figure 8.4.10 Hourly Load with Extreme Peak Load Applied to 10 kVA Center-Tap Transformer

The aging acceleration factor along with the aging cumulative hours calculations are reported in Table 8.13. The hottest spot and the spot name are provided, too. The computations are based on aging rate constant equals to 14580 and normal insulation life equals to 150000.

Table 8.13 Aging Calculation for 10 kVA Transformer and for 24 Hours Period

Time	Load (pu)	Amb. Temp. (ºC)	Hottest Spot Temp (ºC)	Spot Name	LOIL (%)	Cumulative LOIL (%)
0:00:00	0.599	20.611	42.784	L11	0.000000169	0.000000169
1:00:00	0.577	20.000	40.575	L11	0.000000122	0.000000291
2:00:00	0.555	20.000	39.037	L11	0.000000097	0.000000388
3:00:00	0.544	19.389	37.678	L11	0.000000079	0.000000467
4:00:00	0.544	19.389	37.678	L11	0.000000079	0.000000546
5:00:00	0.566	18.889	38.684	L11	0.000000092	0.000000638
6:00:00	0.655	18.889	45.398	L11	0.000000247	0.000000885
7:00:00	0.844	19.389	63.447	L11	0.000002873	0.000003757
8:00:00	0.955	20.611	77.083	L11	0.000015523	0.000019281
9:00:00	1.021	23.278	87.868	L11	0.000053860	0.000073140
10:00:00	1.054	26.111	94.967	L11	0.000117384	0.000190524
11:00:00	1.077	28.889	100.797	L11	0.000217716	0.000408240

Table 8.13 Aging Calculation for 10 kVA Transformer and for 24 Hours Period (continued)

Time	Load (pu)	Amb. Temp. (ºC)	Hottest Spot Temp (ºC)	Spot Name	LOIL (%)	Cumulative LOIL (%)
12:00:00	1.088	30.000	103.394	L11	0.000284908	0.000693148
13:00:00	1.099	30.611	105.503	L11	0.000353506	0.001046654
14:00:00	1.099	31.722	106.615	L11	0.000395718	0.001442371
15:00:00	1.11	31.722	108.127	L11	0.000460785	0.001903157
16:00:00	1.4	31.722	153.443	L11	0.026797767	0.028700923
17:00:00	1.077	31.111	103.078	L11	0.000275797	0.028976720
18:00:00	0.977	30.000	89.147	L11	0.000062115	0.029038836
19:00:00	0.91	27.778	79.057	L11	0.000019605	0.029058440
20:00:00	0.877	26.722	74.331	L11	0.000011163	0.029069603
21:00:00	0.866	26.111	72.527	L11	0.000008967	0.029078570
22:00:00	0.832	25.000	67.834	L11	0.000005017	0.029083587
23:00:00	0.788	24.389	62.801	L11	0.000002643	0.029086230

The expected transformer loss of insulation life during that day is 0.029 %.

8.5 Modeling of Residential/Commercial Smart Building Appliances and Resources

A major model component of the management system is the smart residential/commercial building. In fact, to be able to achieve the objectives outlined in the project goals, real time, comprehensive, and physically based models of a residential/commercial building appliances and other energy resources are developed. A description of every appliance model is discussed followed by brief discussion about various energy resources that can be integrated with the building such as roof top solar photovoltaic. Note that the discussion, in this section, is rather focused upon providing description regarding smart house appliances and resources. However, if properly sized, the house model can be used to represent a commercial building.

8.5.1 Modeling of House Appliances

8.5.1.1 Smart Dishwasher Model

8.5.1.1.1 Introduction

This section discusses the devolvement of the dishwasher load profile. The dishwasher load is modeled mathematically as a constant active and reactive power at the fundamental frequency (60 Hz). The electrical load is computed according to a specified rated power and device efficiency. Based on a specified power factor, the reactive power is then calculated. Typical voltage connection is line to ground with voltage rating approximately ranges between 110-130 V. The basic electrical circuit is illustrated in Figure 8.5.1.

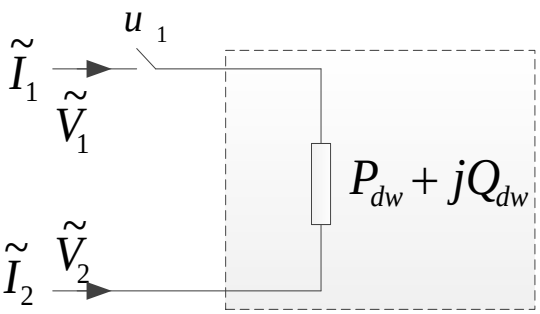

Figure 8.5.1 Electric Circuit of the Dishwasher Model

In this model, the following assumptions are made:

- A constant power factor and fixed efficiency during the operation of the dishwasher.
- Constant active and reactive power consumption during every stage of the dishwasher cycle.
- Constant load level during every operation cycle.
- A one operation cycle of the dishwasher is defined as the duration of time when the dishwasher is switched on until it's switched off.
- Dishwasher operation starts at a specified time and lasts for specified period of time. These two variables are input to the dishwasher model.
- Several operations during the day can be programmed.

Figure 8.5.2 shows the dishwasher model interface window in the WinIGS program.

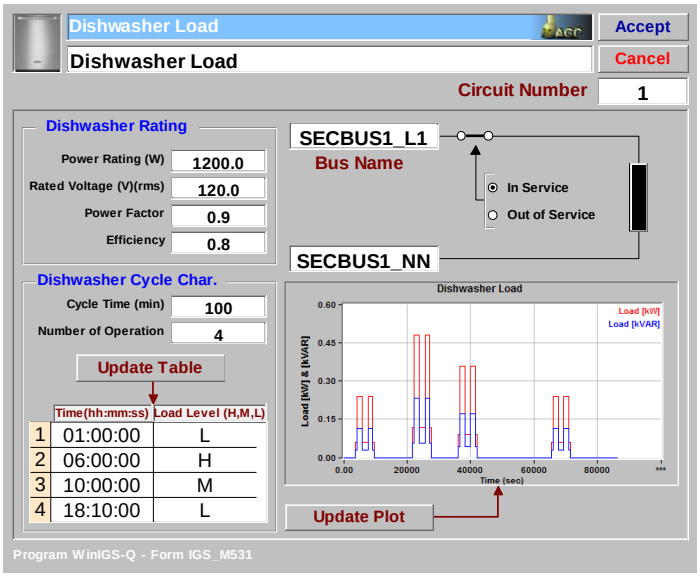

Figure 8.5.2 Smart Dishwasher Model User Interface Window in the WinIGS Program

There are two main factors that affect the power consumption of the dishwasher: the load level inside the dishwasher and the power profile of the cycle. These two factors are explained next.

8.5.1.1.2 Load Level

It is considered that there are three different levels that can be selected from to represent the dishwasher internal loading. These are high, medium, and light. It is assumed that if the "High" option is selected, it corresponds to 100% of the dishwasher power profile will be used; "Medium" option corresponds to 75 % of the dishwasher power profile will be utilized, and "Low" option corresponds to 50 % of the dishwasher power profile will be utilized. The three load levels are summarized in Table 8.14.

Table 8.14 Smart Dishwasher Load levels

Load	Load Level (u_2) [%] of the Dishwasher Power Profile
High	100
Medium	75
Light	50

8.5.1.1.3 Dishwasher Power Profile

The dishwasher cycle can be simulated assuming different profiles. Fixed active and reactive power over the operation cycle profile is widely used. However, in this project, a more detailed profile is considered to more reflect more realistic energy consumption. For every operation cycle, it is assumed there are five different stages as the following: pre-wash, main wash, rinse, rinse and heat, and drying. One cycle duration of time is different from one to another based on the dishwasher model rating and technical specification. It usually ranges between 60 - 200 minutes per cycle. Short technical explanation of each one of these process is provided next:

1. **Pre-wash:**
   In the pre-wash cycle, water is pumped and sprayed to loosen particles stuck on dishes, utensils, pans, and other stuff inside the dishwasher. Water sprayed is not heated up and usually regular in temperature. The water is then pumped out to prepare the dishwasher for the next cycle.

2. **Main wash:**
   After the pre-wash cycle, fresh water is sprayed and mixed with the detergent. The water used in this cycle is heated up to become between 125 - 140 ^{o}F (50 - 70 ^{o}C). When the cycle is over, the water is pumped out.

3. **Rinse:**
   With a cold water, the inside dishwasher is sprayed to clean the residuals from the previous cycle.

4. **Rinse and heat:**
   In this cycle, water is sprayed again. Rinse aid soap could be mixed with sprayed water. Water temperature is increased up to about 140 ^{o}F (70 ^{o}C). By the end of the cycle, hot water is pumped out.

5. **Dry:**
   After pumping all the water in the previous cycle, a heating element positioned on the bottom of the dishwasher is used to provide more heat and dry the left of water and kills bacteria.

Typical power consumption and time usage to perform each one of the stages discussed above is summarized in Table 8.15. Figure 8.5.3 presents the implemented power profile.

Table 8.15 Summary of Power and Time Used at Every Stage of the Operating Cycle

Stage	Power Consumption (u_3) [%] of the Dishwasher Maximum Power	Time [%] of the Dishwasher Total Cycle Time
Pre-wash	25	10
Main wash	100	25
Rinse	25	30
Rinse and heat	100	25
Dry	25	10
The entire cycle	-	100

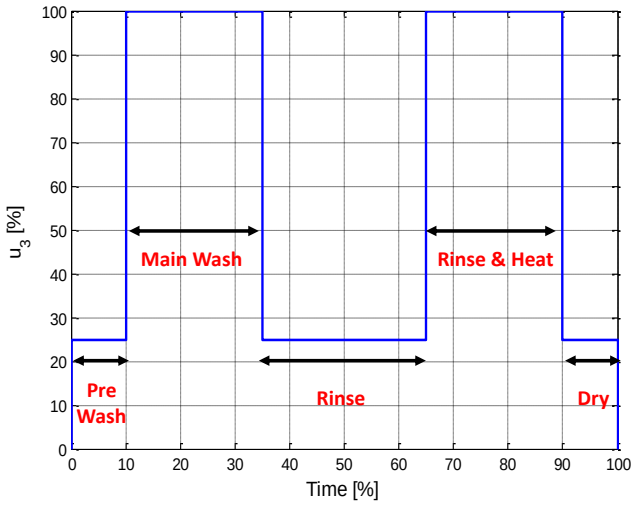

Figure 8.5.3 Smart Dishwasher Power Profile

Based on these characteristics, the mathematical model is developed. The model equations in a compact form are provided in Appendix C.

8.5.1.1.4 Simulation

The same test system used to test the transformer is reused in this case. The simulation is performed over 24 hours. The high side of the electro-thermal transformer is connected to phase A; while the lower side is connected to the residential house via a service drop. Two types of load are included in the test case yet: dishwasher and a constant impedance loads. The dishwasher is assumed to operate three times during the simulation period.

Results presented are for the electro-thermal transformer low side L1 current, dishwasher load current, and dishwasher power. Figure 8.5.4 shows these waveforms. It is clearly shown that when the dishwasher is on, designated power is drawn from the circuit. Otherwise, power is zero. This gives opportunity to the house energy management system to shift the operation of the dishwasher to a later time to avoid any excessive stress on the center-tap transformer.

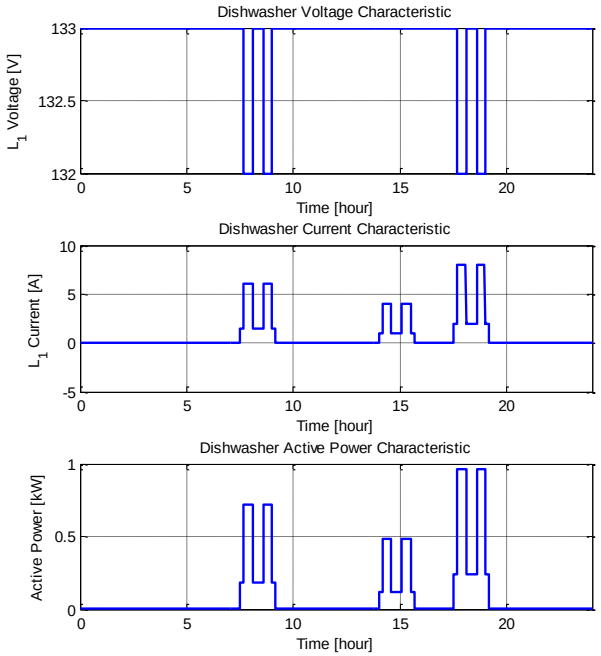

Figure 8.5.4 Waveforms Results of the Simulation Study

8.5.1.2 Electro-Thermal Model of a Top Mount Refrigerator

8.5.1.2.1 Introduction

A detailed and physically based refrigerator electro-thermal model corresponds to a refrigerator with two compartments, fresh food and freezer, is modeled. To monitor the gradient temperatures of the refrigerator model, several temperature spots have been defined. In total, seven temperature spots are assumed. Specifically, the fresh food compartment of the refrigerator is assigned a spot; and the freezer compartment is also assigned a spot. Due to the temperature difference between the internal and external wall of each one of the fresh food and freezer compartments, two temperature spots are selected for each of internal and external wall temperature. The model is connected to the kitchen temperature (assuming that the refrigerator is in the kitchen). In both compartments, the

thermal capacity is the sum of the thermal capacity of every element inside the compartment. During refrigerator internal load changes, the door of the compartment is opened and one or several elements mass would decrease or increase – these changes are incorporated into the refrigerator model in real time. Typical voltage connection is line to ground with voltage rating approximately ranges between 110-130 V. The model is assumed to work at the fundamental frequency. Figure 8.5.5 shows the dishwasher model interface window in the WinIGS program.

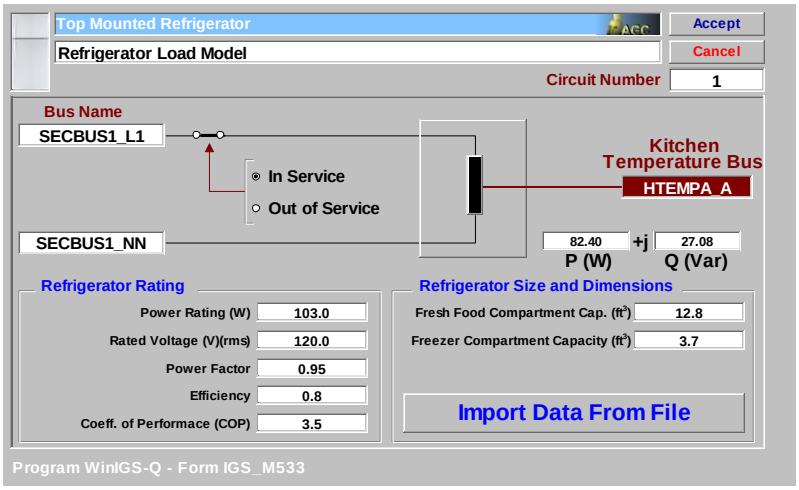

Figure 8.5.5 Electro-Thermal Refrigerator Model User Interface Window in the WinIGS Program

8.5.1.2.2 Temperature Spots, Thermal Conductance, Heat Capacity, and Heat Rate

Temperature Spots:

As stated before, seven temperature spots are assumed. They are listed as the following,

T_{fr}: Fresh food compartment main temperature spot in [^{o}C].

T_{friw}: Fresh food compartment internal wall temperature spot in [^{o}C].

T_{frew}: Fresh food compartment external wall temperature spot in [^{o}C].

T_{fz}: Freezer compartment temperature spot in [^{o}C].

T_{fziw}: Freezer compartment internal wall temperature spot in [^{o}C].

T_{fzew}: Freezer compartment external wall temperature spot in [^{o}C].

T_{k}: Kitchen temperature spot in [^{o}C].

Thermal Conductance:

It is assumed that for every temperature spot in the physical device, there one or several thermal conductances connected to it. Below is a summary of the assumed thermal

conductances as they are also been presented in thermal circuit model of the refrigerator section,

G_{fr}: Thermal conductance between the fresh food compartment mass and the fresh food compartment internal wall in [Btu/^{o}C h].

G_{fz}: Thermal conductance between the freezer compartment mass and the freezer compartment internal wall in [Btu/^{o}C h].

$G_{friw\text{-}fziw}$: Thermal conductance between the fresh food compartment internal wall and the freezer compartment internal wall mass in [Btu/^{o}C h].

$G_{friw\text{-}frew}$: Thermal conductance of the fresh food compartment wall in [Btu/^{o}C h].

$G_{fziw\text{-}fzew}$: Thermal conductance of the freezer compartment wall in [Btu/^{o}C h].

$G_{frew\text{-}fzew}$: Thermal conductance of the fresh food and freezer compartments external walls in [Btu/^{o}C h].

$G_{frew\text{-}K}$: Thermal conductance between the fresh food compartment external wall and the Kitchen air mass in [Btu/^{o}C h].

$G_{fzew\text{-}K}$: Thermal conductance between the freezer compartment external wall and the Kitchen air mass in [Btu/^{o}C h].

Thermal Capacity:

The thermal capacitance is defined as the amount of the heat energy required to raise the temperature specific amount. It is assumed that there is a thermal capacitance associates with each one of fresh food compartment and freezer compartment. The thermal capacitance is connected between the corresponding spot and a specific reference near to the corresponding spot as provided in Table 8.16. Below is a summary of the assumed thermal capacitances as they are also been presented in thermal circuit model of the refrigerator section:

C_{fr}: The sum of the heat capacity of every element inside the fresh food compartment in [Btu/^{o}C].

C_{friw}: Heat capacity of internal door mass in the fresh food compartment in [Btu/^{o}C].

C_{frew}: Heat capacity of external door mass in the fresh food compartment in [Btu/^{o}C].

C_{fz}: The sum of the heat capacity of every element inside the freezer compartment in [Btu/^{o}C]

C_{fziw}: Heat capacity of internal door mass in the freezer compartment in [Btu/^{o}C].

C_{fzew}: Heat capacity of external door mass in the freezer compartment in [Btu/^{o}C].

Table 8.16 Electro-Thermal Refrigerator Thermal Capacitance Connections

Thermal Capacitance (C_{th})	Spot 1	Spot 2
C_{fr}	T_{fr}	T_{friw}
C_{friw}	T_{friw}	T_{frew}
C_{frew}	T_{frew}	T_{K1r}
C_{fz}	T_{fz}	T_{fziw}
C_{fziw}	T_{fziw}	T_{fzew}
C_{fzew}	T_{fzew}	T_{K1r}

Heat Sources:

The heat flow rate is the rate of the heat flow between two systems. Therefore, there is one main heat source provides cooling to both the fresh food and freezer compartments, that is the heat rate provided by the refrigerator $\dot{Q}_r$, shown in Figure 8.5.6. The heat rate provided to the fresh food compartment is assumed to be (k1 = 60%) of the total heat generated by the refrigerator. Alternatively, the heat rate provided to the freezer compartment is assumed to the rest, (k2 = 40%), of the total heat generated by the refrigerator.

8.5.1.2.3 Electrical Model

The electrical load is computed according to specified rated power consumption and specified approximated efficiency. Assuming a constant power factor, the reactive power is then computed. It is also assumed constant active and reactive power consumption during the refrigerator operation. The electrical circuit model used is illustrated in Figure 8.5.6.

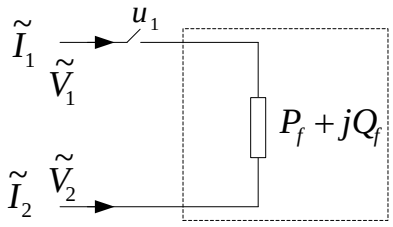

Figure 8.5.6 Electrical Model Circuit of the Refrigerator

8.5.1.2.4 Thermal Model

To monitor the gradient temperatures of the refrigerator model, several temperature spots have to be selected. In this work, seven temperature spots are selected. Location of each one of these spots is illustrated in Figure 8.5.7.

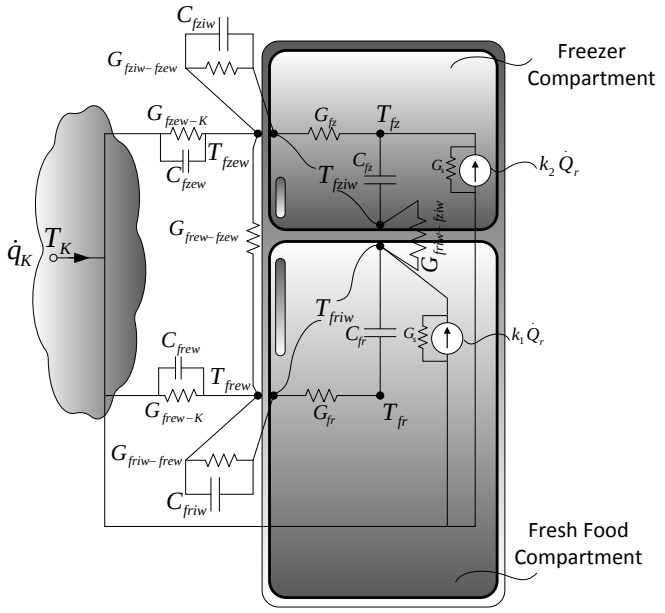

Figure 8.5.7 Refrigerator Thermal Circuit Elements and Temperature Spots Locations

The electrical and thermal model equations are provided in a compact form in Appendix D.

8.5.1.2.5 Computation of Thermal Quantities

The methods used to compute the thermal capacitance and conductance are presented in this section.

Thermal Capacitance (Cth):

The heat capacity of every element inside whether the fresh food compartment or the freezer compartment is a function of the mass of the element and its specific heat as given by:

$$C_{th} = m\, C_p \tag{8.12}$$

where
m: the mass of the element in [kg]
Cp: Specific heat of the element in [Btu/kg. ^{o}C]

When all elements heat capacities are computed, their volumes can be calculated by using the following the equation:

$$Vol = m/\rho \tag{8.13}$$

where

Vol: the volume in [m^3]
ρ: the mass density [kg/m^3]

The list of elements can include all various elements such as various vegetables, fruits, liquids (juice, milk, and water), meat … etc.

Air Heat Capacity

Air is assumed to fill the volume of the refrigerator less the sum of the elements volumes. To compute the heat capacity of the air, it is a function of the volume, mass density, and specific heat of the matter as given by:

$$C_{th} = Vol\ \rho\ C_p \tag{14}$$

Door Opening and Load Change

In case of door opening, the duration of time, while the door is opened, is assumed to be enough for the entire cold air to escape and replace with air that is having kitchen temperature. In addition, the volume that was occupied by the cold air is the same for the hot air, unless if there is load changes. As a result, the temperature inside the refrigerator has to be reinitialized. For example, if the fresh food compartment door is opened, the new initialized temperature value can be computed using the following equation:

$$\theta_{fr}^{new} - \theta_{friw} = \frac{C_{fr}(\theta_{fr} - \theta_{friw}) + C_{fr-door}(\theta_K - \theta_{friw})}{C_{fr} + C_{fr-door}} \tag{15}$$

where $C_{fr\text{-}door}$: The heat capacity of the mass air with kitchen temperature.

This is also applied for the when the freezer compartment door is opened, but with related temperatures and thermal capacities. In case of refrigerator load changes, the heat capacities for the elements, which experience mass change, are become different. For example, if the mass of water is increased by 5% in the fresh food compartment, the heat capacity of the water is changed accordingly. The extra mass is assumed to have a Kitchen temperature and a heat capacity. As a result, the temperature inside the fresh food compartment has to be reinitialized and the sum of the all elements heat capacities, C_{fr}, should be updated. The new initialized temperature value is computed as the following:

$$\theta_{fr}^{new} - \theta_{friw} = \frac{C_{fr}(\theta_{fr} - \theta_{friw}) + \Delta C_{fr1}(\theta_K - \theta_{friw})}{C_{fr} + \Delta C_{fr1}} \tag{16}$$

where
ΔC_{fr1}: Heat capacity due to extra mass element change.

This is also applied for the when any element's mass in the freezer compartment has changed, but with related temperatures and thermal capacities.

Thermal Conductance (Gth):

The thermal conductance circuit parameters are computed considering the refrigerator rated data Rated temperature assumed are provided in Table 8.17. Also, it is assumed that the thermal conductance between the two compartments internal walls is 0.02 of the thermal conductance the freezer door. In addition, the thermal conductance between the two compartments external walls is assumed to be 100 times the thermal conductance between the Kitchen air mass temperature and the fresh food compartment external temperature.

Table 8.17 Rated Temperature at each Temperature Spot (^oC)

Temperature Spot	Rated Temp [^oC]
T_{fr}	2.0
T_{friw}	5.0
T_{frew}	28.0
T_{fz}	-5.0
T_{fziw}	0.0
T_{fzew}	28
T_{K1}	33.0

To compute the thermal conductance, the steady state equations of the set equations (D.1)-(D.11) are used as they are provided below. The linear system resulted is solved to determine the values of the circuit thermal conductances. The following important appliance, the air conditioner, is discussed next.

8.5.1.2.6 Simulation Results

A 13.8 kV system used to test the dishwasher model. The test system consists of mainly slack generator, step up and down transformers, transmission line, distribution substation (13.8 kV), overhead distribution line, thermal distribution transformer, service drop, and loads as illustrated in Figure 8.5.8. The simulation is performed over 24 hours. The high side of the electro-thermal transformer is connected to phase A; while the lower side is connected to the residential house via a service drop. Several types of load are included in the test case yet: refrigerator, dishwasher, and a constant impedance loads. The dishwasher is assumed o operate three times during the simulation period. Refrigerator is assumed to be half full. The temperature set for the refrigerator is 2.5 with 1 degree dead-band. The kitchen temperature is assumed to be fixed and equals 33 ^oC.

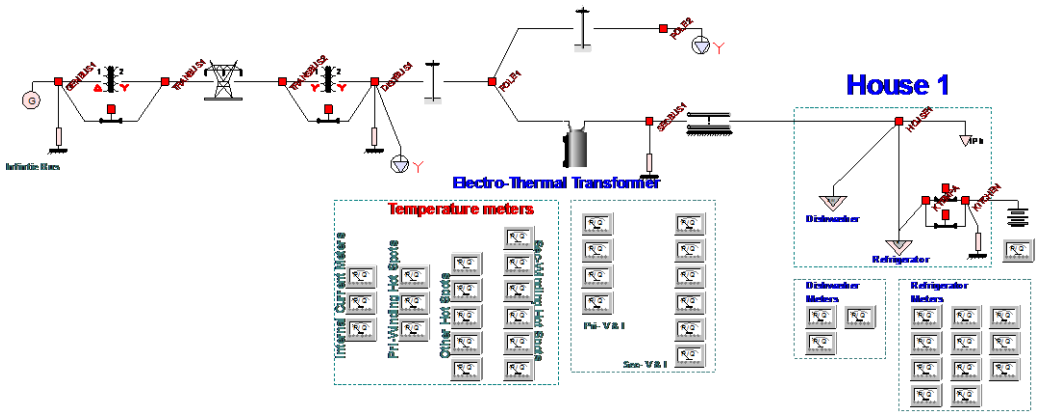

Figure 8.5.8 Refrigerator Test System

In this case, the refrigerator is assumed to be half full. Fresh food and freezer temperature are reported in Figure 8.5.9, Figure 8.5.10, and Figure 8.5.11.

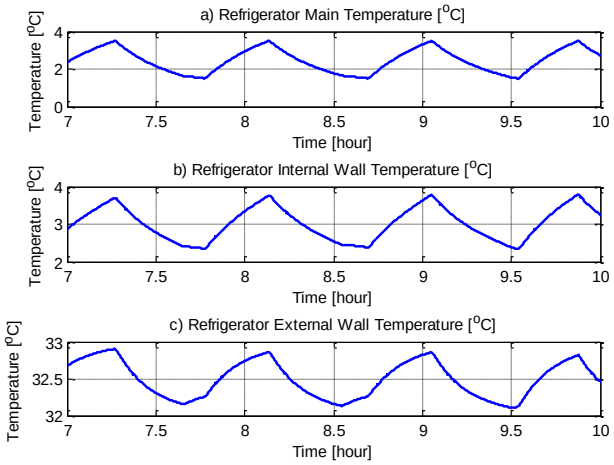

Figure 8.5.9 Refrigerator Fresh Food Chamber Characteristics

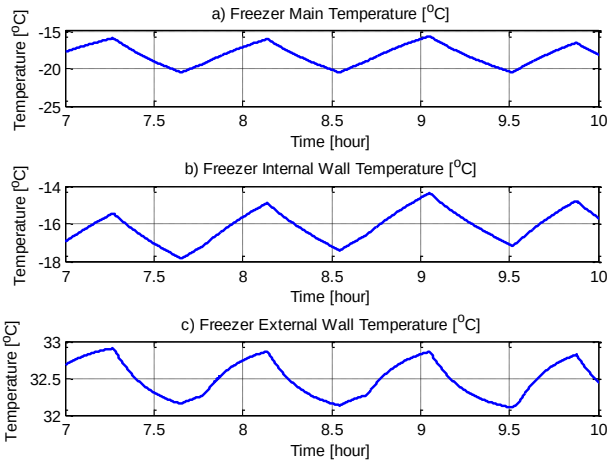

Figure 8.5.10 Freezer Chamber Characteristics

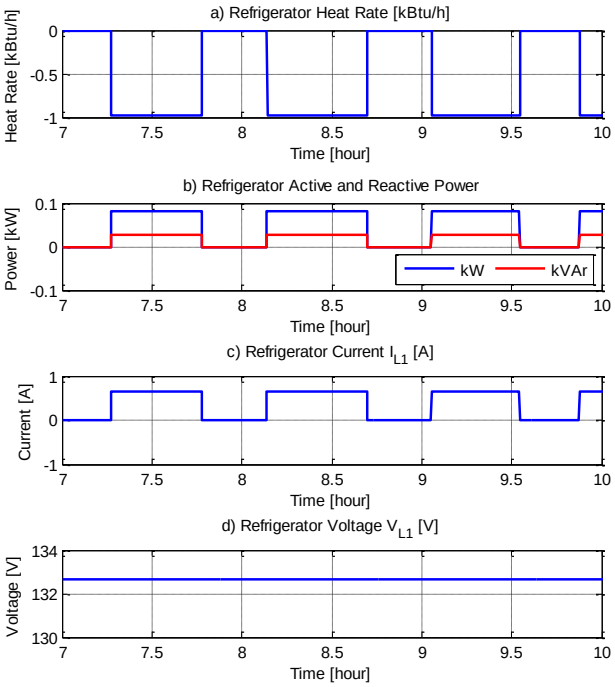

Figure 8.5.11 Refrigerator Heat Rate, Active and Reactive Power, Current, and Voltage Characteristics

8.5.1.3 Air Conditioner Electro-Thermal Model

This section presents the mathematical model of the air conditioner load. The electrical load is modeled as a constant active and reactive power and computed according to the rated air conditioner heat. Figure 8.5.12 shows the model window in the WinIGS program. The electrical and thermal circuits are illustrated by Figure 8.5.13. The upper part shows the electrical circuit; while the lower part shows the thermal circuit. Typical voltage

connection is line to line with voltage rating approximately ranges between 210-240 V. The model is assumed to work at the fundamental frequency. It should be noted that the heat generated by the model is assumed until this time to be only cooling.

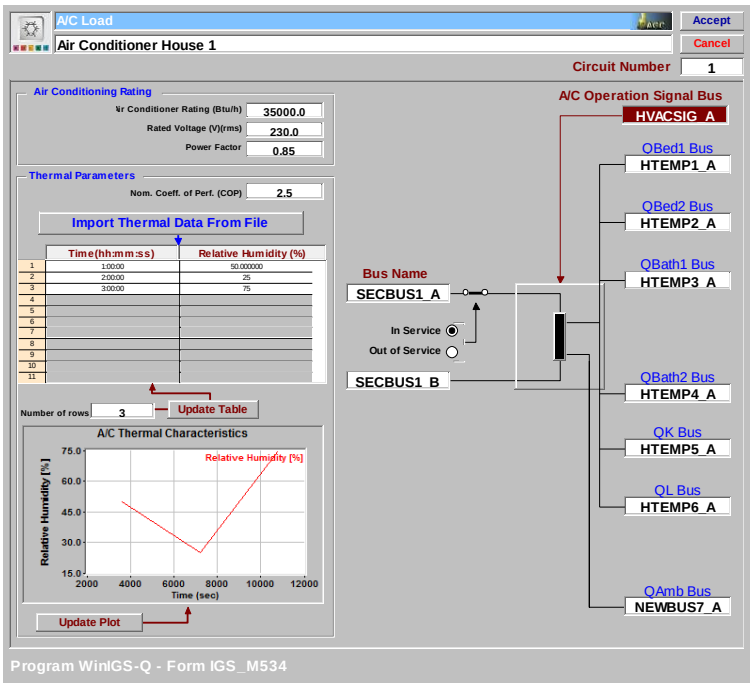

Figure 8.5.12 Electro-Thermal Air Conditioner Model User Interface Window in the WinIGS Program

The characteristics of the air conditioner, rated heat size (BR) and coefficient of performance (COP), are function of the outside temperature. This makes output electrical active and reactive power change according to the environmental conditions. The top part of Figure 8.5.14 shows how the air conditioner rating changes based on the outside temperature. As the temperature drops, the heat rating is increased. Similarly, the air conditioner coefficient of performance increases when the temperature drops as shown in bottom part of Figure 8.5.14. The heat rate (Qhvac) generated by the air conditioner is computed based on the nominal size of the air conditioner, the outside temperature, the relative humidity, and the coefficient of the performance. The model is designed with six ducts to distribute the generated heat (cooling) among various rooms in the house model according the ducts sizes (K1, …, K6). A control signal (u2) is used to control the operation of the air conditioner via a thermostat control model, where the desired temperature can be specified. A full description about the model parameters as well as its equations is provided in Appendix E. The model simulation is included in with the thermal house model simulation.

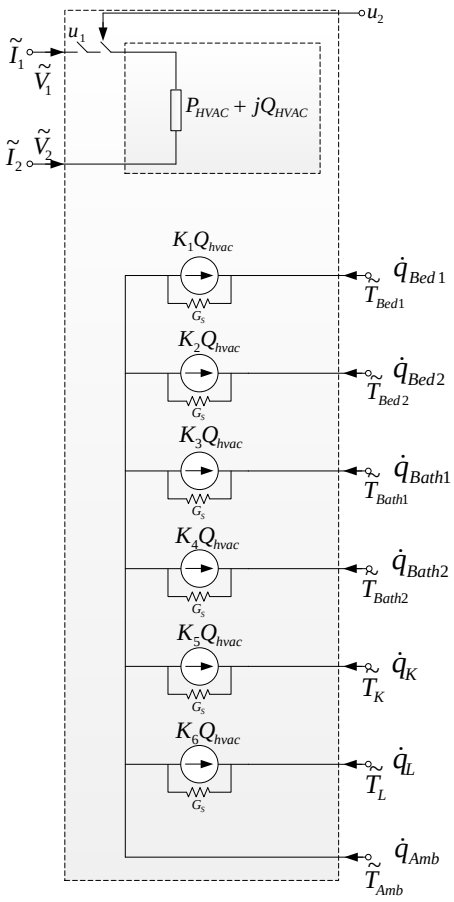

Figure 8.5.13 Air Conditioner Electrical and Thermal Circuit Model

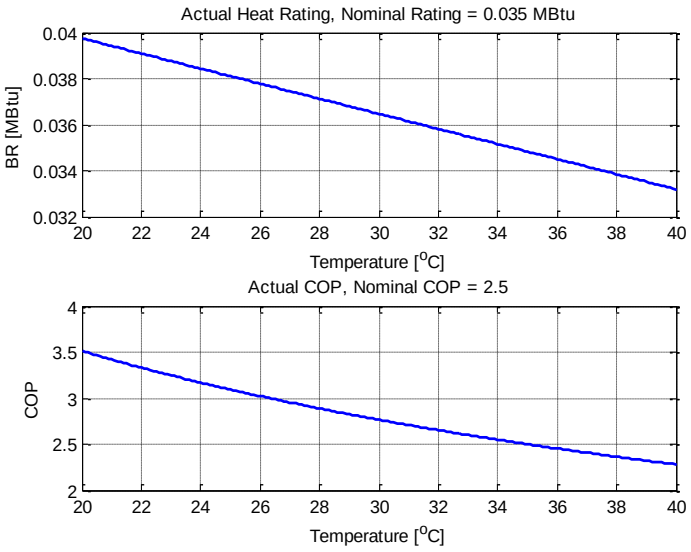

Figure 8.5.14 Air Conditioner Heat Rating (BR, Top Figure) and Coefficient of Performance (COP, Bottom Figure) Characteristics

8.5.1.4 Thermal House Model

The air conditioner model discussed in the previous section can be integrated with a residential/commercial building. In this project, an example of a single story house with two bedrooms and two bathrooms layout is adopted. This layout is illustrated on Figure 8.5.15. The model provides an accurate estimate of the temperature inside the house, which effects the operation of some of the house appliances such as the refrigerator and air conditioner. In other word, a better estimate of the house various temperature spots provide a better estimate of the power consumption of the house appliances.

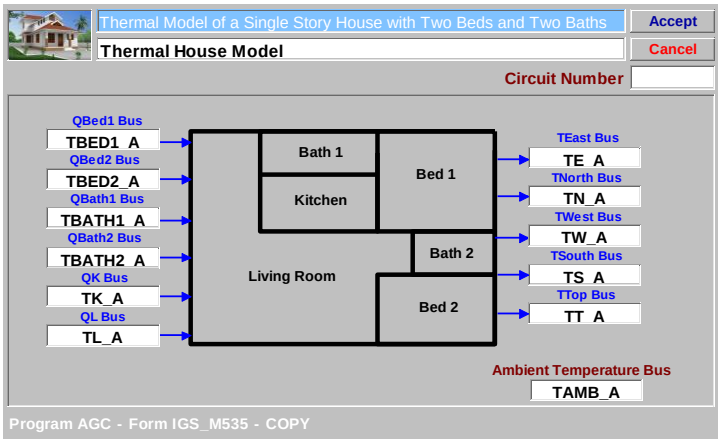

Figure 8.5.15 Adopted House Model User Interface Window in the WinIGS Program

8.5.1.4.1 Definition of the House Thermal Model Parameters

An approximately 1200 ft2 single story house with two bedrooms two bathrooms is considered. The house, however, simplified to have six main spaces as the following: two bedrooms, two bathrooms, a kitchen, and a living room. Extra spaces such as closets and storages are merged with their associated space. The thermal parameters of the house are defined as the following:

1. Temperature Spots:

To monitor the gradient temperatures of the model, several temperature spots have to be selected. In this work, 17 temperature spots are selected. Location of each one of these spots is illustrated in Figure 8.5.16. Specifically, every space is assigned two temperature spots; a main spot and an internal wall spot. To capture the temperature outside the house, every direction including the top of the house is assigned a spot. The definition of each of the spot temperature is given next.

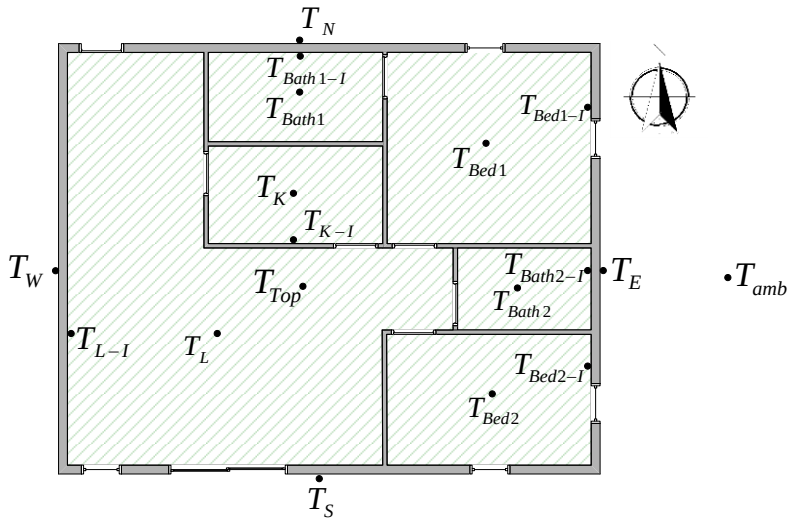

Figure 8.5.16 House Model Internal and External Temperature Spots Locations

- **Bedroom One Spots (Bed1):**
  TBed1: Bedroom 1 temperature spot in [^{o}C].
  TBed1-I: Bedroom 1 internal wall temperature spot in [^{o}C].
- **Bedroom Two Spots (Bed2):**
  TBed2: Bedroom 2 temperature spot in [^{o}C].
  TBed2-I: Bedroom 2 internal wall temperature spot in [^{o}C].
- **Bathroom One Spots (Bath1):**
  TBath1: Bathroom 1 temperature spot in [^{o}C].
  TBath1-I: Bathroom 1 internal wall temperature spot in [^{o}C].
- **Bathroom Two Spots (Bath2):**
  TBath2: Bathroom 2 temperature spot in [^{o}C].
  TBath2-I: Bathroom 2 internal wall temperature spot in [^{o}C].
- **Kitchen Spots (K):**
  TK: Kitchen temperature spot in [^{o}C].
  TK-I: Kitchen internal wall temperature spot in [^{o}C].
- **Living Room Spots (L):**
  TL: Living room temperature spot in [^{o}C].
  TL-I: Living room internal wall temperature spot in [^{o}C].
- **House External Spots (L):**
  TE: East temperature spot in [^{o}C].
  TN: North temperature spot in [^{o}C].
  TW: West temperature spot in [^{o}C].
  TS: South temperature spot in [^{o}C].
  TTop: Top of the house temperature spot in [^{o}C].

2. Thermal Conductances

The thermal conductance is defined as the quantity of heat transmitted between every temperature spot and another. So, for every temperature spot in the physical device, there one or several thermal conductances connected to it. In the house model, the main space spot has a thermal conductance to the internal wall spot. The internal wall spot has thermal conductances with all its direct connected spots such as external wall, top, and other spaces. Basically, it is assumed that there is a thermal conductance between every temperature spot and its direct neighboring spots. For example, bedroom two internal wall spot is connected with the three external spots, bathroom two internal wall, and living room internal temperature spot. All the thermal conductances that are assumed for bedroom two are shown in Figure 8.5.17.

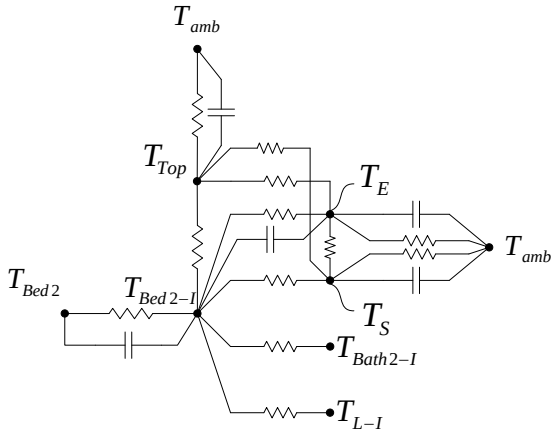

Figure 8.5.17 House Bedroom Two Thermal Circuit Conductance Elements

3. Thermal Capacitances

The thermal capacitance is defined as the amount of the heat energy required to raise the temperature specific amount. The thermal capacitance connections are provided in Table 8.18. Below is a summary of the assumed thermal capacitances:

C_{Bed1}: The sum of the heat capacity of every element inside bedroom one in [Btu/^{o}C].
C_{Bed1_I}: The heat capacity of the wall for bedroom one in [Btu/^{o}C].
C_{Bed2}: The sum of the heat capacity of every element inside bedroom two in [Btu/^{o}C].
C_{Bed2_I}: The heat capacity of the wall for bedroom two in [Btu/^{o}C].
C_{Bath1}: The sum of the heat capacity of every element inside bathroom one in [Btu/^{o}C].
C_{Bath1_I}: The heat capacity of the wall for bathroom one in [Btu/^{o}C].
C_{Bath2}: The sum of the heat capacity of every element inside bathroom two in [Btu/^{o}C].
C_{Bath2_I}: The heat capacity of the wall for bathroom two in [Btu/^{o}C].
C_K: The sum of the heat capacity of every element inside the kitchen in [Btu/^{o}C].
C_{K_I}: The heat capacity of the wall for kitchen in [Btu/^{o}C].
C_L: The sum of the heat capacity of every element inside the living room in [Btu/^{o}C].
C_{L_I}: The heat capacity of the wall for living room in [Btu/^{o}C].
C_E: East side spot heat capacity in [Btu/^{o}C].

C_N: North side spot heat capacity in [Btu/^{o}C].
C_W: West side spot heat capacity in [Btu/^{o}C].
C_S: South side spot heat capacity in [Btu/^{o}C].
C_{Top}: Top side spot heat capacity in [Btu/^{o}C].

Table 8.18 House Model Thermal Capacitance Connections

Thermal Capacitance (C_{th})	Spot 1	Spot 2
C_{Bed1}	T_{bed1}	$T_{bed1\text{-}I}$
$C_{Bed1\text{-}I}$	$T_{bed1\text{-}I}$	T_E
C_{Bed2}	T_{bed2}	$T_{bed2\text{-}I}$
$C_{Bed2\text{-}I}$	$T_{bed2\text{-}I}$	T_S
C_{Bath1}	T_{Bath1}	$T_{Bath1\text{-}I}$
$C_{Bath1\text{-}I}$	$T_{Bath1\text{-}I}$	T_N
C_{Bath2}	T_{Bath2}	$T_{Bath2\text{-}I}$
$C_{Bath2\text{-}I}$	$T_{Bath2\text{-}I}$	T_E
C_K	T_K	$T_{K\text{-}I}$
$C_{K\text{-}I}$	$T_{K\text{-}I}$	T_{Top}
C_L	T_L	$T_{L\text{-}I}$
$C_{L\text{-}I}$	$T_{L\text{-}I}$	T_W
C_E	T_E	T_{amb}
C_N	T_N	T_{amb}
C_W	T_W	T_{amb}
C_S	T_S	T_{amb}
C_{Top}	T_{Top}	T_{amb}

8.5.1.4.2 Thermal House Mathematical Model

This section presents the mathematical model of the thermal house. The thermal circuit of the house is assumed to have 44 thermal conductances, 17 heat capacity, and 6 heat sources. The dynamic of the temperature given by (8.8) is used to derive the thermal model of the house. The set of equations for the thermal house model is provided in a compact form in 0.

8.5.1.4.3 Thermal House and Air Conditioner Models Simulation

A 13.8 KV system used to test the air conditioner model. The test system consists of mainly slack generator, step up and down transformers, transmission line, distribution substation (13.8 KV), overhead distribution line, thermal distribution transformer, service drop, and loads as illustrated in Figure 8.5.18. The high side of the electro-thermal transformer is connected to phase A; while the lower side is connected to the air conditioner and other loads. It should be noted that since typical air conditioner voltage is 210-240 V, its electrical terminal is connected to L1 and L2 of the center tap transformer. The thermostat controller is set to monitor the temperature in bedroom one in the house model. It is set on 25 ^{o}C with three degrees deadband.

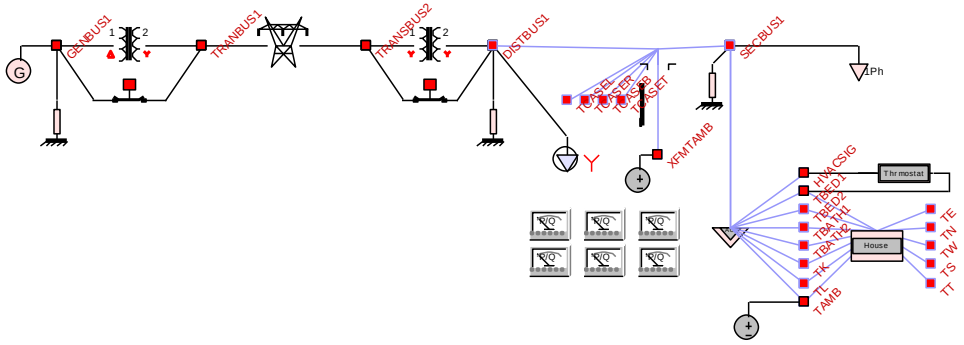

Figure 8.5.18 Test Case System

As shown in Figure 8.5.19, the outside temperature and relative humidity are specified to be changed during the simulation. Various temperature spots measurements of the house are presented in Figure 8.5.19 c. The temperature swings between the deadband limit. A complete operation cycle is about 50 minutes. This, of course, changes as the temperature setting changes and the environmental characteristics change too. The air conditioner various characteristics are shown in Figure 8.5.20. The active and reactive power generated by the air conditioner model is shown in Figure 8.5.20 a. During the operation of the air conditioner to cool the house, the power consumption is not flat. As the outside temperature increases, the efficiency of the thermal cycle inside the air conditioner decreases and thus more active power is drawn from the grid. The heat rate generated by the model is shown in Figure 8.5.20 b. The negative sign in the heat rate plot indicates a cooling setting. In Figure 8.5.20 c, the operation control signal provided by the thermostat controller is depicted. Also, both the heat rating of the air conditioner and the coefficient of performance are presented in Figure 8.5.20 c and d.

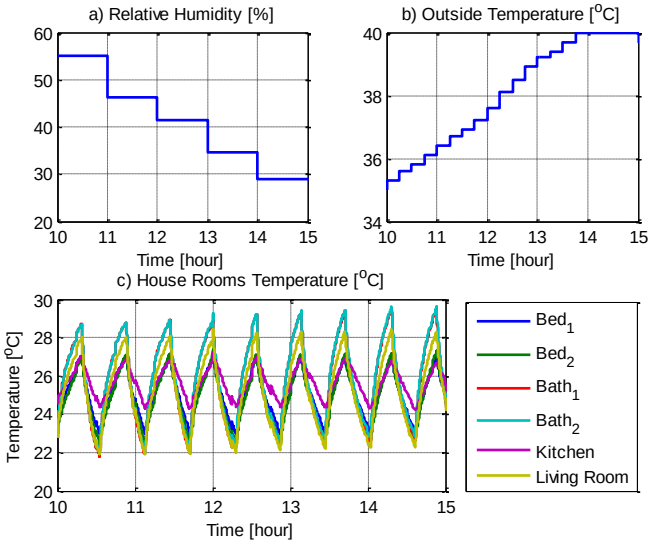

Figure 8.5.19 House Temperature Characteristics

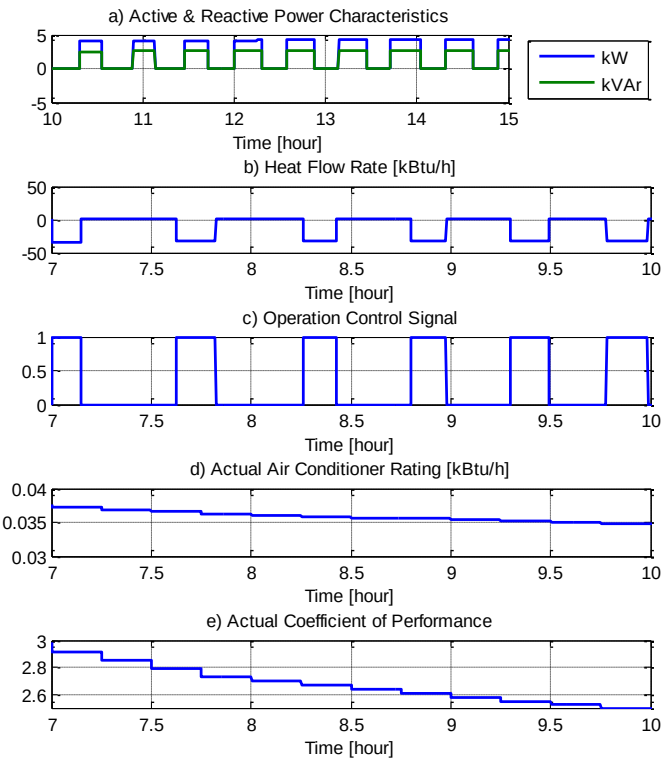

Figure 8.5.20 Air Conditioner Characteristics

8.5.1.5 Other Load Models

So far, several house appliances are physically modeled including dishwasher, refrigerator, and air conditioner. However, to be able to fully capture the energy consumption of the house/ building whether residential or commercial, other appliances consumptions such as lighting, cloth washer and dryer, etc., should be included. For this purpose, a time varying load is developed. The variable load is modeled mathematically as a specified constant active and reactive power at the fundamental frequency (60 Hz) for every time period. The model can, also, adopt different voltage configurations, weather line to line or line to ground, as it is in the physical world. A picture of the variable load model window in the program is illustrated in Figure 8.5.21. The basic electrical circuit is illustrated in Figure 8.5.22. The mathematical model in a compact form is provided in Appendix G.

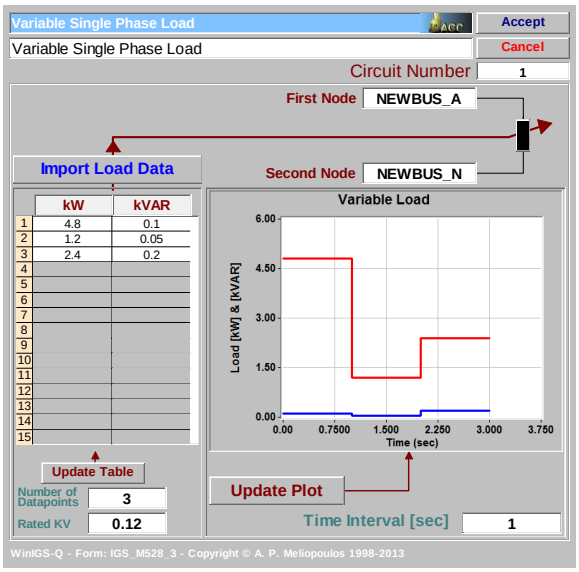

Figure 8.5.21 Variable Load Model User Interface Window in the WinIGS Program

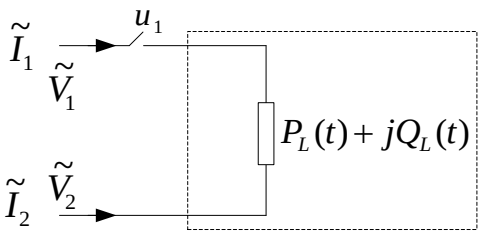

Figure 8.5.22 Electric Circuit of the Variable Load Model

8.5.2 Modeling of Residential House Distributed Energy Resources

Energy distributed resources are considered important part of a smart residential/commercial building. In this section, various resources that can be integrated with a building are physically based modeled.

8.5.2.1 Roof-Top Solar PV Model

The solar photovoltaic array is modeled based on [84]. The model is a dependent on the environment conditions, i.e. temperature and solar irradiance. Figure 8.5.23 shows the equivalent electrical circuit of the single diode solar cell. The mathematical model of the photovoltaic solar cell is provided in a compact form 0.

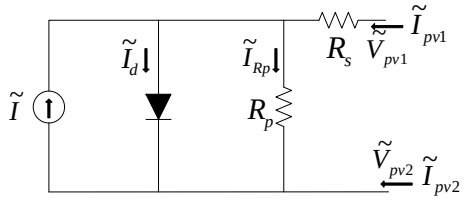

Figure 8.5.23 Equivalent Electrical Circuit of the Solar Cell

Data that are required to perform simulation are usually provided by the solar array manufacturer except the series and parallel resistances. Algorithm provided in [84] was used to find the optimized values of the both resistance. Data used to test the developed model was taken from [85]. Table 8.19 shows the parameters used from the data sheet to test the modeled cell.

Table 8.19 Parameters Used on the Modeled PV Cell

$\boldsymbol{P_{max}}$	260 W	$\boldsymbol{R_s}$	0.373
$\boldsymbol{I_{sc}}$	9.01 A	$\boldsymbol{R_p}$	824.25
$\boldsymbol{V_{oc}}$	38.3 V	$\boldsymbol{K_I}$	0.047
$\boldsymbol{N_s}$	60 in series	$\boldsymbol{K_V}$	-0.335

Figure 8.5.24 shows the current – voltage and voltage – power characteristics of the cell at the nominal temperature using the data in Table 8.19. It also shows the characteristics of the cell for different solar irradiance ranged from the very low solar irradiance to the maximum. On the other hand, Figure 8.5.25 depicts the cell output current and voltage at the maximum attained solar irradiance considering various temperatures.

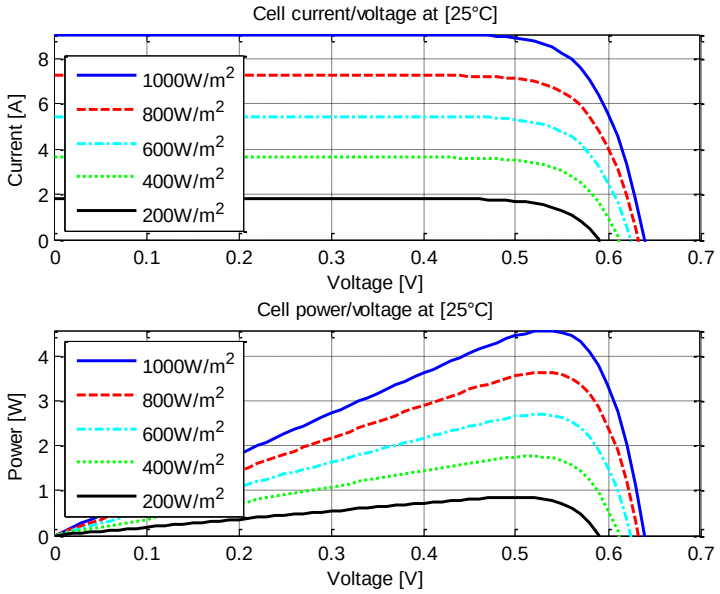

Figure 8.5.24 Solar Cell I-V and P-V Characteristics

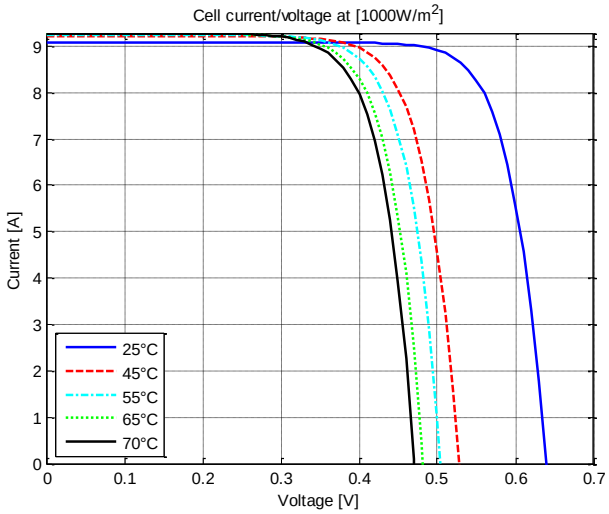

Figure 8.5.25 Cell Current and Voltage at Maximum Solar Irradiance at Various Temperature Conditions

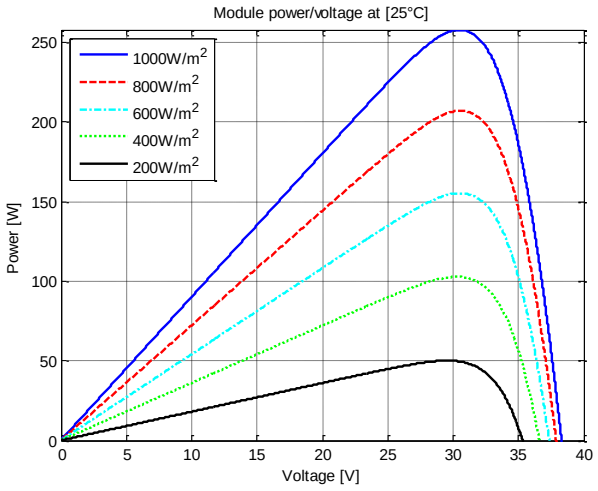

Figure 8.5.26 P-V Characteristics of the PV Module

The solar photovoltaic is connected to a power electronic based DC-DC boost converter to step up the voltage to a level that is comparable to the building voltage level. The average model of the boost converter is discussed next.

8.5.2.2 Single Phase Average DC-DC Boost Converter Model

The DC-DC boost converters are used as a mean to regulate the input voltage, which is regularly an unregulated dc voltage. Stepping up the input voltage can be achieved by using the boost type DC-DC converter. The circuit diagram of this type is shown in Figure 8.5.27. As the name implies, the output voltage is greater than the input, which is controlled by the duty ratio, D. Typical switching frequency used is 60 kHz. The model is designed to work with three different control schemes as the following:

- DC voltage control: It maintains a constant DC output voltage.
- Real power control: It maintains a constant real output power.
- Maximum power point tracking (MPPT) control: In case if the boost converter is connected to a solar photovoltaic (PV), this control option is chosen. It, basically, regulates the converter duty cycle (D) to maintain a constant output voltage. Several MPPT algorithms can be implemented such as perturb and observe, incremental conductance, fuzzy logic, current sweep … etc [86]. In this project, perturb and observe (P&O) algorithm is implemented, which is explained next.

Perturb and observe (P&O) algorithm is used to achieve maximum tracking.

Figure Figure 8.5.28 shows a schematic diagram of (P&O) used. The algorithm makes use of the relation between the output power and the voltage of the PV to determine whether increasing or decreasing the duty cycle.

The equations of the compact model that describe the averaged single phase DC-DC boost converter in the frequency domain and with every control scheme are given in 0.

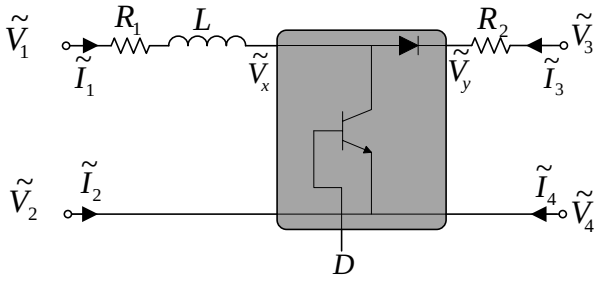

Figure 8.5.27 Equivalent Device Circuit Model of the Single Phase DC-DC Boost Converter

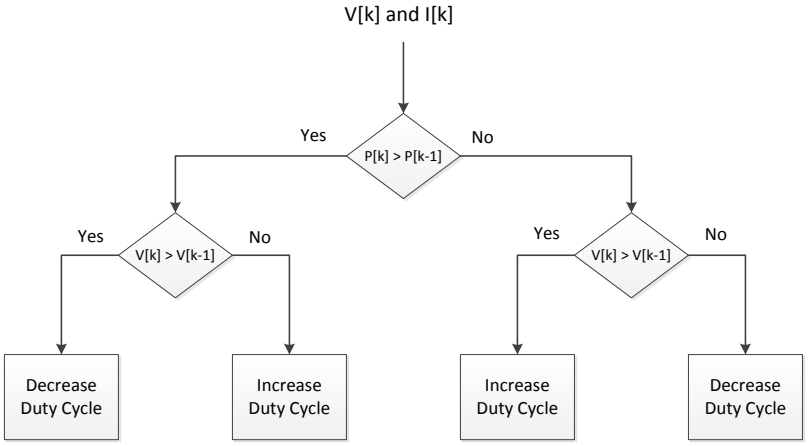

Figure 8.5.28 Perturb and Observe Maximum Tracking Algorithm

8.5.2.3 Single Phase Full Bridge Average DC-AC Inverter Model

The DC-AC inverters are used as a mean to convert input dc current or voltage to ac current or voltage. The circuit diagram of this type is shown in Figure 8.5.29. As the name implies, the output voltage is ac waveforms, which is controlled by the modulation index, M. The model is equipped with two different controls as the following:

VQ Control: It maintains an input dc voltage equals to dc reference voltage and constant reactive power equals to an imaginary power reference.

PQ Control: It maintains a constant real and imaginary power equal to a specified real and imaginary power references.

The mathematical model with every control is provided in Appendix J.

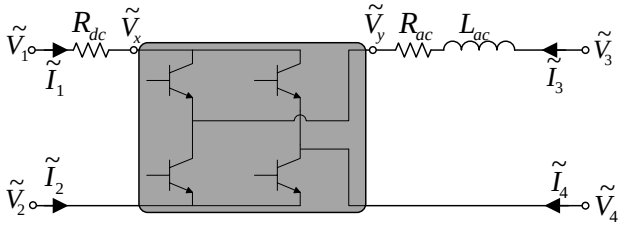

Figure 8.5.29 Equivalent Device Circuit Model of the Single Phase Full Bridge DC-AC Inverter

8.5.2.4 Electro-Thermal Battery Energy Storage System (BESS) Model

Battery based, energy storage system is modeled as part of the smart residential/commercial building DER. Several types of battery could be used for the storage function. However, the mostly and widely used type for photovoltaic and building application is the Lead Acid battery type. It is economically attractive and easily maintained and can last for a long time. Dynamical simulation models are already developed and existed in the literature. Among these, a highly used, validated, and accurate the model developed according [87-89]. It is a third order model and accounted for the following:

The model is dynamic and built mainly for lead acid batteries.

- Surrounding and internal battery temperature variation is considered (thermal model).
- Internal gassing current is modeled.
- Battery self-discharging characteristic is neglected.

The overall battery's configuration is shown in Figure 8.5.30. It is shown with two control switches, which responsible of identifying the operation modes. The first switch, u1, determines the connection status of the battery, which is either standby or connected; whereas, the second switch, u2, governs the battery's mode of operation, either charging or discharging. The mathematical model for every model of operation is provided in Appendix K.

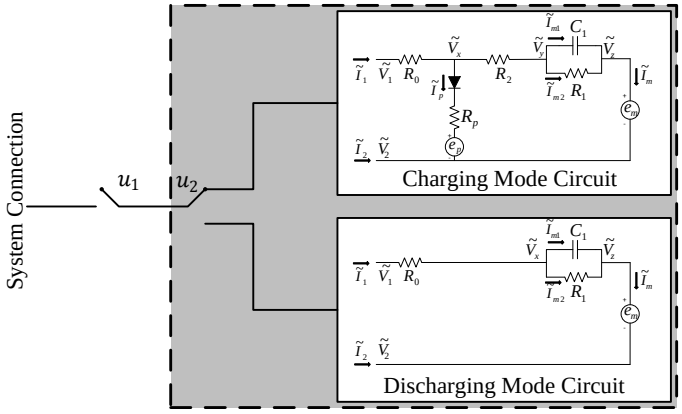

Figure 8.5.30 Configuration of Lead-Acid Battery with the Control Switches

When the first control switch is closed, two modes of operation can be deduced from the battery, charging and discharging. The following sections provide a detailed formulation of the mathematical models in the Frequency domain.

8.5.2.4.1 Lead Acid Battery Simulation

The model represented by (K.1)-(K.14) is simulated and results are reported. All three mode operations, discharging, charging, and stand by, are tested using a battery's numerical values provided in Table 8.20. The battery is assumed to have a charge capacity = 500 Ah for 10 hours.

Table 8.20 Lead Acid Battery Parameters [87]

Main branch				
E_{m0}=2.135 V	R_{00}=2 mΩ	R_{10}=0.7 mΩ	R_{20}=15 mΩ	τ_1=5000 sec
A_0=-0.3	A_{21}=-8.0	A_{22}=-8.45	K_E=0.58 mV/^{o}C	
Parasitic branch				
E_p=1.95 V	V_{p0}=0.1 V	G_{p0}=2 pS	A_p=2.0	
Charge and capacity				
I^*=49 A	$C_0{}^*$=261.9 Ah	K_c=1.18	θ_f=-40 ^{o}C	ξ=1.29	δ=1.4
Thermal model				
C_θ=15 Wh/^{o}C		R_θ=0.2 ^{o}C/W		

Figure 8.5.31 shows the battery when it is in a discharging mode for different levels of discharging currents. The battery was assumed to be fully charged first.

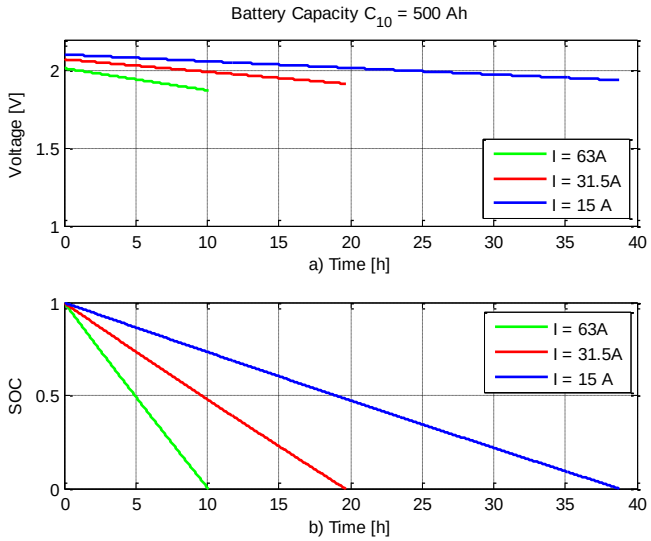

Figure 8.5.31 Lead Acid Battery in Discharge Mode, a) Battery Voltage [V], b) State of Charge (SOC)

In the charging mode the battery was assumed to be fully empty. At the fifth hour, the charging process begins for different level of charging currents, shown in Figure 8.5.32.

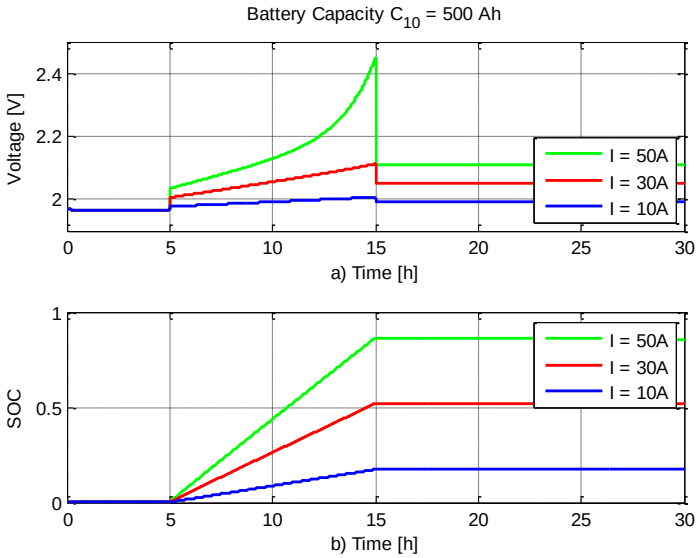

Figure 8.5.32 Lead Acid Battery in Charging Mode

8.5.2.5 Electric Vehicle Model

The unfavorable impacts due to integrating large number of electric vehicles can be mitigated by appropriate controls of the time when charging/discharging the electric vehicles take place. To be able to do this, a physical based electro thermal model of the electric vehicle. In particular, the electric vehicle is modeled as lithium ion battery with

appropriate size. The next section explains the lithium ion battery model adopted in this project.

8.5.2.5.1 Lithium-Ion Battery Model

A dynamic model of the lithium-ion battery is built according to [90]. The model accounts for the following:

- The model is dynamic and built mainly for lithium-ion batteries.
- Surrounding and internal battery temperature variation is considered (thermal model).
- Battery self-discharging characteristic is neglected.

The overall battery's configuration is shown in Figure 8.5.33. It is shown with one control switch, which responsible of identifying the operation modes. The switch, u1, determines the connection status of the battery, which is either standby or connected. The mathematical model in a compact form is provided in Appendix L.

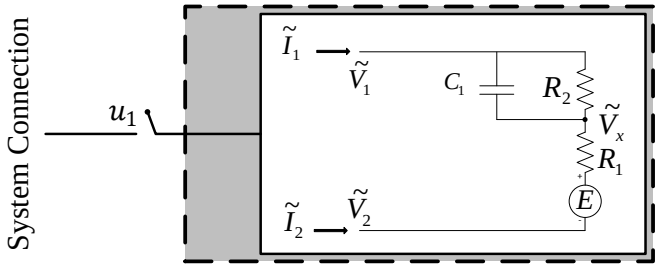

Figure 8.5.33 Configuration of Lithium-Ion Battery with the Control Switch

8.5.2.5.2 Lithium-Ion Model Simulation

The model represented by (L.12)-(L.21) is simulated and results are reported. The model is tested for 1 cell lithium-ion battery using a battery's numerical values provided in Table 8.21.

Table 8.21 Lithium-Ion Battery Parameters [87]

$V_{internal}$= 4.124 V	$SOC_{initial}$ = 1.0 (Discharging)	$SOC_{initial}$ =1e-6 (Charging)
$R_1 = 0.08\,\Omega$	$R_2 = 0.04\,\Omega$	$C_1 = 4\,F$
$Q_r = 0.5\,rate$	$m = 41\text{x}10^{-3}Kg$	$c_p = 925(\frac{J}{Kg}/K)$
$h_c = 10(\frac{W}{m^2}/K)$	$A = 4.3\text{e}^{-3}m^2$	$T_a = 25$

The voltage and state of charge of the battery model during charging mode is presented in Figure 8.5.34. It takes about 2.7 hours to charge the battery from empty to full. On the other hand, Figure 8.5.35 shows the battery voltage and SOC during discharging mode. The model is scalable and, with appropriate sizing, it will be used to model the electric vehicle.

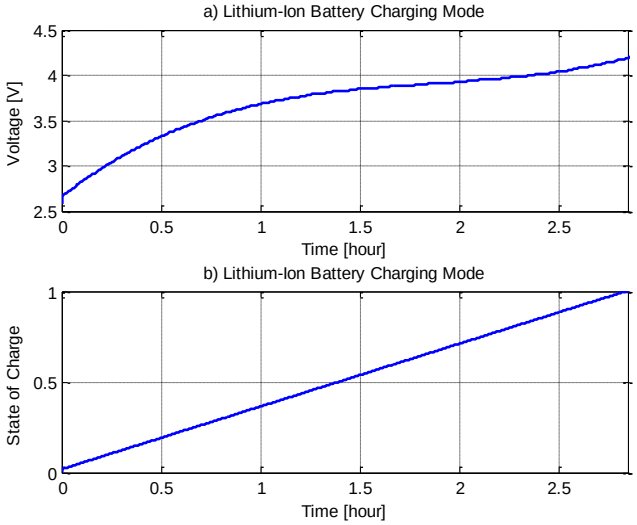

Figure 8.5.34 Lithium-Ion Battery Charging Mode Voltage and SOC

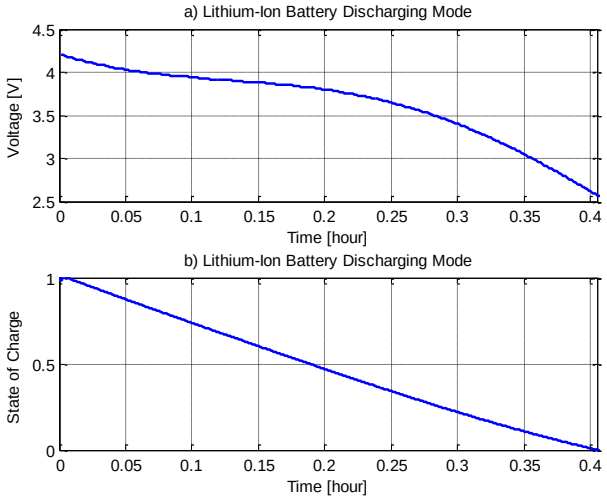

Figure 8.5.35 Lithium-Ion Battery Discharging Mode Voltage and SOC

8.5.2.6 Battery Charger Model

The battery charger, whether lead acid or lithium ion, is assumed to be a single phase DC-DC buck-boost converter. The DC-DC buck boost converters are used as a mean to step up or down the input dc voltage. Stepping up the input voltage can be achieved by using the boost type DC-DC converter. On other hand, stepping down can be done by using the buck converter. The circuit diagram of the buck-boost converter is shown in Figure 8.5.36.

The output voltage is controlled by the duty ratio, D. The mathematical model of the buck-boost converter is provided in Appendix M. The model is equipped with two different controls as the following:

- DC Voltage Control: It maintains an input dc voltage equals to dc reference voltage.
- Real Power Control: It maintains a constant real power equals to a specified real power reference.

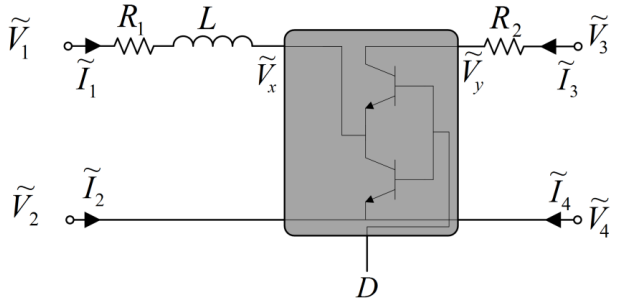

Figure 8.5.36 Equivalent Circuit Model of the Single Phase DC-DC Buck-Boost Converter

8.6 Summary

In this section, we presented physically based models of various components that are considered to be part of the overall model of the system. These include energy resources such as roof top solar PV, energy storage system in the form of lead acid battery system … etc and house appliances such as smart dishwasher, refrigerator, and air conditioner. Averaged models of power electronics converters are used to connect various parts of the system together. A demonstration case study of most of these new models is also provided to display the various characteristics of the model. Note that these models can be used as commercial building appliances, if appropriately scaled. Each model is cast in one common object oriented based frame to make it accessible for developing new models without changing the existing once. Also note that the overall model is integrated by connecting the various components in the way they laid out in the physical system. In a residential house for example, if the refrigerator is located in the kitchen, it is connected to the kitchen model, etc. The overall model is managed by a house management system that provides appropriate control for the entire system connected to a distribution transformer. This may include the transformer and one or more houses.

9. Distributed State Estimation (DSE)

The second major building block of the proposed approach is the distributed state estimator. It provides a reliable real time model that is necessary for the model based coordinated control used in the house management system.

The location of the DSE is determined based on the goals set by the power system operators. Real time synchronized data gathered by various types of metering devices including that monitor the system components are sent to DSE, which is set to receive synchronized measurement and fit the data into a highly accurate model. A general illustration of the DSE algorithm is shown in Figure 9.1. This scheme results to a real time monitoring of the system [91-94]. The DSE will estimate the states of the house, which are a collection of external and internal states of all components states that are connected to the house. The external states include the phasor voltages of the bus as well as the devices. On the other hand, the internal states are algebraic or dynamic states which are existed inside the device. Measurements will also include the state of the control devices, such as switches, dishwasher operation time, converter controllers, which will be used by the optimization algorithm to achieve specified objectives. The mathematical formulation of the DSE is discussed next. Basically, DSE consists of several blocks as the following: Devices, State Set, Measurements Set, State Estimation Algorithm, Detection and Identification of bad data and error analysis.

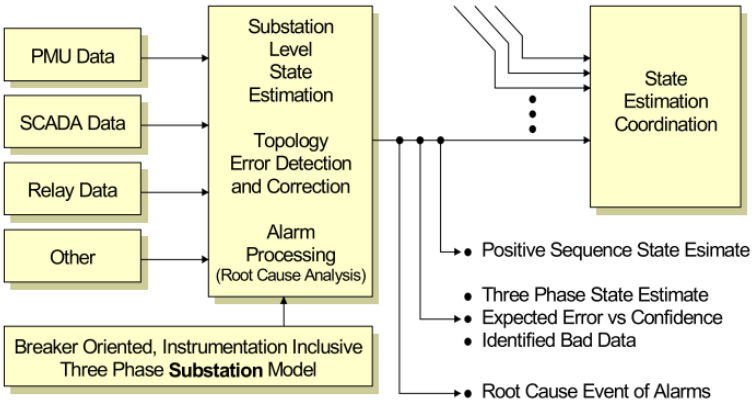

Figure 9.1 A General Description of the Distributed State Estimation Algorithm [94, 95]

1. Three Phase Device Model

Due to single phase loads and feeders, the system imbalances and asymmetries are common. To capture this, the power system has to be modeled on a three phase base (including neutral and grounds) using the physical model of each component.

2. State Set

It is defined as the set of the voltage phasors of every node of the system that describes the operating conditions. So for every three phase bus i of the system the states are defined as,

$$\widetilde{\mathbf{V}}_{\mathbf{i}} = \left[\widetilde{\mathbf{V}}_{\mathbf{i,A}} \quad \widetilde{\mathbf{V}}_{\mathbf{i,B}} \quad \widetilde{\mathbf{V}}_{\mathbf{i,C}} \quad \widetilde{\mathbf{V}}_{\mathbf{i,N}}\right]^{\mathbf{T}} \tag{9.1}$$

3. Measurement Set

The measurements, GPS-synchronized or non-synchronized, are expressed as nonlinear functions in terms of the states of order at most quadratic. The generic form of the measurement is as follows,

$$\mathbf{z_k} = \mathbf{c_k} + \sum_{\mathbf{i}} \mathbf{a_{k,i}}\, \mathbf{x_i} + \sum_{\mathbf{i,j}} \mathbf{b_{k,i,j}}\, \mathbf{x_i}\, \mathbf{x_j} + \eta_{\mathbf{k}} \tag{9.2}$$

where
zk: is the measured value
ck: is the constant term
ak,i: are the linear coefficients
bk,i: are the nonlinear coefficients
ηk: is the error term

4. State Estimation Algorithm

Using the least square approach, the objective is to estimate the states x. Therefore, the problem is formulated as follows,

$$\mathbf{Min}\ \mathbf{J(x)} = \eta^{\mathbf{T}}\mathbf{W}\eta \tag{9.3}$$

where
$\eta = z - h(x)$, and W is a diagonal matrix whose non-zero entries are equal to the inverse of the variance of the measurement errors given by:

$$\mathbf{W} = \mathbf{diag}\left[\frac{\mathbf{1}}{\boldsymbol{\sigma}_{\mathbf{v}}^{\mathbf{2}}}\right] \tag{9.4}$$

Then, the following iterative algorithm is used to obtain the best estimate of the system state,

$$\hat{\mathbf{x}}^{\mathbf{j+1}} = \hat{\mathbf{x}}^{\mathbf{j}} + (\mathbf{H}^{\mathbf{T}}\mathbf{W}\mathbf{H})^{-\mathbf{1}}\mathbf{H}^{\mathbf{T}}\mathbf{W}\left(\mathbf{z_a} - \mathbf{h}(\hat{\mathbf{x}}^{\mathbf{j}})\right) \tag{9.5}$$

, where $\hat{x}$ refers to the best estimate of the state vector and H is the Jacobian matrix of the measurement equations.

5. State Estimation Accuracy Quantification

Chi-square test is used to find the accuracy of the state estimate and the estimation confidence. Given the number of measurements m and the number of states n, the degrees of freedom can simply be calculated as ν=m-n. Calculating the value ζ of the objective

function based on the state estimates, the estimation confidence level is given by the probability,

$$\Pr[\chi^2 \geq \zeta\,] \;=\; 1.0 \;-\; \Pr[\chi^2 \;\leq \zeta\,] \;=\; 1.0 \;-\; \Pr(\zeta\,, \mathrm{v}) \tag{9.6}$$

For an acceptable confidence level, the accuracy of the solution is computed via the covariance matrix as follows,

$$\mathrm{C_x} = \mathrm{E}[(\hat{\mathrm{x}} - \bar{\mathrm{x}})(\hat{\mathrm{x}} - \bar{\mathrm{x}})^{\mathrm{T}}] \tag{9.7}$$

, where $\bar{\mathrm{x}}$ denotes the true state value and $\hat{\mathrm{x}}$ the estimated value, and computed as,

$$\mathrm{C_x} = (\mathrm{H^T W H})^{-1} \tag{9.8}$$

Once the information matrix of the solution has been computed, the standard deviation of a component of the solution vector is given by,

$$\sigma_{\mathrm{x_i}} = \sqrt{\mathrm{C_x(i,i)}} \tag{9.9}$$

, where Cx(i,i) is the ith diagonal entry of the Cx.

The estimates of the measurements can also be computed as,

$$\hat{\mathrm{b}} = \; \mathrm{h}(\hat{\mathrm{x}}, \hat{\mathrm{y}}) \tag{10}$$

, which covariance matrix is proved to be,

$$\mathrm{Cov}\big(\hat{\mathrm{b}}\big) = \mathrm{H}(\mathrm{H^T W H})^{-1}\mathrm{H^T} \tag{9.11}$$

It should be noted that DSE in this formulation is scalable.

10. House System Optimization

10.1 Introduction

In this section, the optimization function that is the core of the management system is discussed. The house model that is optimized can accommodate roof-top solar PV, energy storage (lead-acid type batteries), distribution transformers, controllable and non-controllable house appliances including air conditioner, dishwasher, and plug-in electric vehicle (EVs) modeled as lithium-Ion battery with/without the capability to generate. Averaged models of power electronic converters are used to link various parts of the house system together. The management system with its optimization functionality can control/manage more than one house to be fed by one distribution transformer as this may be also quite usual. As noted before that the house components can be connected in any arrangement depending on what exists in reality and how they are connected to the distribution transformer, the optimization is designed in an object orientation format to be able to accept various configuration that can be set up, which is discussed next. A symbolic view of the overall model is shown in Figure 10.1.

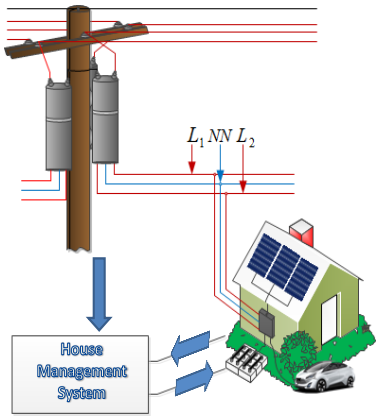

Figure 10.1 Illustration of One Smart House Connected to a Center-Tap Transformer

10.2 Mathematical Formulation of the Optimization Problem

The house management system optimization problem is defined as the optimal scheduling of house resources and smart appliances such as lead acid battery charging/discharging, electric vehicle charging/discharging, and dishwasher over a specified a short planning period, mostly one day. For the formulation of this problem it is assumed that the following are given:

1. House(s) and distribution transformer topology, including distributed resources and appliances.
2. House distributed resources and appliances status including state of charge of storage and others.
3. System time series parameters forecasting such as solar irradiance, temperature, and relative humidity.

Given this information, the optimization problem determines the optimal operating conditions for the house distributed resources and appliances subject to meeting no convenience being incur to the house residents. Optimal operating conditions include the best charging and discharging time for the energy storage system (lead acid battery) and electric vehicle, optimal real and reactive power injection/absorption of the inverter-interfaced distributed resources, and smart dishware. The object-oriented adopted approach enables the ability to implement different objective functions based on the power system operators' desired goals. The management system can provide control of peak load demand, which will elongate the economic life of the distribution transformer by avoiding volatile loading of the transformer and meet other objectives as necessary. In case of variable electricity rates, for example hour of the day rates, it can optimize the cost of electricity by utilizing the capabilities of the electric vehicles stored energy and other resources of the house such as postponing the operation of smart appliances during peak electricity price rate. The most vulnerable part of this system is the distribution transformer – the proposed management system may monitor the transformer loss of life and manage the consumption to elongate the life of the transformer. A general mathematical formulation of the optimization problem is given by,

$$\mathbf{min} = \mathbf{f}(\mathbf{x}, \mathbf{u}) \tag{10.1}$$

Subject to,

$$\begin{aligned} \mathbf{g_i}(\mathbf{x}, \mathbf{u}) &= \mathbf{0}, \quad \mathbf{i} = \mathbf{1}, \dots, \mathbf{m} \\ \mathbf{h_i}(\mathbf{x}, \mathbf{u}) &\geq \mathbf{0}, \quad \mathbf{i} = \mathbf{1}, \dots, \mathbf{p} \end{aligned} \tag{10.2}$$

where
f(x,u): The objective function to be minimized over x and u.
hi(x,u) $\geq$ 0: The inequality constraints of the formulation optimization problem. This includes all the house model constraints such as the temperature set of the house and the time when the dishwasher load must be ready.
gi(x,u) = 0: The equality constraints. This basically represents the dynamic of the house and the overall system. This set of equations provides the power flow in the system.
x: the system states variables.
u: the system control variables.

Demonstrative examples for the house system with/without the management system are provided in the next section.

11. Demonstrative Example

A demonstrative case study is used to provide an understanding of the benefits of the house management system and its ability to optimally coordinate the operation of house assets/resources that also may include EVs and PHEVs. Required input data are described first. After that, two case studies are presented one for normal day operation and the second is for a peak day operation. Discussion on every simulation case results is provided accordingly.

11.1 Input Data Description

To monitor and optimize the operation of system, input data such as the house surrounding environmental conditions should be used. Real data for a single story house at Glasgow, KY area are used. They are corresponding to the peak load day of the year, July, 1st 2013. The data include the loading condition for various house resources and appliances, outside temperature, and relative humidity. These data will be used by various house distributed resource and appliances models.

Solar irradiance data used in the simulation was recorded with 10 minutes resolution. These data are used by the house/commercial building roof-top solar PV model. The environmental condition of that day was happened to be a cloudy day; therefore, a lot of transient is expected in the output of the roof top solar PV. Figure 11.1 presents the solar irradiance data. The maximum value of the solar power density is about 790 W/m2 at 1:20 pm.

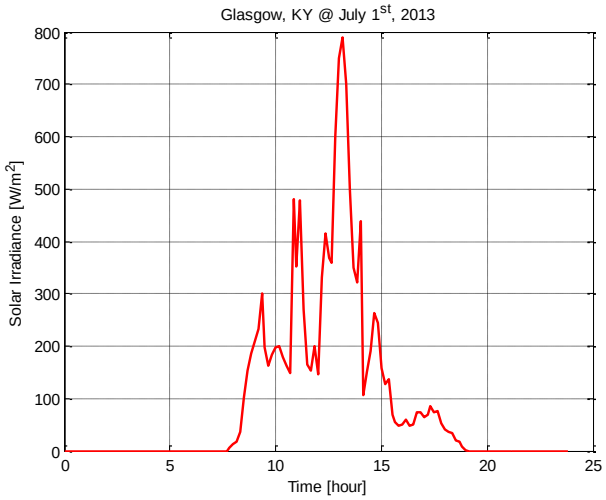

Figure 11.1 Solar Irradiance Input Data

Temperature data for the simulated day is presented in Figure 11.2. The data is with 10 minutes resolution, also. During this peak day, the highest temperature registered was about 40 ^{o}C and the lowest temperature was 24.4 ^{o}C. This large envelope of temperature variation

is expected to have an impact on the temperature inside the house and the operation of some of the house appliances. The models that will make use of temperature data are solar PV, single phase center-tap transformer, thermal house, air conditioner, and electric vehicle (lithium-ion battery) models.

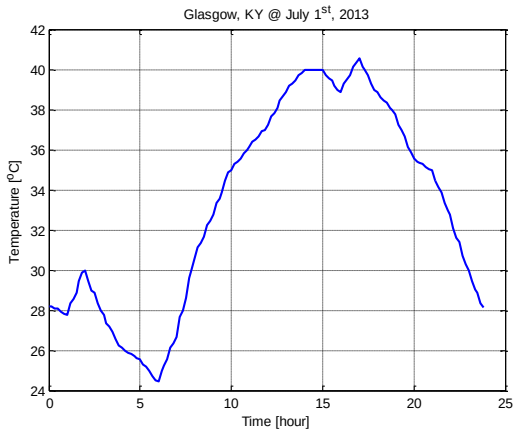

Figure 11.2 Temperature Input Data

Relative humidity data with 10 minutes resolution are presented in Figure 11.3. The maximum and minimum values recorded at the peak day are 100% and 17.5% respectively. These data have an impact on the actual heat rating of the air conditioner model.

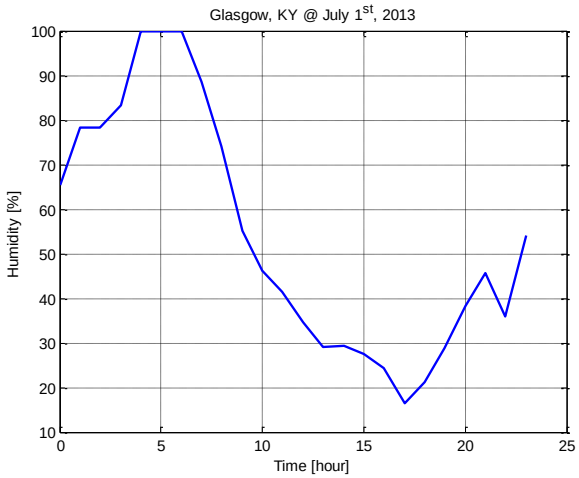

Figure 11.3 Relative Humidity Input Data

Various non-controlled loads for the house under simulation are represented by a time variable active and reactive power load model as shown in Figure 11.4. This figure presents the aggregated value of the load. However, these data are split into two loads and each one is connected to a different phase of the house power network. It is noticed that there are more energy consumption during the time 05:00-10:00 am and 01:00-06:00 pm.

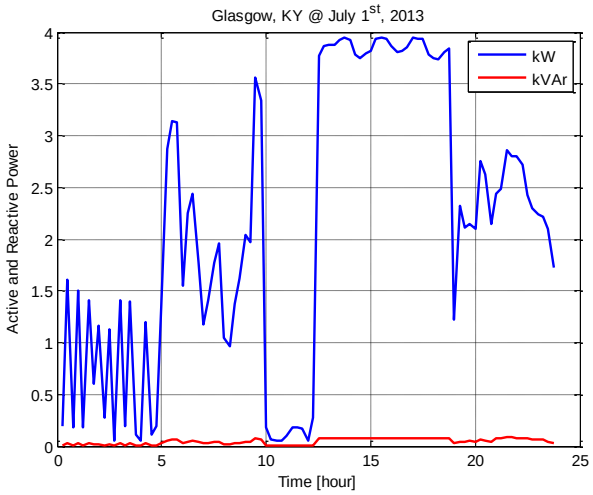

Figure 11.4 Aggregated Active and Reactive Power of House Non-Controlled Appliances

11.2 Test System Description

A test case system with variable distributed resources and house appliances models are built. The test system consists of mainly a 13.8 kV slack generator, 13.8/115 kV delta-why power transformer, transmission line, 115/13.8 kV why-why power transformer, and distribution network. The test system, additionally, has 10 kVA 13.8/7.2 kV single phase electro-thermal distribution transformer connected to phase A to ground, double line and neutral L1-NN-L2 service drop, solar PV, storages, and appliances (air conditioner, refrigerator, dishwasher, variable load). The diagram of the test system is illustrated in Figure 11.5. The simulation is performed over 24 hours with 1 second time step.

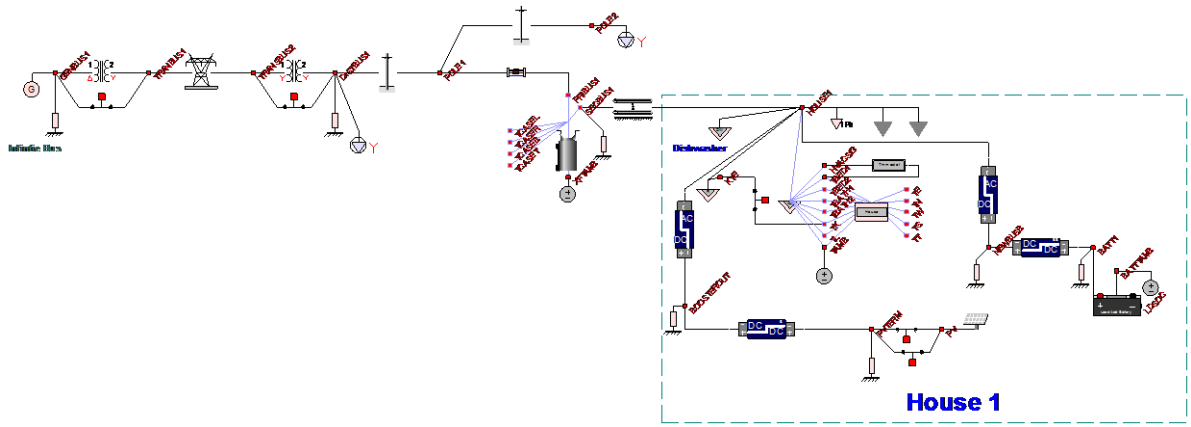

Figure 11.5 Demonstrative Case Study Test System

Electro-thermal center-tap transformer used to step the voltage down to a voltage that is comparable to the house voltage is rated 10 kVA 7.2/0.24 kV. Electrical circuit parameters provided in Table 8.5 is used in this case. Physical parameters such as the oil tank size are taken from [81]. The transformer outside temperature data are presented in Figure 11.2.

Dishwasher input data are provided in Table 11.1. This dishwasher is assumed to be controllable by the management system and their operation can be shifted without violating any constraints or the customer convenience. In this case, based on the data of the house in Glasgow, the dishwasher was operated twice that day at specific times. To simulate real case, the smart dishwasher is set to operate two times during the simulation period as in the real observed house. The operation of the dishwasher is presented in Figure 11.6. Their operation times are summarized in Table 11.2.

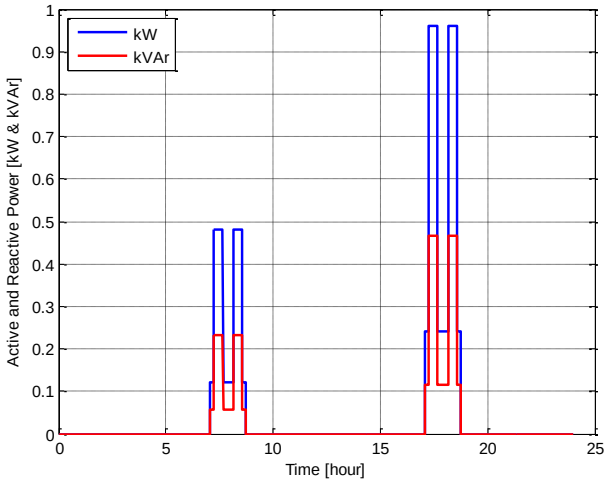

Figure 11.6 Smart Dishwasher Operation Characteristics over the Day

Table 11.1 Dishwasher Input Data

$P_{dwrated}$ =1200 W	V_{rms} = 130 V	*Efficiency = 0.8*
Pf = 0.9	*Cycle Time = 100 min*	*Connection L1-NN*

Table 11.2 Dishwasher Operation and Power Characteristics

Dishwasher Operation	***Power Level***	***Time***	***Ready By***
Operation 1	*L*	*7:00 am*	*9:00 am*
Operation 2	*H*	*17:00 pm*	*04:30 am*

A top mount house refrigerator with 16.5 ft3 capacity is included in the simulation and assumed to be half full both fresh food compartment and freezer. The temperature set for the refrigerator is 2.5 with 1 degree dead-band. The refrigerator is assumed to be in the kitchen room where its temperature is not fixed since it is part of the thermal house model. Basic input data to the refrigerator model is provided in Table 11.3. Physical characteristics of the refrigerator are provided in Table 11.4 [96].

Table 11.3 Refrigerator Input Data

$P_{refrated}$ =100 W	V_{rms} = 130 V	Efficiency = 0.8
Pf = 0.95	COP = 3.5	Connection L1-NN

Table 11.4 Refrigerator Physical Characteristics [26]

Fresh Food Compartment Capacity =12.8 ft^3	Freezer Compartment Capacity =3.7 ft^3

An air conditioner with six ducts model as described in Section 8.5.1.3 is used in this case study. The environmental conditions, outside temperature and relative humidity, data are presented in Figure 11.2 and Figure 11.3. Other necessary model parameters are provided in Table 11.5. The model operation is controlled by a thermostat controller with temperature equals to 25 ^{o}C.

Table 11.5 Air Conditional Model Parameters

Heat Rate =35 kBtu	V_{rms} = 230 V	Nominal COP = 2.5
Pf = 0.85	Thermostat Controlled	Connection L1-L2

The house roof-top solar PV is sized as the following, 6 panels with 60 cells in each panel. Typical characteristics data for every panel is provided in Table 11.6 and taken from [85]. Perturb and Observe MPPT algorithm is used to obtain the maximum power. The electric vehicle is sized typical as 3 kW. It is assumed to be connected to the house network at 6:00 pm for three hours for charging purpose. However, the customer wants the car to be fully charged in the morning at 5:00 am. This gives the house management system enough time to postpone the charge for a later time. Lead acid batteries are connected to the house mode; however, they set on standby mode during the simulation. Power electronics boost, buck-boost, and inverter are used with typical parameters.

Table 11.6 House Roof-Top Data Parameters

Rated Power =0.26 kW/panel	V_{oc} = 38.3 V	I_{sc} = 9.09 A
R_s = 0.4 Ω	R_p=850 Ω	P&O MPPT Algorithm

11.3 Case Study Results

In this case, two devices are assumed to be controlled dishwasher and electric vehicle charging time. The objective is to minimize the total demand peak load. House active and

reactive power data over the simulated day time, July 1st 2013, are presented in Figure 11.7. It was found that the house load was peaked to 11.7 kW around 5:43 pm. The peak load was about 20 % more than the center-tap transformer rating, which is expected to increase the hot spot temperature, and thus increase the deterioration of the transformer insulation.

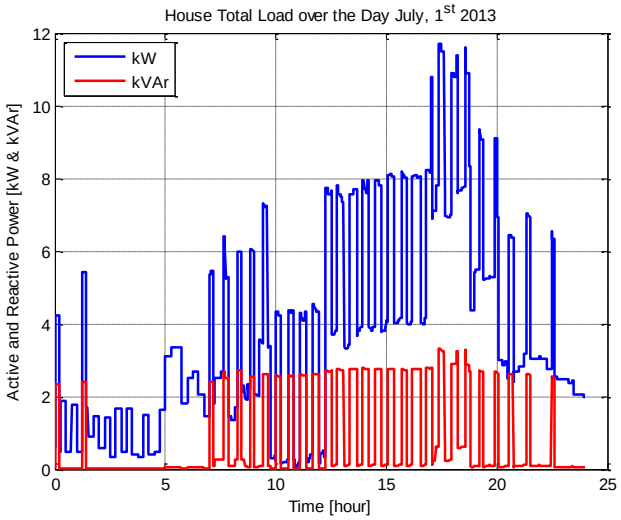

Figure 11.7 House Total Peak Load

Simulation results for the system with and without proper coordination and control of the house controllable EV charging time and smart dishwasher operating time are provided. Figure 11.8 and Figure 11.9 show the dishwasher active, reactive, voltage, and current characteristics when the house is managed with smart management system and without the management system applied. When the optimization scheme is applied, the dishwasher operation starting time is shift from 5:05 pm and scheduled to start operate at 6:45 pm for one full cycle (100 minutes) without interruption as presented in Figure 11.8. In the same figure, it is shown that the first operating cycle of the dishwasher, which is scheduled to operate at 7:00 am, does not experience any operating time rescheduling. However, the second scheduled operating cycle is rescheduled to operate at a later time as mentioned before, at 6:45 pm. The voltage waveform, as shown in the top of Figure 11.9, is maintained fluctuation with acceptable limits. Additionally, the current waveform, which is shown in the bottom of Figure 11.9, reflects the same envelope as the dishwasher power.

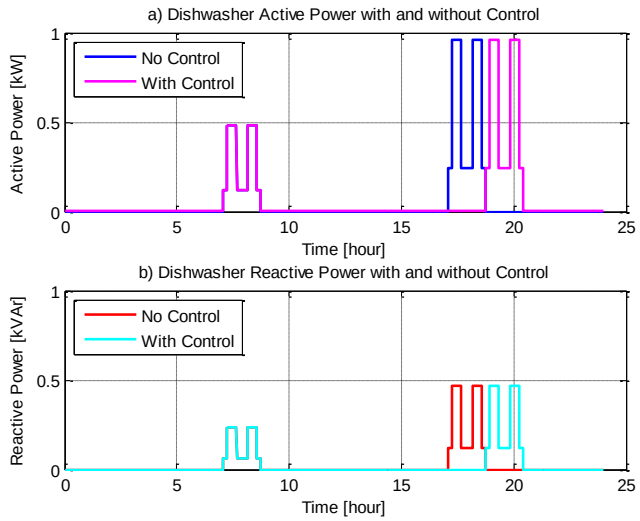

Figure 11.8 Smart Dishwasher Active and Reactive Power Characteristics during the Simulation

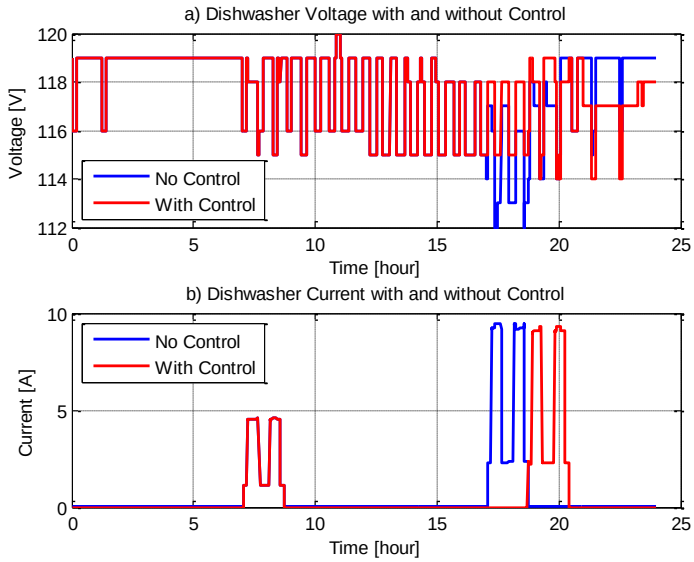

Figure 11.9 Smart Dishwasher Voltage and Current Characteristics

The second controllable resource is the electric vehicle charging time. The electric vehicle is originally scheduled to start as soon as it is connected to the house power network, i.e. at 06:00 pm. With the optimization scheme is applied, the electric vehicle charging time is rescheduled to start at 9:30 pm and maintain charging mode status for three consecutive hours as shown in Figure 11.10.

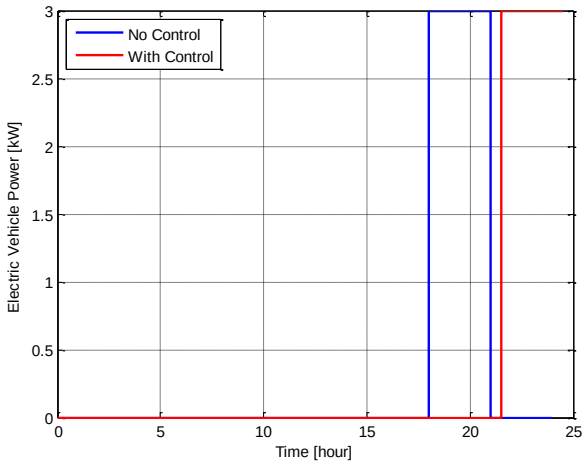

Figure 11.10 Electric Vehicle Operation Characteristics

The thermostat controller senses the temperature of bedroom 1 and provides a control signal to control the operation of the air conditioner model. Figure 11.11 shows the variation of the bedroom 1 main temperature spot, bedroom 1 internal wall temperature spot, north side temperature spot, top of the house temperature spot, air conditioner control signal, air conditioner active and reactive power, and heat rate produced by air conditioner model.

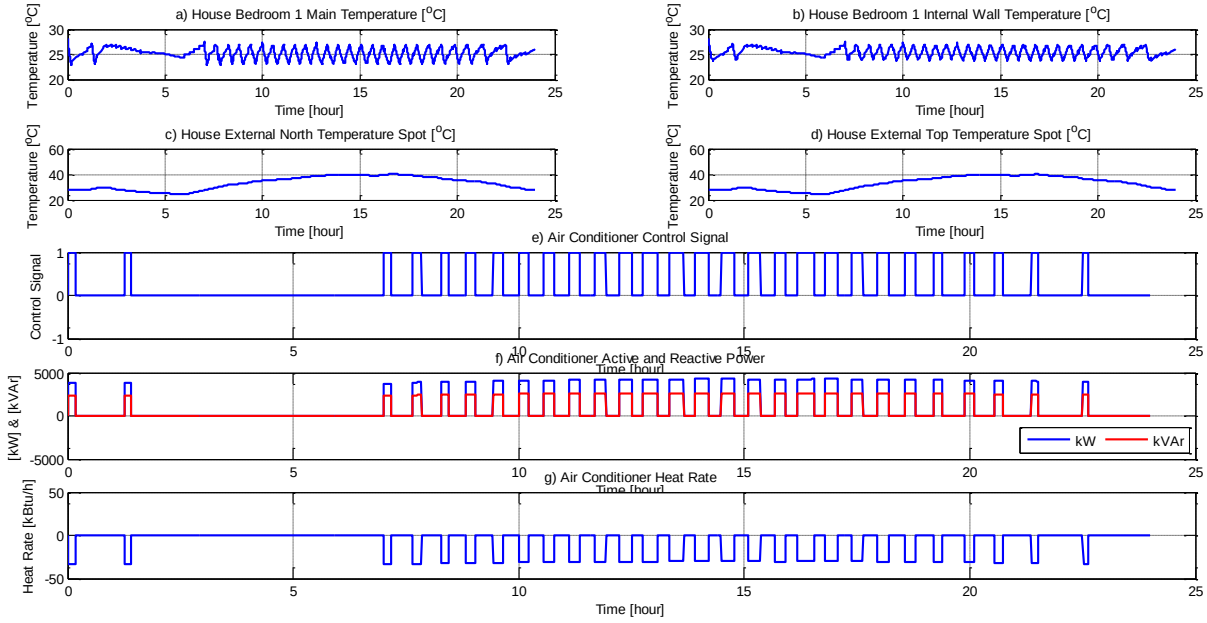

Figure 11.11 House and Air Conditioner Models Characteristics

The following transformer temperature spots, Th1, TL11, TCT, TTOT, and $T_{CaseTop}$ are depicted in Figure 11.2. Note that these waveforms are for the house that does not deploy any control strategy (no optimization and control). The hot spot is found to be L11 spot.

Therefore, it is used to determine the loss of transformer insulation life. During the peak load, the temperature at the hot spot is risen to 152 ^{o}C at 5:30 pm.

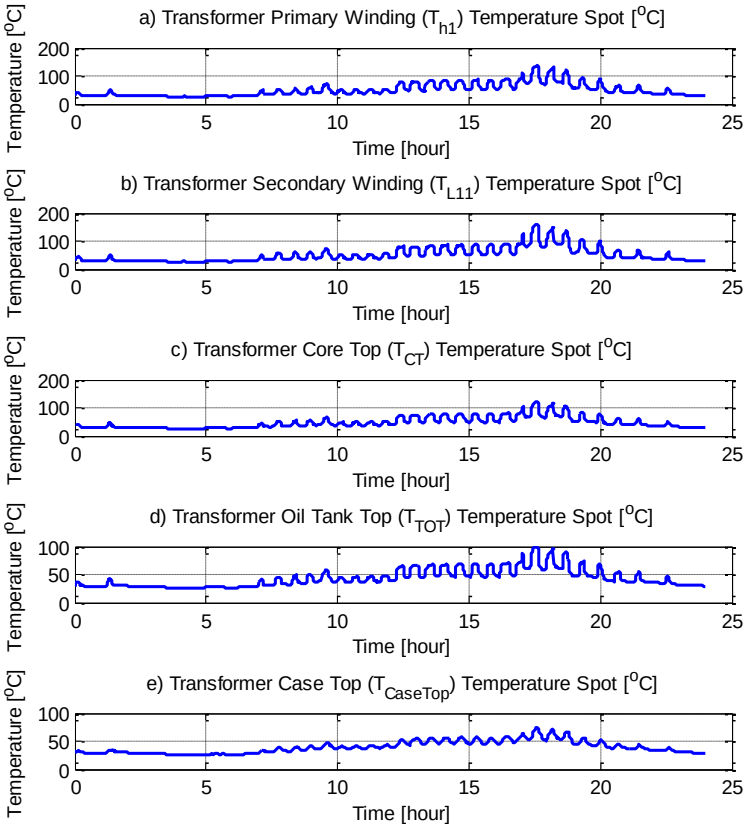

Figure 11.12 Temperature Spots Waveforms of Some of the Transformer Temperature Spots

The total house load with and without shifting smart dishwasher load and electric vehicle charging time is presented in Figure 11.13. With proper and coordinated control (Dishwasher Starts at 6:45 pm and EV charging starts at 9:30 pm), the total load peak has been reduced by approximately 18 % of the peak with no control applied to house system. The new peak is become 9.5 kW at 10:00 pm as shown in the top of Figure 11.3. The peak hot spot, in fact, becomes less the center tap transformer rating. Thus, with smart controls, the current center tap transformer can meet the load during the peak and no replacement is required. In addition, the hot spot temperature has been also reduced by approximately 30 %, which is substantial. The new peak hot spot is approximately 107 ^{o}C, which occurs at 10:00 pm at the peak load demand. Thus, the transformer insulation expected life deterioration has been decreased.

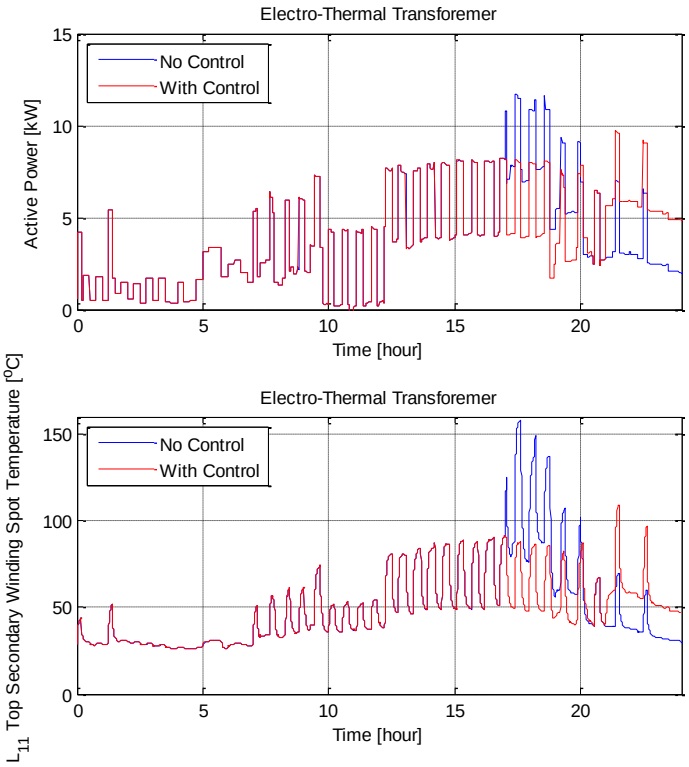

Figure 11.13 Top: Electro-Thermal Transformer Active Power, Bottom: Electro-Thermal Transformer Hot spot Temperature L11

11.4 Conclusion

It has been widely known and accepted that the percentage of EVs/PHEVs will rise in the future resulting in increased end user residential demand. With growing load, more stress is expected to take place on the distribution system components such as the distribution center tap transformer. This negative impact would then result in decreasing the economic life of the distribution power grid assets. In addition, the reliability and power delivery distribution system to the customers would be questionable. However, the unfavorable impacts on the environment, economy, and reliability, can be averted if it is appropriately managed and controlled by deploying smart-grid optimization schemes. Moreover, it can be extremely valuable because it has the potential to provide important ancillary services that can assist the regulation of the power grid when needed by implementing certain control signals. Therefore, the benefits of integrating EVs/PHEVs to the power grid can be exploited by additional deployment of control algorithms and using appropriate devices or circuits.

Towards this purpose, a house management system is developed that maximizes the benefits associated with the existing of EVs/PHEVs. The operation of the management system requires an advanced infrastructure. This infrastructure, continuously, monitors the operation of the system at the residential and commercial level and provides control functionally of the building loads in such a way that the distribution grid components are

not overloaded, thus avoiding loss of life. In addition, the developed infrastructure provides at the same time load management services to the utility. Distributed energy resources and loads, distributed state estimation, and optimization are the major three components of the infrastructure.

Major part of the infrastructure is modeling various assets including center tap transformers, service drops, and the residential house energy resources and loads. The modeling approach used in this project is a physically based object orientated approach. It helps unified the format of various power devices, applications, and associated controls. Therefore, it can easily handle system expansion with new models. Various house energy resources and loads are then physically modeled and developed into a standard syntax, named SCAQCF format. Measurements gathered from various house resources and loads, distribution circuits, transformer, switches, and other are collected and sent to the distributed state estimation, which is the second component of the infrastructure. The measurements are utilized with the object oriented models to perform state estimation. The final result of the estimation process is a reliable and verified real time model of the house building and the distribution circuits. This reliable and verified real time model is sent to the house management system to perform optimization; this is the third major component of the advanced infrastructure. An optimization is performed considering various constraints among the residential house devices. Several objectives can be used. For example, minimization of peak demand, or, in case of variable electricity rates, the objective is minimization of total cost. The solution of the optimization problem is in terms of schedules for EV charging, smart appliances, etc. The optimal schedules signals are sent back to the devices. There are several benefits of the developed management system: (1) minimization of distribution transformer loss of life since the optimal solution limits the peak loading of the transformer and avoids peak transformer loading, (2) scheduled use of electricity at low prices to minimize the electricity bill. The management system can provide the power utility provider some important services such as voltage regulation, etc. Other usages of the management system could be the provision of cyber security functionalities such as coding collected energy usage data that are regularly sent to the power utility provider to maintain high level of residential customer privacy. Note that, this system can be used to not only manage one house, but also with several houses connected to one distribution transformer, as this configuration is usual. Moreover, the management system can manage a commercial building as well, if all the components are appropriately modeled.

A demonstrative case study is developed to show the benefits of the house management system. A distribution center tap transformer is connected to a residential house through a service drop. The residential house is assumed to include domestic appliances such as dishwasher, refrigerator, and air conditioner. Other loads are also considered as time variable loads. In addition, energy house resources such as roof top solar PV and energy storage system (lead acid batteries), and EV are also included. In this case, two devices are assumed to be controllable. These two are the dishwasher and EV charging. In particular, the operating starting time of the dishwasher and the time when the charging process of EV begins are two of the control variables. With no optimization considered, the system is peaked to 11.7 kW and the transformer hot spot temperature reaches 152 ^{o}C. This

temperature is above the capability of the transformer, which signals the need for resizing the transformer. However, with smart control strategies in place, the management system delays the operating time of the dishwasher and the charging of EV to avoid more stress on the distribution circuits. The new demand peak has been reduced by 2.2 kW and the peak time has been shifted away from the critical time. All these are taken place without violating the system physical constraints and without incurring any inconvenience to the customer.

In summary coordinated control of the various resources in residential and commercial buildings can provide real benefits to the customer and the utility alike and will maximize the value of EVs and PHEVs. Coordinated control can achieve these objectives without inconveniencing customers. However, coordinated control requires an infrastructure that enables monitoring of the system all the way to the customer level with a distributed state estimator and enables the real time control of EVs, PHEVs and smart appliances and other resources in houses and commercial buildings.

12. Scheduling Flexible Loads for Ancillary Service Provision in Multi-settlement Electricity Markets

12.1 Introduction

Demand flexibility is one of the key enablers of demand response. Flexible loads, i.e. loads not bound to a specific instantaneous power consumption trajectory, comprise a considerable portion of the current load and are hence potential demand response providers. Moreover, plug-in electric vehicle (PEV) charging, which is projected to be a considerable future load, has shown to be very flexible [97]. This flexibility not only enables displacement of electric energy consumption by flexible loads to the time when it is more abundant and hence cheaper, but also helps counterbalance the intermittency and uncertainty of renewable sources, should the proper communication, control and service infrastructure be in place. Furthermore, flexibility can be used to match renewable generation to maximize its utilization without need for expensive storage.

Utilizing demand flexibility and instigating demand response, however, is a challenging task. As restructured electricity markets become standard in the US and around the world, economy becomes the main driver of supply demand balance. However, a considerable portion of flexible demand has been shielded from market prices through utilities and Retail Energy Provider Companies (REPCo) for technical and non-technical reasons. The major infrastructure challenges, i.e., fine grained measurement of consumption over time and communication of prices to the consumer, are being addressed by smart grids and other innovative communication mechanisms like OpenADR. However, new services should be offered over this infrastructure to enable full utilization of demand side assets. Due to the diversity in flexible loads and their preferences, as discussed in [98], common pricing of electricity such as Time of Use (ToU) and dynamic pricing cannot fully utilize the potential of flexible loads and may result in undesired behavior at network level, as demonstrated in [97].

In this context, an Energy Services Company (ESCo) or Load Aggregator (LA), which can be a part of a REPCo, can orchestrate flexible demands and aggregate them to a level that can participate in the electricity market at the wholesale level. The motivation for such organization of flexible loads goes beyond facilitation of operations and market participation to more control on the aggregate level load, avoiding distribution network (DN) congestion, and enabling provision of Ancillary Services (AS) in a reliable manner, which is required by most Independent System Operators (ISO) as a part of market rules. Ancillary Services, and particularly frequency regulation service (REG), are basically reserves provisioned by the system operator to cover supply-demand imbalances and maintain system stability. By modulating the instantaneous consumption of a large enough group of flexible loads, the LA can operate flexible loads as a REG provider while they are actually net consumers.

Aggregating flexible loads by the LA, however, is a technically challenging problem due to the wholesale market structure and inherent uncertainties in the process. Most wholesale electricity markets are organized in a multi-settlement fashion with at least two stages: The forward stage, which we refer to as the day-ahead market (DAM), plays an operations

planning role. It is also where the reserves and unit commitment decisions are usually made, in co-optimization with energy decisions, to ensure reliable operation of the grid. Most markets also incorporate a "real-time" market (RTM), acting as a recourse stage, which is usually implemented as an adjustment market.

The DAM is usually cleared hours before the actual operation time, when information about flexible loads is available. Although LA can solely participate in the RTM for energy purchases, offering AS usually requires participating in the DAM. Moreover, participating in DAM can potentially result in better total costs of energy to LA, if it can buy energy at a lower cost. On the other hand, making day-ahead commitments are challenging as there are various uncertainties faced by the LA in real-time in addition to load arrivals and departures, including changes in real-time prices and distribution network congestion situation.

Scheduling and participation in multi-settlement markets have been studied by many authors in the past and using various approaches. The major part of the past work [99-105] has focused on the strategic behavior of generation entities and firm resources in multi-settlement markets and how various aspects, like risk, offering ancillary services and market rules affect the results. Various approaches have been taken by the authors, from Supply Function Equilibria (SFE) [99,102] methods to simulation based approaches [105]. However, optimal participation of collections of demand side resources in multi-settlement markets is much more challenging and is not studied as extensively. One the most challenging aspects, from the perspective of this work, is the uncertainty in availability of resources which would add a technically challenging dimension to the problem.

Caramanis and Foster [106-108] take an aggregation based approach and hypothesize that only the total purchases of energy and sales of AS for each group of users with the same deadline needs to be tracked and scheduled and an optimal algorithm to distribute the optimal totals among the flexible resources can be found. Using this assumption and focusing on PEVs, they model the multi-settlement market consisting of a day-ahead and an hour-ahead market and consider the interaction between various entities in the market. They particularly aim at modeling the decision problem faced by the Load Aggregator, which is obtaining optimal bids for energy and reserves in both markets. They propose a stochastic dynamic programming formulation for this problem and discuss its extension to other classes of flexible loads like HVAC systems. They, however, do not discuss tractability of their model and have not shown any numerical results as to how their model performs should approximate techniques be used to tractably solve the problem. In their follow up work [107], the authors suggest modifications to the market structure to enable better integration of flexible loads in the multi-settlement market by opening the possibility of complex bids.

Jin et al. [109] propose a scheduling model for co-optimizing PEV load and energy storage in a multi-settlement market as well as a communication infrastructure model to support their scheduling algorithm. They show that their model admits a mixed integer linear program and propose a heuristic method to tackle its tractability which is essentially rounding a continuous relaxation of the original problem. They study the performance of

their model through simulation and show major reduction in total cost by optimal scheduling compared to uncontrolled charging. Moreover, they show that the loss of performance due to their heuristic solution to the mixed integer program is acceptable. The major short coming of their work, however, is adopting a deterministic model and resorting to the flexibility of the energy storage asset to tackle the uncertainties faced by the system.

Subramanian et al. [110] consider the problem of a "Cluster Manager (CM)" (i.e. Load Aggregator) which participates in a two stage market. The CM has to satisfy the demand of a group of flexible and non-flexible loads by purchasing energy on their behalf in the market and has access to an intermittent cheap generation asset (e.g. a wind farm). Unlike typical models, they also assume that the CM has to buy reserve capacity to cover its deviations from its base points cleared in the market. They aim at obtaining cost minimizing decisions for bulk energy and reserve purchases in the day-ahead market. They present their results for the case of fully flexible loads and non-flexible loads. They obtain the optimal energy purchase policies for the two cases by solving the dynamic programming problem resulting from their model. Besides the fact that their model does not match the established market rules in terms of reserve provision, their theoretical results apply only to extreme cases they consider, i.e. the fully flexible loads and non-flexible loads. While providing some insight into the nature of the problem, the simplifying assumptions in studying the two extreme cases limit the applicability of the model by relaxing essential constraints in the model. Consequently, it is hard to generalize the result or numerically evaluate the performance of the full model using the presented results.

Al-Awami and Sortomme [111], similar to the work presented here, approach the problem of optimal decisions in DAM and RTM using stochastic programming. However, they differ from our work in that they assume availability of multiple generation resources, both intermittent and firm, to the load aggregator and do not consider the possibility of AS provision by the flexible loads, nor the distribution network constraints that the load aggregator might be subject to. They also factor in the trading risk between DAM and RTM by adding a conditional value at risk term to their objective. Their model results in a stochastic mixed integer linear program which they solve using CPLEX. Their model, however, captures uncertainty only in wind production scenarios and assumes PEV demand is known. Therefore, their scenario generation technique is completely different from what is presented here. Their results only show modest gains from coordination, about 3% improvement in total cost. Unsurprisingly, their results show that including risk in their objective improves the Conditional Value at Risk (CVaR) measure substantially.

In this section, we extend our previous work and propose a model focused on the challenges in capturing the uncertainties in flexible loads, particularly PEV loads, in a systematic way. The first contribution of this work is to propose a stochastic programming approach that fits well with the multi-settlement structure of the market and provides a realistic scheduling mechanism for implementation by the load aggregators. The proposed scenario generation technique which can handle heterogeneous scenarios is the second main contribution of this work.

The rest of this section is organized as follows: In Section 7.2 we introduce our system model. In Section 7.3 we present our formulation for the planning method for DAM scheduling and our proposed scenario generation technique. In Section 7.4 we analyze the performance of the proposed stochastic programming approach through numerical simulation. Finally, in Section 7.5 we conclude and discuss our future directions.

12.2 System Model

To fully utilize the demand response potential of flexible loads, a systematic approach should be adopted for market participation and load scheduling by the LA. This is the problem we tackle in this section by proposing a model for the decision problem faced by the LA in the context of a multi-settlement electricity market. To this end, similar to [98], we assume a general information and power flow architecture which can be implemented on smart grids or even independently. As illustrated in Figure 12.1, we assume the LA communicating with the ISO for wholesale related operations, namely bidding in the DAM and RTM for purchasing energy and offering AS as well as other wholesale level information. The LA also communicates with the distribution network operator to ensure feasibility of energy transfers and AS services scheduled without overloading the network. Finally, the LA communicates with the flexible loads to gather their energy requests and preferences and implement the energy delivery schedule and AS deployment commands. The LA is assumed to participate in both DAM and RTM as a price taker, i.e. its decisions will not affect the prices.

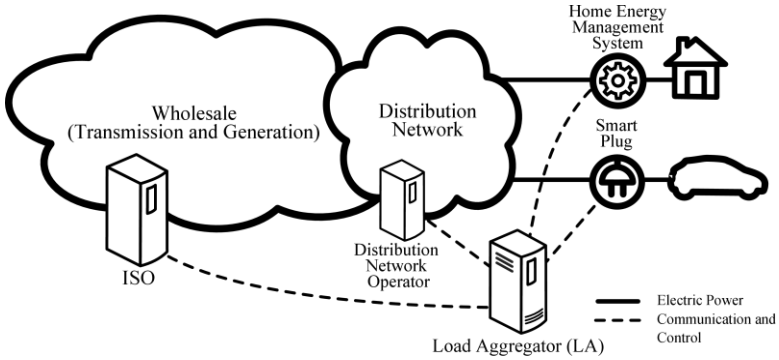

Figure 12.1: Interactions of the Load Aggregator (LA) with other entities

The multi-settlement structure of the market calls for two main stages for decision making, namely day-ahead and real-time. Day-ahead decisions consist of bids for total energy purchased and offers for reserves for every interval, usually an hour, in the following day. The decision problem faced in real-time, however, has a multi-stage structure itself, i.e. at every interval, which is usually five to fifteen minutes long, the LA should decide its bids for energy, and reserves, and should there be a real-time market for reserves.1 Moreover, the LA should decide the amount of energy transferred to each flexible load as well as the portion of reserves provided by it at every real-time stage. These decisions are subject to

[1] In RTM, the bids might be only allowed to change once every couple of intervals, e.g. once every hour, although the market is run for every interval, e.g. 5 min.

distribution network constraints and individual load capacity constraints. Figure 12.2 depicts the decision time-line where the square corresponds to the day-ahead decisions and the circles denote the decisions made at each real-time stage and T denotes the number of real-time stages considered by the LA.

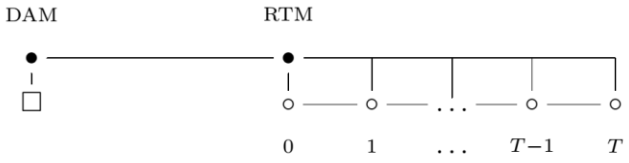

Figure 12.2 Decision Time-line and Stages

Let us first introduce our notation. We denote the arrival time, departure time/deadline and electric demand of each flexible load, e.g. a plug-in electric vehicle (PEV), by t_i^a, t_i^d and d_i respectively where $i \in I$ is the set of flexible loads. We assume that the ESCo has to supply the flexible load its desired demand, d_i, up to the given deadline at some pre-negotiated rate and any shortfall in the energy delivery is penalized at s^{EV} \$/kWh, which can be seen as a proxy for price of gasoline in case of plug-in hybrid electric vehicles (PHEV) like Chevy Volt. We further assume that the instantaneous rate of energy delivered to each load can be varied continuously between zero and $\bar{x}_i$. In other words, each load is assumed to have an individual capacity of $\bar{x}_i$ kW. In case of a PEV, t_i^d denotes the desired departure time, d_i can be the depleted capacity of the EV battery and $\bar{x}_i$ represents the Electric Vehicle Supply Equipment (EVSE) capacity.

For simplicity, we assume a single feeder which we model to a single capacity limited element. We denote excess capacity of this element by C_t. As will be discussed later, our method can be extended for handling more sophisticated radial distribution networks as well as multi-feeder setups, where feeders are all in the same load hub.

Participation in DAM and RTM has a very different nature in the sense that DAM a is forward market whose corresponding decisions are made without the exact knowledge of the flexible loads availability and demand. Moreover, only the aggregate amount of power needed for serving flexible load is to be decided. Finally, the time resolution in DAM is usually different from RTM (e.g. 1hr vs. 5min in ERCOT). This implies that the decisions made for DAM should be good for multiple market intervals in RTM. We denote the DAM and RTM interval lengths by Δt^{DA} and Δt^{RT} respectively. For simplicity, we assume $m = \frac{\Delta t^{DA}}{\Delta t^{RT}}$ to be an integer. Since we are assuming all the loads under the same bus, from the bulk power system perspective, we only have to consider a single set of energy and

reserves, in particular regulation, prices. Since our focus here is to address the coupling between DAM and RTM, we assume that the ESCo participates in the market as a price taker and does not focus on optimal bidding. That is, unlike our previous work in [98] and Kefayati and Caramanis (2010), the ESCo estimates prices for DAM and forms its offers based on its marginal penalty (s^{EV}). We denote the DAM predicted prices for energy and reserves by $p_t^{e,DA}$ and $p_t^{r,DA}$ respectively. In RTM, we assume that the ESCo is only allowed to purchase or sell energy, whose price is denoted by $p_t^{e,RT}$. We assume only statistical information of the real-time prices are available to the ESCo.

The multi-settlement setup of the market implies two main set of decisions to be made by the ESCo. In DAM, the ESCo should decide amounts of total energy to purchase and reserves to sell for each time interval, which we denote by $x_t^{e,DA}$ and $x_t^{r,DA}$ respectively. In real-time operation, in contrast, amount of energy to be delivered to each load as well the share of the committed AS is to be decided besides the amount of purchases/sales of energy to achieve a balanced schedule.

12.3 Scheduling in Multi-settlement Electricity Markets

12.3.1 Participation in the Day-Ahead Market (DAM)

To address the day-ahead decisions, we adopt a stochastic optimization model in accordance with the two stage structure of the problem. Our first stage planning decisions consist of the quantities of energy purchased and reserves offered in the day-ahead market. These decisions are used as nominal values for total energy consumption and reserves offered in the recourse stage, i.e. real-time. Constructing the recourse expected cost, as a function of the planning stage decisions, however, is a challenging problem since the recourse is a multi-stage problem itself. Moreover, in practice, only historical sample information is available about load availability and demand amount, rather than their distribution and patterns. We formulate the DAM planning problem as follows:

$$\begin{aligned} \min_{\mathbf{x}^{e;DA};\mathbf{x}^{r;DA}} & (\mathbf{p}^{e;DA}\mathbf{x}^{e;DA} - \mathbf{p}_t^{r;DA}\mathbf{x}^{e;DA})\Delta t^{DA} + E_{\xi}[h(\mathbf{x}^{DA};\xi)] \\ st. \quad & \mathbf{x}^{e;DA};\mathbf{x}^{r;DA} \geq 0; \\ & \mathbf{1}_{|T^{DA}|}^{\intercal}\mathbf{x}^{e;DA} \leq \overline{x}^{\,e;DA}; \end{aligned} \tag{12.1}$$

where:

Vectorization is done with respect to the DAM time index, $t \in T^{DA}$;

T^{DA} is the set of DAM time indices;

$\mathbf{p}^{e,DA}$, $\mathbf{p}^{r,DA}$ represent the expected day-ahead prices for energy and regulation in a row vector format;

$\mathbf{1}_n$ denotes the column vector of all ones with length n;

$|A|$ denotes the number of elements of set A;

$\mathbf{x}^{DA}=(\mathbf{x}^{e,DA},\mathbf{x}^{r,DA})$;

$\xi\in\Xi$ is the random variable indexing different potential scenarios;

Ξ is the scenario set;

$\overline{\mathbf{x}}^{e,DA}$, the upper bound on the total DAM energy purchases;

Δt^{DA} is the time interval length for the DA market;

$h(\mathbf{x}^{DA},\xi)$ is the optimal objective of the real-time (RT) problem.

The upper bound on the total energy purchases in DAM, $\overline{\mathrm{x}}^{\mathrm{e,DA}}$, is added as a regulatory constraint to decrease the scheduler's tendency towards DAM-RTM trading and arbitrage, particularly because risk is not directly modeled in this formulation. In this work we have set $\overline{\mathrm{x}}^{\mathrm{e,DA}}$ to $\min_{\xi}\sum_{i\in I_\xi}\mathrm{d}_{i,\xi}$, that is, the ESCo is required not to buy more energy in DAM more than it almost surely is going to consume. We will comment on this constraint later in this section.

In the recourse stage, the LA actually serves the PEVs and responds to the regulation signal dispatched by the ISO. The impact of the planning stage decision on this stage is the total amount of energy purchased at DA (at DA price) and the regulation commitments. Hence, we have the following problem in recourse (not considering the bidding process):

$$h(\mathbf{x}^{DA},\xi)=\min_{\mathbf{x}^{e,RT}_{I,\xi},\,\mathbf{x}^{r,RT}_{I,\xi}} \quad \mathbf{p}^{e,RT}_{\xi}(\mathbf{x}^{e,RT}_{\xi}-M\mathbf{x}^{e,DA})\Delta t^{RT} + s^{AS}\Delta t^{RT}\mathbf{1}^{\intercal}_{|T^{RT}|}(M\mathbf{x}^{r,DA}-\mathbf{x}^{r,RT}_{\xi}) + s^{EV}\sum_{i\in I_\xi}(d_{i,\xi}-\Delta t^{RT}\mathbf{1}^{\intercal}_{|T^{RT,EV}_{i,\xi}|}\mathbf{x}^{e,RT}_{i,\xi}) \tag{12.2}$$

$$\text{st.} \quad \mathbf{x}^{e,RT}_{\xi}=W_\xi\sum_{i\in I_\xi}\mathbf{x}^{e,RT}_{i,\xi}, \tag{12.3}$$

$$\mathbf{x}_{\xi}^{r,RT} = W_{\xi} \sum_{i} \mathbf{x}_{i,\xi}^{r,RT}, \tag{12.4}$$

$$\mathbf{x}_{\xi}^{e,RT} + \mathbf{x}_{\xi}^{r,RT} \leq \mathbf{C}_{\xi} \tag{12.5}$$

$$\mathbf{x}_{i,\xi}^{e,RT} + \mathbf{x}_{i,\xi}^{r,RT} \leq \overline{\mathbf{x}}_{i,\xi}, \qquad \forall i \in I_{\xi}, \tag{12.6}$$

$$\mathbf{x}_{i,\xi}^{r,RT} \leq \mathbf{x}_{i,\xi}^{e,RT}, \qquad \forall i \in I_{\xi}, \tag{12.7}$$

$$\Delta t^{RT} \mathbf{1}_{|T^{RT}|}^{\intercal} \mathbf{x}_{i,\xi}^{e,RT} \leq d_{i,\xi}, \qquad \forall i \in I_{\xi}, \tag{12.8}$$

$$x_{\tau,i,\xi}^{e,RT} = 0, \qquad \forall \tau \notin [t_{i,\xi}^{a}, t_{i,\xi}^{d}), i \in I_{\xi}, \tag{12.9}$$

$$\mathbf{x}_{i,\xi}^{e}, \mathbf{x}_{i,\xi}^{r} \geq 0, \qquad \forall i \in I_{\xi}, \tag{12.10}$$

where:

- Vectorization is done with respect to the RTM time index, τ, $\tau \in T^{RT}$;
- T^{RT} denotes the set of RTM time indices (as seen in the planning stage) for all variables except the ones that are indexed by i, the PEV index, for which, $\tau \in T_{\xi}^{RT,EV} = [\min\{TRT\}, \max_i t_{i,\xi}^{d} - \min\{TRT\}]$;
- I_{ξ} is the PEV index set for scenario ξ;
- M is the time synchronization matrix between markets which is defined as:

$$\mathrm{M} = \mathrm{I}_{|\mathrm{TDA}|} \otimes 1_{\mathrm{m}}; \tag{12.11}$$

- $m = \Delta t^{DA} \Delta t^{RT}$ as defined previously;
- $\mathbf{I}_n$ denotes the $n \times n$ identity matrix;
- $\otimes$ denotes Kronecker product;
- $\mathbf{p}_{\xi}^{e,RT}$ is the real-time price of electricity in row format;
- s^{AS} captures the penalty for unsatisfied regulation commitment;
- s^{EV} captures the penalty for the unserved EV demand;
- Δt^{RT} is the period of the real-time market;

- $\mathbf{C}_\xi$ represents the excess capacity of the distribution network available for charging;
- $t^a_{i,\xi}, t^d_{i,\xi}, d_{i,\xi}, \overline{\mathbf{x}}_{i,\xi}$ represent arrival time, departure time, energy demand and EVSE capacity for each vehicle;
- W_ξ is the time wrapping matrix, defined as:

$$W_\xi = cols\left(\left[1 : \left|T^{RT,EV}\right| \bmod \left|T^{RT}\right|\right], \otimes I_{|TRT|}, \left[1 : \left|T^{RT,EV}\right|\right]\right); \quad (12.12)$$

- *cols*(*M*,*A*) denoted the columns of *M* whose indices appear in set *A*;

W_ξ is essentially a horizontal repetition of the identity matrix with width truncated to $\left|T^{RT,EV}_\xi\right|$. The main purpose of using this time wrapping matrix is to give the optimization problem a consistent rolling view of time. Time wrapping basically wraps the time line of each of the PEVs back in T^{RT} range. Let us elaborate on time wrapping by going through an example. Consider a PEV that arrives at 5pm and leaves at 8am next day. Assuming Δt^{DA}=1hr and Δt^{RT}=15min with a 24 hour planning horizon, the time span of the PEV stay goes beyond the planning horizon for a particular day. However, when time wrapped, the period between 12am to 8am is mapped back to the same period in the problem's time span, as if some other PEV has previously started at 5pm yesterday and is finishing today at 8am. In other words, time wrapping folds individual PEV time lines and aligns them to the DAM and RTM time windows.

As discussed, constraints (12.3) and (12.4) define the time wrapped total energy and AS variables, $x^{e,RT}_\xi$, $x^{r,RT}_\xi$. Constraint (12.5) ensures that total PEV energy consumption and head room reserved for REG down remain below distribution network capacity. Constraint (12.6) ensures individual PEV capacity limits of EVSE are similarly observed. Constraint (12.7) guarantees feasibility of down REG. Constraint (12.8) prevents over-satisfaction of individual PEVs. Constraint (12.9) ensures that energy can be consumed only over the availability window of the PEV. Finally, constraint (12.10) ensures unidirectional flow of power, i.e. no-V2G.

There are couple of parameters that are potentially different in each scenario. We overload ξ to represent the particular realization of these parameters as:

$$\xi = (\boldsymbol{\rho}^{e,RT}_\xi, \mathbf{C}_\xi, \{(t^a_{i,\xi}, t^d_{i,\xi}, d_{i,\xi}, \overline{\mathbf{x}}_{i,\xi}) | i \in I_\xi\}). \quad (12.13)$$

That is, we can have uncertainty in real-time prices, (excess) distribution network capacity, and the PEV parameter set which includes demand arrivals, departures, amount of energy requested by each EV and its EVSE capacity. Consequently, each scenario has a realization

of all of the above parameters. Note that the parameters in the above triplet is a set, whose size, namely the number of PEVs, is scenario dependent and hence imposes a challenge in forming the distribution needed for scenario generation.

12.3.2 Participation in the Real-Time Market (RTM)

The stochastic program proposed above results in DAM market positions,x^{DA}. In real-time however, the ESCo faces another multi stage problem as the PEVs show up and prices change. The problem in real-time, however, is very similar to the problem we studied in [98] and Kefayati and Caramanis (2010). Therefore, we skip further treatment of the real time decision problem for the sake of brevity and to keep our focus on the effect of DAM planning on the overall cost faced by the ESCo.

12.3.3 Scenario Generation

In this subsection we introduce how we obtain the expected value in (12.1) by discussing our scenario generation approach. The major challenge in obtaining scenarios, which are essentially realizations of (12.13) is the third element of it, which is the set of PEVs and their demands. Generating scenarios for time series data, i.e. prices and distributions network capacity, has been studied in the past, e.g. [112] and the references within. So the main challenge is generating good scenarios for the group of PEVs.

Generating PEV scenarios has a couple of challenging aspects: First, the number of PEVs in each group can be different and hence, the size of each scenario is different. This makes finding a proper probability distribution function rather challenging. Second, the arrival, departure and demand process of the PEVs may have hidden correlations that might be hard to capture by tractable probability distributions. User preferences can be very diverse and capturing the non-stationary and time and location dependent behavior of the users is a challenging problem.

To address these issues, we propose data driven method based on subsetting and sampling for scenario generation. The main motivation here is that the ESCo gathers has access to all the realized charging sessions for PEVs subscribing to its programs at different locations. Using this dataset, the ESCo first subsets the dataset to obtain the relevant data subset, e.g. by time and/or location. Then based on the probability distribution of the number of users in each scenario, it decides the number of users in each scenario. Note that forming a distribution function for the number of users expected to arrive over each day is relatively straightforward. Then, for each scenario ξ, given the$|I_\xi|$, the ESCo picks $|I_\xi|$ samples form the relevant dataset with uniform probability. Alternatively, this method uniformly picks a subset of the relevant set with size$|I_\xi|$. Finally, the probability assigned to each of the scenarios is set to$\frac{1}{|\Xi|}$.

The main advantage of the proposed scenario generation method is simplicity and the fact that it does not need to form the distribution functions (empirical or parametric) from the

data and then sample them for scenario generation. This would be particularly challenging since the correlation between various aspects of the loads and their potential correlation with each other would be hard to capture. Moreover the dimensionality of the joint distributions does not pose an issue in the proposed method.

The major downside of the proposed scenario generation method, however, is inability in capturing low probability tail scenarios. We do not believe that this would pose an issue in our case since rare behavior patterns can only minimally affect the bulk transactions in DAM and the ESCo usually has an adequate amount of flexibility in recourse.

12.4 Performance Analysis

To establish the effectiveness of our proposed method, we measure the cost reductions compared to various localized charging policies through simulation. We also measure the amount of reserves offered by the LA and their reliability in terms of deviations of reserves offered in real-time from day-ahead offers. Finally, we study the aggregate load to measure the distribution level impacts of our proposed method.

To generate the simulation model and furnish it with data, we use the transportation induced PEV dataset we introduced in [97], similar to [98], where we use ERCOT prices for Houston load zone as our reference prices, ERCOT's diurnal load pattern as the pattern from which we drive out excess distribution network capacity and the PEV dataset resulting from everywhere charging with min dwell time of three hours. More specifically, the prices are generated by perturbing the historical prices with Gaussian samples with roughly 5%-10% standard deviation. The distribution network is first obtained by subtracting the ERCOT minutely average diurnal pattern from 120% of its max (as the feeder capacity) and then scaling the total energy capacity in the pattern appropriately so that 50% excess capacity loading is achieved.

We implemented the stochastic program in its deterministic expansion form. The entire simulation process in implemented in MATLABTM, including scenario generation, and YALMIP [113] is used as the optimization modeling interface to the solvers. We have experimented with various solvers including CPLEX 12.6, Gurobi 5.6, MOSEK 7, and GLPK, where the first three are commercial and were available on an academic license and the latter is an open source solver. Our computational experience with these solvers in our application was mixed, and sometimes contrary to established benchmarks. All the commercial solvers performed much better than GLPK as expected. CPLEX performed worst among the commercial solvers, ranging between 2-3 times slower than Gurobi. To our surprise, however, MOSEK performed better in most cases, our performing Gurobi between 10% and 20% in terms of run time.

We assume roughly 50 charging sessions per day scenario (since the exact number depends on the scenario and day of week). To achieve a consistent result from the DAM stochastic program we experimented with the number of scenarios. Based on our dataset and sampling, we found out that the total cost of the DAM planning problem does not change more than

10^{-3} for number of scenarios greater than 250 scenarios; therefore, we ran each day of planning with 250 scenarios.

We have performed the simulations for the complete year of 2012 to minimize the effect of fluctuations in prices. Figure 12.3 summarizes the results in terms of the average normalized cost over 2012. In comparison with uncoordinated charging, there is substantial amount of saving even when the coordinated users are subject to capacity constraints while uncoordinated users are not. We have also demonstrated the effect of savings on the total cost as the stacked block. That is, if the savings from AS offering, which can only happen if the ESCo participates in the market, are taken off the ESCo's balance sheet, the cost will go up by the block on top of the cost for the scheduled users. Note that this is a rough estimate of the contribution of AS provision in total costs since if the ESCo forgoes the AS provision option, its schedule would most likely change. In other words, the AS savings block shown here is an upper bound on the contribution of AS in total cost reduction.

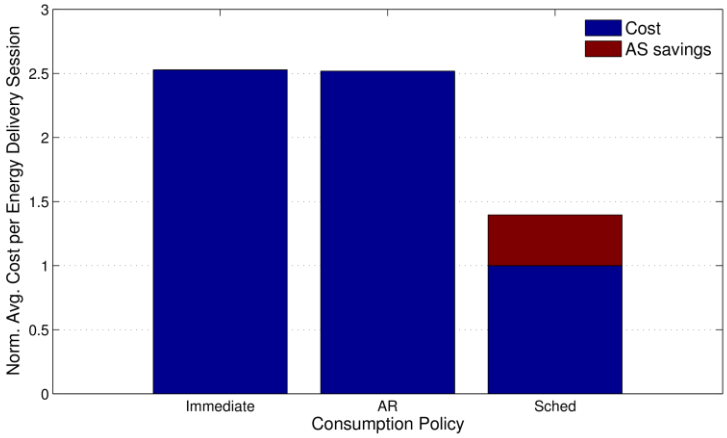

Figure 12.3 Average Cost Comparison between Immediate Charging, AR Charging and Multi-settlement Scheduling

As demonstrated by Figure 12.3, scheduling in DAM reduces the energy cost to approximately half that of price insensitive methods. Also, roughly one fourth of the savings comes from the AS provision. In order to get a more detailed view and observe the seasonality in costs, we have also plotted the monthly averages of cost per PEV charging session in Figure 12.4. This figure shows that the main monthly trend of the costs remain the same and are mostly influenced by the trend of electricity and AS prices.

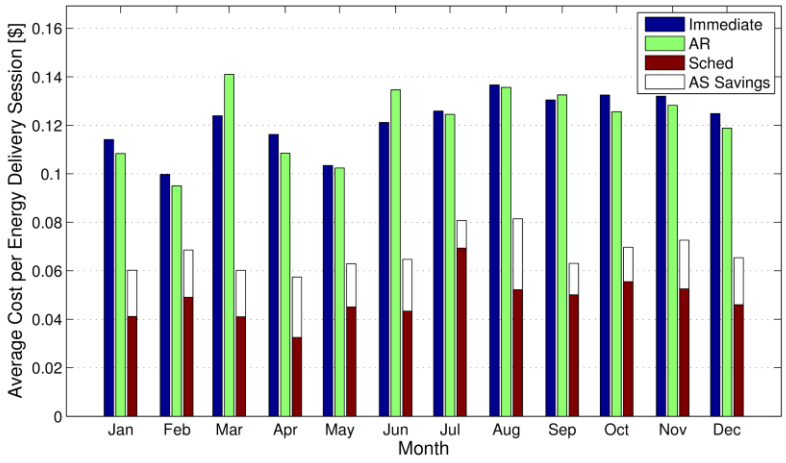

Figure 12.4 Average Cost of Multi-settlement Scheduling per Month over the Year

Finally, we study the ratio of AS capacity offered to energy served in Figure 12.12.5, where we have plotted this ratio for year 2012 on a monthly basis. Based on this figure, the ratio of AS capacity offered to energy served remains above 50% for all months and relatively steady. This is good news since it suggests that overall, the PEV load can be seen as a substantial and reliable source of AS in terms of capacity.

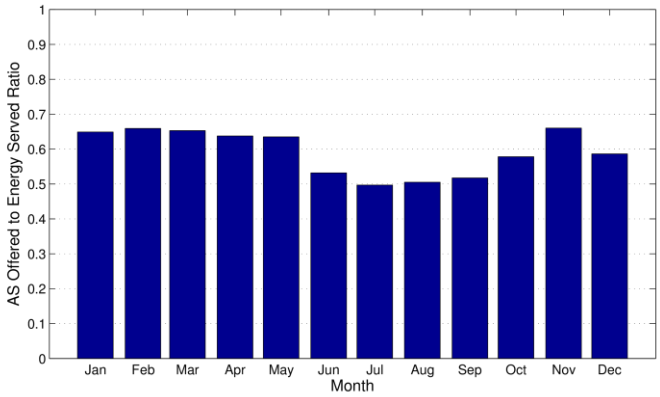

Figure 12.5 Monthly AS offered to energy served ratio.

Careful investigation of the source of cost savings, revealed that some of the savings, in some cases a major portion of it, came from the ESCo ceasing the DAM-RTM trading opportunities. Since we have assumed that unused DAM purchases can be sold back to the market, when prices are expected to be better in DAM, the ESCo purchases considerable amounts in those times, almost regardless of its schedule and sells it in RTM. Since we expect these arbitrage opportunities to be short lived, we tried to set in place measures to prevent extensive occurrence of such situations. In this work, as discussed in the formulation, we have bound the total amount energy purchase volume in DAM to be the minimum amount of total energy demand over the scenarios. We believe, however, that systematic modeling of risk in DAM-RTM decisions, through including a systematic

measure of risk into the objective function, e.g. CVaR, would help with such situations. Finally, we believe there is nothing systematically wrong in ESCo seeking profit maximization in any possible way, if the risks of such decision making is modeled properly. We have left investigation of this path for future work.

12.5 Conclusion

In this section we proposed a systematic method for an Energy Services Company, particularly one that serves PEV load, to participate in a multi-settlement market structure. We focused on the DAM planning problem and formulated it as a stochastic program. We then discussed the challenges in scenario generation in case of PEV load and proposed a data driven approach for generating scenarios. We finally presented our performance analysis on the proposed method and showed that adopting the proposed method can result in cost reductions of about 50%, roughly half of which is due to AS sales by the ESCo. Moreover, we observed that the ESCo would offer roughly 50% of its served load back in the market as AS.

We plan to add a measure of risk to our future implementation of our proposed method to have a more realistic view of the decision making process by the ESCo. Moreover, we are working on more efficient implementation of the proposed stochastic program though L-shaped method and similar techniques.

13. Conclusions

This report mainly focuses on the following two points: 1) analysis on the relationship between EV movement and its SOC; 2) communication network establishment to integrate EV charging stations from various vendors.

In order to obtain the impact of EV movement on its SOC, a model is introduced to simulate the energy consumption of EV according to its movement. Besides, a stochastic way of generating driving cycle is proposed considering the uncertainties such as human behaviors, and etc. Various factors have been taken into account during the simulation such as the velocity, standard deviation of the driving speed, with or without regenerative brake, stop times, wind speed, and etc. and their respective impact is evaluated in the report. Among all the factors considered, the inclination of the ground has the greatest effect on EV's energy consumption. Besides, the frequency of changing speed and the stop times of EV also have relatively greater impact on EV's SOC compared with other factors. Moreover, it has been proved that the regenerative braking which is one of those factors which differentiate EV from conventional vehicles can help save energy. It can be speculated that the regenerative braking can greatly help saving energy in the future especially for EVs running in the city where they will have to stop a lot when the efficiency of the conversion from kinetic energy to electricity energy is improved.

After the analysis, an algorithm is proposed to calculate the optimal velocity to optimize the battery energy consumption which is a nonlinear function with regard to different factors such as velocity, stop times, and etc. The mound-shaped curve can be obtained to describe the relationship between the average velocity and the total energy consumption. Such algorithm can be integrated into the vehicle system to give drivers suggestions and thus help save battery energy.

In order to set up communication network to integrate charging stations from various vendors, a survey was done among different vendors on their network and communication protocols, their services to EV drivers and charging station owners and so on. Considering the great variety in their communication scheme, we propose the concept of "Communication Center" in this report to integrate the communication from charging stations provided by different vendors. The functionality of the proposed Communication Center include: communication realization and management, data acquisition and management, information provision to drivers, control and optimization, and interaction with other entities. The advantages of adopting and realizing the Communication Center are elaborated in the report including efficiency in utilizing charging resources, relatively easy to implement, compatible with future aggregative architecture, data and communication management, and etc. The according design of a communication center is also discussed in the report including its multi-layer communication structure, the communication protocol to be adopted, and some necessary components it should have like database, etc.

However, due to some limitations, the proposed functionalities cannot be fully realized at this moment especially for those control functions, since the concept of Communication

Center has not been yet widely accepted. We believe that with the popularization of EVs and wider acceptance of the concept of communication center, the communication center will be able to realize more functionalities. Under the existing limitation, the functionality of the communication center should be somehow adjusted and we here can realize the functionality of collecting and managing data from charging stations provided by different vendors.

The way how to realize the communication between charging infrastructures and our proposed communication center is discussed in this report including the data requirement and practical data acquisition analysis, database design for the communication center according to the practical availability of the data, and the methods to establish the communication to obtain data. Usually, the vendors are responsible to collect data from infrastructure provided by them and then transmit the data to the charging station owner. Therefore, what we can do is to establish the communication between different vendors and communication center. For some vendors, they are able to transmit the data through API. However, API may not be available for every vendor, for those who do not have API, data can still be transmitted through email at fixed frequency. This report discusses the way how to acquire data both through the API and email automatically and then put those data into the database we design and establish for the communication center.

References

[1] Pieltain Fernández, L.; Román, T.G.S.; Cossent, R.; Domingo, C.M.; Frías, P., "Assessment of the Impact of Plug-in Electric Vehicles on Distribution Networks," *Power Systems, IEEE Transactions on*, vol.26, no.1, pp.206, 213, Feb. 2011

[2] S. Soylu (2011, Aug.). Electric Vehicles – The Benefits and Barriers. (1st Ed.) [Online]. Available: http:// www.intechopen.com.

[3] S. W. Hadley and A. A. Tsvetkova, "Potential impacts of plug-in hybrid electric vehicles on regional power generation," Electr. J., vol. 22, no. 10, pp. 56–68, 2009

[4] Roe, C.; Meliopoulos, A.P.; Meisel, J.; Overbye, T., "Power System Level Impacts of Plug-In Hybrid Electric Vehicles Using Simulation Data," *Energy 2030 Conference, 2008. ENERGY 2008. IEEE*, vol., no., pp.1, 6, 17-18 Nov. 2008

[5] Sakis Meliopoulos, Jerome Meisel, George Cokkinides, Thomas Overbye; "Power System Level Impacts of Plug-In Hybrid Vehicles", Power Systems Engineering Research Center, October 2009: Available at www.pserc.wisc.edu/.../meliopoulos_phev_pserc_report_t-34_2009.pdf

[6] Mladen Kezunovic (lead), Ross Baldick, and Ivan Damnjanovic; " PHEVs as Dynamically Configurable Dispersed Energy Storage", Power Systems Engineering Research Center, August 2011: Available at http://www.pserc.wisc.edu/documents/publications/reports/2011_reports/Kezunovic_PSERC_Final_Report_Project_T-40_2011.pdf

[7] Pang, C.; Dutta, P.; Kim, S.; Kezunovic, M.; Damnjanovic, I., "PHEVs as dynamically configurable dispersed energy storage for V2B uses in the smart grid," *Power Generation, Transmission, Distribution and Energy Conversion (MedPower 2010), 7th Mediterranean Conference and Exhibition on*, vol., no., pp.1, 6, 7-10 Nov. 2010

[8] Underwriters Laboratories approves SAE J1772 charging plug [Online]. Available: http://green.autoblog.com/2009/06/28/underwriters-laboratories-approves-sae-j1772-charging-plug/

[9] Rawson, M. and Kateley, S., "Electric Vehicle Charging Equipment Design and Health and Safety Codes," SAE Technical Paper 1999-01-2941, 1999, doi: 10.4271/1999-01-2941.

[10] Yan, Q.; Mladen, K., "Impact analysis of Electric Vehicle charging on distribution system," *North American Power Symposium (NAPS), 2012*, vol., no., pp.1, 6, 9-11 Sept. 2012

[11] M. Dubarry, V. Svoboda, R. Hwu, B.Y. Liaw, Capacity Loss in Rechargeable Lithium Cells during Cycle Life Testing: The Importance of Determining State of Charge, *Journal of Power Sources* (2007), doi: 10.1016/j.jpowsour.2007.06.185.

[12] Bor Yann Liaw, Matthieu Dubarry, From driving cycle analysis to understanding battery performance in real-life electric hybrid vehicle operation, *Journal of Power Sources*, Volume 174, Issue 1, 22 November 2007, Pages 76-88, ISSN 0378-7753

[13] Habib AL JED, André MIEZE, Jean-Michel VINASSA, Rémi SIMON, Mathematical modeling of aging factors for Li-ion battery cells, *IEEE VPPC*, September 2010

[14] A. A. Frank, "Plug-in hybrid vehicles for a sustainable future," Amer. *Sci.*, vol. 95, no. 2, pp. 158–165, Mar. /Apr. 2007.

[15] Shahidinejad, S.; Bibeau, E.; Filizadeh, S., "Statistical Development of a Duty Cycle for Plug-in Vehicles in a North American Urban Setting Using Fleet Information,"

Vehicular Technology, IEEE Transactions on, vol.59, no.8, pp.3710, 3719, Oct. 2010
[16] Chrenko, D.; Garcia Diez, I.; Le Moyne, L., "Artificial driving cycles for the evaluation of energetic needs of electric vehicles," *Transportation Electrification Conference and Expo (ITEC), 2012 IEEE* , vol., no., pp.1,5, 18-20 June 2012
[17] T Markel, A Brooker, T Hendricks, V Johnson, K Kelly, B Kramer, M O'Keefe, S Sprik, K Wipke, ADVISOR: a systems analysis tool for advanced vehicle modeling, *Journal of Power Sources*, Volume 110, Issue 2, 22 August 2002, Pages 255-266, ISSN 0378-7753
[18] Shi Qingsheng; Zhang Chenghui; Cui Naxin; Zhang Xiaoping, "Battery state-of-charge estimation in electric vehicle using elman neural network method," *Control Conference (CCC), 2010 29th Chinese*, vol., no., pp.5999, 6003, 29-31 July 2010
[19] Chaoui, H. and P. Sicard, Accurate State of Charge (SOC) Estimation for Batteries using a Reduced-order Observer. *2011 IEEE International Conference on Industrial Technology (Icit)*, 2011
[20] Yan, J.Y., et al., A Novel On-line Self-learning State-of-charge Estimation of Battery Management System for Hybrid Electric Vehicle. *2009 IEEE Intelligent Vehicles Symposium*, vols 1 and 2, 2009: p. 1161-1166.
[21] Yan, J.Y., et al., Battery State-of-charge Estimation based on H (infinity) Filter for Hybrid Electric Vehicle. *2008 10th International Conference on Control Automation Robotics & Vision*: Icarv 2008, vols 1-4, 2008: p. 464-469
[22] Guo Chun-lin; Wu Li; Wang Dan; Qi Wen-bo; Xiao Xiang-ning, "Impact of electric vehicle charging on power grid," *Electrical and Control Engineering (ICECE), 2011 International Conference on*, vol., no., pp.2270, 2274, 16-18 Sept. 2011
[23] R. H. Yi Yun Tu, Can Li, Lin Cheng, Lin Le, "Impact of Electric Vehicles on Power System through Vehicle to Grid Technology," Advanced Materials Research, no. 347-353, pp. 3928-3934, 2011
[24] Wikipedia. *Charging Station*. Available: http://en.wikipedia.org/wiki/Charging_station
[25] Fox, G.H., "Electric Vehicle Charging Stations: Are We Prepared?" *Industry Applications Magazine, IEEE*, vol.19, no.4, pp.32,38, July-Aug. 2013
[26] Rawson, M. and Kateley, S., "Electric Vehicle Charging Equipment Design and Health and Safety Codes," SAE Technical Paper 1999-01-2941, 1999
[27] Y. Jingyu, X. Guoqing, X. Yangsheng, and X. Benliang, "Battery state-of-charge estimation based on H<inf>∞</inf> filter for hybrid electric vehicle," presented at the Control, Automation, Robotics and Vision, 2008. ICARCV 2008. 10th International Conference on, 2008.
[28] G. Qiuming, L. Yaoyu, and P. Zhong-Ren, "Trip-Based Optimal Power Management of Plug-in Hybrid Electric Vehicles," Vehicular Technology, IEEE Transactions on, vol. 57, pp. 3393-3401, 2008.
[29] G. Qiuming, L. Yaoyu, and P. Zhong-Ren, "Trip Based Power Management of Plug-in Hybrid Electric Vehicle with Two-Scale Dynamic Programming," in Vehicle Power and Propulsion Conference, 2007. VPPC 2007. IEEE, 2007, pp. 12-19.
[30] N. Jinrui, S. Fengchun, and R. Qinglian, "A Study of Energy Management System of Electric Vehicles," in Vehicle Power and Propulsion Conference, 2006. VPPC '06. IEEE, 2006, pp. 1-6.
[31] P. Notten, H. Bergveld, and W. Kruijt, "Battery Management Systems: Design by

modeling," ed: Kluwer Academic Publisher, 2002.
[32] G. L. Plett, "Extended Kalman filtering for battery management systems of LiPB-based HEV battery packs: Part 2. Modeling and identification," Journal of power sources, vol. 134, pp. 262-276, 2004.
[33] S. Piller, M. Perrin, and A. Jossen, "Methods for state-of-charge determination and their applications," Journal of power sources, vol. 96, pp. 113-120, 2001.
[34] V. Coroban, I. Boldea, and F. Blaabjerg, "A novel on-line state-of-charge estimation algorithm for valve regulated lead-acid batteries used in hybrid electric vehicles," in Electrical Machines and Power Electronics, 2007. ACEMP '07. International Aegean Conference on, 2007, pp. 39-46.
[35] K. W. E. Cheng, B. P. Divakar, W. Hongjie, K. Ding, and H. Ho Fai, "Battery-Management System (BMS) and SOC Development for Electrical Vehicles," Vehicular Technology, IEEE Transactions on, vol. 60, pp. 76-88, 2011.
[36] C. Bingham, C. Walsh, and S. Carroll, "Impact of driving characteristics on electric vehicle energy consumption and range," Intelligent Transport Systems, IET, vol. 6, pp. 29-35, 2012.
[37] H. Xiaoling and J. W. Hodgson, "Modeling and simulation for hybrid electric vehicles. I. Modeling," Intelligent Transportation Systems, IEEE Transactions on, vol. 3, pp. 235-243, 2002.
[38] H. Xiaoling and J. W. Hodgson, "Modeling and simulation for hybrid electric vehicles. II. Simulation," Intelligent Transportation Systems, IEEE Transactions on, vol. 3, pp. 244-251, 2002.
[39] L. Der-Tsai, S. Shaw-Ji, L. Chien-Ming, and W. Ying-Chung, "State-of-Charge Estimation for Electric Scooters by Using Learning Mechanisms," Vehicular Technology, IEEE Transactions on, vol. 56, pp. 544-556, 2007.
[40] S. G. Li, S. M. Sharkh, F. C. Walsh, and C. N. Zhang, "Energy and Battery Management of a Plug-In Series Hybrid Electric Vehicle Using Fuzzy Logic," Vehicular Technology, IEEE Transactions on, vol. 60, pp. 3571-3585, 2011.
[41] H. A. Jed, A. Mieze, R. Simon, and J. Vinassa, "An electric vehicle model and a driving cycle for mail delivery use," in Power Electronics and Applications (EPE 2011), Proceedings of the 2011-14th European Conference on, 2011, pp. 1-8.
[42] R. Sadoun, N. Rizoug, P. Bartholomeus, B. Barbedette, and P. Le Moigne, "Influence of the drive cycles on the sizing of hybrid storage system battery-supercapacitor supplying an electric vehicle," in IECON 2011 - 37th Annual Conference on IEEE Industrial Electronics Society, 2011, pp. 4106-4112.
[43] L. Guzzella and A. Sciarretta, Vehicle propulsion systems: Springer, 2007.
[44] M. André, "The ARTEMIS European driving cycles for measuring car pollutant emissions," Science of The Total Environment, vol. 334–335, pp. 73-84, 12/1/ 2004.
[45] D. D. Brandt, "Driving cycle testing of electric vehicle batteries and systems," Journal of Power Sources, vol. 40, pp. 73-79, 12// 1992.
[46] O. Shiqi, Z. Yafu, L. Jing, J. Pu, and T. Baoyu, "Development of hybrid city bus's driving cycle," in Electric Information and Control Engineering (ICEICE), 2011 International Conference on, 2011, pp. 2112-2116.
[47] H. Y. Tong, W. T. Hung, and C. S. Cheung, "Development of a driving cycle for Hong Kong," Atmospheric Environment, vol. 33, pp. 2323-2335, 7/1/ 1999.
[48] D. Chrenko, I. Garcia Diez, and L. Le Moyne, "Artificial driving cycles for the

evaluation of energetic needs of electric vehicles," in Transportation Electrification Conference and Expo (ITEC), 2012 IEEE, 2012, pp. 1-5.
[49] G. Souffran, L. Miegeville, and P. Guerin, "Simulation of real-world vehicle missions using a stochastic Markov model for optimal design purposes," in Vehicle Power and Propulsion Conference (VPPC), 2011 IEEE, 2011, pp. 1-6.
[50] S. Shahidinejad, E. Bibeau, and S. Filizadeh, "Statistical Development of a Duty Cycle for Plug-in Vehicles in a North American Urban Setting Using Fleet Information," Vehicular Technology, IEEE Transactions on, vol. 59, pp. 3710-3719, 2010.
[51] T. Di, L. Yutao, and H. Xiangdong, "Statistic Driving Cycle Analysis and application for hybrid electric vehicle parametric design," in Consumer Electronics, Communications and Networks (CECNet), 2011 International Conference on, 2011, pp. 5259-5263.
[52] Online available: http://www.ieahev.org/by-country/belgium-charging-infrastructure/
[53] US Department of Transportation, Bureau of Transportation Statistics, Omnibus Household Survey. "From Home to Work, the Average Commute is 26.4 Minutes". OmniStats 3 (4). Retrieved 2009-10-15.
[54] Wikipedia. Charging Station. Available:
http://en.wikipedia.org/wiki/Charging_station
[55] Dharmakeerthi, C.H.; Mithulananthan, N.; Saha, T.K., "Planning of electric vehicle charging infrastructure," Power and Energy Society General Meeting (PES), 2013 IEEE, vol., no., pp.1, 5, 21-25 July 2013
[56] Fox, G.H., "Electric Vehicle Charging Stations: Are We Prepared?," Industry Applications Magazine, IEEE , vol.19, no.4, pp.32,38, July-Aug. 2013
[57] Rawson, M. and Kateley, S., "Electric Vehicle Charging Equipment Design and Health and Safety Codes," SAE Technical Paper 1999-01-2941, 1999
[58] Bohn, T.; Chaudhry, H., "Overview of SAE standards for plug-in electric vehicle," Innovative Smart Grid Technologies (ISGT), 2012 IEEE PES, vol., no., pp.1, 7, 16-20 Jan. 2012
[59] Hybrid Committe, "SAE Electric Vehicle and Plug in Hybrid Electric
Vehicle Conductive Charge Coupler," SAE International, Detroit,Michigan, Standard J1772, Jan, 2010
[60] US Department of Energy, Energy Efficiency & Renewable Energy, Developing Infrastructure to Charge Plug-In Electric Vehicles, available: http://www.afdc.energy.gov/fuels/electricity_infrastructure.html
[61] G. H. Fox, "Getting ready for electric vehicle charging stations." pp. 1-7
[62] Vehicle Technologies Program: US Department of Energy, Office of Energy and Renewable Energy and the National Renewable Energy Lab, 2011
[63] M. Yilmaz, and P. T. Krein, "Review of charging power levels and infrastructure for plug-in electric and hybrid vehicles." pp. 1-8
[64] Wikipedia, Communications protocol, available:
http://en.wikipedia.org/wiki/Communications_protocol
[65] Marsden 1986, Section 6.3 - Advantages of standardization, p. 66-67
[66] R. J. Bessa and M. A. Matos, "The role of an aggregator agent for EV in the electricity market," in Power Generation, Transmission, Distribution and Energy Conversion (MedPower 2010), 7th Mediterranean Conference and Exhibition on, 2010, pp. 1-9.
[67] L. Junfeng, N. G. Tszwang, E. K. W. Cheng, and Z. Jun, "The study of distributed EV charging station based on network," in Power Electronics Systems and Applications

(PESA), 2011 4th International Conference on, 2011, pp. 1-5.
[68] C. Quinn, D. Zimmerle, and T. H. Bradley, "The effect of communication architecture on the availability, reliability, and economics of plug-in hybrid electric vehicle-to-grid ancillary services," Journal of Power Sources, vol. 195, pp. 1500-1509, 2010.
[69] Wikipedia. Database normalization. Available: http://en.wikipedia.org/wiki/Database_normalization
[70] Wikipedia. Application programming interface. Available: http://en.wikipedia.org/wiki/Application_programming_interface
[71] Wikipedia. SQL. Available: http://en.wikipedia.org/wiki/SQL
[72] G. C. A. P. Sakis Meliopoulos, Renke Huang, Evangelos Farantatos, Sungyun Choi, Yonghee Lee, and Xuebei Yu, "Smart Grid Technologies for Autonomous Operation and Control," IEEE TRANSACTIONS ON SMART GRID, vol. 2, pp. 1-10, March 2011.
[73] G. J. C. a. G. S. A. P. Sakis Meliopoulos, "Symbolic Integration of Dynamical Systems by Collocation Methods," IEEE PES Power Systems Conference and Exposition, pp. 362 - 367, Oct. 29-Nov. 1 2006.
[74] G. J. C. George. K. Stefopoulos, and A. P. Sakis Meliopoulos, "Quadratized Model of Nonlinear Saturable-Core Inductor for Time-Domain Simulation," IEEE Power & Energy Society General Meeting, pp. 1 - 8, 26-30 July 2009.
[75] G. K. S. a. A. P. S. Meliopoulos, "Quadratized Three-Phase Induction Motor Model for Steady-State and Dynamic Analysis," 38th North American Power Symposium, pp. 65 - 75, 2006.
[76] G. J. C. A. P. Meliopoulos, and George K. Stefopoulos, "Quadratic Integration Method," International Conference on Power Systems Transients (IPST'05), June 19-23 2005.
[77] A. P. Sakis Meliopoulos, Jerome Meisel, George Cokkinides, Thomas Overbye, "Power System Level Impacts of Plug-In Hybrid Vehicles," October 2009.
[78] IEEE, "IEEE Guide for Loading Mineral-Oil Immersed Transformers," in IEEE Std C57.91-2011 (Revision of IEEE Std C57.91-1995) - Redline ed, 2012, pp. 1-172.
[79] A. S. Meliopoulos, G. Cokkinides, and R. James, "Transformer Diagnostic System for Loss of Life and Coil Integrity," in Proceedings of the 1998 Georgia Tech Fault and Disturbance Analysis Conference, pp. 4-5.
[80] ANSI/IEEE, "IEEE Guide for Loading Mineral-Oil-Immersed Overhead and Pad-Mounted Distribution Transformers Rated 500 kVa and Less With 65 Degrees C Or 55 Degrees C Average Winding Rise," in ANSI/IEEE Std C57.91-1981, ed, 1981.
[81] ABB. (Feburary). Single Phase Center Tap Transformer Datasheet. Available: http://alturl.com/g45p4
[82] P. Partener. (February). Single Phase Center Tap Transformer Datasheet. Available: http://alturl.com/nfw42
[83] C. P. Systems. (February). Single Phase Center Tap Transformer Datasheet. Available: http://alturl.com/e93ib
[84] M. G. Villalva, J. R. Gazoli, and E. R. Filho. (2009) Comprehensive approach to modeling and simulation of Photovoltaic Arrays. IEEE Transaction on Power Electronics. 1198-1208.
[85] (Septemper, 2013). Datasheet. Available: Available: http://alturl.com/vqkmq
[86] T. Esram and P. L. Chapman, "Comparison of Photovoltaic Array Maximum Power Point Tracking Techniques," IEEE Transaction at the Energy Conversio, vol. 22, pp. 439 -

449, 2007.
[87] M. Ceraolo, "New Dynamical Models of Lead–Acid Batteries," IEEE TRANSACTIONS ON POWER SYSTEMS, vol. VOL. 15 NOVEMBER 2000.
[88] [18] R. A. Jackey, "A Simple, Effective Lead-Acid Battery Modeling Process for Electrical System Component Selection," 2007.
[89] M. C. S Barsali, "Dynamical models of lead-acid batteries: implementation issues," IEEE Transactions on Energy Conversion, vol. 17, pp. 16-23, March 2002 2002.
[90] S. L. Lijun Gao, Roger A. Dougal, "Dynamic Lithium-Ion Battery Model for System Simulation," IEEE TRANSACTIONS ON COMPONENTS AND PACKAGING TECHNOLOGIES, vol. VOL. 25, SEPTEMBER 2002.
[91] A. P. S. C. Meliopoulos, G.J. ; Galvan, F. ; Fardanesh, B. ; Myrda, P., "Distributed state estimator – Advances and demonstration,," Proceedings of the 41st Annual Hawaii International Conference on System Sciences, p. 163, 2008.
[92] A. P. S. C. Meliopoulos, G.J. ; Galvan, F. ; Fardanesh, B. ; Myrda, P. , "Advances in the SuperCalibrator Concept – Practical Implementations," 40th Annual Hawaii International Conference on System Sciences, (HICSS), p. 118, 2007.
[93] S. A. Mohagheghi, R.H. ; Cokkinides, G.J. ; Meliopoulos, A.P.S. , "Distributed state estimation based on the SuperCalibrator concept – Laboratory Implementation," iREP Symposium on Bulk Power System Dynamics and Control pp. 1-9, 2007.
[94] A. P. S. C. Meliopoulos, G.J. ; Hedrington, C. ; Conrad, T.L. , "The SuperCalibrator – A Fully Distributed State Estimator," IEEE Power and Energy Society General Meeting, pp. 1-8, 2010.
[95] A. P. S. C. Meliopoulos, G.J. ; Galvan, F. ; Fardanesh, B. ; Myrda, P. , "Delivering accurate and timely data to all," Power and Energy Magazine, IEEE vol. 5, pp. 74-86, 2007.
[96] (March 2014). Frigidaire Available: http://www.frigidaire.com/
[97] Mahdi Kefayati and Ross Baldick. Harnessing demand flexibility to match renewable production using localized policies. In 50th Annual Allerton Conference on Communication, Control and Computing, Allerton, IL, October 2012a.
[98] Mahdi Kefayati and Ross Baldick. Energy delivery transaction pricing for flexible electrical loads. In 2011 IEEE International Conference on Smart Grid Communications (SmartGridComm), pages 363–368, Brussels, Belgium, October 2011. ISBN 978-1-4577-1704-8.
[99] Steven Craig Anderson. Analyzing strategic interaction in multi-settlement electricity markets: A closed-loop supply function equilibrium model. PhD thesis, Harvard University Cambridge, Massachusetts, 2004.
[100] K.W. Cheung, P. Shamsollahi, David Sun, J. Milligan, and M. Potishnak. Energy and ancillary service dispatch for the interim iso new england electricity market. In Power Industry Computer Applications, 1999. PICA '99. Proceedings of the 21st 1999 IEEE International Conference, pages 47–53, Jul 1999.
[101] R. Kamat and S.S. Oren. Multi-settlement systems for electricity markets: zonal aggregation under network uncertainty and market power. In Proceedings of the 35th Annual Hawaii International Conference onSystem Sciences (HICSS), pages 739–748, Jan 2002.
[102] Hui Niu, R. Baldick, and Guidong Zhu. Supply function equilibrium bidding strategies with fixed forward contracts. Power Systems, IEEE Transactions on, 20 (4): 1859–1867, Nov 2005. ISSN 0885-8950.

[103] Daniel J. Veit, Anke Weidlich, Jian Yao, and Shmuel S. Oren. Simulating the dynamics in two-settlement electricity markets via an agent-based approach. International Journal of Management Science and Engineering Management, 1 (2): 83–97, 2006.
[104] J. Yao, S.S. Oren, and I. Adler. Computing cournot equilibria in two settlement electricity markets with transmission constraint. In Proceedings of the 37th Annual Hawaii International Conference on System Sciences (HICSS), pages 1–9, Jan 2004.
[105] Taiyou Yong, C.R. Philbrick, R. Entriken, and A. Tuohy. Multi-settlement simulation of reserve procurement using stochastic optimal power flow. In Power and Energy Society General Meeting, 2012 IEEE, pages 1–7, July 2012.
[106] M.C. Caramanis and J.M. Foster. Coupling of day ahead and real-time power markets for energy and reserves incorporating local distribution network costs and congestion. In Communication, Control, and Computing (Allerton), 2010 48th Annual Allerton Conference on, pages 42–49, Sept 2010.
[107] M.C. Caramanis, E. Goldis, P.A. Ruiz, and A. Rudkevich. Power market reform in the presence of flexible schedulable distributed loads. new bid rules, equilibrium and tractability issues. In Communication, Control, and Computing (Allerton), 2012 50th Annual Allerton Conference on, pages 1089–1096, Oct 2012.
[108] Michael C. Caramanis, Justin M. Foster, and Evegeniy A. Goldis. Load participation in electricity markets: Day-Ahead and Hour-Ahead market coupling with Wholesale/Transmission and Retail/Distribution cost and congestion modeling. In IEEE SmartGridComm., pages 513–518, Gaithersburg, MD, 2010.
[109] Chenrui Jin, Jian Tang, and P. Ghosh. Optimizing electric vehicle charging with energy storage in the electricity market. Smart Grid, IEEE Transactions on, 4 (1): 311–320, March 2013. ISSN 1949-3053.
[110] Subramanian, J.A. Taylor, E. Bitar, D. Callaway, K. Poolla, and P. Varaiya. Optimal power and reserve capacity procurement policies with deferrable loads. In Decision and Control (CDC), 2012 IEEE 51st Annual Conference on, pages 450–456, Dec 2012.
[111] A.T. Al-Awami and E. Sortomme. Coordinating vehicle-to-grid services with energy trading. Smart Grid, IEEE Transactions on, 3 (1): 453–462, March 2012. ISSN 1949-3053.
[112] Heejung Park. Electric transmission system expansion planning for the system with uncertain intermittent renewable resources. PhD thesis, The University of Texas at Austin, Austin, TX, 2013.
[113] J. Löfberg. YALMIP : A toolbox for modeling and optimization in MATLAB. In Proceedings of the CACSD Conference, Taipei, Taiwan, 2004. URL http://users.isy.liu.se/johanl/yalmip.

Appendix A. Object Oriented Device Modeling Approach

A.1 Standard Form of the Mathematical Model

The quadratized model of a device can have any combination of a differential equation part, linear part, and quadratic part. The differential equations involved the model can be cast in the following equations format:

$$A_1 \begin{bmatrix} i(t) \\ 0 \end{bmatrix} + A_2 \frac{d}{dt} \begin{bmatrix} i(t) \\ 0 \end{bmatrix} = B_1 x(t) + B_2 \frac{dx(t)}{dt} \tag{A.1}$$

, whereas the algebraic equations are cast in the below form:

$$\begin{bmatrix} i(t) \\ 0 \end{bmatrix} = B_3 x(t) + \begin{bmatrix} x(t)^T F_{eq1} x(t) \\ x(t)^T F_{eq2} x(t) \\ \vdots \end{bmatrix} + K_{eq} \tag{A.2}$$

, where

$$\begin{bmatrix} i(t) \\ 0 \end{bmatrix} = \begin{bmatrix} i_1(t) \\ i_2(t) \\ \vdots \\ 0 \\ 0 \\ \vdots \end{bmatrix}, \quad x(t) = \begin{bmatrix} x_1(t) \\ x_2(t) \\ \vdots \\ x_n(t) \end{bmatrix}$$

i (t): Vector defining the through variable of the model.
x (t): Vector defining the external and internal states of the model.
n: Number of internal and external state variables

Differential equations:

A_1: Identity matrix defining the linear part of the through variables with appropriate dimension.
A_2: Matrix defining the coefficients of the differential part of the through variables with appropriate dimension.
B_1: Matrix defining the linear part with appropriate dimension.
B_2: Matrix defining the coefficients of the differential part with appropriate dimension.

Algebraic equations:

B_3: Matrix defining the linear part with appropriate dimension.
F_{eq}: Matrix defining the quadratic part with appropriate dimension.
K_{eq}: Vector defining the constant part.

A.2 Quadratic Integration Method

The differential equations of the quadratized model that is cast in the form of (A.1) have to be integrated yielding to algebraic equations. The method used to perform the numerical integration is called Quadratic Integration. Simply, this method performs the integration over three points $x(t\text{-}h)$, $x(t_m)$, and $x(t)$ that defines a quadratic function in the interval $[t\text{-}h, t]$. Thus, when the function is integrated over time interval $[t\text{-}h, t]$, it yields

$$A_1\left[\frac{h}{6}i(t-h)+\frac{2h}{3}i(t_m)+\frac{h}{6}i(t)\right]+A_2[i(t)-i(t-h)] = B_1\left[\frac{h}{6}x(t-h)+\frac{2h}{3}x(t_m)+\frac{h}{6}x(t)\right]+B_2[x(t)-x(t-h)]$$

And when it is integrated over time interval $[t\text{-}h, t_m]$, it produces

$$A_1\left[\frac{5h}{24}i(t-h)+\frac{h}{3}i(t_m)-\frac{h}{24}i(t)\right]+A_2[i(t_m)-i(t-h)] = B_1\left[\frac{5h}{24}x(t-h)+\frac{h}{3}x(t_m)-\frac{h}{24}x(t)\right]+B_2[x(t_m)-x(t-h)]$$

Thus, by expressing the above two equations in one compact form, it yields

$$\begin{bmatrix} \frac{h}{6}A_1+A_2 & 0 & \frac{2h}{3}A_1 & 0 \\ 0 & 0 & 0 & 0 \\ -\frac{h}{24}A_1 & 0 & \frac{h}{3}A_1+A_2 & 0 \\ 0 & 0 & 0 & 0 \end{bmatrix}\begin{bmatrix} i(t) \\ 0 \\ i(t_m) \\ 0 \end{bmatrix} = \begin{bmatrix} \frac{h}{6}B_1+B_2 & \frac{2h}{3}B_1 \\ -\frac{h}{24}B_1 & \frac{h}{3}B_1+B_2 \end{bmatrix}\begin{bmatrix} x(t) \\ x(t_m) \end{bmatrix} - \begin{bmatrix} B_2-\frac{h}{6}B_1 \\ B_2-\frac{5h}{24}B_1 \end{bmatrix}[x(t-h)] - \begin{bmatrix} \frac{h}{6}A_1-A_2 & 0 \\ 0 & 0 \\ \frac{5h}{24}A_1-A_2 & 0 \\ 0 & 0 \end{bmatrix}\begin{bmatrix} i(t-h) \\ 0 \end{bmatrix} \quad \text{(A.3)}$$

By assigning the following:

$$D = \begin{bmatrix} \frac{h}{6}A_1 + A_2 & 0 & \frac{2h}{3}A_1 & 0 \\ 0 & 0 & 0 & 0 \\ -\frac{h}{24}A_1 & 0 & \frac{h}{3}A_1 + A_2 & 0 \\ 0 & 0 & 0 & 0 \end{bmatrix}$$

Since A_1 is the identity matrix, sized according to the number of through variables in (A.1), and A_2 can be assumed to be zero, E is the pseudo-inverse of D, which is given by

$$E = \begin{bmatrix} \frac{4}{h}I & 0 & -\frac{8}{h}I & 0 \\ 0 & I & 0 & 0 \\ \frac{1}{2h}I & 0 & \frac{2}{h}I & 0 \\ 0 & 0 & 0 & I \end{bmatrix}$$

Let:

$$F_1 = \begin{bmatrix} \frac{h}{6}B_1 + B_2 & \frac{2h}{3}B_1 \\ -\frac{h}{24}B_1 & \frac{h}{3}B_1 + B_2 \end{bmatrix}$$

$$F_2 = \begin{bmatrix} B_2 - \frac{h}{6}B_1 \\ B_2 - \frac{5h}{24}B_1 \end{bmatrix}$$

$$F_3 = \begin{bmatrix} \frac{h}{6}I & 0 \\ 0 & 0 \\ \frac{5h}{24}I & 0 \\ 0 & 0 \end{bmatrix}$$

Thus, the final form after the integration is performed can be written as the following:

$$\begin{bmatrix} i(t) \\ 0 \\ i(t_m) \\ 0 \end{bmatrix} = E\, F_1 \begin{bmatrix} x(t) \\ x(t_m) \end{bmatrix} - b_{eq} \qquad \text{(A.4)}$$

, where $b_{eq} = E\, F_2[x(t-h)] + E\, F_3 \begin{bmatrix} i(t-h) \\ 0 \end{bmatrix}$

A.3 Final Form of AQCF and SCAQCF

Both forms shown in (A.2) and (A.4) are expressed in one matrix form as the following

$$\begin{bmatrix} i(t) \\ 0 \\ i(t_m) \\ 0 \end{bmatrix} = Y_{eq} \begin{bmatrix} x(t) \\ x(t_m) \end{bmatrix} + \begin{bmatrix} x(t)^T F_{eq1} x(t) \\ x(t)^T F_{eq2} x(t) \\ \vdots \\ x(t_m)^T F_{eq1} x(t_m) \\ x(t_m)^T F_{eq2} x(t_m) \\ \vdots \end{bmatrix} - b_{eq} \tag{A.5}$$

$$b_{eq} = \begin{bmatrix} b_1(t-h) \\ b_2(t-h) \end{bmatrix} = N_{eq}[x(t-h)] + M_{eq} \begin{bmatrix} i(t-h) \\ 0 \end{bmatrix} - K_{eq} \tag{A.6}$$

$$Y_{eq} = E\, F_1 + \begin{bmatrix} B_3 & 0 \\ 0 & B_3 \end{bmatrix} \tag{A.7}$$

$$N_{eq} = E\, F_2 \tag{A.8}$$

$$M_{eq} = E\, F_3 \tag{A.9}$$

, where
Y_{eq}: Matrix defining the linear part of the model.
N_{eq}: Matrix defining the contribution from the previous time step states.
M_{eq}: Matrix defining the contribution of the previous time step through variables.
K_{eq}: Vector defining the constant part of the model.

A.4 Matrix and Vector Dimensions

Assume that there are *n* state variables with *n* equations. Also, assume that there are *m* equations are differential equations for the through variables and (*n-m*) are algebraic equations. Therefore, the dimension of the matrices and vectors defining the AQCF is given by the below table:

$\begin{bmatrix} i(t) \\ 0 \end{bmatrix}$	(n by 1)	$x(t)$	(n by 1)	D	(2n by 2n)
$\begin{bmatrix} i(t_m) \\ 0 \end{bmatrix}$	(n by 1)	$x(t_m)$	(n by 1)	Y_{eq}	(2n by 2n)
$\begin{bmatrix} i(t-h) \\ 0 \end{bmatrix}$	(n by 1)	$x(t-h)$	(n by 1)	N_{eq}	(2n by n)
B_1, B_2, B_3	(n by n)	E	(2n by 2n)	M_{eq}	(2n by n)
A_1	$I(m\ by\ m)$	F_1	(2n by 2n)	K_{eq}	(2n by 1)
		F_2	(2n by n)	b_{eq}	(2n by 1)
		F_3	(2n by n)	F_{eq1}, F_{eq2}	(n by n)

A.5 Network Synthesis

At each node of the system, the connectivity constrains obtained from Kirchhoff's current law is applied. The solution of the network is then achieved at time *t* and t_m. To accomplish this, the set of internal device equations are appended yielding to the following expression,

$$\sum_k A^k i^k(t) = 0 \tag{A.10}$$

$$\sum_k A^k i_m^k(t) = 0 \tag{A.11}$$

, where
i^k (*t*) is the device current injection from device *k* at time t.
Ik(t_m) is the device current injection from device *k* at time t_m.
A^k is the incident matrix given by

$$A_{ij}^k = \begin{cases} 1, & if\ node\ j\ of\ device\ k\ is\ connected\ to\ node\ i \\ 0, & otherwisw \end{cases}$$

Similarly, the terminal voltage for each device v^k (*t*) is related to the constructed nodal voltage vector *v*(*t*). This can be mathematically expressed by:

$$v^k(t) = A^k I\ v(t) \tag{A.12}$$

, where
I: a 2 by 2 identity matrix.

The device currents in the system of equations expressed by the final AQCF in (A.5) are eliminated with the use of equation (A.10) and (A.11). The resulted set of equations is only in terms of the external and internal state variables. Thus, the set of equations can be expressed by the following format,

$$g\big(x(t), x(t_m)\big) = Y_{eq}\begin{bmatrix} x(t) \\ x(t_m) \end{bmatrix} + \begin{bmatrix} x(t)^T F_{eq1} x(t) \\ x(t)^T F_{eq2} x(t) \\ \vdots \\ x(t_m)^T F_{eq1} x(t_m) \\ x(t_m)^T F_{eq2} x(t_m) \\ \vdots \end{bmatrix} - b_{eq} = 0.0 \tag{A.13}$$

A.6 Solution Solver

The system of equations represented by (A.13) is solved using Newton's method. This method is particularly chosen because it is ideally suited for the solution of quadratic equations. Specifically, the solution is given by the following expression,

$$\begin{bmatrix} x^{v+1}(t) \\ x^{v+1}(t_m) \end{bmatrix} = \begin{bmatrix} x^{v}(t) \\ x^{v}(t_m) \end{bmatrix} - J_g^{-1} \left[Y_{eq} \begin{bmatrix} x^{v}(t) \\ x^{v}(t_m) \end{bmatrix} + \begin{bmatrix} (x^{v}(t))^T F_{eq1} x^{v}(t) \\ (x^{v}(t))^T F_{eq2} x^{v}(t) \\ \vdots \\ (x^{v}(t_m))^T F_{eq1} x^{v}(t_m) \\ (x^{v}(t_m))^T F_{eq1} x^{v}(t_m) \\ \vdots \end{bmatrix} - b_{eq} \right] \quad \text{(A.14)}$$

, where v is the iteration step number, b_{eq} is the contribution from the previous time step given by (A.6) and J_g is the Jacobian matrix of equation (A.14). Particularly, the Jacobian matrix takes the following form:

$$J_g = Y_{eq} + \begin{bmatrix} (x^{v}(t))^T (F_{eq1} + F_{eq1}^T) \\ (x^{v}(t))^T (F_{eq2} + F_{eq2}^T) \\ \vdots \\ (x^{v}(t_m))^T (F_{eq1} + F_{eq1}^T) \\ (x^{v}(t_m))^T (F_{eq2} + F_{eq2}^T) \\ \vdots \end{bmatrix} \quad \text{(A.15)}$$

Note that the SCAQCF form of the model can be easily deduced from the AQCF form.

A.7 Quadratic and Trapezoidal Integration Methods Case Study

The RLC circuit that was used in the simulation is shown in Figure A-1. Circuit parameters are tabulated in Table A-1. The results of the simulation of the capacitor voltage and inductor current are shown in Figure A-2 and Figure A-3, respectively. The absolute error of the circuit inductor current for the trapezoidal and quadratic integration methods, compared to the analytical solution is shown in Figure A-4. The vertical axis is logarithmic scale. In this particular case, the quadratic integration method is found to be almost three orders of magnitude more accurate than the trapezoidal method.

Table A-1 RLC Circuit Parameters

R = 1 Ω	L = 10 mH	C = 20 μF
Simulation time = 0.1 sec	Time step (h) = 1 μsec	V=$110\sqrt{2}\sin(120\pi t)$

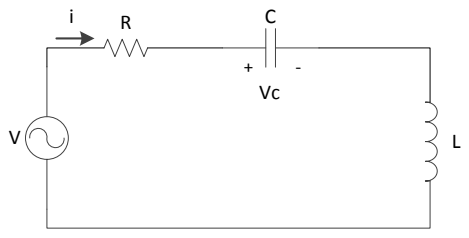

Figure A-1 Series RLC Circuit

Time domain model of the circuit:

$$\frac{dv_c(t)}{dt} = \frac{1}{C}i(t) \tag{A.16}$$

$$\frac{di(t)}{dt} = -\frac{1}{L}v_c(t) - \frac{R}{L}i(t) + \frac{1}{L}\left(10\sqrt{3}\sin(120\pi t)\right) \tag{A.17}$$

The time domain equations are formulated in the standard format and then quadratized as necessary as the following:

$$0.0 = \frac{dv_c(t)}{dt} - \frac{1}{C}i(t) \tag{A.18}$$

$$0.0 = \frac{di(t)}{dt} - x_1(t) \tag{A.19}$$

$$0.0 = x_1(t) + \frac{1}{L}v_c(t) + \frac{R}{L}i(t) - \frac{1}{L}\left(110\sqrt{2}\sin(120\pi t)\right) \tag{A.20}$$

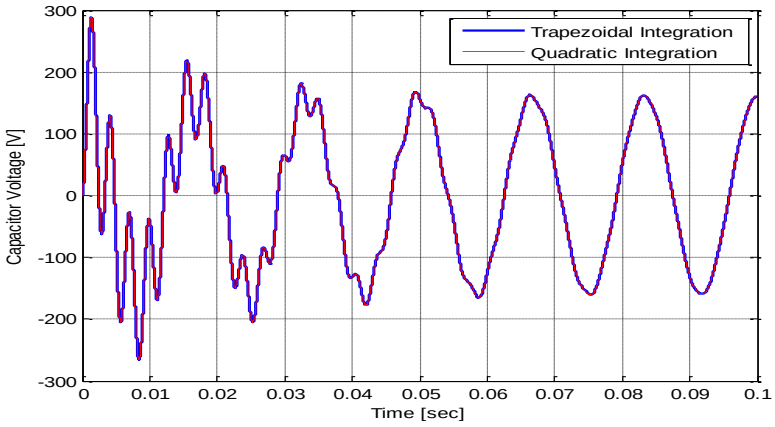

Figure A-2 Capacitor Voltage Waveform

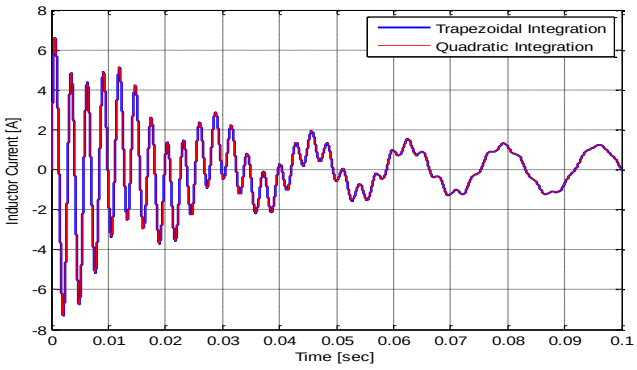

Figure A-3 Circuit Current Waveform

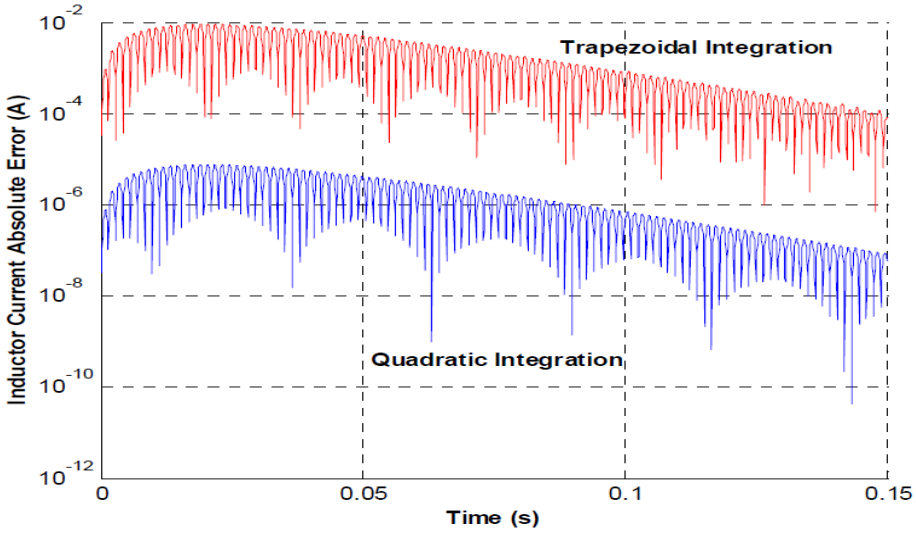

Figure A-4 Absolute Error of the Inductor Current Between the Analytic Solution and Trapezoidal and Quadratic Integration Methods, taken from [77].

Appendix B. Single Phase Center-Tap Distribution Transformer

B.1 Electrical and Thermal Mathematical Model

B.1.1 Electrical Model

Model equations of a single phase center-tap transformer are given by the following equations:

$$\tilde{I}_1 = Y_1\tilde{V}_1 - Y_1\tilde{V}_2 - Y_1\tilde{E} \tag{B.1}$$

$$\tilde{I}_2 = -\tilde{I}_1 \tag{B.2}$$

$$\tilde{I}_{L1} = Y_2\tilde{V}_{L1} - Y_2\tilde{V}_{NN} - \frac{t}{2}Y_2\tilde{E} \tag{B.3}$$

$$\tilde{I}_{NN} = -(\tilde{I}_{L1} + \tilde{I}_{L2}) \tag{B.4}$$

$$\tilde{I}_{L2} = -Y_2\tilde{V}_{NN} + Y_2\tilde{V}_{L2} + \frac{t}{2}Y_2\tilde{E} \tag{B.5}$$

$$0.0 = -Y_1\tilde{V}_1 + Y_1\tilde{V}_2 - \frac{t}{2}Y_2\tilde{V}_{L1} + \frac{t}{2}Y_2\tilde{V}_{L2} + (Y_m + Y_1 + \frac{t^2}{2}Y_2)\tilde{E} \tag{B.6}$$

B.1.2 Thermal Model

The model equations of the thermal model of a single phase center-tap transformer are given by the following set of equations

$$\begin{aligned}\dot{q}_{caseT} = {} & C_{TOT}\frac{d}{dt}(\theta_{CaseT} - \theta_{TOT}) + C_{CaseT}\frac{d}{dt}(\theta_{CaseT} - \theta_{amb}) \\ & + G_{h1-CaseT}(\theta_{CaseT} - \theta_{h1}) + G_{h2-CaseT}(\theta_{CaseT} - \theta_{h2}) \\ & + G_{h3-CaseT}(\theta_{CaseT} - \theta_{h3}) + G_{L11-CaseT}(\theta_{CaseT} - \theta_{L11}) \\ & + G_{L12-CaseT}(\theta_{CaseT} - \theta_{L12}) + G_{L13-CaseT}(\theta_{CaseT} - \theta_{L13}) \\ & + G_{L21-CaseT}(\theta_{CaseT} - \theta_{L21}) + G_{L22-CaseT}(\theta_{CaseT} - \theta_{L22}) \\ & + G_{L23-CaseT}(\theta_{CaseT} - \theta_{L23}) + G_{CT-CaseT}(\theta_{CaseT} - \theta_{CT}) \\ & + G_{CB-CaseT}(\theta_{CaseT} - \theta_{CB}) + G_{CR-CaseT}(\theta_{CaseT} - \theta_{CR}) \\ & + G_{CL-CaseT}(\theta_{CaseT} - \theta_{CL}) + G_{TOT-CaseT}(\theta_{CaseT} - \theta_{TOT}) \\ & + G_{BOT-CaseT}(\theta_{CaseT} - \theta_{BOT}) + G_{ROT-CaseT}(\theta_{CaseT} - \theta_{ROT}) \\ & + G_{LOT-CaseT}(\theta_{CaseT} - \theta_{LOT}) + G_{CaseT-CaseB}(\theta_{CaseT} - \theta_{CaseB}) \\ & + G_{CaseT-CaseR}(\theta_{CaseT} - \theta_{CaseR}) \\ & + G_{CaseT-CaseL}(\theta_{CaseT} - \theta_{CaseL}) + G_{CaseT-amb}(\theta_{CaseT} - \theta_{amb})\end{aligned} \tag{B.7}$$

$$\begin{aligned}\dot{q}_{caseB} = {} & C_{TOB}\frac{d}{dt}(\theta_{CaseB} - \theta_{BOT}) + C_{CaseB}\frac{d}{dt}(\theta_{CaseB} - \theta_{amb}) \\ & + G_{h1-CaseB}(\theta_{CaseB} - \theta_{h1}) + G_{h2-CaseB}(\theta_{CaseB} - \theta_{h2}) \\ & + G_{h3-CaseB}(\theta_{CaseB} - \theta_{h3}) + G_{L11-CaseB}(\theta_{CaseB} - \theta_{L11}) \\ & + G_{L12-CaseB}(\theta_{CaseB} - \theta_{L12}) + G_{L13-CaseB}(\theta_{CaseB} - \theta_{L13}) \\ & + G_{L21-CaseB}(\theta_{CaseB} - \theta_{L21}) + G_{L22-CaseB}(\theta_{CaseB} - \theta_{L22}) \\ & + G_{L23-CaseB}(\theta_{CaseB} - \theta_{L23}) + G_{CT-CaseB}(\theta_{CaseB} - \theta_{CT}) \\ & + G_{CB-CaseB}(\theta_{CaseB} - \theta_{CB}) + G_{CR-CaseB}(\theta_{CaseB} - \theta_{CR}) \\ & + G_{CL-CaseB}(\theta_{CaseB} - \theta_{CL}) + G_{TOT-CaseB}(\theta_{CaseB} - \theta_{TOT}) \\ & + G_{BOT-CaseB}(\theta_{CaseB} - \theta_{BOT}) + G_{ROT-CaseB}(\theta_{CaseB} - \theta_{ROT}) \\ & + G_{LOT-CaseB}(\theta_{CaseB} - \theta_{LOT}) + G_{CaseT-CaseB}(\theta_{CaseB} - \theta_{CaseT}) \\ & + G_{CaseB-CaseR}(\theta_{CaseB} - \theta_{CaseR}) \\ & + G_{CaseB-CaseL}(\theta_{CaseB} - \theta_{CaseL}) \\ & + G_{CaseB-amb}(\theta_{CaseB} - \theta_{amb})\end{aligned} \tag{B.8}$$

$$\begin{aligned}\dot{q}_{caseR} = {} & C_{ROT}\frac{d}{dt}(\theta_{CaseR} - \theta_{ROT}) + C_{CaseR}\frac{d}{dt}(\theta_{CaseR} - \theta_{amb}) \\ & + G_{h1-CaseR}(\theta_{CaseR} - \theta_{h1}) + G_{h2-CaseR}(\theta_{CaseR} - \theta_{h2}) \\ & + G_{h3-CaseR}(\theta_{CaseR} - \theta_{h3}) + G_{L11-CaseR}(\theta_{CaseR} - \theta_{L11}) \\ & + G_{L12-CaseR}(\theta_{CaseR} - \theta_{L12}) + G_{L13-CaseR}(\theta_{CaseR} - \theta_{L13}) \\ & + G_{L21-CaseR}(\theta_{CaseR} - \theta_{L21}) + G_{L22-CaseR}(\theta_{CaseR} - \theta_{L22}) \\ & + G_{L23-CaseR}(\theta_{CaseR} - \theta_{L23}) + G_{CT-CaseR}(\theta_{CaseR} - \theta_{CT}) \\ & + G_{CB-CaseR}(\theta_{CaseR} - \theta_{CB}) + G_{CR-CaseR}(\theta_{CaseR} - \theta_{CR}) \\ & + G_{CL-CaseR}(\theta_{CaseR} - \theta_{CL}) + G_{TOT-CaseR}(\theta_{CaseR} - \theta_{TOT}) \\ & + G_{BOT-CaseR}(\theta_{CaseR} - \theta_{BOT}) + G_{ROT-CaseR}(\theta_{CaseR} - \theta_{ROT}) \\ & + G_{LOT-CaseR}(\theta_{CaseR} - \theta_{LOT}) + G_{CaseT-CaseR}(\theta_{CaseR} - \theta_{CaseT}) \\ & + G_{CaseB-CaseR}(\theta_{CaseR} - \theta_{CaseB}) \\ & + G_{CaseR-CaseL}(\theta_{CaseR} - \theta_{CaseL}) \\ & + G_{CaseR-amb}(\theta_{CaseR} - \theta_{amb})\end{aligned} \tag{B.9}$$

$$\begin{aligned}\dot{q}_{caseL} = {} & C_{LOT}\frac{d}{dt}(\theta_{CaseL} - \theta_{LOT}) + C_{CaseL}\frac{d}{dt}(\theta_{CaseL} - \theta_{amb}) \\ & + G_{h1-CaseL}(\theta_{CaseL} - \theta_{h1}) + G_{h2-CaseL}(\theta_{CaseL} - \theta_{h2}) \\ & + G_{h3-CaseL}(\theta_{CaseL} - \theta_{h3}) + G_{L11-CaseL}(\theta_{CaseL} - \theta_{L11}) \\ & + G_{L12-CaseL}(\theta_{CaseL} - \theta_{L12}) + G_{L13-CaseL}(\theta_{CaseL} - \theta_{L13}) \\ & + G_{L21-CaseL}(\theta_{CaseL} - \theta_{L21}) + G_{L22-CaseL}(\theta_{CaseL} - \theta_{L22}) \\ & + G_{L23-CaseL}(\theta_{CaseL} - \theta_{L23}) + G_{CT-CaseL}(\theta_{CaseL} - \theta_{CT}) \\ & + G_{CB-CaseL}(\theta_{CaseL} - \theta_{CB}) + G_{CR-CaseL}(\theta_{CaseL} - \theta_{CR}) \\ & + G_{CL-CaseL}(\theta_{CaseL} - \theta_{CL}) + G_{TOT-CaseL}(\theta_{CaseL} - \theta_{TOT}) \\ & + G_{BOT-CaseL}(\theta_{CaseL} - \theta_{BOT}) + G_{ROT-CaseL}(\theta_{CaseL} - \theta_{ROT}) \\ & + G_{LOT-CaseL}(\theta_{CaseL} - \theta_{LOT}) + G_{CaseT-CaseL}(\theta_{CaseL} - \theta_{CaseT}) \\ & + G_{CaseB-CaseL}(\theta_{CaseL} - \theta_{CaseB}) \\ & + G_{CaseR-CaseL}(\theta_{CaseL} - \theta_{CaseR}) + G_{CaseL-amb}(\theta_{CaseL} - \theta_{amb})\end{aligned} \tag{B.10}$$

$$\dot{q}_{amb} = C_{CaseT}\frac{d}{dt}(\theta_{amb} - \theta_{CaseT}) + C_{CaseB}\frac{d}{dt}(\theta_{amb} - \theta_{CaseB}) + C_{CaseR}\frac{d}{dt}(\theta_{amb} - \theta_{CaseR}) + C_{CaseL}\frac{d}{dt}(\theta_{amb} - \theta_{CaseR}) + \dot{Q}_{h1} + \dot{Q}_{h2} + \dot{Q}_{h3} + \dot{Q}_{L11} + \dot{Q}_{L12} + \dot{Q}_{L13} + \dot{Q}_{L21} + \dot{Q}_{L22} + \dot{Q}_{L23} + \dot{Q}_{CT} + \dot{Q}_{CB} + \dot{Q}_{CR} + \dot{Q}_{CL} + G_{CaseT-amb}(\theta_{amb} - \theta_{CaseT}) + G_{CaseB-amb}(\theta_{amb} - \theta_{CaseB}) + G_{CaseB-amb}(\theta_{amb} - \theta_{CaseR}) + G_{CaseL-amb}(\theta_{amb} - \theta_{CaseL}) \quad \text{(B.11)}$$

$$\dot{Q}_{h1} = C_{h1}\frac{d}{dt}(\theta_{h1} - \theta_{CT}) + G_{h1-h2}(\theta_{h1} - \theta_{h2}) + G_{h1-h3}(\theta_{h1} - \theta_{h3}) + G_{h1-L11}(\theta_{h1} - \theta_{L11}) + G_{h1-L12}(\theta_{h1} - \theta_{L12}) + G_{h1-L13}(\theta_{h1} - \theta_{L13}) + G_{h1-L21}(\theta_{h1} - \theta_{L21}) + G_{h1-L22}(\theta_{h1} - \theta_{L22}) + G_{h1-L23}(\theta_{h1} - \theta_{L23}) + G_{h1-CT}(\theta_{h1} - \theta_{CT}) + G_{h1-CB}(\theta_{h1} - \theta_{CB}) + G_{h1-CR}(\theta_{h1} - \theta_{CR}) + G_{h1-CL}(\theta_{h1} - \theta_{CL}) + G_{h1-TOT}(\theta_{h1} - \theta_{TOT}) + G_{h1-BOT}(\theta_{h1} - \theta_{BOT}) + G_{h1-ROT}(\theta_{h1} - \theta_{ROT}) + G_{h1-LOT}(\theta_{h1} - \theta_{LOT}) + G_{h1-CaseT}(\theta_{h1} - \theta_{CaseT}) + G_{h1-CaseB}(\theta_{h1} - \theta_{CaseB}) + G_{h1-CaseR}(\theta_{h1} - \theta_{CaseR}) + G_{h1-CaseL}(\theta_{h1} - \theta_{CaseL}) \quad \text{(B.12)}$$

$$\dot{Q}_{h2} = C_{h2}\frac{d}{dt}(\theta_{h2} - \theta_{CL}) + G_{h1-h2}(\theta_{h2} - \theta_{h1}) + G_{h2-h3}(\theta_{h2} - \theta_{h3}) + G_{h2-L11}(\theta_{h2} - \theta_{L11}) + G_{h2-L12}(\theta_{h2} - \theta_{L12}) + G_{h2-L13}(\theta_{h2} - \theta_{L13}) + G_{h2-L21}(\theta_{h2} - \theta_{L21}) + G_{h2-L22}(\theta_{h2} - \theta_{L22}) + G_{h2-L23}(\theta_{h2} - \theta_{L23}) + G_{h2-CT}(\theta_{h2} - \theta_{CT}) + G_{h2-CB}(\theta_{h2} - \theta_{CB}) + G_{h2-CR}(\theta_{h2} - \theta_{CR}) + G_{h2-CL}(\theta_{h2} - \theta_{CL}) + G_{h2-TOT}(\theta_{h2} - \theta_{TOT}) + G_{h2-BOT}(\theta_{h2} - \theta_{BOT}) + G_{h2-ROT}(\theta_{h2} - \theta_{ROT}) + G_{h2-LOT}(\theta_{h2} - \theta_{LOT}) + G_{h2-CaseT}(\theta_{h2} - \theta_{CaseT}) + G_{h2-CaseB}(\theta_{h2} - \theta_{CaseB}) + G_{h2-CaseR}(\theta_{h2} - \theta_{CaseR}) + G_{h2-CaseL}(\theta_{h2} - \theta_{CaseL}) \quad \text{(B.13)}$$

$$\dot{Q}_{h3} = C_{h3}\frac{d}{dt}(\theta_{h3} - \theta_{CB}) + G_{h1-h3}(\theta_{h3} - \theta_{h1}) + G_{h2-h3}(\theta_{h3} - \theta_{h2}) + G_{h3-L11}(\theta_{h3} - \theta_{L11}) + G_{h3-L12}(\theta_{h3} - \theta_{L12}) + G_{h3-L13}(\theta_{h3} - \theta_{L13}) + G_{h3-L21}(\theta_{h3} - \theta_{L21}) + G_{h3-L22}(\theta_{h3} - \theta_{L22}) + G_{h3-L23}(\theta_{h3} - \theta_{L23}) + G_{h3-CT}(\theta_{h3} - \theta_{CT}) + G_{h3-CB}(\theta_{h3} - \theta_{CB}) + G_{h3-CR}(\theta_{h3} - \theta_{CR}) + G_{h3-CL}(\theta_{h3} - \theta_{CL}) + G_{h3-TOT}(\theta_{h3} - \theta_{TOT}) + G_{h3-BOT}(\theta_{h3} - \theta_{BOT}) + G_{h3-ROT}(\theta_{h3} - \theta_{ROT}) + G_{h3-LOT}(\theta_{h3} - \theta_{LOT}) + G_{h3-CaseT}(\theta_{h3} - \theta_{CaseT}) + G_{h3-CaseB}(\theta_{h3} - \theta_{CaseB}) + G_{h3-CaseR}(\theta_{h3} - \theta_{CaseR}) + G_{h3-CaseL}(\theta_{h3} - \theta_{CaseL}) \quad \text{(B.14)}$$

$$\dot{Q}_{L11} = C_{L11}\frac{d}{dt}(\theta_{L11} - \theta_{CT}) + G_{h1-L11}(\theta_{L11} - \theta_{h1}) + G_{h2-L11}(\theta_{L11} - \theta_{h2}) + G_{h3-L11}(\theta_{L11} - \theta_{h3}) + G_{L11-L12}(\theta_{L11} - \theta_{L12}) + G_{L11-L13}(\theta_{L11} - \theta_{L13}) + G_{L11-L21}(\theta_{L11} - \theta_{L21}) + G_{L11-L22}(\theta_{L11} - \theta_{L22}) + G_{L11-L23}(\theta_{L11} - \theta_{L23}) + G_{L11-CT}(\theta_{L11} - \theta_{CT}) + G_{L11-CB}(\theta_{L11} - \theta_{CB}) + G_{L11-CR}(\theta_{L11} - \theta_{CR}) + G_{L11-CL}(\theta_{L11} - \theta_{CL}) + G_{L11-TOT}(\theta_{L11} - \theta_{TOT}) + G_{L11-BOT}(\theta_{L11} - \theta_{BOT}) + G_{L11-ROT}(\theta_{L11} - \theta_{ROT}) + G_{L11-LOT}(\theta_{L11} - \theta_{LOT}) + G_{L11-CaseT}(\theta_{L11} - \theta_{CaseT}) + G_{L11-CaseB}(\theta_{L11} - \theta_{CaseB}) + G_{L11-CaseR}(\theta_{L11} - \theta_{CaseR}) + G_{L11-CaseL}(\theta_{L11} - \theta_{CaseL}) \quad \text{(B.15)}$$

$$\dot{Q}_{L12} = C_{L12}\frac{d}{dt}(\theta_{L12} - \theta_{CR}) + G_{h1-L12}(\theta_{L12} - \theta_{h1}) + G_{h2-L12}(\theta_{L12} - \theta_{h2}) + G_{h3-L12}(\theta_{L12} - \theta_{h3}) + G_{L11-L12}(\theta_{L12} - \theta_{L11}) + G_{L12-L13}(\theta_{L12} - \theta_{L13}) + G_{L12-L21}(\theta_{L12} - \theta_{L21}) + G_{L12-L22}(\theta_{L12} - \theta_{L22}) + G_{L12-L23}(\theta_{L12} - \theta_{L23}) + G_{L12-CT}(\theta_{L12} - \theta_{CT}) + G_{L12-CB}(\theta_{L12} - \theta_{CB}) + G_{L12-CR}(\theta_{L12} - \theta_{CR}) + G_{L12-CL}(\theta_{L12} - \theta_{CL}) + G_{L12-TOT}(\theta_{L12} - \theta_{TOT}) + G_{L12-BOT}(\theta_{L12} - \theta_{BOT}) + G_{L12-ROT}(\theta_{L12} - \theta_{ROT}) + G_{L12-LOT}(\theta_{L12} - \theta_{LOT}) + G_{L12-CaseT}(\theta_{L12} - \theta_{CaseT}) + G_{L12-CaseB}(\theta_{L12} - \theta_{CaseB}) + G_{L12-CaseR}(\theta_{L12} - \theta_{CaseR}) + G_{L12-CaseL}(\theta_{L12} - \theta_{CaseL}) \quad \text{(B.16)}$$

$$\dot{Q}_{L13} = C_{L13}\frac{d}{dt}(\theta_{L13} - \theta_{CR}) + G_{h1-L13}(\theta_{L13} - \theta_{h1}) + G_{h2-L13}(\theta_{L13} - \theta_{h2}) + G_{h3-L13}(\theta_{L13} - \theta_{h3}) + G_{L11-L13}(\theta_{L13} - \theta_{L11}) + G_{L12-L13}(\theta_{L13} - \theta_{L12}) + G_{L13-L21}(\theta_{L13} - \theta_{L21}) + G_{L13-L22}(\theta_{L13} - \theta_{L22}) + G_{L13-L23}(\theta_{L13} - \theta_{L23}) + G_{L13-CT}(\theta_{L13} - \theta_{CT}) + G_{L13-CB}(\theta_{L13} - \theta_{CB}) + G_{L13-CR}(\theta_{L13} - \theta_{CR}) + G_{L13-CL}(\theta_{L13} - \theta_{CL}) + G_{L13-TOT}(\theta_{L13} - \theta_{TOT}) + G_{L13-BOT}(\theta_{L13} - \theta_{BOT}) + G_{L13-ROT}(\theta_{L13} - \theta_{ROT}) + G_{L13-LOT}(\theta_{L13} - \theta_{LOT}) + G_{L13-CaseT}(\theta_{L13} - \theta_{CaseT}) + G_{L13-CaseB}(\theta_{L13} - \theta_{CaseB}) + G_{L13-CaseR}(\theta_{L13} - \theta_{CaseR}) + G_{L13-CaseL}(\theta_{L13} - \theta_{CaseL}) \quad \text{(B.17)}$$

$$\dot{Q}_{L21} = C_{L21}\frac{d}{dt}(\theta_{L21} - \theta_{CR}) + G_{h1-L21}(\theta_{L21} - \theta_{h1}) + G_{h2-L21}(\theta_{L21} - \theta_{h2}) + G_{h3-L21}(\theta_{L21} - \theta_{h3}) + G_{L11-L21}(\theta_{L21} - \theta_{L11}) + G_{L12-L21}(\theta_{L21} - \theta_{L12}) + G_{L13-L21}(\theta_{L21} - \theta_{L13}) + G_{L21-L22}(\theta_{L21} - \theta_{L22}) + G_{L21-L23}(\theta_{L21} - \theta_{L23}) + G_{L21-CT}(\theta_{L21} - \theta_{CT}) + G_{L21-CB}(\theta_{L21} - \theta_{CB}) + G_{L21-CR}(\theta_{L21} - \theta_{CR}) + G_{L21-CL}(\theta_{L21} - \theta_{CL}) + G_{L21-TOT}(\theta_{L21} - \theta_{TOT}) + G_{L21-BOT}(\theta_{L21} - \theta_{BOT}) + G_{L21-ROT}(\theta_{L21} - \theta_{ROT}) + G_{L21-LOT}(\theta_{L21} - \theta_{LOT}) + G_{L21-CaseT}(\theta_{L21} - \theta_{CaseT}) + G_{L21-CaseB}(\theta_{L21} - \theta_{CaseB}) + G_{L21-CaseR}(\theta_{L21} - \theta_{CaseR}) + G_{L21-CaseL}(\theta_{L21} - \theta_{CaseL}) \quad \text{(B.18)}$$

$$\dot{Q}_{L22} = C_{L22}\frac{d}{dt}(\theta_{L22} - \theta_{CR}) + G_{h1-L22}(\theta_{L22} - \theta_{h1}) + G_{h2-L22}(\theta_{L22} - \theta_{h2}) + G_{h3-L22}(\theta_{L22} - \theta_{h3}) + G_{L11-L22}(\theta_{L22} - \theta_{L11}) + G_{L12-L22}(\theta_{L22} - \theta_{L12}) + G_{L13-L22}(\theta_{L22} - \theta_{L13}) + G_{L21-L22}(\theta_{L22} - \theta_{L21}) + G_{L22-L23}(\theta_{L22} - \theta_{L23}) + G_{L22-CT}(\theta_{L22} - \theta_{CT}) + G_{L22-CB}(\theta_{L22} - \theta_{CB}) + G_{L22-CR}(\theta_{L22} - \theta_{CR}) + G_{L22-CL}(\theta_{L22} - \theta_{CL}) + G_{L22-TOT}(\theta_{L22} - \theta_{TOT}) + G_{L22-BOT}(\theta_{L22} - \theta_{BOT}) + G_{L22-ROT}(\theta_{L22} - \theta_{ROT}) + G_{L22-LOT}(\theta_{L22} - \theta_{LOT}) + G_{L22-CaseT}(\theta_{L22} - \theta_{CaseT}) + G_{L22-CaseB}(\theta_{L22} - \theta_{CaseB}) + G_{L22-CaseR}(\theta_{L22} - \theta_{CaseR}) + G_{L22-CaseL}(\theta_{L22} - \theta_{CaseL}) \quad \text{(B.19)}$$

$$\dot{Q}_{L23} = C_{L23}\frac{d}{dt}(\theta_{L23} - \theta_{CB}) + G_{h1-L23}(\theta_{L23} - \theta_{h1}) + G_{h2-L23}(\theta_{L23} - \theta_{h2}) + G_{h3-L23}(\theta_{L23} - \theta_{h3}) + G_{L11-L23}(\theta_{L23} - \theta_{L11}) + G_{L12-L23}(\theta_{L23} - \theta_{L12}) + G_{L13-L23}(\theta_{L23} - \theta_{L13}) + G_{L21-L23}(\theta_{L23} - \theta_{L21}) + G_{L22-L23}(\theta_{L23} - \theta_{L22}) + G_{L23-CT}(\theta_{L23} - \theta_{CT}) + G_{L23-CB}(\theta_{L23} - \theta_{CB}) + G_{L23-CR}(\theta_{L23} - \theta_{CR}) + G_{L23-CL}(\theta_{L23} - \theta_{CL}) + G_{L23-TOT}(\theta_{L23} - \theta_{TOT}) + G_{L23-BOT}(\theta_{L23} - \theta_{BOT}) + G_{L23-ROT}(\theta_{L23} - \theta_{ROT}) + G_{L23-LOT}(\theta_{L23} - \theta_{LOT}) + G_{L23-CaseT}(\theta_{L23} - \theta_{CaseT}) + G_{L23-CaseB}(\theta_{L23} - \theta_{CaseB}) + G_{L23-CaseR}(\theta_{L23} - \theta_{CaseR}) + G_{L23-CaseL}(\theta_{L23} - \theta_{CaseL}) \quad \text{(B.20)}$$

$$\dot{Q}_{CT} = C_{h1}\frac{d}{dt}(\theta_{CT} - \theta_{h1}) + C_{L11}\frac{d}{dt}(\theta_{CT} - \theta_{L11}) + C_{CT}\frac{d}{dt}(\theta_{CT} - \theta_{TOT}) + G_{h1-CT}(\theta_{CT} - \theta_{h1}) + G_{h2-CT}(\theta_{CT} - \theta_{h2}) + G_{h3-CT}(\theta_{CT} - \theta_{h3}) + G_{L11-CT}(\theta_{CT} - \theta_{L11}) + G_{L12-CT}(\theta_{CT} - \theta_{L12}) + G_{L13-CT}(\theta_{CT} - \theta_{L13}) + G_{L21-CT}(\theta_{CT} - \theta_{L21}) + G_{L22-CT}(\theta_{CT} - \theta_{L22}) + G_{L23-CT}(\theta_{CT} - \theta_{L23}) + G_{CT-CB}(\theta_{CT} - \theta_{CB}) + G_{CT-CR}(\theta_{CT} - \theta_{CR}) + G_{CT-CL}(\theta_{CT} - \theta_{CL}) + G_{CT-TOT}(\theta_{CT} - \theta_{TOT}) + G_{CT-BOT}(\theta_{CT} - \theta_{BOT}) + G_{CT-ROT}(\theta_{CT} - \theta_{ROT}) + G_{CT-LOT}(\theta_{CT} - \theta_{LOT}) + G_{CT-CaseT}(\theta_{CT} - \theta_{CaseT}) + G_{CT-CaseB}(\theta_{CT} - \theta_{CaseB}) + G_{CT-CaseR}(\theta_{CT} - \theta_{CaseR}) + G_{CT-CaseL}(\theta_{CT} - \theta_{CaseL}) \quad \text{(B.21)}$$

$$\dot{Q}_{CB} = C_{h3}\frac{d}{dt}(\theta_{CB} - \theta_{h3}) + C_{L23}\frac{d}{dt}(\theta_{CB} - \theta_{L23}) + C_{CB}\frac{d}{dt}(\theta_{CB} - \theta_{BOT}) + G_{h1-CB}(\theta_{CB} - \theta_{h1}) + G_{h2-CB}(\theta_{CB} - \theta_{h2}) + G_{h3-CB}(\theta_{CB} - \theta_{h3}) + G_{L11-CB}(\theta_{CB} - \theta_{L11}) + G_{L12-CB}(\theta_{CB} - \theta_{L12}) + G_{L13-CB}(\theta_{CB} - \theta_{L13}) + G_{L21-CB}(\theta_{CB} - \theta_{L21}) + G_{L22-CB}(\theta_{CB} - \theta_{L22}) + G_{L23-CB}(\theta_{CB} - \theta_{L23}) + G_{CT-CB}(\theta_{CB} - \theta_{CT}) + G_{CB-CR}(\theta_{CB} - \theta_{CR}) + G_{CB-CL}(\theta_{CB} - \theta_{CL}) + G_{CB-TOT}(\theta_{CB} - \theta_{TOT}) + G_{CB-BOT}(\theta_{CB} - \theta_{BOT}) + G_{CB-ROT}(\theta_{CB} - \theta_{ROT}) + G_{CB-LOT}(\theta_{CB} - \theta_{LOT}) + G_{CB-CaseT}(\theta_{CB} - \theta_{CaseT}) + G_{CB-CaseB}(\theta_{CB} - \theta_{CaseB}) + G_{CB-CaseR}(\theta_{CB} - \theta_{CaseR}) + G_{CB-CaseL}(\theta_{CB} - \theta_{CaseL}) \quad \text{(B.22)}$$

$$\dot{Q}_{CR} = C_{L12}\frac{d}{dt}(\theta_{CR} - \theta_{L12}) + C_{L13}\frac{d}{dt}(\theta_{CR} - \theta_{L13}) + C_{L21}\frac{d}{dt}(\theta_{CR} - \theta_{L21}) + C_{L22}\frac{d}{dt}(\theta_{CR} - \theta_{L22}) + C_{CR}\frac{d}{dt}(\theta_{CR} - \theta_{ROT}) + G_{h1-CR}(\theta_{CR} - \theta_{h1}) + G_{h2-CR}(\theta_{CR} - \theta_{h2}) + G_{h3-CR}(\theta_{CR} - \theta_{h3}) + G_{L11-CR}(\theta_{CR} - \theta_{L11}) + G_{L12-CR}(\theta_{CR} - \theta_{L12}) + G_{L13-CR}(\theta_{CR} - \theta_{L13}) + G_{L21-CR}(\theta_{CR} - \theta_{L21}) + G_{L22-CR}(\theta_{CR} - \theta_{L22}) + G_{L23-CR}(\theta_{CR} - \theta_{L23}) + G_{CT-CR}(\theta_{CR} - \theta_{CT}) + G_{CB-CR}(\theta_{CR} - \theta_{CB}) + G_{CR-CL}(\theta_{CR} - \theta_{CL}) + G_{CR-TOT}(\theta_{CR} - \theta_{TOT}) + G_{CR-BOT}(\theta_{CR} - \theta_{BOT}) + G_{CR-ROT}(\theta_{CR} - \theta_{ROT}) + G_{CR-LOT}(\theta_{CR} - \theta_{LOT}) + G_{CR-CaseT}(\theta_{CR} - \theta_{CaseT}) + G_{CR-CaseB}(\theta_{CR} - \theta_{CaseB}) + G_{CR-CaseR}(\theta_{CR} - \theta_{CaseR}) + G_{CR-CaseL}(\theta_{CR} - \theta_{CaseL}) \quad \text{(B.23)}$$

$$\dot{Q}_{CL} = C_{h2}\frac{d}{dt}(\theta_{CL} - \theta_{h2}) + C_{CL}\frac{d}{dt}(\theta_{CL} - \theta_{LOT}) + G_{h1-CL}(\theta_{CL} - \theta_{h1}) + G_{h2-CL}(\theta_{CL} - \theta_{h2}) + G_{h3-CL}(\theta_{CL} - \theta_{h3}) + G_{L11-CL}(\theta_{CL} - \theta_{L11}) + G_{L12-CL}(\theta_{CL} - \theta_{L12}) + G_{L13-CL}(\theta_{CL} - \theta_{L13}) + G_{L21-CL}(\theta_{CL} - \theta_{L21}) + G_{L22-CL}(\theta_{CL} - \theta_{L22}) + G_{L23-CL}(\theta_{CL} - \theta_{L23}) + G_{CT-CL}(\theta_{CL} - \theta_{CT}) + G_{CB-CL}(\theta_{CL} - \theta_{CB}) + G_{CR-CL}(\theta_{CL} - \theta_{CR}) + G_{CL-TOT}(\theta_{CL} - \theta_{TOT}) + G_{CL-BOT}(\theta_{CL} - \theta_{BOT}) + G_{CL-ROT}(\theta_{CL} - \theta_{ROT}) + G_{CL-LOT}(\theta_{CL} - \theta_{LOT}) + G_{CL-CaseT}(\theta_{CL} - \theta_{CaseT}) + G_{CL-CaseB}(\theta_{CL} - \theta_{CaseB}) + G_{CL-CaseR}(\theta_{CL} - \theta_{CaseR}) + G_{CL-CaseL}(\theta_{CL} - \theta_{CaseL}) \quad \text{(B.24)}$$

$$0.0 = C_{CT}\frac{d}{dt}(\theta_{TOT} - \theta_{CT}) + C_{TOT}\frac{d}{dt}(\theta_{TOT} - \theta_{CaseT}) + G_{h1-TOT}(\theta_{TOT} - \theta_{h1}) + G_{h2-TOT}(\theta_{TOT} - \theta_{h2}) + G_{h3-TOT}(\theta_{TOT} - \theta_{h3}) + G_{L11-TOT}(\theta_{TOT} - \theta_{L11}) + G_{L12-TOT}(\theta_{TOT} - \theta_{L12}) + G_{L13-TOT}(\theta_{TOT} - \theta_{L13}) + G_{L21-TOT}(\theta_{TOT} - \theta_{L21}) + G_{L22-TOT}(\theta_{TOT} - \theta_{L22}) + G_{L23-TOT}(\theta_{TOT} - \theta_{L23}) + G_{CT-TOT}(\theta_{TOT} - \theta_{CT}) + G_{CB-TOT}(\theta_{TOT} - \theta_{CB}) + G_{CR-TOT}(\theta_{TOT} - \theta_{CR}) + G_{CL-TOT}(\theta_{TOT} - \theta_{CL}) + G_{TOT-BOT}(\theta_{TOT} - \theta_{BOT}) + G_{TOT-ROT}(\theta_{TOT} - \theta_{ROT}) + G_{TOT-LOT}(\theta_{TOT} - \theta_{LOT}) + G_{TOT-CaseT}(\theta_{TOT} - \theta_{CaseT}) + G_{TOT-CaseB}(\theta_{TOT} - \theta_{CaseB}) + G_{TOT-CaseR}(\theta_{TOT} - \theta_{CaseR}) + G_{TOT-CaseL}(\theta_{TOT} - \theta_{CaseL}) \quad \text{(B.25)}$$

$$
\begin{aligned}
0.0 = {} & C_{CB}\frac{d}{dt}(\theta_{BOT}-\theta_{CB}) + C_{BOT}\frac{d}{dt}(\theta_{BOT}-\theta_{CaseB}) \\
& + G_{h1-BOT}(\theta_{BOT}-\theta_{h1}) + G_{h2-BOT}(\theta_{BOT}-\theta_{h2}) \\
& + G_{h3-BOT}(\theta_{BOT}-\theta_{h3}) + G_{L11-BOT}(\theta_{BOT}-\theta_{L11}) \\
& + G_{L12-BOT}(\theta_{BOT}-\theta_{L12}) + G_{L13-BOT}(\theta_{BOT}-\theta_{L13}) \\
& + G_{L21-BOT}(\theta_{BOT}-\theta_{L21}) + G_{L22-BOT}(\theta_{BOT}-\theta_{L22}) \\
& + G_{L23-BOT}(\theta_{BOT}-\theta_{L23}) + G_{CT-BOT}(\theta_{BOT}-\theta_{CT}) \\
& + G_{CB-BOT}(\theta_{BOT}-\theta_{CB}) + G_{CR-BOT}(\theta_{BOT}-\theta_{CR}) \\
& + G_{CL-BOT}(\theta_{BOT}-\theta_{CL}) + G_{TOT-BOT}(\theta_{BOT}-\theta_{TOT}) \\
& + G_{BOT-ROT}(\theta_{BOT}-\theta_{ROT}) + G_{BOT-LOT}(\theta_{BOT}-\theta_{LOT}) \\
& + G_{BOT-CaseT}(\theta_{BOT}-\theta_{CaseT}) + G_{BOT-CaseB}(\theta_{BOT}-\theta_{CaseB}) \\
& + G_{BOT-CaseR}(\theta_{BOT}-\theta_{CaseR}) + G_{BOT-CaseL}(\theta_{BOT}-\theta_{CaseL})
\end{aligned}
\tag{B.26}
$$

$$
\begin{aligned}
0.0 = {} & C_{L21}\frac{d}{dt}(\theta_{ROT}-\theta_{CR}) + C_{ROT}\frac{d}{dt}(\theta_{ROT}-\theta_{CaseR}) \\
& + G_{h1-ROT}(\theta_{ROT}-\theta_{h1}) + G_{h2-ROT}(\theta_{ROT}-\theta_{h2}) \\
& + G_{h3-ROT}(\theta_{ROT}-\theta_{h3}) + G_{L11-ROT}(\theta_{ROT}-\theta_{L11}) \\
& + G_{L12-ROT}(\theta_{ROT}-\theta_{L12}) + G_{L13-ROT}(\theta_{ROT}-\theta_{L13}) \\
& + G_{L21-ROT}(\theta_{ROT}-\theta_{L21}) + G_{L22-ROT}(\theta_{ROT}-\theta_{L22}) \\
& + G_{L23-ROT}(\theta_{ROT}-\theta_{L23}) + G_{CT-ROT}(\theta_{ROT}-\theta_{CT}) \\
& + G_{CB-ROT}(\theta_{ROT}-\theta_{CB}) + G_{CR-ROT}(\theta_{ROT}-\theta_{CR}) \\
& + G_{CL-ROT}(\theta_{ROT}-\theta_{CL}) + G_{TOT-ROT}(\theta_{ROT}-\theta_{TOT}) \\
& + G_{BOT-ROT}(\theta_{ROT}-\theta_{BOT}) + G_{ROT-LOT}(\theta_{ROT}-\theta_{LOT}) \\
& + G_{ROT-CaseT}(\theta_{ROT}-\theta_{CaseT}) + G_{ROT-CaseB}(\theta_{ROT}-\theta_{CaseB}) \\
& + G_{ROT-CaseR}(\theta_{ROT}-\theta_{CaseR}) + G_{ROT-CaseL}(\theta_{ROT}-\theta_{CaseL})
\end{aligned}
\tag{B.27}
$$

$$
\begin{aligned}
0.0 = {} & C_{CL}\frac{d}{dt}(\theta_{LOT}-\theta_{CL}) + C_{LOT}\frac{d}{dt}(\theta_{LOT}-\theta_{CaseL}) + G_{h1-LOT}(\theta_{LOT}-\theta_{h1}) \\
& + G_{h2-LOT}(\theta_{LOT}-\theta_{h2}) + G_{h3-LOT}(\theta_{LOT}-\theta_{h3}) \\
& + G_{L11-LOT}(\theta_{LOT}-\theta_{L11}) + G_{L12-LOT}(\theta_{LOT}-\theta_{L12}) \\
& + G_{L13-LOT}(\theta_{LOT}-\theta_{L13}) + G_{L21-LOT}(\theta_{LOT}-\theta_{L21}) \\
& + G_{L22-LOT}(\theta_{LOT}-\theta_{L22}) + G_{L23-LOT}(\theta_{LOT}-\theta_{L23}) \\
& + G_{CT-LOT}(\theta_{LOT}-\theta_{CT}) + G_{CB-LOT}(\theta_{LOT}-\theta_{CB}) \\
& + G_{CR-LOT}(\theta_{LOT}-\theta_{CR}) + G_{CL-LOT}(\theta_{LOT}-\theta_{CL}) \\
& + G_{TOT-LOT}(\theta_{LOT}-\theta_{TOT}) + G_{BOT-LOT}(\theta_{LOT}-\theta_{BOT}) \\
& + G_{ROT-LOT}(\theta_{LOT}-\theta_{ROT}) + G_{LOT-CaseT}(\theta_{LOT}-\theta_{CaseT}) \\
& + G_{LOT-CaseB}(\theta_{LOT}-\theta_{CaseB}) + G_{LOT-CaseR}(\theta_{LOT}-\theta_{CaseR}) \\
& + G_{LOT-CaseL}(\theta_{LOT}-\theta_{CaseL})
\end{aligned}
\tag{B.28}
$$

Equations (B.1)-(B.28) cast into a compact matrix form as follows:

$$
\begin{bmatrix} I \\ 0 \end{bmatrix} = Y_{eq}\begin{bmatrix} V \\ Y \end{bmatrix} + K_{eq} \tag{B.29}
$$

, where

$I = [\tilde{I}_1 \quad \tilde{I}_2 \quad \tilde{I}_{L1} \quad \tilde{I}_{NN} \quad \tilde{I}_{L2} \quad \dot{q}_{caseT} \quad \dot{q}_{caseB} \quad \dot{q}_{caseR} \quad \dot{q}_{caseL} \quad \dot{q}_{amb}]^T$,

$V = [\tilde{V}_1 \quad \tilde{V}_2 \quad \tilde{V}_{L1} \quad \tilde{V}_{NN} \quad \tilde{V}_{L2} \quad \theta_{caseT} \quad \theta_{caseB} \quad \theta_{caseR} \quad \theta_{caseL} \quad \theta_{amb}]^T$

$Y = [\tilde{E} \quad \theta_{h1} \quad \theta_{h2} \quad \theta_{h3} \quad \theta_{L11} \quad \theta_{L12} \quad \theta_{L13} \quad \theta_{L21} \quad \theta_{L22} \quad \theta_{L23} \quad \theta_{CT} \quad \theta_{CB} \quad \theta_{CR}$

$\theta_{CL} \quad \theta_{TOT} \quad \theta_{BOT} \quad \theta_{ROT} \quad \theta_{LOT}]^T$

Y_{eq}: Matrix defining the linear part of the model.
K_{eq}: Vector containing the constant part of the model.
Note that there 28 states with 28 equations are identified.

B.2 Single Phase Center-Tap Thermal Conductance

To compute the thermal conductance, a percentage of each one is assumed based on the below tables table B-1-table B-21.

Table B-1 Transformer T_{h1} Conductances

T_{h1} Conductances	(%) of G_{h1}
$G_{\_h1\_h2}$	20
$G_{\_h1\_h3}$	9
$G_{\_h1\_L11}$	6
$G_{\_h1\_L12}$	5
$G_{\_h1\_L13}$	4
$G_{\_h1\_L21}$	3
$G_{\_h1\_L22}$	2
$G_{\_h1\_L23}$	1
$G_{\_h1\_CT}$	7
$G_{\_h1\_CB}$	5
$G_{\_h1\_CR}$	3
$G_{\_h1\_CL}$	10
$G_{\_h1\_TOT}$	3.5
$G_{\_h1\_BOT}$	2.5
$G_{\_h1\_ROT}$	1
$G_{\_h1\_LOT}$	8
$G_{\_h1\_CaseT}$	2.5
$G_{\_h1\_CaseB}$	1.5
$G_{\_h1\_CaseR}$	1
$G_{\_h1\_CaseL}$	5

Table B-2 Transformer T_{h2} Conductances

T_{h2} Conductances	(%) of G_{h2}
$G_{\_h2\_h3}$	20
$G_{\_h2\_L11}$	3
$G_{\_h2\_L12}$	3.5
$G_{\_h2\_L13}$	3.5
$G_{\_h2\_L21}$	3
$G_{\_h2\_L22}$	3.5
$G_{\_h2\_L23}$	3.5
$G_{\_h2\_CT}$	5.5
$G_{\_h2\_CB}$	5.5
$G_{\_h2\_CR}$	2
$G_{\_h2\_CL}$	10
$G_{\_h2\_TOT}$	1
$G_{\_h2\_BOT}$	1
$G_{\_h2\_ROT}$	0.8
$G_{\_h2\_LOT}$	8
$G_{\_h2\_CaseT}$	0.5
$G_{\_h2\_CaseB}$	0.5
$G_{\_h2\_CaseR}$	0.2
$G_{\_h2\_CaseL}$	5

Table B-3 Transformer T_{h3} Conductances

T_{h3} Conductances	(%) of G_{h3}
$G_{\_h3\_L11}$	*1*
$G_{\_h3\_L12}$	*2*
$G_{\_h3\_L13}$	*3*
$G_{\_h3\_L21}$	*4*
$G_{\_h3\_L22}$	*5*
$G_{\_h3\_L23}$	*6*
$G_{\_h3\_CT}$	*5*
$G_{\_h3\_CB}$	*7*
$G_{\_h3\_CR}$	*3*
$G_{\_h3\_CL}$	*10*
$G_{\_h3\_TOT}$	*2.5*
$G_{\_h3\_BOT}$	*3.5*
$G_{\_h3\_ROT}$	*1*
$G_{\_h3\_LOT}$	*8*
$G_{\_h3\_CaseT}$	*1.5*
$G_{\_h3\_CaseB}$	*2.5*
$G_{\_h3\_CaseR}$	*1*
$G_{\_h3\_CaseL}$	*5*

Table B-4 Transformer T_{L11} Conductances

T_{L11} Conductances	(%) of G_{L11}
$G_{\_L11\_L12}$	15
$G_{\_L11\_L13}$	12
$G_{\_L11\_L21}$	9
$G_{\_L11\_L22}$	6
$G_{\_L11\_L23}$	3
$G_{\_L11\_CT}$	6
$G_{\_L11\_CB}$	4
$G_{\_L11\_CR}$	7
$G_{\_L11\_CL}$	3
$G_{\_L11\_TOT}$	5
$G_{\_L11\_BOT}$	3
$G_{\_L11\_ROT}$	5.5
$G_{\_L11\_LOT}$	1
$G_{\_L11\_CaseT}$	3
$G_{\_L11\_CaseB}$	2
$G_{\_L11\_CaseR}$	5
$G_{\_L11\_CaseL}$	0.5

Table B-5 Transformer T_{L12} Conductances

T_{L12} Conductances	(%) of G_{L12}
$G_{\_L12\_L13}$	15
$G_{\_L12\_L21}$	12
$G_{\_L12\_L22}$	9
$G_{\_L12\_L23}$	6
$G_{\_L12\_CT}$	4.5
$G_{\_L12\_CB}$	3.5
$G_{\_L12\_CR}$	6
$G_{\_L12\_CL}$	2.5
$G_{\_L12\_TOT}$	3
$G_{\_L12\_BOT}$	2
$G_{\_L12\_ROT}$	3.5
$G_{\_L12\_LOT}$	1
$G_{\_L12\_CaseT}$	2
$G_{\_L12\_CaseB}$	1
$G_{\_L12\_CaseR}$	3
$G_{\_L12\_CaseL}$	0.5

Table B-6 Transformer T_{L13} Conductances

T_{L13} Conductances	(%) of G_{L13}
$G_{\_L13\_L21}$	15
$G_{\_L13\_L22}$	12
$G_{\_L13\_L23}$	9
$G_{\_L13\_CT}$	3.5
$G_{\_L13\_CB}$	3
$G_{\_L13\_CR}$	4
$G_{\_L13\_CL}$	1
$G_{\_L13\_TOT}$	3
$G_{\_L13\_BOT}$	2.5
$G_{\_L13\_ROT}$	3.5
$G_{\_L13\_LOT}$	0.8
$G_{\_L13\_CaseT}$	2
$G_{\_L13\_CaseB}$	1
$G_{\_L13\_CaseR}$	2
$G_{\_L13\_CaseL}$	0.2

Table B-7 Transformer T_{L21} Conductances

T_{L21} Conductances	(%) of G_{L21}
$G_{\_L21\_L22}$	15
$G_{\_L21\_L23}$	12
$G_{\_L21\_CT}$	3
$G_{\_L21\_CB}$	3.5
$G_{\_L21\_CR}$	4
$G_{\_L21\_CL}$	1
$G_{\_L21\_TOT}$	2.5
$G_{\_L21\_BOT}$	3
$G_{\_L21\_ROT}$	3.5
$G_{\_L21\_LOT}$	0.8
$G_{\_L21\_CaseT}$	1
$G_{\_L21\_CaseB}$	2
$G_{\_L21\_CaseR}$	2.5
$G_{\_L21\_CaseL}$	0.2

Table B-8 Transformer T_{L22} Conductances

T_{L22} Conductances	(%) of G_{L22}
$G_{\_L22\_L23}$	15
$G_{\_L22\_CT}$	3.5
$G_{\_L22\_CB}$	4.5
$G_{\_L22\_CR}$	6
$G_{\_L22\_CL}$	2.5
$G_{\_L22\_TOT}$	2
$G_{\_L22\_BOT}$	3
$G_{\_L22\_ROT}$	3.5
$G_{\_L22\_LOT}$	1
$G_{\_L22\_CaseT}$	1
$G_{\_L22\_CaseB}$	2
$G_{\_L22\_CaseR}$	3
$G_{\_L22\_CaseL}$	0.5

Table B-9 Transformer T_{L23} Conductances

T_{L23} Conductances	(%) of G_{L23}
$G_{\_L23\_CT}$	4
$G_{\_L23\_CB}$	6
$G_{\_L23\_CR}$	7
$G_{\_L23\_CL}$	3
$G_{\_L23\_TOT}$	3
$G_{\_L23\_BOT}$	5
$G_{\_L23\_ROT}$	5.5
$G_{\_L23\_LOT}$	1
$G_{\_L23\_CaseT}$	2
$G_{\_L23\_CaseB}$	3
$G_{\_L23\_CaseR}$	4.8
$G_{\_L23\_CaseL}$	0.2

Table B-10 Transformer T_{CT} Conductances

T_{CT} Conductances	(%) of G_{CT}
$G_{\_CT\_CB}$	7
$G_{\_CT\_CR}$	10
$G_{\_CT\_CL}$	10
$G_{\_CT\_TOT}$	8
$G_{\_CT\_BOT}$	2
$G_{\_CT\_ROT}$	5
$G_{\_CT\_LOT}$	5
$G_{\_CT\_CaseT}$	5
$G_{\_CT\_CaseB}$	1
$G_{\_CT\_CaseR}$	2.5
$G_{\_CT\_CaseL}$	2.5

Table B-11 Transformer T_{CB} Conductances

T_{CB} Conductances	(%) of G_{CB}
$G_{\_CB\_CR}$	10
$G_{\_CB\_CL}$	10
$G_{\_CB\_TOT}$	2
$G_{\_CB\_BOT}$	8
$G_{\_CB\_ROT}$	5
$G_{\_CB\_LOT}$	5
$G_{\_CB\_CaseT}$	1
$G_{\_CB\_CaseB}$	5
$G_{\_CB\_CaseR}$	2.5
$G_{\_CB\_CaseL}$	2.5

Table B-12 Transformer T_{CR} Conductances

T_{CR} Conductances	(%) of G_{CR}
$G_{\_CR\_CL}$	7
$G_{\_CR\_TOT}$	4
$G_{\_CR\_BOT}$	4
$G_{\_CR\_ROT}$	12.9
$G_{\_CR\_LOT}$	1
$G_{\_CR\_CaseT}$	2
$G_{\_CR\_CaseB}$	2
$G_{\_CR\_CaseR}$	5
$G_{\_CR\_CaseL}$	0.1

Table B-13 Transformer T_{CL} Conductances

T_{CL} Conductances	(%) of G_{CL}
$G_{\_CL\_TOT}$	4
$G_{\_CL\_BOT}$	4
$G_{\_CL\_ROT}$	2
$G_{\_CL\_LOT}$	12.9
$G_{\_CL\_CaseT}$	1.25
$G_{\_CL\_CaseB}$	1.25
$G_{\_CL\_CaseR}$	0.1
$G_{\_CL\_CaseL}$	4.5

Table B-14 Transformer T_{TOT} Conductances

T_{TOT} Conductances	(%) of G_{TOT}
$G_{\_TOT\_BOT}$	5
$G_{\_TOT\_ROT}$	10
$G_{\_TOT\_LOT}$	10
$G_{\_TOT\_CaseT}$	15
$G_{\_TOT\_CaseB}$	2
$G_{\_TOT\_CaseR}$	7.25
$G_{\_TOT\_CaseL}$	7.25

Table B-15 Transformer T_{BOT} Conductances

T_{BOT} Conductances	(%) of G_{BOT}
$G_{\_BOT\_ROT}$	10
$G_{\_BOT\_LOT}$	10
$G_{\_BOT\_CaseT}$	2
$G_{\_BOT\_CaseB}$	15
$G_{\_BOT\_CaseR}$	7.25
$G_{\_BOT\_CaseL}$	7.25

Table B-16 Transformer T_{ROT} Conductances

T_{ROT} Conductances	(%) of G_{ROT}
$G_{\_ROT\_LOT}$	4
$G_{\_ROT\_CaseT}$	6
$G_{\_ROT\_CaseB}$	6
$G_{\_ROT\_CaseR}$	10
$G_{\_ROT\_CaseL}$	1.3

Table B-17 Transformer T_{LOT} Conductances

T_{LOT} Conductances	(%) of G_{LOT}
$G_{\_LOT\_CaseT}$	5.75
$G_{\_LOT\_CaseB}$	5.75
$G_{\_LOT\_CaseR}$	1
$G_{\_LOT\_CaseL}$	10

Table B-18 Transformer T_{CaseT} Conductances

T_{CaseT} Conductances	(%) of G_{CaseT}
$G_{\_CaseT\_CaseB}$	3
$G_{\_CaseT\_CaseR}$	8
$G_{\_CaseT\_CaseL}$	8
$G_{\_CaseT\_amb}$	27.5

Table B-19 Transformer T_{CaseB} Conductances

T_{CaseB} Conductances	(%) of G_{CaseB}
$G_{\_CaseB\_CaseR}$	8
$G_{\_CaseB\_CaseL}$	8
$G_{\_CaseB\_amb}$	27.5

Table B-20 Transformer T_{CaseR} Conductances

T_{CaseR} Conductances	(%) of G_{CaseR}
$G_{\_CaseR\_CaseL}$	4
$G_{\_CaseR\_amb}$	21.9

Table B-21 Transformer T_{CaseL} Conductances

T_{CaseL} Conductances	(%) of G_{CaseL}
$G_{\_CaseL\_amb}$	27.5

Appendix C. Smart Dishwasher Mathematical Model

The mathematical model of the dishwasher is given by the following equations,

$$\tilde{I}_1 = \left(\frac{P_{dw} + jQ_{dw}}{\tilde{V}_1 - \tilde{V}_2}\right)^* (1 - u_1)u_2u_3z_t \quad \text{(C.1)}$$

$$\tilde{I}_2 = -\left(\frac{P_{dw} + jQ_{dw}}{\tilde{V}_1 - \tilde{V}_2}\right)^* (1 - u_1)u_2u_3z_t \quad \text{(C.2)}$$

, where:
P_{dw}: Maximum active power consumption of the dishwasher in [W] computed as the following,

$$P_{dw} = P_{rated}Eff$$

Q_{dw}: Maximum reactive power consumption of the dishwasher [VAr] computed as the following,

$$Q_{dw} = P_{dw}\tan(\cos^{-1}(pf))$$

u_1: Dishwasher On/Off status (main service of operation),

$$u_1 = \begin{cases} 0 & , Dishwasher\ Power\ On \\ 1 & , Dishwasher\ Power\ Off \end{cases}$$

u_2: Dishwasher load level variable. It is specified according to the chosen input load level as given in Table 8.14.

u_3: Power consumption at each stage of the cycle. During every cycle, u_3 will change according to the stage. Every stage of the simulation is determined based on the progress of the simulation time inside the cycle. So, u_3 can be evaluated as the following,

$$\begin{aligned} u_3 = {} & 0.25\left[U\left(t - t_{0_i}\right) - U\left(t - t_{0_i} - 0.1t_c\right)\right] \\ & + \left[U\left(t - t_{0_i} - 0.1t_c\right) - U\left(t - t_{0_i} - 0.35t_c\right)\right] \\ & + 0.25\left[U\left(t - t_{0_i} - 0.35t_c\right) - U\left(t - t_{0_i} - 0.65t_c\right)\right] \\ & + \left[U\left(t - t_{0_i} - 0.65t_c\right) - U\left(t - t_{0_i} - 0.9t_c\right)\right] \\ & + 0.25\left[U\left(t - t_{0_i} - 0.9t_c\right) - U\left(t - t_{0_i} - t_c\right)\right] \end{aligned}$$

z_t: a unit step function defined by

$$z_t = U\left(t - t_{0_i}\right) - U\left(t - t_{0_i} - t_c\right)$$

P_{rated}: Rated power of the dishwasher in [W].

V_{rated}: Rated voltage in root mean square value of the dishwasher in [V].
Eff: The dishwasher efficiency. A value of 0.8 is typical for a dishwasher.
pf: Power factor of the device. A value of 0.9 is typical for a dishwasher.
t_c: Duration time for one full cycle of the dishwasher in [min].
t_{0i}: The time at *i* when the dishwasher is turned on in this form [hh:mm:ss]. For multiple operations, the duration time of full cycle should be taken into account.

The model then is cast into a compact matrix form as follows:

$$\begin{bmatrix} I \\ 0 \end{bmatrix} = Y_{eq} V + K_{eq} \tag{C.3}$$

, where
$I = [\tilde{I}_1 \quad \tilde{I}_2]^T$,
$V = [\tilde{V}_1 \quad \tilde{V}_2]^T$
I: Through variables of the model.
V: Across external states variables of the model.
Y_{eq}: Matrix defining the linear part of the model.
K_{eq}: Vector containing the constant part of the model.

Appendix D. Electro-Thermal Model of Refrigerator

The mathematical model of the electro-thermal refrigerator with six temperature spots is given by the following equations:

$$\tilde{I}_1 = \left(\frac{P_f + jQ_f}{\tilde{V}_1 - \tilde{V}_2}\right)^* (1-u_1)u_2 \tag{D.1}$$

$$\tilde{I}_2 = -\left(\frac{P_f + jQ_f}{\tilde{V}_1 - \tilde{V}_2}\right)^* (1-u_1)u_2 \tag{D.2}$$

$$\begin{aligned}\dot{q}_1 = {} & C_{frew}\frac{d}{dt}\left(T_{K1}(t) - T_{frew}(t)\right) + C_{fzew}\frac{d}{dt}\left(T_{K1}(t) - T_{fzew}(t)\right) \\ & + G_{frew-k}\left(T_{K1}(t) - T_{frew}(t)\right) + G_{fzew-k}\left(T_{K1}(t) - T_{fzew}(t)\right)\end{aligned} \tag{D.3}$$

$$\dot{q}_2 = G_s\left(T_{K2}(t) - T_{fr}(t)\right) + G_s\left(T_{K2}(t) - T_{fz}(t)\right) + k_1\dot{Q}_r + k_2\dot{Q}_r \tag{D.4}$$

$$P_f\,(1-u_1)u_2 = k_{factor}\frac{-\dot{Q}_r}{COP} \tag{D.5}$$

$$\begin{aligned}0.0 = {} & C_{fr}\frac{d}{dt}\left(T_{fr}(t) - T_{friw}(t)\right) + G_{fr}\left(T_{fr}(t) - T_{friw}(t)\right) \\ & + G_s\left(T_{fr}(t) - T_{K2}(t)\right) - k_1\,\dot{Q}_r\end{aligned} \tag{D.6}$$

$$\begin{aligned}0.0 = {} & C_{fr}\frac{d}{dt}\left(T_{friw}(t) - T_{fr}(t)\right) + C_{friw}\frac{d}{dt}\left(T_{friw}(t) - T_{frew}(t)\right) \\ & + G_{fr}\left(T_{friw}(t) - T_{fr}(t)\right) + G_{friw-fziw}\left(T_{friw}(t) - T_{fziw}(t)\right) \\ & + G_{friw-frew}\left(T_{friw}(t) - T_{frew}(t)\right)\end{aligned} \tag{D.7}$$

$$\begin{aligned}0.0 = {} & C_{friw}\frac{d}{dt}\left(T_{frew}(t) - T_{friw}(t)\right) + C_{frew}\frac{d}{dt}\left(T_{frew}(t) - T_{K1}(t)\right) \\ & + G_{friw-frew}\left(T_{frew}(t) - T_{friw}(t)\right) \\ & + G_{frew-fzew}\left(T_{frew}(t) - T_{fzew}(t)\right) \\ & + G_{frew-K}\left(T_{frew}(t) - T_{K1}(t)\right)\end{aligned} \tag{D.8}$$

$$\begin{aligned}0.0 = {} & C_{fz}\frac{d}{dt}\left(T_{fz}(t) - T_{fziw}(t)\right) + G_{fz}\left(T_{fz}(t) - T_{fziw}(t)\right) \\ & + G_s\left(T_{fz}(t) - T_{K2}(t)\right) - k_2\,\dot{Q}_r\end{aligned} \tag{D.9}$$

$$\begin{aligned}0.0 = {} & C_{fz}\frac{d}{dt}\left(T_{fziw}(t) - T_{fz}(t)\right) + C_{fziw}\frac{d}{dt}\left(T_{fziw}(t) - T_{fzew}(t)\right) \\ & + G_{fz}\left(T_{fziw}(t) - T_{fz}(t)\right) + G_{friw-fziw}\left(T_{fziw}(t) - T_{friw}(t)\right) \\ & + G_{fziw-fzew}\left(T_{fziw}(t) - T_{fzew}(t)\right)\end{aligned} \tag{D.10}$$

$$
\begin{aligned}
0.0 = C_{fziw}\frac{d}{dt}\left(T_{fzew}(t) - T_{fziw}(t)\right) + C_{fzew}\frac{d}{dt}\left(T_{fzew}(t) - T_{K1}(t)\right) \\
+ G_{fziw-fzew}\left(T_{fzew}(t) - T_{fziw}(t)\right) \\
+ G_{frew-fzew}\left(T_{fzew}(t) - T_{frew}(t)\right) \\
+ G_{fzew-K}\left(T_{frew}(t) - T_{K1}(t)\right)
\end{aligned}
\tag{D.11}
$$

Equations (D.1)-(D.11) are cast into a compact matrix form as follows:

$$
\begin{bmatrix} I \\ 0 \end{bmatrix} = Y_{eq}\begin{bmatrix} V \\ Y \end{bmatrix} + \begin{bmatrix} V & Y \end{bmatrix} F_{eq}\begin{bmatrix} V \\ Y \end{bmatrix} + K_{eq} \tag{D.12}
$$

, where

$I = [\tilde{I}_1 \quad \tilde{I}_2 \quad \dot{q}_1 \quad \dot{q}_2]^T$,

$V = [\tilde{V}_1 \quad \tilde{V}_2 \quad T_{K1}(t) \quad T_{K2}(t)]^T$

$Y = \left[T_{fr}(t) \quad T_{friw}(t) \quad T_{frew}(t) \quad T_{fz}(t) \quad T_{fziw}(t) \quad T_{fzew}(t) \quad \dot{Q}_r\right]^T$

I: Through variables of the model.
V: Across external states variables of the model.
Y: Internal states variables of the model.
Y_{eq}: Matrix defining the linear part of the model.
F_{eq}: Nonlinear and differential parts of the model.
K_{eq}: Vector containing the constant part of the model.
P_f: Maximum active power consumption of the refrigerator in [MW] computed as the following,

$$P_f = P_{rated}Eff$$

Q_f: Maximum reactive power consumption of the refrigerator [MVAr] computed as the following,

$$Q_f = P_f \tan(\cos^{-1}(pf))$$

u_1: Refrigerator On/Off status (main service of operation).

$$u_1 = \begin{cases} 0, & Power\ ON \\ 1, & Power\ OFF \end{cases}$$

u_2: Refrigerator temperature control.

$$u_2 = \begin{cases} 0, & Refrigerator\ OFF \\ 1, & Refrigerator\ ON \end{cases}$$

k_{factor}: A conversion factor (1 MW ~ 3.414 MBtu/h)
P_{rated}: Rated power of the refrigerator in [W].
V_{rated}: Rated voltage rms of the refrigerator in [V].

Eff: The refrigerator electrical efficiency. A value of 0.8 is typical for a refrigerator.
pf: Power factor of the device. A value of 0.9 is typical for a refrigerator.
COP: Coefficient of performance. A value of 3.5 is typical for a refrigerator.
k_1 and k_2: Constant depends on the refrigerator manufacture design. Typical values are 0.6 and 0.4 respectively.
$\dot{Q}_r$: Heat flow rate of the refrigerator [MBtu/h].
$\dot{q}_1$: Heat flow through variable 1 [MBtu/h].
$\dot{q}_2$: Heat flow through variable 2 [MBtu/h].
T_{fr}: Fresh food compartment temperature spot in [^oC].
T_{fz}: Freezer compartment temperature spot in [^oC].
T_{friw}: Internal wall of the fresh food compartment temperature spot in [^oC].
T_{frew}: External wall of the fresh food compartment temperature spot in [^oC].
T_{fziw}: Internal wall of the freezer compartment temperature spot in [^oC].
T_{fzew}: External wall of the freezer compartment temperature spot in [^oC].
T_{k1}: Across external state variable kitchen terminal 1 temperature spot in [^oC].
T_{k2}: Across external state variable kitchen terminal 2 temperature spot in [^oC].
G_{fr}: Thermal conductance between the fresh food compartment mass and the fresh food compartment internal wall in [MBtu/^oC h].
G_{fz}: Thermal conductance between the freezer compartment mass and the freezer compartment internal wall in [MBtu/^oC h].
$G_{friw\text{-}fziw}$: Thermal conductance between the fresh food compartment internal wall and the freezer compartment internal wall mass in [MBtu/^oC h].
$G_{friw\text{-}frew}$: Thermal conductance of the fresh food compartment wall in [MBtu/^oC h].
$G_{fziw\text{-}fzew}$: Thermal conductance of the freezer compartment wall in [MBtu/^oC h].
$G_{frew\text{-}fzew}$: Thermal conductance of the fresh food and freezer compartments external walls in [MBtu/^oC h].
$G_{frew\text{-}K}$: Thermal conductance between the fresh food compartment external wall and the Kitchen air mass in [MBtu/^oC h].
$G_{fzew\text{-}K}$: Thermal conductance between the freezer compartment external wall and the Kitchen air mass in [MBtu/^oC h].
G_s: Thermal conductance of the heat source in [MBtu/^oC h].
C_{fr}: The sum of the heat capacity of every element inside the fresh food compartment in [MBtu/^oC].
C_{friw}: Heat capacity of internal door mass in the fresh food compartment in [MBtu/^oC].
C_{frew}: Heat capacity of external door mass in the fresh food compartment in [MBtu/^oC].
C_{fz}: The sum of the heat capacity of every element inside the freezer compartment in [MBtu/^oC].
C_{fziw}: Heat capacity of internal door mass in the freezer compartment in [MBtu/^oC].
C_{fzew}: Heat capacity of external door mass in the freezer compartment in [MBtu/^oC].
Vol_{fr}: Fresh Food Compartment Capacity in [ft^3].
Vol_{fz}: Freezer Compartment Capacity in [ft^3].
θ_{set}: Refrigerator desired internal temperature in [^oC]. Typical value is 1-5 ^{o}C.
$\theta_{dead\text{-}band}$: Temperature control dead-band in [^oC]. Typically, it is 1-2 ^{o}C.

It should be noted that $C_{fr}(t)$ is the sum of each element heat capacity, including cool air, inside the fresh food compartment at every time *t*. It is mathematically expressed as the following:

$$C_{fr}(t) = \Delta C_{fr0}(t) + \Delta C_{fr1}(t) + \Delta C_{fr2}(t) + \cdots + \Delta C_{fri}(t)$$

, where
$\Delta C_{fr0}(t)$: Thermal capacitance of element 0 in the fresh food compartment at time *t* [MBtu/k^{o}C].
$\Delta C_{fr1}(t)$: Thermal capacitance of element 1 in the fresh food compartment at time *t* [MBtu/k^{o}C].
$\Delta C_{fr2}(t)$: Thermal capacitance of element 2 in the fresh food compartment at time *t* [MBtu/k^{o}C].
$\Delta C_{fri}(t)$: Thermal capacitance of element *i* in the fresh food compartment at time *t* [MBtu/k^{o}C].
i: The total number of elements inside the fresh food compartment.

Also, $C_{fz}(t)$ is the sum of each element heat capacity, including cold air, inside the freezer compartment at every time *t*. It is mathematically expressed as the following:

$$C_{fz}(t) = \Delta C_{fz0}(t) + \Delta C_{fz1}(t) + \Delta C_{fz2}(t) + \cdots + \Delta C_{fzj}(t)$$

, where
$\Delta C_{fz0}(t)$: Thermal capacitance of element 0 in the freezer compartment at time *t* [MBtu/k^{o}C].
$\Delta C_{fz1}(t)$: Thermal capacitance of element 1 in the freezer compartment at time *t* [MBtu/k^{o}C].
$\Delta C_{fz2}(t)$: Thermal capacitance of element 2 in the freezer compartment at time *t* [MBtu/k^{o}C].
$\Delta C_{fzj}(t)$: Thermal capacitance of element *j* in the freezer compartment at time *t* [MBtu/k^{o}C].
j: The total number of elements inside the fresh food compartment.

Note that data regarding both refrigerator and freezer elements are specified in the csv file found in the device folder. This file contains the following information,

- Time when the event takes place enter the form (hh:mm:ss)
- Door openings for both fresh food and freezer compartments.
- Mass in (*kg*) for every element inside both the fresh food and freezer compartments.

Appendix E. Electro-Thermal Model of Air Conditioner

The mathematical model of the electro-thermal air conditioner is given by the following equations:

$$\tilde{I}_1 = \left(\frac{P_{HVAC} + jQ_{HVAC}}{\tilde{V}_1 - \tilde{V}_2}\right)^* (1 - u_1)u_2 \tag{E.1}$$

$$\tilde{I}_2 = -\left(\frac{P_{HVAC} + jQ_{HVAC}}{\tilde{V}_1 - \tilde{V}_2}\right)^* (1 - u_1)u_2 \tag{E.2}$$

$$0.0 = 0.0\, u_2 \tag{E.3}$$

$$\dot{q}_{Bed1} = G_S\left(\tilde{T}_{Bed1} - \tilde{T}_{Amb}\right) - K_1\dot{Q}_{hvac} \tag{E.4}$$

$$\dot{q}_{Bed2} = G_S\left(\tilde{T}_{Bed2} - \tilde{T}_{Amb}\right) - K_2\dot{Q}_{hvac} \tag{E.5}$$

$$\dot{q}_{Bath1} = G_S\left(\tilde{T}_{Bath1} - \tilde{T}_{Amb}\right) - K_3\dot{Q}_{hvac} \tag{E.6}$$

$$\dot{q}_{Bath2} = G_S\left(\tilde{T}_{Bath2} - \tilde{T}_{Amb}\right) - K_4\dot{Q}_{hvac} \tag{E.7}$$

$$\dot{q}_K = G_S\left(\tilde{T}_K - \tilde{T}_{Amb}\right) - K_5\dot{Q}_{hvac} \tag{E.8}$$

$$\dot{q}_L = G_S\left(\tilde{T}_L - \tilde{T}_{Amb}\right) - K_6\dot{Q}_{hvac} \tag{E.9}$$

$$\dot{q}_{Amb} = -G_S\left(\tilde{T}_{Bed1} + \tilde{T}_{Bed2} + \tilde{T}_{Bath1} + \tilde{T}_{Bath2} + \tilde{T}_K + \tilde{T}_L - 6\,\tilde{T}_{Amb}\right) + (K_1 + K_2 + K_3 + K_4 + K_5 + K_6)\dot{Q}_{hvac} \tag{E.10}$$

$$P_{HVAC} = \frac{k_{factor}\ \dot{Q}_{hvac}\, m}{COP}(1 - u_1)u_2 \tag{E.11}$$

$$Q_{HVAC} = \tan(\cos^{-1}(pf))\, P_{HVAC} \tag{E.12}$$

$$\dot{Q}_{hvac} = \frac{BR}{m}(1 - u_1)\, u_2 \tag{E.13}$$

$$BR = BR_0\left(1.4892 - 0.0052\left(\left(\frac{9}{5}a\tilde{T}_{Amb}\right) + 32\right)\right) \tag{E.14}$$

$$m = 1.1 + \frac{m_l}{1 + \exp(4 - 0.1\rho)} \tag{E.15}$$

$$COP = \frac{COP_{nom}}{-0.01364 + 0.01067\left(\left(\left(\frac{9}{5}a\tilde{T}_{Amb}\right) + 32\right)\right)} \tag{E.16}$$

Equations (E.1)-(E.16) cast into a compact matrix form as follows:

$$\begin{bmatrix} I \\ 0 \end{bmatrix} = Y_{eq}\begin{bmatrix} V \\ Y \end{bmatrix} + [V \quad Y]F_{eq}\begin{bmatrix} V \\ Y \end{bmatrix} + K_{eq} \tag{E.17}$$

, where
$I = [\tilde{I}_1 \quad \tilde{I}_2 \quad 0.0 \quad \dot{q}_{Bed1} \quad \dot{q}_{Bed2} \quad \dot{q}_{Bath1} \quad \dot{q}_{Bath2} \quad \dot{q}_K \quad \dot{q}_L \quad \dot{q}_{Amb}]^T$,

$V = [\tilde{V}_1 \quad \tilde{V}_2 \quad u_2 \quad \tilde{T}_{Bed1} \quad \tilde{T}_{Bed2} \quad \tilde{T}_{Bath1} \quad \tilde{T}_{Bath2} \quad \tilde{T}_K \quad \tilde{T}_L \quad \tilde{T}_{Amb}]^T$
$Y = [P_{HVAC} \quad Q_{HVAC} \quad \dot{Q}_{hvac} \quad BR \quad m \quad COP]^T$

Y_{eq}: Matrix defining the linear part.
F_{eq}: Nonlinear and differential parts of the model.
K_{eq}: Vector containing the constant part of the model.
P_{HVAC}: Air conditioner active power consumption in [MW].
Q_{HVAC}: Air conditioner reactive power consumption in [MVAr].
V_{rated}: Rated voltage rms of air conditioner in [V].
Eff: The air conditioner electrical efficiency.
pf: Power factor of the device.
G_s: Heat source internal thermal conductance, added for numerical stability purpose in [MBtu/k^{o}C h].
$\dot{Q}_{hvac}$: Heat rate generated by the air conditioner in [MBtu/h].
q_{bed1},q_L: Heat rate through variables in [MBtu/h].
$T_{Bed1,\ldots}$, *TL*: Temperature across states variables in [k ^{o}C].
k_{factor}: a conversion factor (1 MW ~ 3.414 MBtu/h).
BR_o: Nominal Btu rating of the air conditioner system (at 35 ^{o}C) in [MBtu/h].
m: Fraction of the cooling load [unit-less].
COP_o: Nominal cooling coefficient of performance (at 35 ^{o}C) [unit-less].
ρ: Outside relative humidity [%].
$K_{1,\ldots}K_6$: Constant based on the house layout of ducts.
a: scale factor equals 1000.
u_1: Air conditioner On/Off power service given by

$$u_1 = \begin{cases} 0, & Power\ ON \\ 1, & Power\ OFF \end{cases}$$

u_2: Air conditioner operation control signal

$$u_2 = \begin{cases} 0, & A/C\ OFF \\ 1, & A/C\ ON \end{cases}$$

Appendix F. Thermal Model of a Single Story House with Two Bedrooms and Two Bathrooms

The mathematical model of the house is given by the following equations:

$$\dot{q}_{Bed1} = C_{Bed1}\frac{d}{dt}(T_{Bed1} - T_{Bed1-I}) + G_{Bed1}(T_{Bed1} - T_{Bed1-I}) \tag{F.1}$$

$$\dot{q}_{Bed2} = C_{Bed2}\frac{d}{dt}(T_{Bed2} - T_{Bed2-I}) + G_{Bed2}(T_{Bed2} - T_{Bed2-I}) \tag{F.2}$$

$$\dot{q}_{Bath1} = C_{Bath1}\frac{d}{dt}(T_{Bath1} - T_{Bath1-I}) + G_{Bath1}(T_{Bath1} - T_{Bath1-I}) \tag{F.3}$$

$$\dot{q}_{Bath2} = C_{Bath2}\frac{d}{dt}(T_{Bath2} - T_{Bath2-I}) + G_{Bath2}(T_{Bath2} - T_{Bath2-I}) \tag{F.4}$$

$$\dot{q}_{K} = C_{K}\frac{d}{dt}(T_{K} - T_{K-I}) + G_{K}(T_{K} - T_{K-I}) \tag{F.5}$$

$$\dot{q}_{L} = C_{L}\frac{d}{dt}(T_{L} - T_{L-I}) + G_{L}(T_{L} - T_{L-I}) \tag{F.6}$$

$$\begin{aligned}\dot{q}_{E} = {} & C_{Bed1I}\frac{d}{dt}(T_{E} - T_{Bed1-I}) + C_{Bath2I}\frac{d}{dt}(T_{E} - T_{Bath2-I}) + C_{E}\frac{d}{dt}(T_{E} \\ & - T_{amb}) + G_{Bed1IE}(T_{E} - T_{Bed1-I}) + G_{Bed2IE}(T_{E} - T_{Bed2-I}) \\ & + G_{Bath2IE}(T_{E} - T_{Bath2-I}) + G_{EN}(T_{E} - T_{N}) \\ & + G_{ETop}\left(T_{E} - T_{Top}\right) + G_{ES}(T_{E} - T_{S}) + G_{EAmb}(T_{E} - T_{amb})\end{aligned} \tag{F.7}$$

$$\begin{aligned}\dot{q}_{N} = {} & C_{Bath1I}\frac{d}{dt}(T_{N} - T_{Bath1-I}) + C_{N}\frac{d}{dt}(T_{N} - T_{amb}) \\ & + G_{Bed1IN}(T_{N} - T_{Bed1-I}) + G_{Bath1IN}(T_{N} - T_{Bath1-I}) \\ & + G_{LIN}(T_{N} - T_{L-I}) + G_{EN}(T_{N} - T_{E}) + G_{NW}(T_{N} - T_{W}) \\ & + G_{NTop}\left(T_{N} - T_{Top}\right) + G_{NAmb}(T_{N} - T_{amb})\end{aligned} \tag{F.8}$$

$$\begin{aligned}\dot{q}_{W} = {} & C_{LI}\frac{d}{dt}(T_{W} - T_{L-I}) + C_{W}\frac{d}{dt}(T_{W} - T_{amb}) + G_{LIW}(T_{W} - T_{L-I}) \\ & + G_{WS}(T_{W} - T_{S}) + G_{NW}(T_{W} - T_{N}) + G_{WTop}\left(T_{W} - T_{Top}\right) \\ & + G_{WAmb}(T_{W} - T_{amb})\end{aligned} \tag{F.9}$$

$$\begin{aligned}\dot{q}_{S} = {} & C_{Bed2I}\frac{d}{dt}(T_{S} - T_{Bed2-I}) + C_{S}\frac{d}{dt}(T_{S} - T_{amb}) + G_{Bed2IS}(T_{S} - T_{Bed2-I}) \\ & + G_{LIS}(T_{S} - T_{L-I}) + G_{ES}(T_{S} - T_{E}) + G_{WS}(T_{S} - T_{W}) \\ & + G_{STOP}\left(T_{S} - T_{Top}\right) + G_{SAmb}(T_{S} - T_{amb})\end{aligned} \tag{F.10}$$

$$\begin{aligned}\dot{q}_{Top} = {} & C_{KI}\frac{d}{dt}(T_{Top} - T_{K-I}) + C_{Top}\frac{d}{dt}(T_{Top} - T_{amb}) \\ & + G_{Bed1ITop}\left(T_{Top} - T_{Bed1-I}\right) + G_{Bed2ITop}\left(T_{Top} - T_{Bed2-I}\right) \\ & + G_{Bath1ITop}\left(T_{Top} - T_{Bath1-I}\right) + G_{Bath2Top}\left(T_{Top} - T_{Bath2-I}\right) \\ & + G_{KITop}\left(T_{Top} - T_{K-I}\right) + G_{LITop}\left(T_{Top} - T_{L-I}\right) \\ & + G_{ETop}\left(T_{Top} - T_{E}\right) + G_{WTop}\left(T_{Top} - T_{W}\right) \\ & + G_{NTop}\left(T_{Top} - T_{N}\right) + G_{STop}\left(T_{Top} - T_{S}\right) \\ & + G_{TopAmb}\left(T_{Top} - T_{amb}\right)\end{aligned} \tag{F.11}$$

$$\dot{q}_{amb} = C_E \frac{d}{dt}(T_{amb} - T_E) + C_N \frac{d}{dt}(T_{amb} - T_N) + C_W \frac{d}{dt}(T_{amb} - T_W) + C_S \frac{d}{dt}(T_{amb} - T_S) + C_{Top} \frac{d}{dt}(T_{amb} - T_{Top}) + G_{EAmb}(T_{amb} - T_E) + G_{NAmb}(T_{amb} - T_N) + G_{SAmb}(T_{amb} - T_S) + G_{WAmb}(T_{amb} - T_W) + G_{TopAmb}\left(T_{amb} - T_{Top}\right) \quad \text{(F.12)}$$

$$0.0 = C_{Bed1} \frac{d}{dt}(T_{Bed1-I} - T_{Bed1}) + C_{Bed1I} \frac{d}{dt}(T_{Bed1-I} - T_E) + G_{Bed1}(T_{Bed1-I} - T_{Bed1}) + G_{Bed1IE}(T_{Bed1-I} - T_E) + G_{Bed1IN}(T_{Bed1-I} - T_N) + G_{Bed1ITop}\left(T_{Bed1-I} - T_{Top}\right) + G_{Bed1IBath1I}(T_{Bed1-I} - T_{Bath1-I}) + G_{Bed1IBath2I}(T_{Bed1-I} - T_{Bath2-I}) + G_{Bed1IKI}(T_{Bed1-I} - T_{K-I}) + G_{Bed1ILI}(T_{Bed1-I} - T_{L-I}) \quad \text{(F.13)}$$

$$0.0 = C_{Bed2} \frac{d}{dt}(T_{Bed2-I} - T_{Bed2}) + C_{Bed2I} \frac{d}{dt}(T_{Bed2-I} - T_S) + G_{Bed2}(T_{Bed2-I} - T_{Bed2}) + G_{Bed2IE}(T_{Bed2-I} - T_E) + G_{Bed2IS}(T_{Bed2-I} - T_S) + G_{Bed2ITop}\left(T_{Bed2-I} - T_{Top}\right) + G_{Bed2IBath2I}(T_{Bed2-I} - T_{Bath2-I}) + G_{Bed2ILI}(T_{Bed2-I} - T_{L-I}) \quad \text{(F.14)}$$

$$0.0 = C_{Bath1} \frac{d}{dt}(T_{Bath1-I} - T_{Bath1}) + C_{Bath1I} \frac{d}{dt}(T_{Bath1-I} - T_N) + G_{Bath1}(T_{Bath1-I} - T_{Bath1}) + G_{Bath1IN}(T_{Bath1-I} - T_N) + G_{Bath1ITop}\left(T_{Bath1-I} - T_{Top}\right) + G_{Bed1IBath1I}(T_{Bath1-I} - T_{Bed1-I}) + G_{Bath1IKI}(T_{Bath1-I} - T_{K-I}) + G_{Bath1ILI}(T_{Bath1-I} - T_{L-I}) \quad \text{(F.15)}$$

$$0.0 = C_{Bath2} \frac{d}{dt}(T_{Bath2-I} - T_{Bath2}) + C_{Bath2I} \frac{d}{dt}(T_{Bath2-I} - T_E) + G_{Bath2}(T_{Bath2-I} - T_{Bath2}) + G_{Bath2IE}(T_{Bath2-I} - T_E) + G_{Bath2ITop}\left(T_{Bath2-I} - T_{Top}\right) + G_{Bed1IBath2I}(T_{Bath2-I} - T_{Bed1-I}) + G_{Bed2IBath2I}(T_{Bath2-I} - T_{Bed2-I}) + G_{Bath2ILI}(T_{Bath2-I} - T_{L-I}) \quad \text{(F.16)}$$

$$0.0 = C_K \frac{d}{dt}(T_{K-I} - T_K) + C_{KI} \frac{d}{dt}(T_{K-I} - T_{Top}) + G_K(T_{K-I} - T_K) + G_{KITop}\left(T_{K-I} - T_{Top}\right) + G_{Bed1IKI}(T_{K-I} - T_{Bed1-I}) + G_{Bath1IKI}(T_{K-I} - T_{Bath1-I}) + G_{KILI}(T_{K-I} - T_{L-I}) \quad \text{(F.17)}$$

$$0.0 = C_L \frac{d}{dt}(T_{L-I} - T_L) + C_{LI} \frac{d}{dt}(T_{L-I} - T_W) + G_L(T_{L-I} - T_L) + G_{LIS}(T_{L-I} - T_S) + G_{LIW}(T_{L-I} - T_W) + G_{LIN}(T_{L-I} - T_N) + G_{LITop}\left(T_{L-I} - T_{Top}\right) + G_{Bed1ILI}(T_{L-I} - T_{Bed1-I}) + G_{Bed2ILI}(T_{L-I} - T_{Bed2-I}) + G_{Bath1ILI}(T_{L-I} - T_{Bath1-I}) + G_{Bath2ILI}(T_{L-I} - T_{Bath2-I}) + G_{KILI}(T_{L-I} - T_{K-I}) \quad \text{(F.18)}$$

Equations (F.1)-(F.18) can be cast into a compact matrix form as follows:

$$\begin{bmatrix} I \\ 0 \end{bmatrix} = Y_{eq} \begin{bmatrix} V \\ Y \end{bmatrix} + K_{eq} \tag{F.19}$$

, where

$I = [\dot{q}_{Bed1} \quad \dot{q}_{Bed2} \quad \dot{q}_{Bath1} \quad \dot{q}_{Bath2} \quad \dot{q}_K \quad \dot{q}_L \quad \dot{q}_E \quad \dot{q}_N \quad \dot{q}_W \quad \dot{q}_S \quad \dot{q}_{Top} \quad \dot{q}_{amb}]^T$

$V = [T_{Bed1} \quad T_{Bed2} \quad T_{Bath1} \quad T_{Bath2} \quad T_K \quad T_L \quad T_E \quad T_N \quad T_W \quad T_S \quad T_{Top} \quad T_{amb}]^T$

$Y = [T_{Bed1-I} \quad T_{Bed2-I} \quad T_{Bath1-I} \quad T_{Bath2-I} \quad T_{K-I} \quad T_{L-I}]^T$

Y_{eq}: Matrix defining the linear part.
K_{eq}: Vector containing the constant part of the model.
Note that there 30 states with 30 equations are identified.

Appendix G. Variable Load Model

The mathematical model of the variable load is given by the following equations,

$$\tilde{I}_1 = \left(\frac{P_L(t) + jQ_L(t)}{\tilde{V}_1 - \tilde{V}_2}\right)^* \quad \text{(G.1)}$$

$$\tilde{I}_2 = -\left(\frac{P_L(t) + jQ_L(t)}{\tilde{V}_1 - \tilde{V}_2}\right)^* \quad \text{(G.2)}$$

, where:
$P_L(t)$: Load active power consumption at time *t* in [MW].
$Q_L(t)$: Load reactive power consumption of the dishwasher [MVAr] computed as the following,

The model then is cast into a compact matrix form as follows:

$$\begin{bmatrix} I \\ 0 \end{bmatrix} = Y_{eq}V + K_{eq} \quad \text{(G.3)}$$

, where
$I = [\tilde{I}_1 \quad \tilde{I}_2]^T$,
$V = [\tilde{V}_1 \quad \tilde{V}_2]^T$
I: Through variables of the model.
V: Across external states variables of the model.
Y_{eq}: Matrix defining the linear part of the model.
K_{eq}: Vector containing the constant part of the model.

Appendix H. Solar Cell Mathematical Model

The mathematical model used for the solar cell is represented by the following equations:

$$I = I_{pv} - I_0 \left[\exp\left(\frac{V + IR_s}{V_t a}\right) - 1\right] - \frac{V + IR_s}{R_P} \quad \text{(H.1)}$$

$$I_{pv} = (I_{pv_n} + K_I\, \Delta T)\frac{S}{S_n} \quad \text{(H.2)}$$

$$I_0 = (I_{sc_n} + K_I\, \Delta T) / \left[\exp\left(\frac{\left(V_{oc_n} + K_V\, \Delta T\right)}{aV_t}\right) - 1\right] \quad \text{(H.3)}$$

$$I_{pv_n} = \frac{R_p + R_s}{R_p} I_{sc_n} \quad \text{(H.4)}$$

$$V_t = \frac{N_s kT}{q} \quad \text{(H.5)}$$

$$\Delta T = T - T_n \quad \text{(H.6)}$$

, where
I: the array output current [A]
V: the array output voltage [V]
I_{pv}: Light generated current [A]
$I_{pv,n}$: Light generated current at the nominal condition [A]
I_0: the reverse saturation or the leakage current of the diode [A]
R_s: the equivalent series resistance of the array [Ω]
R_p: the equivalent parallel resistance of the array [Ω]
$I_{sc,\,n}$: Short circuit current provided by the data sheet [A]
$V_{oc,\,n}$: Open circuit voltage provided by the data sheet [V]
S: Current solar irradiance [W/m^2]
S_n: Nominal solar irradiance = 1000[W/m^2]
T: Weather temperature [K]
T_n: Nominal temperature = 273.15 [K]
V_t: the equivalent thermal voltage of the array [V]
N_s: the number of cells in series provided by the data sheet
a: Diode constant $1 \leq a \leq 1.5$
K_I: Short circuit current temperature coefficient provided by the data sheet
K_V: Open circuit voltage temperature coefficient provided by the data sheet
k: Boltzmann constant = 1.3806503 x 10^{-23} [J/K]
q: the electron charge = 1.60217646 x 10^{-19} [C]

Appendix I. Single Phase Average Model DC-DC Boost Converter

I.1 DC Voltage Control

The mathematical model of the DC-DC boost converter with dc voltage control is given by the following equations,

$$\tilde{I}_1 = (G_1 - jB)\left(\tilde{V}_1 - \tilde{V}_x\right) \tag{I.1}$$

$$\tilde{I}_2 = -(G_1 - jB)\left(\tilde{V}_1 - \tilde{V}_x\right) \tag{I.2}$$

$$\tilde{I}_3 = G_2(\tilde{V}_3 - \tilde{V}_y) \tag{I.3}$$

$$\tilde{I}_4 = -G_2(\tilde{V}_3 - \tilde{V}_y) \tag{I.4}$$

$$0.0 = \left(\tilde{V}_x - \tilde{V}_2\right) - (1 - D)(\tilde{V}_y - \tilde{V}_4) \tag{I.5}$$

$$0.0 = \tilde{I}_1(1 - D) + \tilde{I}_3 \tag{I.6}$$

Controller 1: Voltage control

$$0.0 = -V_{dc\,ref} + \tilde{V}_y - \tilde{V}_4 \tag{I.7}$$

For simplicity, equations (I.1)-(I.7) can be cast into a compact matrix form as follows:

$$\begin{bmatrix} I \\ 0 \end{bmatrix} = A \begin{bmatrix} V \\ Y \end{bmatrix} + N + C \tag{I.8}$$

, where
$I = [\tilde{I}_1 \quad \tilde{I}_2]^T$,
$V = [\tilde{V}_1 \quad \tilde{V}_2 \quad \tilde{V}_3 \quad \tilde{V}_4]^T$
$Y = \left[\tilde{V}_x \quad \tilde{V}_y \quad D\right]^T$

A: Matrix defining the linear part.
N: Nonlinear and differential parts of the model.
C: Vector containing the constant part of the model.
Note that there 7 states with 7 equations are identified.

I.2 Real Power Control

The mathematical model of the DC-DC boost converter with real power control is given by the following equations,

$$\tilde{I}_1 = (G_1 - jB)\left(\tilde{V}_1 - \tilde{V}_x\right) \tag{I.9}$$

$$\tilde{I}_2 = -(G_1 - jB)\left(\tilde{V}_1 - \tilde{V}_x\right) \tag{I.10}$$

$$\tilde{I}_3 = G_2(\tilde{V}_3 - \tilde{V}_y) \tag{I.11}$$

$$\tilde{I}_4 = -G_2(\tilde{V}_3 - \tilde{V}_y) \tag{I.12}$$

$$0.0 = \left(\tilde{V}_x - \tilde{V}_2\right) - (1 - D)(\tilde{V}_y - \tilde{V}_4) \tag{I.13}$$

$$0.0 = \tilde{I}_1(1 - D) + \tilde{I}_3 \tag{I.14}$$

Controller 2: Real power control

$$\begin{aligned} 0.0 &= -P_{ref} + \tilde{I}_1\left(\tilde{V}_1 - \tilde{V}_2\right) - \frac{\tilde{I}_1^2}{G}, \\ OR\ \ 0.0 &= -P_{ref} + \tilde{I}_1\left(\tilde{V}_x - \tilde{V}_2\right) \end{aligned} \tag{I.15}$$

For simplicity, equations (I.9)-(I.15) can be cast into a compact matrix form as follows:

$$\begin{bmatrix} I \\ 0 \end{bmatrix} = A \begin{bmatrix} V \\ Y \end{bmatrix} + N + C \tag{I.16}$$

, where
$I = [\tilde{I}_1 \quad \tilde{I}_2]^T$,
$V = [\tilde{V}_1 \quad \tilde{V}_2 \quad \tilde{V}_3 \quad \tilde{V}_4]^T$
$Y = \left[\tilde{V}_x \quad \tilde{V}_y \quad D\right]^T$

A: Matrix defining the linear part.
N: Nonlinear and differential parts of the model.
C: Vector containing the constant part of the model.
Note that there 7 states with 7 equations are identified.

I.3 Maximum Power Point Tracking (MPPT) Control

The mathematical model of the DC-DC boost converter with MPPT control is given by the following equations,

$$\tilde{I}_1 = (G_1 - jB)\left(\tilde{V}_1 - \tilde{V}_x\right) \tag{I.17}$$

$$\tilde{I}_2 = -(G_1 - jB)\left(\tilde{V}_1 - \tilde{V}_x\right) \tag{I.18}$$

$$\tilde{I}_3 = G_2(\tilde{V}_3 - \tilde{V}_y) \tag{I.19}$$

$$\tilde{I}_4 = -G_2(\tilde{V}_3 - \tilde{V}_y) \tag{I.20}$$

$$0.0 = \left(\tilde{V}_x - \tilde{V}_2\right) - (1 - D)(\tilde{V}_y - \tilde{V}_4) \tag{I.21}$$

$$0.0 = \tilde{I}_1(1 - D) + \tilde{I}_3 \tag{I.22}$$

For simplicity, equations (I.17)-(I.22) can be cast into a compact matrix form as follows:

$$\begin{bmatrix} I \\ 0 \end{bmatrix} = A \begin{bmatrix} V \\ Y \end{bmatrix} + N + C \tag{I.23}$$

, where
$I = [\tilde{I}_1 \quad \tilde{I}_2]^T$,
$V = [\tilde{V}_1 \quad \tilde{V}_2 \quad \tilde{V}_3 \quad \tilde{V}_4]^T$
$Y = \begin{bmatrix} \tilde{V}_x & \tilde{V}_y \end{bmatrix}^T$

A: Matrix defining the linear part.
N: Nonlinear and differential parts of the model.
C: Vector containing the constant part of the model.
Note that there 6 states with 6 equations are identified.

Appendix J. Single Phase Full-Bridge Average Model of DC-AC Inverter

J.1 VQ Control

The mathematical model of the DC-AC inverter with VQ control is given by the following equations,

$$\tilde{I}_1 = G_{dc}(\tilde{V}_1 - \tilde{V}_x) \tag{J.1}$$

$$\tilde{I}_2 = -G_{dc}(\tilde{V}_1 - \tilde{V}_x) \tag{J.2}$$

$$\tilde{I}_3 = (G_{dc} - jB_{ac})(\tilde{V}_3 - \tilde{V}_y) \tag{J.3}$$

$$\tilde{I}_4 = -(G_{dc} - jB_{ac})(\tilde{V}_3 - \tilde{V}_y) \tag{J.4}$$

$$0.0 = \left|\tilde{V}_y\right| - \left|\tilde{V}_4\right| - \sqrt{2}\, m\left(\tilde{V}_x - \tilde{V}_2\right) \tag{J.5}$$

$$\begin{gathered} 0.0 = \tilde{I}_1 + m\tilde{I}_3 \\ OR\ 0.0 = \tilde{I}_1\left(\tilde{V}_x - \tilde{V}_2\right) + Re\left\{\tilde{I}_3^*\left(\tilde{V}_y - \tilde{V}_4\right)\right\} \end{gathered} \tag{J.6}$$

$$0.0 = -V_{dc\,ref} + \tilde{V}_x - \tilde{V}_2 \tag{J.7}$$

$$0.0 = Q_{ref} + Im\left\{\tilde{I}_3^*\left(\tilde{V}_y - \tilde{V}_4\right)\right\} \tag{J.8}$$

For simplicity, equations (J.1)-(J.8) can be cast into a compact matrix form as follows:

$$\begin{bmatrix} I \\ 0 \end{bmatrix} = Y_{eq}\begin{bmatrix} V \\ Y \end{bmatrix} + [V \quad Y]F_{eq}\begin{bmatrix} V \\ Y \end{bmatrix} + K_{eq} \tag{J.9}$$

, where
$I = [\tilde{I}_1 \quad \tilde{I}_2 \quad \tilde{I}_3 \quad \tilde{I}_4]^T$,
$V = [\tilde{V}_1 \quad \tilde{V}_2 \quad \tilde{V}_3 \quad \tilde{V}_4]^T$
$Y = \left[\tilde{V}_x \quad \tilde{V}_y \quad m\right]^T$
Y_{eq}: Matrix defining the linear part.
F_{eq}: Nonlinear and differential parts of the model.
K_{eq}: Vector containing the constant part of the model.
Note that there 7 states with 7 equations are identified.

J.2 PQ Control

The mathematical model of the DC-AC inverter with PQ control is given by the following equations,

$$\tilde{I}_1 = G_{dc}(\tilde{V}_1 - \tilde{V}_x) \tag{J.10}$$

$$\tilde{I}_2 = -G_{dc}(\tilde{V}_1 - \tilde{V}_x) \tag{J.11}$$

$$\tilde{I}_3 = (G_{dc} - jB_{ac})(\tilde{V}_3 - \tilde{V}_y) \quad \text{(J.12)}$$

$$\tilde{I}_4 = -(G_{dc} - jB_{ac})(\tilde{V}_3 - \tilde{V}_y) \quad \text{(J.13)}$$

$$0.0 = \left|\tilde{V}_y\right| - \left|\tilde{V}_4\right| - \sqrt{2}\, m\left(\tilde{V}_x - \tilde{V}_2\right) \quad \text{(J.14)}$$

$$0.0 = \tilde{I}_1 + m\tilde{I}_3$$
$$OR\ 0.0 = \tilde{I}_1\left(\tilde{V}_x - \tilde{V}_2\right) + Re\left\{\tilde{I}_3^*\left(\tilde{V}_y - \tilde{V}_4\right)\right\} \quad \text{(J.15)}$$

$$0.0 = P_{ref} + Re\left\{\tilde{I}_3^*\left(\tilde{V}_y - \tilde{V}_4\right)\right\} \quad \text{(J.16)}$$

$$0.0 = Q_{ref} + Im\left\{\tilde{I}_3^*\left(\tilde{V}_y - \tilde{V}_4\right)\right\} \quad \text{(J.17)}$$

For simplicity, equations (J.10)-(J.17) can be cast into a compact matrix form as follows:

$$\begin{bmatrix} I \\ 0 \end{bmatrix} = Y_{eq} \begin{bmatrix} V \\ Y \end{bmatrix} + [V \quad Y] F_{eq} \begin{bmatrix} V \\ Y \end{bmatrix} + K_{eq} \quad \text{(J.18)}$$

, where
$I = [\tilde{I}_1 \quad \tilde{I}_2 \quad \tilde{I}_3 \quad \tilde{I}_4]^T$,
$V = [\tilde{V}_1 \quad \tilde{V}_2 \quad \tilde{V}_3 \quad \tilde{V}_4]^T$
$Y = \left[\tilde{V}_x \quad \tilde{V}_y \quad m\right]^T$
Y_{eq}: Matrix defining the linear part.
F_{eq}: Nonlinear and differential parts of the model.
K_{eq}: Vector containing the constant part of the model.
Note that there 7 states with 7 equations are identified.

Appendix K. Electro-Thermal Lead Acid Battery Model

The lead acid electrical circuit is shown in Figure K-1.

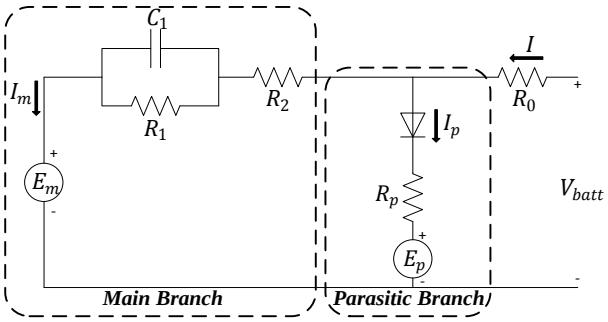

Figure K-1 Equivalent Lead Acid Electric Circuit Model

K.1 Mathematical Model

Main Branch

The main branch voltage is a function of the state of charge and the electrolyte temperature and given by,

$$E_m = E_{m0} - K_E(273 + \theta)(1 - SOC) \quad \text{(K.1)}$$

, where
E_m: Open circuit voltage in [V]
E_{m0}: Open circuit voltage when the battery is full of charge in [V]
T: Electrolyte temperature in [^{o}C]
SOC: State of charge
K_E: Constant in [V/^{o}C]

The main branch resistance and capacitance are given by,

$$R_1 = -R_{10} \ln(DOC) \quad \text{(K.2)}$$

$$C_1 = \tau_1 / R_1 \quad \text{(K.3)}$$

, where
R_1: the main branch resistance in [Ω]
C_1: the main branch capacitance in [F]
R_{10}: Constant in [Ω]
DOC: Battery depth of charge
τ_1: the main branch time constant in [sec]

The main branch second resistance is given by,

$$R_2 = R_{20} \exp[A_{21}(1 - SOC)] / (1 + \exp(A_{22} I_m / I^*) \quad \text{(K.4)}$$

, where
R_2: is the main branch second resistance in [Ω]
R_{20}: Constant in [Ω]
A_{21}: Constant
A_{22}: Constant
I_m: The main branch current in [A]
I^*: Battery nominal current in [A]

The terminal resistance of the battery is given by,

$$R_0 = R_{00}[1 + A_0(1 - SOC)] \quad \text{(K.5)}$$

, where
R_0: the resistance in [Ω]
R_{00}: Constant in [Ω] and equals to the value of R_0 the battery is full of charge
A_0: Constant

Parasitic Branch

The behavior of the parasitic branch is strongly non-linear. However, the value of the current flowing in the branch, which is a function of the parasitic branch voltage, can be computed by the Tafel gassing – current relationship which is given by,

$$I_p = V_p G_p \quad \text{(K.6)}$$

, where G_p is

$$G_p = G_{p0} \exp\left[\frac{V_p}{V_{p0}} + A_p\left(1 - \frac{T}{T_f}\right)\right] \quad \text{(K.7)}$$

, and thus R_p is

$$R_p = (V_p - E_p)/I_p \quad \text{(K.8)}$$

, where
I_p: the current flowing in the parasitic branch in [A]
V_p: The parasitic branch voltage in [V]
G_{p0}: Constant in [S]
V_{p0}: Constant in [V]
A_p: Constant
T_f: Electrolyte freezing temperature in [^{o}C]

Charge and Battery Capacity

The extracted charge at *t* is given by,

$$Q_e(t) = Q_{init} + \int_0^t -I_m(\tau)d\tau \tag{K.9}$$

The averaged current can be computed by,

$$I_{ave} = I_m/(\tau_1 s + 1) \tag{K.10}$$

The capacity of the battery, which is a function of the battery current *I* and the electrolyte temperature, is given by the following,

$$C(I,T) = \frac{K_c C_{0^*}\left(1 - \frac{T}{T_f}\right)^{\xi}}{1 + (K_c - 1)\left(\frac{I}{I^*}\right)^{\delta}} \tag{K.11}$$

, where
Q_e: the extracted charge in [As]
Q_{init}: the initial extracted charge in [As]
τ: The integration time variable
t: the simulation time in [sec]
K_c: a constant
C_0^*: no load capacity at 0[^{o}C] in [Ah]
ξ and δ: constant

The state of charge and the depth of charge are given by the following equations,

$$SOC = 1 - Q_e/C(0,T) \tag{K.12}$$

$$DOC = 1 - Q_e/C(I_{ave},T) \tag{K.13}$$

Thermal Model

$$\frac{dT}{dt} = 1/C_{th}\left[P_s - \frac{T - T_a}{R_{th}}\right] \tag{K.14}$$

, where
C_{th}: Thermal capacitance in [Wh/^{o}C]
R_{th}: Thermal resistance in [^{o}C/W]
P_s: The heat power loss in the parasitic branch in [W]
T_a: Ambient temperature or the surrounding temperature in [^{o}C]

K.2 Charging Mode

The mathematical model of the lead acid battery in the charging mode is given by the following compact equations,

$$I_1 = G_0(V_1 - V_x) \tag{K.15}$$

$$I_2 = -G_0(V_1 - V_x) \tag{K.16}$$

$$0.0 = G_p\left[(V_x - V_2) - E_p\right] + I_m - G_0(V_1 - V_x) \tag{K.17}$$

$$0.0 = I_m - G_1\left(V_y - V_z\right) - C_1\frac{d}{dt}(V_y - V_z) \tag{K.18}$$

$$0.0 = I_m - G_2(V_x - V_y) \tag{K.19}$$

$$0.0 = (V_z - V_2) - E_{m0} + K_E(273 + T)(1 - SOC) \tag{K.20}$$

$$0.0 = C_1 - \tau_1 G_1 \tag{K.21}$$

$$0.0 = R_0 - R_{00}[1 + A_0(1 - SOC)] \tag{K.22}$$

$$0.0 = I_m + \frac{dQ_e(t)}{dt} \tag{K.23}$$

$$0.0 = SOC\ C(0,T) - C(0,T) + Q_e \tag{K.24}$$

$$0.0 = DOC\ C(I_{ave},T) - C(I_{ave},T) + Q_e \tag{K.25}$$

$$0.0 = \frac{dT}{dt} - \frac{1}{C_{th}}\left[P_s - \frac{T - T_a}{R_{th}}\right] \tag{K.26}$$

$$0.0 = R_0 G_0 - 1 \tag{K.27}$$

$$0.0 = R_1 G_1 - 1 \tag{K.28}$$

$$0.0 = R_2 G_2 - 1 \tag{K.29}$$

$$0.0 = C(0,T) - K_c C_{0^*}\left(1 - \frac{T}{T_f}\right)^{\xi} \tag{K.30}$$

$$0.0 = C\left(I_{avg},T\right) - \frac{K_c C_{0^*}\left(1 - \frac{T}{T_f}\right)^{\xi}}{1 + (K_c - 1)\left(\frac{I_{avg}}{I^*}\right)^{\delta}} \tag{K.31}$$

$$0.0 = C(I_1,T) - \frac{K_c C_{0^*}\left(1 - \frac{T}{T_f}\right)^{\xi}}{1 + (K_c - 1)\left(\frac{I_1}{I^*}\right)^{\delta}} \tag{K.32}$$

$$0.0 = R_2 - R_{20}\exp[\mathrm{A}_{21}(1 - \mathrm{SOC})] \,/\, \left[1 + \exp\left(\frac{\mathrm{A}_{22}\mathrm{I}_{\mathrm{m}}}{\mathrm{I}^*}\right)\right] \tag{K.33}$$

$$0.0 = G_p - G_{p0}\exp\left[\left(\frac{V_x - V_2}{V_{p0}}\right) + A_p\left(1 - \frac{T}{T_f}\right)\right] \tag{K.34}$$

$$0.0 = I_{avg} - \left[\frac{I_m \exp\left(-\frac{t}{\tau_1}\right)}{\tau_1}\right] \tag{K.35}$$

$$0.0 = R_1 + R_{10}\ln(DOC) \tag{K.36}$$

$$0.0 = P_s - G_p[(V_x - V_2) - E_p]^2 \tag{K.37}$$

For simplicity, equations (K.15)-(K.37) can be cast into a compact matrix form as follows:

$$\begin{bmatrix} I \\ 0 \end{bmatrix} = A\begin{bmatrix} V \\ Y \end{bmatrix} + N + C \tag{K.38}$$

Where:
$I = [I_1 \quad I_2]^T$,
$V = [V_1 \quad V_2]^T$
$Y = [V_x \quad V_y \quad V_z \quad R_0 \quad R_1 \quad R_2 \quad G_0 \quad G_1 \quad G_2 \quad G_p \quad C_1 \quad T \quad SOC \quad DOC \quad I_m \quad P_s$
$Q_e \quad I_{avg} \quad C(0,T) \quad C\left(I_{avg},T\right) \quad C(I_1,T)]^T$

K.3 Discharging Mode

The mathematical model of the lead acid battery in the discharging mode is given by the following compact equations,

$$I_1 = G_0(V_1 - V_x) \tag{K.39}$$

$$I_2 = -G_0(V_1 - V_x) \tag{K.40}$$

$$0.0 = I_m - G_0(V_1 - V_x) \tag{K.41}$$

$$0.0 = I_m - G_1(V_x - V_z) - C_1 \frac{d}{dt}(V_x - V_z) \tag{K.42}$$

$$0.0 = (V_z - V_2) - E_{m0} + K_E(273 + \theta)(1 - SOC) \tag{K.43}$$

$$0.0 = C_1 - \tau_1 G_1 \tag{K.44}$$

$$0.0 = R_0 - R_{00}[1 + A_0(1 - SOC)] \tag{K.45}$$

$$0.0 = I_m + \frac{d\ Q_e(t)}{dt} \tag{K.46}$$

$$0.0 = SOC\ C(0, \theta) - C(0, \theta) + Q_e \tag{K.47}$$

$$0.0 = DOC\ C(I_{ave}, \theta) - C(I_{ave}, \theta) + Q_e \tag{K.48}$$

$$0.0 = \frac{d\theta}{dt} - \frac{1}{C_\theta}\left[0 - \frac{\theta - \theta_a}{R_\theta}\right] \tag{K.49}$$

$$0.0 = R_0 G_0 - 1 \tag{K.50}$$

$$0.0 = R_1 G_1 - 1 \tag{K.51}$$

$$0.0 = C(0, \theta) - K_c C_{0^*}\left(1 - \frac{\theta}{\theta_f}\right)^{\xi} \tag{K.52}$$

$$0.0 = C\left(I_{avg}, \theta\right) - \frac{K_c C_{0^*}\left(1 - \frac{\theta}{\theta_f}\right)^{\xi}}{1 + (K_c - 1)\left(\frac{I_{avg}}{I^*}\right)^{\delta}} \tag{K.53}$$

$$0.0 = C(I_1, \theta) - \frac{K_c C_{0^*}\left(1 - \frac{\theta}{\theta_f}\right)^{\xi}}{1 + (K_c - 1)\left(\frac{I_1}{I^*}\right)^{\delta}} \tag{K.54}$$

$$0.0 = I_{avg} - \left[\frac{I_m \exp\left(-\frac{t}{\tau_1}\right)}{\tau_1}\right] \tag{K.55}$$

$$0.0 = R_1 + R_{10} \ln(DOC) \tag{K.56}$$

For simplicity, equations (K.39)-(K.56) can be cast into a compact matrix form as follows,

$$\begin{bmatrix} I \\ 0 \end{bmatrix} = A \begin{bmatrix} V \\ Y \end{bmatrix} + N + C \tag{K.57}$$

Where:
$I = [I_1 \quad I_2]^T$,
$V = [V_1 \quad V_2]^T$
$Y = [V_x \quad V_z \quad R_0 \quad R_1 \quad G_0 \quad G_1 \quad C_1 \quad \theta \quad SOC \quad DOC \quad I_m \quad Q_e \quad I_{avg}$
$C(0,\theta) \quad C\left(I_{avg},\theta\right) \quad C(I_1,\theta)]^T$

Appendix L. Electric Vehicle Model (Lithium Ion Battery Model)

L.1 Lithium-Ion Battery Mathematical Model Derivation

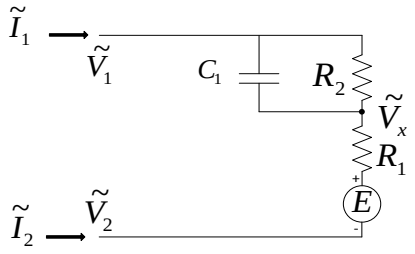

Figure L-1 Equivalent Electrical Circuit of the Battery

In this section, the battery model is reformulated according to the standard device format that is as the following:

$$\tilde{I}_1 = \tilde{x}_1 \tag{L.1}$$

$$\tilde{I}_2 = -\tilde{x}_1 \tag{L.2}$$

, where x_1 is given by:

$$0.0 = -\tilde{x}_1 + G_2\left(\tilde{V}_1 - \tilde{V}_x\right) + j\omega C_1(\tilde{V}_1 - \tilde{V}_x) \tag{L.3}$$

$$0.0 = \tilde{E} - \left(\tilde{V}_1 - \tilde{V}_2\right) + (R_1 + R_2)\tilde{x}_1 \tag{L.4}$$

$$0.0 = -\tilde{V}_1 + \tilde{V}_2 + c_0 + c_1 SOD(t) + c_2 SOD^2(t) + c_3 SOD^3(t) + \Delta E\left(\theta(t)\right) \tag{L.5}$$

Where the coefficients are listed below,

Table L-1 The Terminal Voltage Polynomial Coefficients

$c_0 = 4.121$	$c_1 = -1.624$	$c_2 = 3.587$	$c_3 = -3.581$

$$0.0 = \frac{d}{dt} SOD(t) - \frac{1}{Q_r}\alpha(\tilde{I}_1)\,\beta\left(\theta(t)\right)\tilde{x}_1 \tag{L.6}$$

$$0.0 = -m\,c_p\,\frac{d\theta(t)}{dt} + P_s(t) - h_c A(\theta(t) - \theta_a) \tag{L.7}$$

, where $P_s(t)$ is the electric power loss and given by:

$$0.0 = P_s(t) - \tilde{x}_1^2 R_1 - G_2\left(\tilde{V}_1 - \tilde{V}_x\right)^2 \tag{L.8}$$

The other three fitted to the 2nd degree polynomials are

$$\alpha(\tilde{I}_1) = a_0 + a_1\tilde{x}_1 + a_2\tilde{x}_1^2 \quad \text{(L.9)}$$

$$\beta(\theta(t)) = b_0 + b_1\theta(t) + b_2\theta^2(t) \quad \text{(L.10)}$$

$$\Delta E\big(\theta(t)\big) = d_0 + d_1\theta(t) + d_2\theta^2(t) \quad \text{(L.11)}$$

, where the values of the coefficients are given in the below table,

Table L-2 Polynomails Coefficients

$a_2 = -0.006647$	$a_1 = 0.05215$	$a_0 = 0.9559$
$b_2 = 2.139\text{x}10^{-6}$	$b_1 = -0.001835$	$b_0 = 1.052$
$d_2 = -4.935\text{x}10^{-5}$	$d_1 = 0.01097$	$d_0 = -0.1793$

L.2 Mathematical Model in a Compact Form

The compact form is:

$$\tilde{I}_1 = \tilde{x}_1 \quad \text{(L.12)}$$

$$\tilde{I}_2 = -\tilde{x}_1 \quad \text{(L.13)}$$

$$0.0 = \tilde{E} - \big(\tilde{V}_1 - \tilde{V}_2\big) + (R_1 + R_2)\tilde{x}_1 \quad \text{(L.14)}$$

$$0.0 = -\tilde{V}_1 + \tilde{V}_2 + c_0 + c_1 SOD + c_2 SOD^2 + c_3 SOD^3 + \Delta E(\theta) \quad \text{(L.15)}$$

$$0.0 = -\tilde{x}_1 + G_2\big(\tilde{V}_1 - \tilde{V}_x\big) + j\omega C_1(\tilde{V}_1 - \tilde{V}_x) \quad \text{(L.16)}$$

$$0.0 = P_s - \tilde{I}_1^2 R_1 - G_2\big(\tilde{V}_1 - \tilde{V}_x\big)^2 \quad \text{(L.17)}$$

$$0.0 = SOC - 1 + SOD \quad \text{(L.18)}$$

$$0.0 = -\alpha(\tilde{x}_1) + a_0 + a_1\tilde{x}_1 + a_2\tilde{x}_1^2 \quad \text{(L.19)}$$

$$0.0 = -\beta(\theta) + b_0 + b_1\theta + b_2\theta^2 \quad \text{(L.20)}$$

$$0.0 = -\Delta E(\theta) + d_0 + d_1\theta + d_2\theta^2 \quad \text{(L.21)}$$

For simplicity, equations (L.12)-(L.21) can be cast into a compact matrix form as follows:

$$\begin{bmatrix} I \\ 0 \end{bmatrix} = A \begin{bmatrix} V \\ Y \end{bmatrix} + N + C \quad \text{(L.22)}$$

, where
$I = [\tilde{I}_1 \quad \tilde{I}_2]^T$,
$V = [\tilde{V}_1 \quad \tilde{V}_2]^T$
$Y = [\tilde{V}_x \quad \tilde{E} \quad \tilde{x}_1 \quad SOD \quad P_s \quad \alpha(\tilde{I}_1) \quad \beta(\theta) \quad \Delta E(\theta)]^T$

A: Matrix defining the linear part.
N: Nonlinear and differential parts of the model.

C: Vector containing the constant part of the model.

Appendix M. Battery Charger Model

M.1 DC Voltage Control

The mathematical model of the averaged DC-DC buck boost converter is given in the following compact form,

$$\tilde{I}_1 = (G_1 - jB)\left(\tilde{V}_1 - \tilde{V}_x\right) \quad \text{(M.1)}$$

$$\tilde{I}_2 = -(G_1 - jB)\left(\tilde{V}_1 - \tilde{V}_x\right) \quad \text{(M.2)}$$

$$\tilde{I}_3 = G_2(\tilde{V}_3 - \tilde{V}_y) \quad \text{(M.3)}$$

$$\tilde{I}_4 = -G_2(\tilde{V}_3 - \tilde{V}_y) \quad \text{(M.4)}$$

$$0.0 = \left(\tilde{V}_x - \tilde{V}_2\right) - \frac{1-D}{D}(\tilde{V}_y - \tilde{V}_4) \quad \text{(M.5)}$$

$$0.0 = \frac{\tilde{I}_1(1-D)}{D} + \tilde{I}_3 \quad \text{(M.6)}$$

$$0.0 = -V_{dc\,ref} + \tilde{V}_y - \tilde{V}_4 \quad \text{(M.7)}$$

For simplicity, equations (M.1)-(M.7) can be cast into a compact matrix form as follows:

$$\begin{bmatrix} I \\ 0 \end{bmatrix} = A \begin{bmatrix} V \\ Y \end{bmatrix} + N + C \quad \text{(M.8)}$$

, where
$I = [\tilde{I}_1 \quad \tilde{I}_2]^T$,
$V = [\tilde{V}_1 \quad \tilde{V}_2 \quad \tilde{V}_3 \quad \tilde{V}_4]^T$
$Y = \left[\tilde{V}_x \quad \tilde{V}_y \quad D\right]^T$

A: Matrix defining the linear part.
N: Nonlinear and differential parts of the model.
C: Vector containing the constant part of the model.

M.2 Real Power Control

The mathematical model of the averaged DC-DC buck boost converter is given in the following compact form,

$$\tilde{I}_1 = (G_1 - jB)\left(\tilde{V}_1 - \tilde{V}_x\right) \quad \text{(M.9)}$$

$$\tilde{I}_2 = -(G_1 - jB)\left(\tilde{V}_1 - \tilde{V}_x\right) \quad \text{(M.10)}$$

$$\tilde{I}_3 = G_2(\tilde{V}_3 - \tilde{V}_y) \quad \text{(M.11)}$$

$$\tilde{I}_4 = -G_2(\tilde{V}_3 - \tilde{V}_y) \quad \text{(M.12)}$$

$$0.0 = \left(\tilde{V}_x - \tilde{V}_2\right) - \frac{1-D}{D}(\tilde{V}_y - \tilde{V}_4) \quad \text{(M.13)}$$

$$0.0 = \frac{\tilde{I}_1(1-D)}{D} + \tilde{I}_3 \tag{M.14}$$

$$0.0 = -P_{ref} + \tilde{I}_1(\tilde{V}_1 - \tilde{V}_2) - \frac{\tilde{I}_1^2}{G}, \quad OR \;\; 0.0 = -P_{ref} + \tilde{I}_1(\tilde{V}_x - \tilde{V}_2) \tag{M.15}$$

For simplicity, equations (M.9)-(M.15) can be cast into a compact matrix form as follows:

$$\begin{bmatrix} I \\ 0 \end{bmatrix} = A \begin{bmatrix} V \\ Y \end{bmatrix} + N + C \tag{M.16}$$

, where
$I = [\tilde{I}_1 \quad \tilde{I}_2]^T$,
$V = [\tilde{V}_1 \quad \tilde{V}_2 \quad \tilde{V}_3 \quad \tilde{V}_4]^T$
$Y = \begin{bmatrix} \tilde{V}_x & \tilde{V}_y & D \end{bmatrix}^T$

A: Matrix defining the linear part.
N: Nonlinear and differential parts of the model.
C: Vector containing the constant part of the model.